## General Disclaimer

## One or more of the Following Statements may affect this Document

- This document has been reproduced from the best copy furnished by the organizational source. It is being released in the interest of making available as much information as possible.

- This document may contain data, which exceeds the sheet parameters. It was furnished in this condition by the organizational source and is the best copy available.

- This document may contain tone-on-tone or color graphs, charts and/or pictures, which have been reproduced in black and white.

- This document is paginated as submitted by the original source.

- Portions of this document are not fully legible due to the historical nature of some of the material. However, it is the best reproduction available from the original submission.

Produced by the NASA Center for Aerospace Information (CASI)

"Made available under NASA sponsorship
in the interest of early and wide dis-
semination of Earth Resources Survey
Program information and without liability
for any use made thereof."

7.7 - 1 0.1 4 9.
CR - 152649

# GROUND WATER RECHARGE TO THE AQUIFERS OF NORTHERN SAN LUIS VALLEY, COLORADO: A REMOTE SENSING INVESTIGATION

By

David Huntley

(E77-10149) GROUND WATER RECHARGE TO THE AQUIFERS OF NORTHERN SAN LUIS VALLEY, COLORADO: A REMOTE SENSING INVESTIGATION (Colorado School of Mines, Golden.) 313 p HC A14/MF A01 CSCL 08H G3/43

N77-22578

Unclas
00149

Remote Sensing Report 76-3

NASA Grant NGL 06-001-015
National Aeronautics and Space Administration
Office of University Affairs
Washington, D.C. 20546

MAR 1977
RECEIVED
NASA STI FACILITY
INPUT BRANCH

December 1976

i

**REMOTE SENSING PROJECTS**

DEPARTMENT OF GEOLOGY

COLORADO SCHOOL OF MINES • GOLDEN, COLORADO

# GROUND WATER RECHARGE TO THE AQUIFERS OF NORTHERN SAN LUIS VALLEY, COLORADO: A REMOTE SENSING INVESTIGATION

By

David Huntley

Remote Sensing Report 76-3

Bonanza Remote Sensing Project
Department of Geology
Colorado School of Mines
Golden, Colorado

Original photography may be purchased from:
EROS Data Center
10th and Dakota Avenue
Sioux Falls, SD 57198

NASA Grant NGL 06-001-015

Approved for Publication: ____________

Keenan Lee
Principal Investigator

December 1976

## ABSTRACT

The northern San Luis Basin can be divided into three distinct, but hydrologically connected provinces: the Sangre de Cristo Mountains, a region of relatively low, depth-dependent permeability, low ground water flow rates, and high surface water flow rates; the San Juan Mountains, a region of relatively high, strongly anisotropic permeability, high ground water flow rates, and low surface water flow rates; and San Luis Valley, a region of high permeability and high rates of evapotranspirative discharge. Faults are important in all regions, providing areas of increased permeability in the Sangre de Cristo and San Juan mountains, while acting as ground water barriers in San Luis Valley. Faults have controlled sedimentation patterns in the basin from Paleozoic through Quaternary time.

Ground water is calcium bicarbonate type in the recharge areas of the basin, changing to sodium bicarbonate toward the center of discharge of the basin. A sharp increase in the proportion of sodium relative to calcium in the water of the confined aquifer along the eastern margin of San Luis Valley probably is caused by hyperfiltration of ground water as it flows through confining clays. The distribution of sodium/calcium ratios in water of the confined aquifer can be used to estimate the lateral extent of the confining clays.

Recharge to the aquifers of western San Luis Valley is largely from ground water inflow from the permeable volcanic rocks of the San Juan Mountains. Recharge to the aquifers of eastern San Luis Valley is dominantly from stream seepage into alluvial fans along a narrow strip bordering the Sangre de Cristo Mountains. The limit of flowing wells in San Luis Valley corresponds neither to the limit of confining clays nor the limit of the ground water recharge zone.

Use of aerial photography and thermal-infrared imagery resulted in a significant savings in time and increase in accuracy in this regional ground water study. The most important feature governing the usefulness of aerial photography is the ground resolution. Reflectance measurements of moist and dry soils, saline soils, and volcanic rocks show that, like sedimentary rocks, there is no unique spectral "signature" that can be assigned to a rock or soil type, and that absolute reflectance differences in one part of the spectrum can be extrapolated to the rest of the photographic spectrum. Spectral variations related to vegetation variation, in turn related primarily to water availability, are extremely important in hydrogeologic studies, however. Color-infrared film is the most useful film for such a study.

Both vegetation and saline soils can be used to distinguish between shallow (<4 m) and deep ground water, but saline soil distribution is a more dependable and widespread indicator in San Luis Valley.

Temperature differences seen on thermal-infrared imagery can be related to differences in thermal inertia, solar reflectance, evaporation rates, or subsurface temperature distribution. Increases in soil moisture cause an increase in thermal inertia and a decrease in reflectance, theoretically causing decreased daytime temperatures and increased nighttime temperatures. An increase in evaporative cooling rates with increasing soil moisture partly counteract this effect, however, causing decreased daytime and nighttime temperatures. Temperature effects due to varying ground water depth, while transferred in a damped state to the surface, are completely overshadowed by effects due to varying evaporative cooling rates. Both evaporative cooling and temperature effects due to varying ground water depth affect the diurnal temperature curve in the same manner and are indistinguishable.

# TABLE OF CONTENTS

## ILLUSTRATIONS

## TABLES

# INTRODUCTION

## PURPOSE AND SCOPE

The purpose of this research was twofold; (1) to determine the sources and quantities of ground water recharge to the aquifers of the northern closed basin of San Luis Valley, and (2) to evaluate the application of remote sensing techniques to regional hydrogeologic studies.

The specific objectives were:

1) To map hydrogeologically significant rock units and structures in the Precambrian and Paleozoic rocks of the Sangre de Cristo Mountains and Tertiary volcanic rocks of the San Juan Mountains, and determine their influence on recharge into the aquifers of the San Luis Valley.
2) To map the Cenozoic alluvial and volcanic deposits, as well as their geometry, and determine the influence of these features on ground water recharge and flow in San Luis Valley.
3) To define the water table of the unconfined aquifer and the direction and magnitude of ground water flow.
4) To determine the chemical quality of recharging surface and ground water near the zone of recharge, and

to evaluate the relation between hydrochemical facies and ground water flow directions.

5) To evaluate photographic and thermal-infrared remote sensors in terms of their use as sources of basic data in regional ground water studies.

## GEOGRAPHIC AREA

The northern San Luis Basin, which includes the northern closed basin of San Luis Valley and contributing watersheds of the Sangre de Cristo and San Juan mountains, is a high mountain basin encompassing approximately 7800 square kilometers (3000 sq. mi) of south-central Colorado (Fig. 1). The basin is located 210 km (130 mi) south-west of Denver, along the Rio Grande Rift Zone, a zone of Cenozoic normal faulting, volcanic activity, and high heat flow (Chapin, 1971). The basin is bounded on the east and west by the surface water divides of the Sangre de Cristo and San Juan mountains, respectively, on the north by Poncha Pass, and on the south by a shallow ground and surface water divide north of the Rio Grande River (Fig. 2).

The basin can be divided into three distinct, but hydraulically connected regions (Fig. 2); the Sangre de Cristo Mountains, the San Juan Mountains, and the San Luis Valley. All surface and ground water within the basin drains toward the sump area of San Luis Valley, characterized by surface and

REPRODUCIBILITY OF THE ORIGINAL PAGE IS POOR

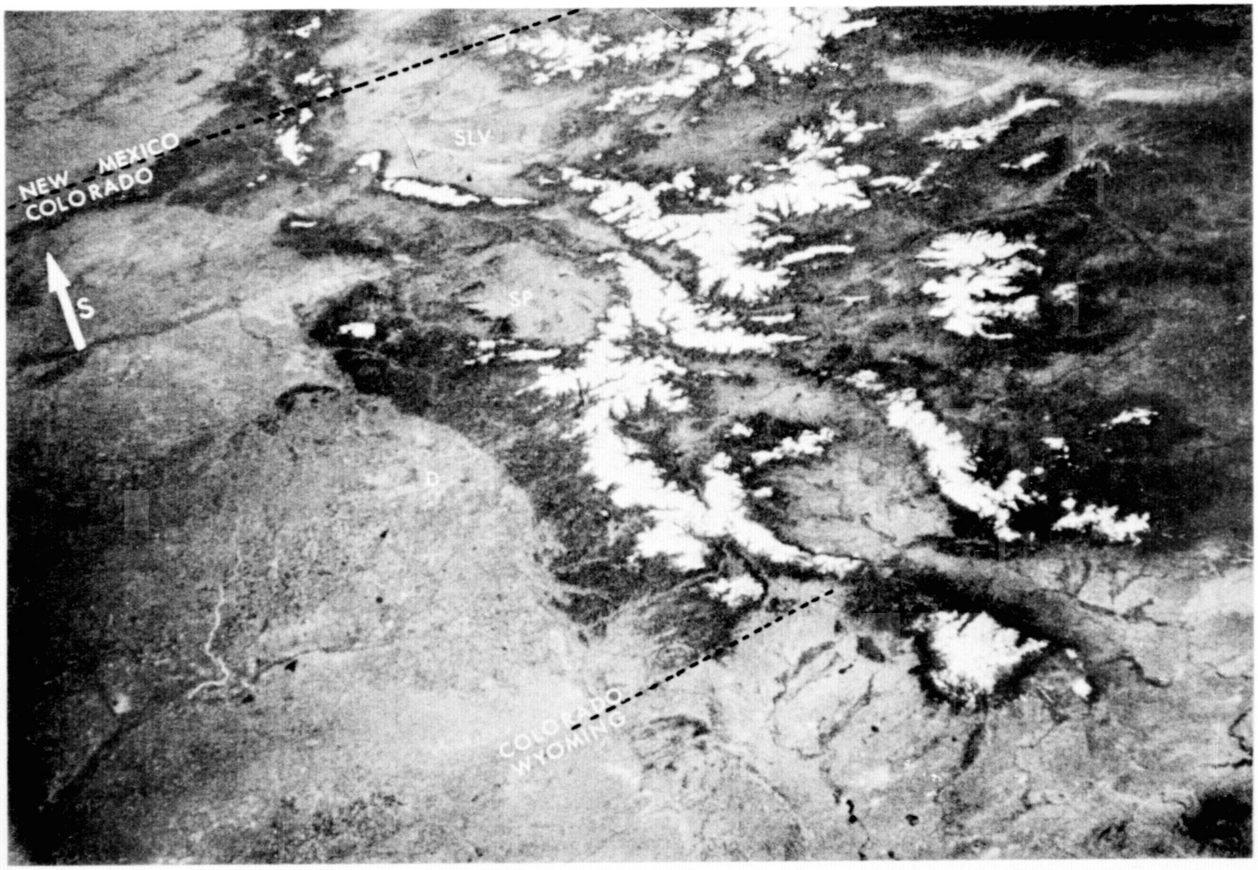




Figure 1: Skylab oblique photograph, showing location of San Luis Valley (SLV) in relation to South Park (SP) and Denver (D).

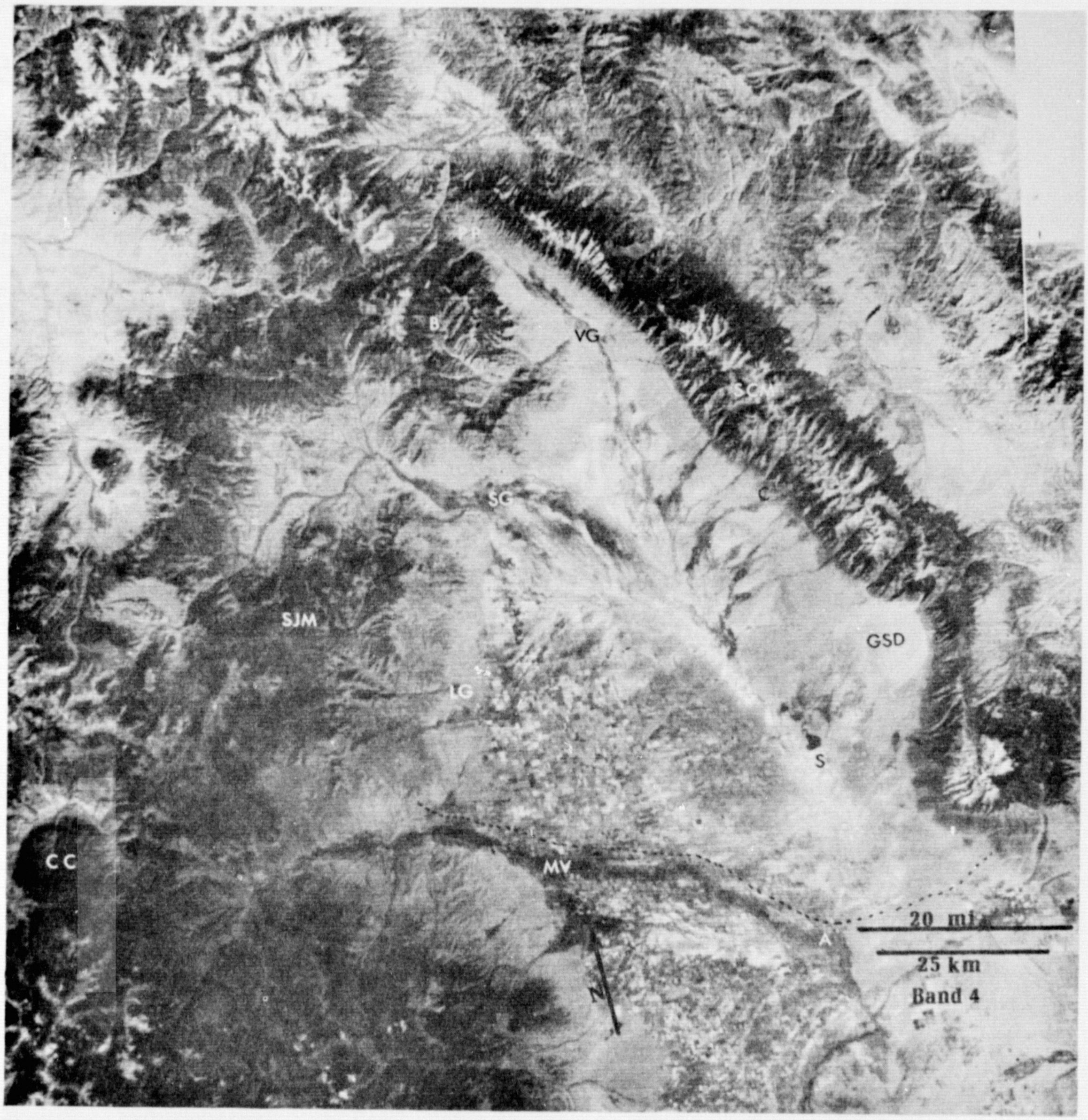


Figure 2: LANDSAT mosaic, showing the major geographic features within the San Luis Basin; Poncha Pass (PP), Bonanza Caldera (B), Villa Grove (VG), Saguache (SG), Crestone (C), La Garita (LG), Great Sand Dunes National Monument (GSD), the sump area (S) of the valley, Monte Vista (MV), Alamosa (A), Creede Caldera (CC), San Juan Mts (SJM), and Sangre de Cristo Mts (SCM). The dashed line north of Monte Vista and Alamosa is the approximate location of the southern ground water divide.

REPRODUCIBILITY OF THE ORIGINAL PAGE IS POOR

shallow ground water of high salinity and high rates of evapotranspiration. Elevations within the valley range from 2285 m (7500 ft) at the sump to 2590 m (8500 ft) at the northern extremity. Most of the valley is between 2285 m and 2440 m (8000 ft) in elevation. Sand dunes within Great Sand Dunes National Monument reach elevations of 2620 m (8600 ft), with a local relief of 244 m (800 ft).

The Sangre de Cristo Mountains (Fig. 3) rise from the floor of San Luis Valley at an elevation of 2440 m (8000 ft) to elevations of over 4267 m (14,000 ft) in less than 8 km (5 mi) and show abundant evidence of alpine glaciation. The San Juan Mountains (Fig. 4), in contrast, are dominated by relatively gentle rolling hills, often capped by resistant, flat-lying rocks. Peaks in this region of the San Juan Mountains seldom reach elevations of 3658 m (12,000 ft).

Topographically, climatically, and structurally, the San Luis Basin resembles more the Basin and Range Province of North America than the Colorado Rocky Mountains.

## VEGETATION

The distribution of vegetation within the basin is controlled by elevation, slope, available moisture, and the quality of available moisture. At the lower elevations, as in San Luis Valley and some parts of the San Juan Mountains, moisture dependence is a primary control. Common phreatophytes

REPRODUCIBILITY OF THE
ORIGINAL PAGE IS POOR

Figure 3: Western flank, Sangre de Cristo Mountains.

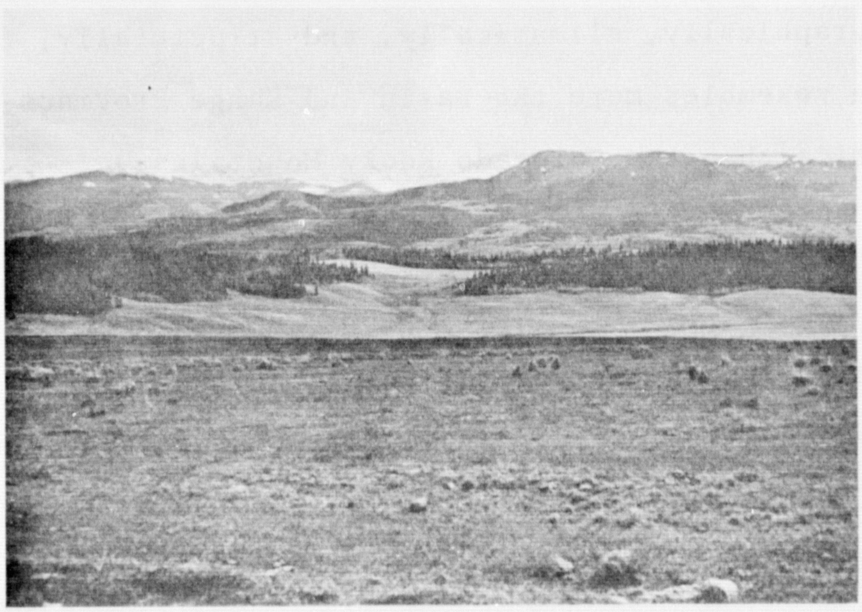

Figure 4: San Juan Mountains, looking west to the Continental Divide.

within this zone include rabbitbrush (*Chrysothamnus nauseosus*), greasewood (*Sarcobatus vermiculatus*), saltbush (*Atriplex canescens*), wiregrass (*Juncus balticus*), willow (*Salix* spp.), and narrowleaf cottonwood (*Populus angustifolia*). In addition, aspen (*Populus tremuloides*) appears to act as a phreatophyte near the border of San Luis Valley, often found in association with narrowleaf cottonwood trees. Common xerophytes found in the valley include sagebrush (*Artemisia tridenta*), and several grasses not identified by the author.

At higher elevations within the valley, antelope brush (*Purshia tridentata*), pinon pine (*Pinus edulis*), and one-seed juniper (*Juniperus monosperma*) become commom, particularly in dry areas with sandy soils. Rock spirea (*Holodiscus dumosus*), scrub oak (*Quercus gambelli*), and gooseberry (*Ribes inerme*) are found in moist areas in this zone.

At higher elevations, within the San Juan and Sangre de Cristo mountains, conifers are the dominant vegetation type, with the distribution of individual species controlled almost entirely by elevation. Conifers found in the mountainous regions of the basin, listed in order of increasing elevation, are ponderosa pine (*Pinus ponderosa*), Douglas fir (*Pseudotsuga menziesii*), Colorado blue spruce (*Picea pungens*), lodgepole pine (*Pinus contorta*), subalpine fir (*Abies lasciocarpa*), bristlecone pine (*Pinus aristata*), and the Engelmann Spruce (*Picea engelmannii*). Aspen trees are found from the edge of San Luis Valley up to timberline, but are generally restricted

to areas where there is sufficient moisture.

## HISTORY OF WATER USE

As early as 1852, farmers in San Luis Valley began irrigating fields with water from the San Juan Mountains (Anon., 1976). Accidental discovery of artesian water in 1887 (Carpenter, 1891) was followed by extensive development of the artesian aquifer. In 1891 there were an estimated 2000 flowing wells (Siebenthal, 1910), a number which grew to 3,234 by 1904 (Siebenthal, 1910), to approximately 5000 by 1916 (White, 1916), to 6,074 in 1936 (Robinson and Waite, 1938), and to an estimated 7000 flowing wells by 1971 (Emery and others, 1971). Development of the shallow aquifer of San Luis Valley has similarly undergone rapid acceleration. Emery and others (1971) report a large increase in the number of large capacity irrigation wells, to an estimated total of 2200 wells in 1971. This increased usage of ground water in San Luis Valley has resulted in a lowering of both the water table and the piezometric surface, and there is evidence that it has resulted in decreased flow in several of the rivers of San Luis Valley. Figure 5 shows both a plot of cumulative Conejos River discharge and cumulative withdrawal from the confined aquifer for the period 1937-1970. A change in slope of the cumulative discharge of the Conejos River occurs in the same time period as a sharp increase in the use of artesian water. Similar plots for other

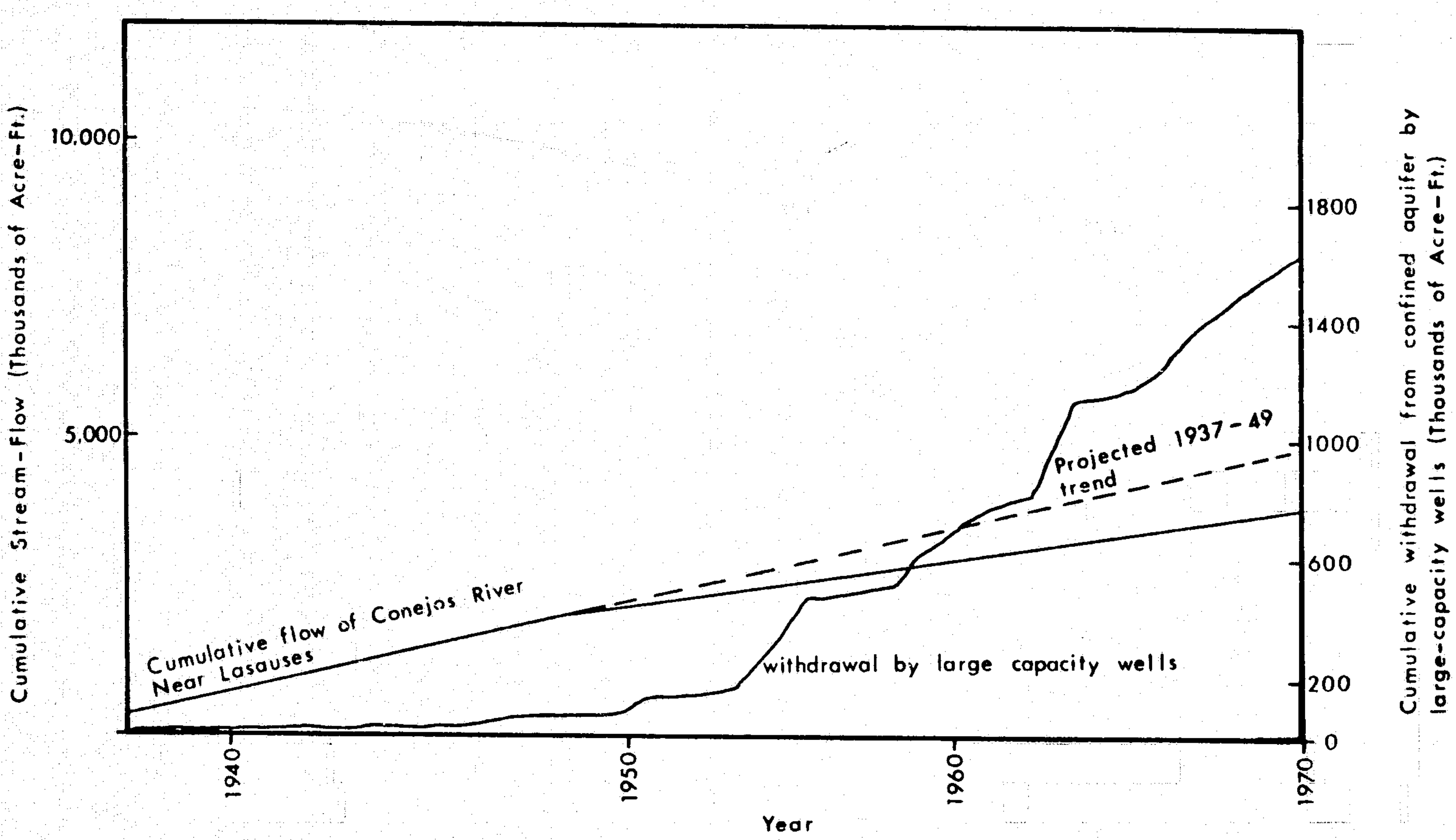


Figure 5: Cumulative river flow and confined aquifer withdrawal (from Emery and others, 1973)

rivers show similar results (J.M. Sinton, personal communication), indicating that increased withdrawal from the aquifers since 1950 has resulted in decreased river flow. This is a serious problem, as Colorado by 1967 had accrued a deficit of 1.16 $(10^9)$ $m^3$ (944,000 acre-feet) of water that was to be delivered to New Mexico by the 1938 Rio Grande Compact (Emery and others, 1971).

Two solutions have been suggested to increase the flow in the Rio Grande and Conejos rivers, the most obvious of which is curtailment of withdrawal from the confined aquifer. Because most of the small artesian wells are uncapped, much of the water discharged from the confined aquifer is wasted. Unfortunately, most of the wells are old, and many of these wells collapse when shut off.

The second method suggested to increase flow in the Rio Grande River is the closed basin drain project proposed by the Bureau of Reclamation in 1940 (Powell, 1958). This proposed project involves the construction of a drainage canal from the area of Russell Lakes, south of Saguache (Fig. 2, p. 4), southeast through the sump area, and south to the Rio Grande River near La Sauses. The purpose of the drain is to lower the water table approximately 3 m (10 ft), thereby decreasing non-beneficial evapotranspiration and discharging the salvaged water to the Rio Grande River (Colorado Water Conservation Board, 1959).

Before implementation, both alternatives need information

on sources of recharge to the aquifers and the degree of hydraulic connection between aquifers, as well as between the aquifers and the surface water. For example, if there is a high degree of hydraulic continuity between the confined and unconfined aquifers, shutting off wells in the confined aquifer may merely increase upward leakage from the confined to the unconfined aquifer, defeating the purpose of the plan.

Similarly, the development of shallow ground water and surface water along the margins of San Luis Valley, associated with the relatively new resort and retirement communities, may accelerate the decrease in piezometric levels throughout the valley. This is especially critical if these communities are located within the ground water recharge areas of the basin.

More recently, there has been active interest in, and exploration for, geothermal resources in San Luis Valley. Future development of geothermal resources in San Luis Valley may make heavy demands upon the water resources of the region and require an understanding of the basin hydrology.

## PREVIOUS WORK

### HYDROGEOLOGY

Previous studies related to the hydrogeology of the northern San Luis Basin can be grouped into two categories; 1) geologic studies of portions of the Sangre de Cristo and San Juan mountains, and 2) general hydrologic studies of San Luis Valley.

Regional geologic studies of the Sangre de Cristo and San Juan mountains have been done by Knepper (1974), Peel (1971), Bolyard (1956), Johnson (1969), Larsen and Cross (1956), and Steven and others (1974). Numerous detailed studies of both regions have been completed, chiefly in the form of theses from Colorado School of Mines, University of Colorado and University of Michigan. Among these is the work of Bruns (1971), Nolting (1970), and Wychgram (1972).

Three major hydrologic studies have been made of the San Luis Valley. Prompted by the rapid development of ground water resources, Siebenthal (1910) completed a study summarizing the geology and the occurrence of ground water in the valley. His ideas have remained largely unchallenged by subsequent work. Powell (1958) did extensive work, consisting of test drilling, description of the shallow valley stratigraphy, and pump tests in the sump area of San Luis Valley, to provide data for the closed basin drain project. His piezometric map of the valley is the first such published map, and is therefore of great benefit to those interested in the changes in the ground water regime since 1958.

The most extensive hydrologic study of San Luis Valley was one undertaken by the United States Geological Survey in 1968 (Emery and others, 1969, 1971, 1972, 1973, 1975). Early work consisted of inventorying water resources and the collection of basin hydrologic data (stream discharge measurements, well levels, water analyses). Later work involved the

description of the water quality of ground and surface water resources and the results of an electric analog study of the valley.

## REMOTE SENSING

Most of the work related to the mapping of hydrogeologic units is part of the general remote sensing literature in the areas of standard geologic mapping. Numerous authors have presented evaluations of aircraft and satellite photography and imagery for geologic applications. Locally, the Colorado School of Mines Remote Sensing Reports 71-1 to 75-7 (1971-1975) present evaluations of the various sensors in a wide variety of geologic environments in Colorado. Howe (1958) summarized techniques of interpreting aerial photography in ground water studies.

Most research relating soil moisture to photographic tone has concentrated on color photography. Kalensky (1968) discussed a technique to correlate photographic tone with soil moisture for individual soil types. Piech and Walker (1974) proposed a method for evaluating soil moisture using ratios of the red and blue spectral bands of a color image.

Idso and others (1975) summarized their research on the determination of soil moisture using daytime and nighttime thermal-infrared images. Patton (1909) determined the relation between soil moisture and thermal diffusivity for six

soil types, finding a rise of diffusivity to a peak, and then a decrease in diffusivity, for increasing soil moisture. Quiel (1975) reported the relationships between soil moisture and thermal conductivity and thermal inertia for some unconsolidated materials.

Robinson (1958) has presented the most complete description of the relation between phreatophyte type and ground water depth and quality. His research focused on vegetation in the arid to semi-arid regions of the western United States and therefore includes many of the vegetation types found in San Luis Valley.

Cartwright (1968a, 1968b, 1970, 1971, 1974) developed the theory for steady-state heat flow between an aquifer and the ground surface. He used this theory as a tool in field exploration for aquifers, successfully detecting aquifers to depths of 30 meters. His work indicates that temperature anomalies depend upon aquifer depth, thickness, and transmissivity. Parsons (1970) studied the lateral change of ground water temperature by digitally solving the equation for simultaneous fluid flow and heat conduction. Myers and Moore (1972) and Chase (1969) claim detection of shallow aquifers using thermal infrared imagery. Watson and others (1971), Watson (1975), and Kahle and others (1975) discussed computer modeling of diurnal temperature changes of materials with varying thermal inertia and under varying meteorologic conditions.

## ACKNOWLEDGEMENTS

This research was supported by the Bonanza Remote Sensing Project at the Colorado School of Mines under NASA Grant NGL 06-001-015. Special thanks are due to the principal investigator of the project and thesis advisor, Dr. Keenan Lee, for his help, encouragement, and critical questioning during the course of this study.

The suggestions from the thesis committee, consisting of Professors W.R. Astle, J.A. Danielson, A.J. Kidnay, K. Lee, and D.T. Snow, greatly aided me during the duration of the research, often pointing me in a different direction when work seemed stymied.

This work has also been aided by the work of several people, including Dr. Karl Newman for his analysis of pollen samples from the AMOCO geothermal test well, and Mr. Duane Moredock, for releasing information to me about the AMOCO test well. This research could not have been completed without the cooperation of the many residents of San Luis Valley, particularly Mr. D.H. MacFadden, of the Colorado State Engineer's Office in Alamosa.

Most of all, thanks must be given to Ms. Kitty Huntley for her help as field assistant, laboratory assistant, draftsperson, typist, and psychologist, without whom this work would never have been completed.

# HYDROGEOLOGY

## WATER BUDGET

### PRECIPITATION

The northern San Luis Basin contains only four stations that either record, or have in the past recorded, precipitation data. Weather stations with limited instrumentation are located at Great Sand Dunes National Monument and at the towns of Saguache and Del Norte. A complete meteorologic station operates at the city of Alamosa. Because these stations are located within the valley, estimates of mountain precipitation must be based on the correlation between observed precipitation and physiographic features. The strong orographic effect on storms in the region produces this necessary correlation (Fig. 6).

Precipitation within the basin falls largely as either winter snow or summer thunder showers. Approximately 65% of the precipitation in the Sangre de Cristo and San Juan mountains falls as snow in the October to April period, varying from 2.52 in/yr (64.0 mm/yr) in Alamosa to over 25 in/yr (635 mm/yr) in parts of the surrounding mountains. Precipitation in the May to September period is largely in the form of

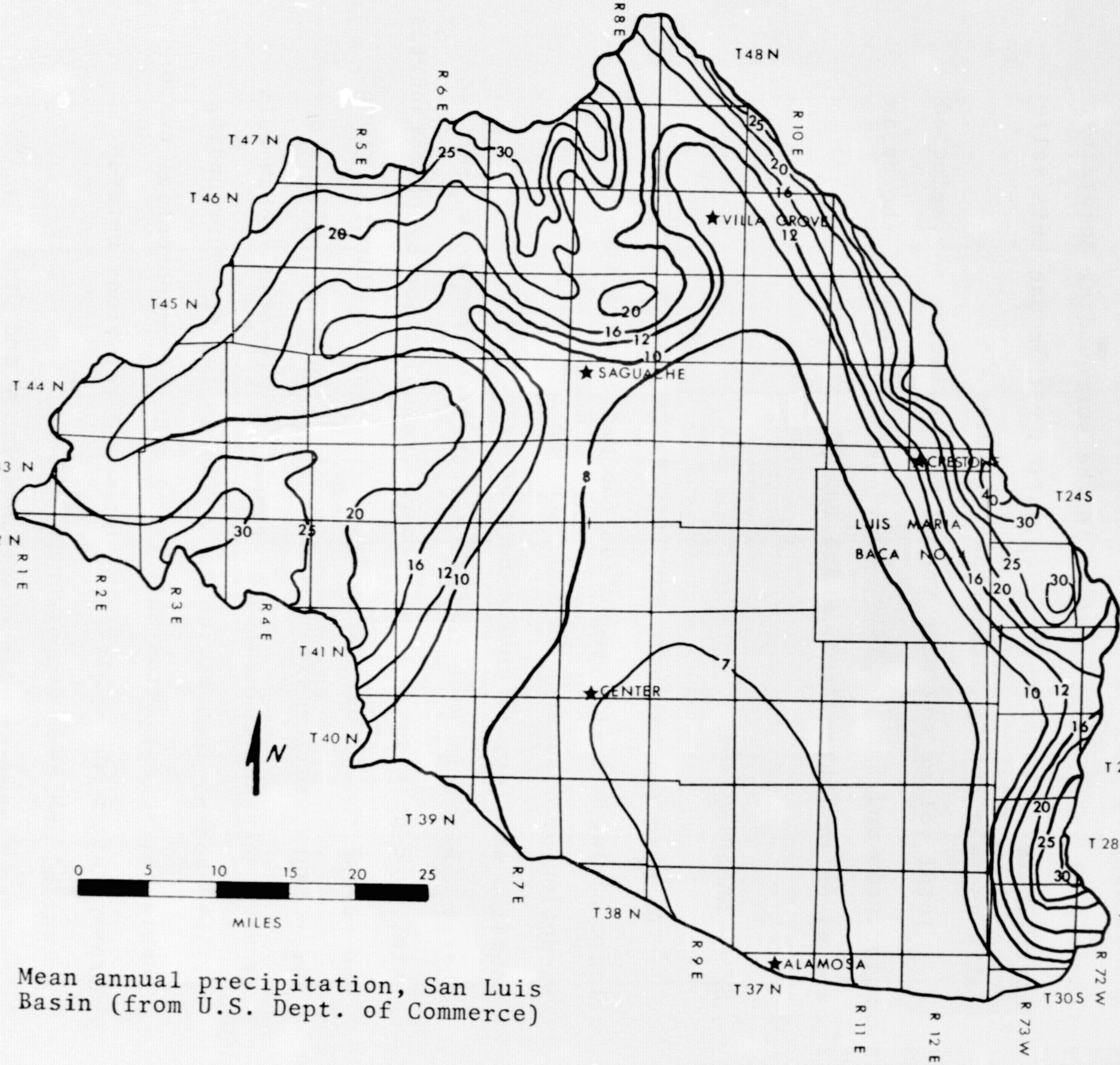


Figure 6: Mean annual precipitation, San Luis Basin (from U.S. Dept. of Commerce)

thunderstorms, varying from 4.04 in/yr (102.6 mm/yr) in Alamosa to over 14 in/yr (355.6 mm/yr) in the surrounding mointains. Approximately 60% of the precipitation within San Luis Valley falls as rain during summer thunderstorms.

Total volume and mean annual precipitation for selected watersheds and for the three hydrologic regions of the basin are given in Tables 2, 3, and 4 (p. 30-32).

## EVAPOTRANSPIRATION

Because the northern San Luis Basin is a closed hydrologic basin, all discharge from the basin, with the minor exception of discharge to southern San Luis Valley in the confined aquifer, is in the form of evapotranspirative discharge. Water is lost through evaporation from snow, surface water, and bare soils and through transpiration by phreatophytes and xerophytes. Loss varies as a function of climate, ground water depth, soil moisture, and vegetation type. Little data is available on real rates of evapotranspiration in San Luis Valley, and no information is available for the surrounding mountains, so estimates must be made based on potential evapotranspiration and empirically observed relations between potential and real evapotranspiration.

The Blaney-Criddle equation (Blaney and Criddle, 1962) is a commonly used empirical formula relating potential evapotranspiration rates to mean monthly air temperature and monthly

percentage of annual daytime hours, by the expression;

$$ET_p = \frac{TP}{100}$$

where $ET_p$ = Potential monthly evapotranspiration in inches.

T = Mean monthly air temperature in degrees fahrenheit.

P = Monthly percentage of annual daytime hours (listed by latitude in Blaney and Criddle, 1962).

This expression requires only mean monthly temperature as input, data which are available for the Alamosa weather station for a sufficient period of time (Table 1).

Table 1: Potential Evapotranspiration computed by the Blaney-Criddle Equation

| Month | Mean Monthly Temperature (°F) | Potential Evapotranspiration (inches) |
|---|---|---|
| January | 17.4 | 0 |
| February | 23.5 | 0 |
| March | 32.1 | 2.7 |
| April | 41.8 | 3.7 |
| May | 50.8 | 5.0 |
| June | 60.0 | 5.9 |
| July | 64.9 | 6.5 |
| August | 63.0 | 6.0 |
| September | 55.7 | 4.7 |
| October | 44.4 | 3.5 |
| November | 29.5 | 0 |
| December | 19.2 | 0 |
| Total | | 38.0 (96.5 cm) |

A second method of estimating potential evapotranspiration is the use of lake evaporation rates presented by Kohler and others (1959). Evaporation for the San Luis Valley varies

between 96.5 cm/yr (38 in/yr) and 106.7 cm/yr (42 in/yr).

For the 1961-1967 period, Emery and others (1971) measured an average class A pan evaporation rate of 132.7 cm/yr (52.25 in/yr) in San Luis Valley. Applying a pan coefficient of 0.69, given by Kohler and others (1959) for San Luis Valley, a third independent estimate, of 91.5 cm/yr (36.0 in/yr), is arrived at for potential evapotranspiration in San Luis Valley. The relative consistancy of values determined by the three methods tends to indicate that potential evapotranspiration in the basin is approximately 94.8 cm/yr (37.3 in/yr), the average of the three values, and it is this value that is used in future computations.

Estimating potential evapotranspiration for the mountains surrounding San Luis Valley is more difficult, as little information is available on air temperature or evaporation from either lakes or evaporation pans. Kohler and others (1959) indicate that lake evaporation in the mountains averages 10.16 cm/yr (4 in/yr) less than in San Luis Valley. Using this figure, an estimate of potential evapotranspiration during the May to September period is 84.14 cm/yr (33.1 in/yr) for the Sangre de Cristo and San Juan mountains. Real evapotranspiration in the mountains is the sum of evapotranspiration during the May to September period and evaporation from snow during the October to April period. Measurements of snow evaporation described in the literature are relatively consistant. Croft (1944) obtained a value of 5.87 cm (2.31 in) for

a 210 day snow period at a station on the Wasatch Plateau, Utah, at an elevation of 2682 m (8800 ft). Wilm and Dunford (1948) similarly obtained a value of 5.92 cm (2.33 in) for the period of snow cover at the Fraser Experimental Forest in Colorado. Halverson (1972) obtained a value of 6.35 cm (2.5 in) for a 6 month snow cover period in the Sierra Nevada Mountains of California at an elevation of 2103 m (6900 ft). A value of 6.1 cm (2.4 in) will be used in this study as a representative value for evaporation from snow.

Real evapotranspirative rates are a function of potential evapotranspiration, vegetation type, ground water depth, and soil moisture. In the forested watersheds surrounding San Luis Valley, there is insufficient information on most of these variables, and no work has been done to establish a quantitative relationship between the variables. Instead, empirical relations observed elsewhere in Colorado must be used to estimate forest evapotranspiration. Betters (1975) analyzed previous observations of forested areas in Colorado and arrived at the expression;

$$E_a = 0.28E_p$$

where $E_a$ = Actual evapotranspiration.

$E_p$ = Real evapotranspiration.

As potential evapotranspiration takes climatic variation into account, the constant term in the above expression takes into account average timber thicknesses, average ground water depths,

and average soil moistures. Using this expression for watersheds that varied in elevation from 2987 m (9800 ft) to 3475 m (11,400 ft), Betters (1975) simulated forest runoff with errors on the order of 10%. Applying this expression to the potential evapotranspiration computed for forested areas above, a value of 23.56 cm (9.27 in) is arrived at for summer evapotranspiration. The average sum of summer evapotranspiration and winter evaporation from snow in the Sangre de Cristo and San Juan mountains is therefore on the order of 29.66 cm/yr (11.68 in/yr).

Considerably more information is available in San Luis Valley that can be used to more accurately estimate real evapotranspiration. Evapotranspiration in agriculturally developed areas can be estimated using potential evapotranspiration and consumptive use coefficients determined by Blaney and Criddle (1962) for various crop types. Crops grown in San Luis Valley are barley, oats, potatoes, and a minor amount of other vegetables. Blaney and Criddle give coefficients that vary between 0.76 for potatoes and 0.78 for grain, with a coefficient of 0.91 given for grass and pastureland. Using the potential evapotranspiration of 96.5 cm/yr (38.0 in/yr), and a coefficient of 0.91 for irrigated pastureland and 0.77 for cropland, evapotranspirations of 87.8 cm/yr (34.6 in/yr) and 74.3 cm/yr (29.3 in/yr), respectively, are obtained for the areas of pertinent land use (Fig. 7).

In unirrigated rangeland, ground water depth is the major factor controlling evapotranspiration in San Luis Valley.

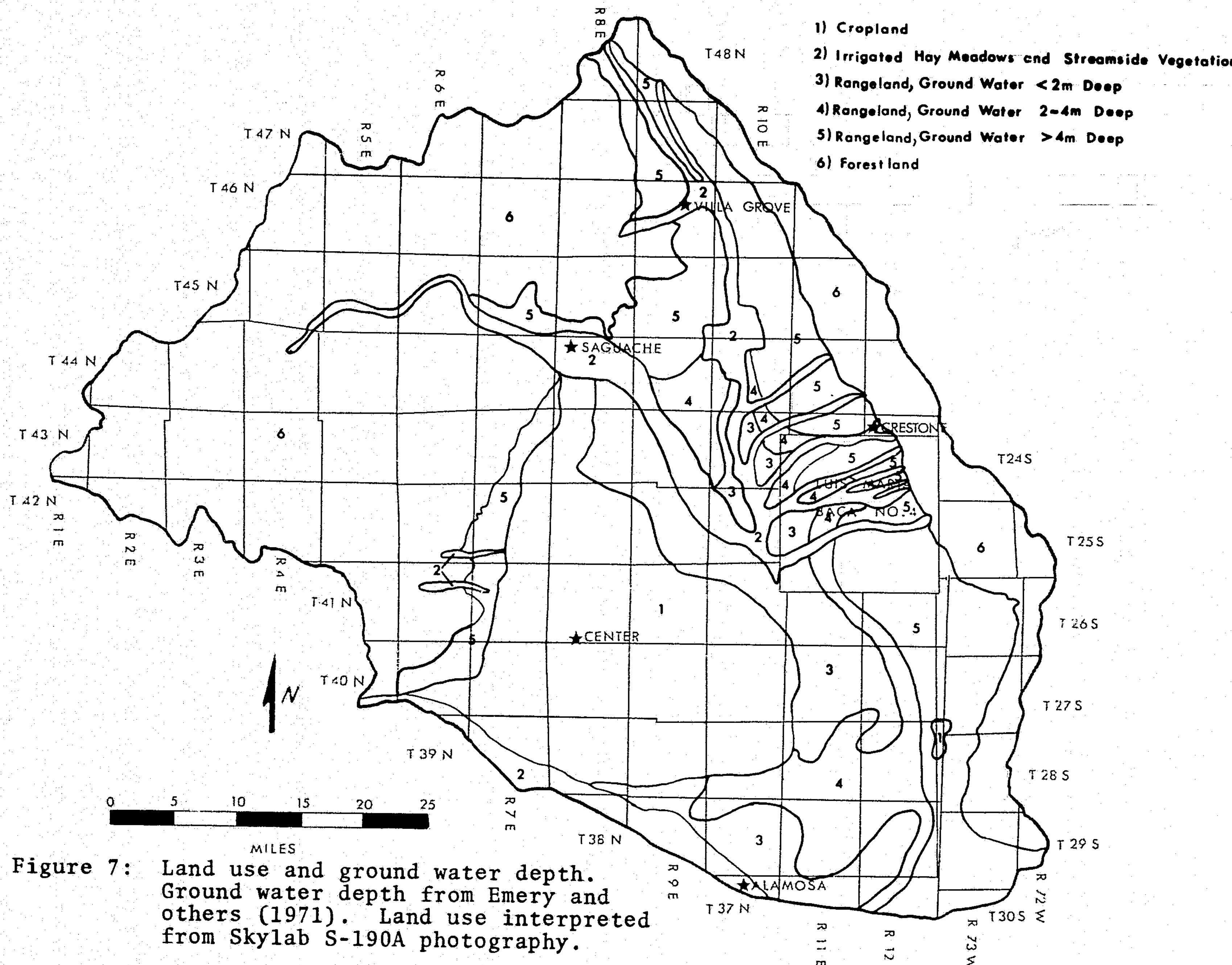


Figure 7: Land use and ground water depth. Ground water depth from Emery and others (1971). Land use interpreted from Skylab S-190A photography.

Emery and others (1971) present a graph relating ground water depth to evapotranspirative rates, using a value of 132.7 cm/yr (52.25 in/yr) for the maximum evapotranspiration (potential evapotranspiration). A modification of this graph (Fig. 8), using the potential rate of 94.8 cm/yr (37.3 in/yr) determined above (p. 20), agrees well with Powell's (1958) determination of evapotranspiration. This relation was used to determine evapotranspiration rates for non-irrigated land with the ground water depths shown in Figure 7.

Evapotranspiration for selected watersheds and the three hydrologic regions are listed in Tables 2, 3, and 4 (p. 30-32).

## SURFACE WATER FLOW

While there is no natural surface inflow or outflow from the San Luis Basin, water importation for irrigation is a source of surface water inflow to the basin. The Sangre de Cristo and San Juan mountain hydrologic regions have no surface water inflow, but a significant part of the outflow from these regions is surface water inflow to the San Luis Valley.

The only streams that discharge from the San Juan Mountains into San Luis Valley are Kerber Creek, Saguache Creek, Carnero Creek, and La Garita Creek. All four creeks have stream gaging stations established at points upstream of significant irrigation diversion or seepage loss to valley-fill sediments. Records have been kept of discharge for 38 years at Kerber Creek, 60 years at Saguache Creek, 30 years at Carnero Creek,

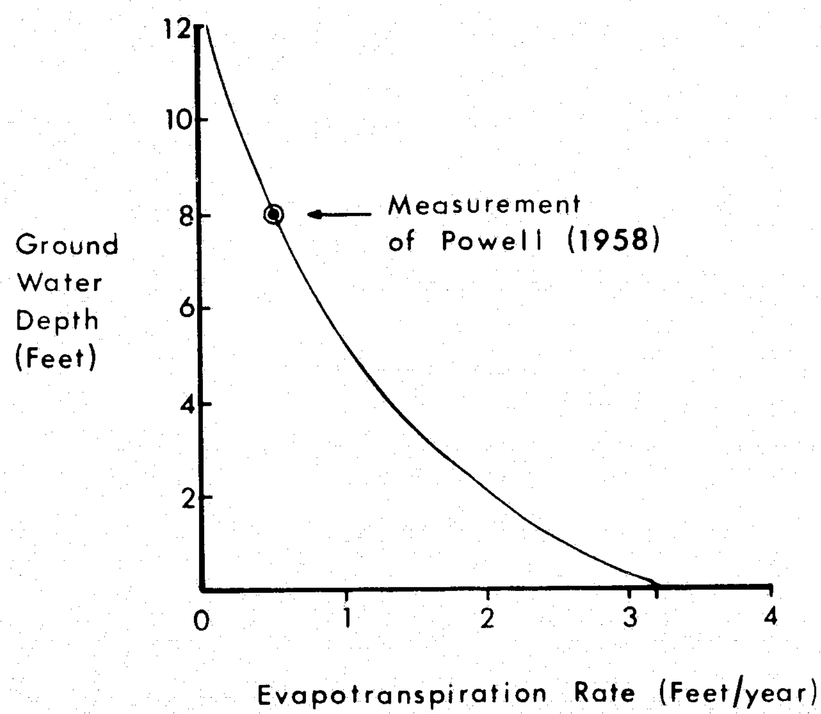


**Figure 8:** Relation between ground water depth and evapotranspiration rates in San Luis Valley. Values given are for average vegetation densities and vegetation commonly found associated with the given ground water depth. Modified from Emery and others (1971).

and 29 years at La Garita Creek. Mean annual discharge for these creeks is presented in Table 3 (p. 31).

Of the many streams that discharge from the Sangre de Cristo Mountains to San Luis Valley, long-term gaging records are available only for North Crestone Creek, which has been recorded for 29 years. Ten other stations have recorded stream discharge intermittently. To determine an average value for surface water discharge from the Sangre de Cristo Mountains, discharge of North Crestone Creek was plotted against that of the eight other creeks which are gaged upstream of any seepage loss, for the recording periods of the smaller creeks (Fig. 9). These plots were then used to estimate surface water discharge for all streams that were gaged in the Sangre de Cristo Mountains (Table 2, p. 30) and to obtain an average value of surface water discharge for the entire region for the recording period of North Crestone Creek. This can be done only because of the relative hydrogeologic uniformity of the watersheds in the Sangre de Cristo Mountains (Plate 1), and because all gaging stations used are located upstream of any seepage loss to the sediments of San Luis Valley.

An important source of surface water inflow to the closed basin of San Luis Valley is that of irrigation canals. Approximately 50% of the flow of the Rio Grande River at Del Norte is diverted to the closed basin in the Rio Grande and Farmers Union canal. As part of Powell's (1958) study of San Luis Valley, P.B. Mutz of the Bureau of Reclamation completed

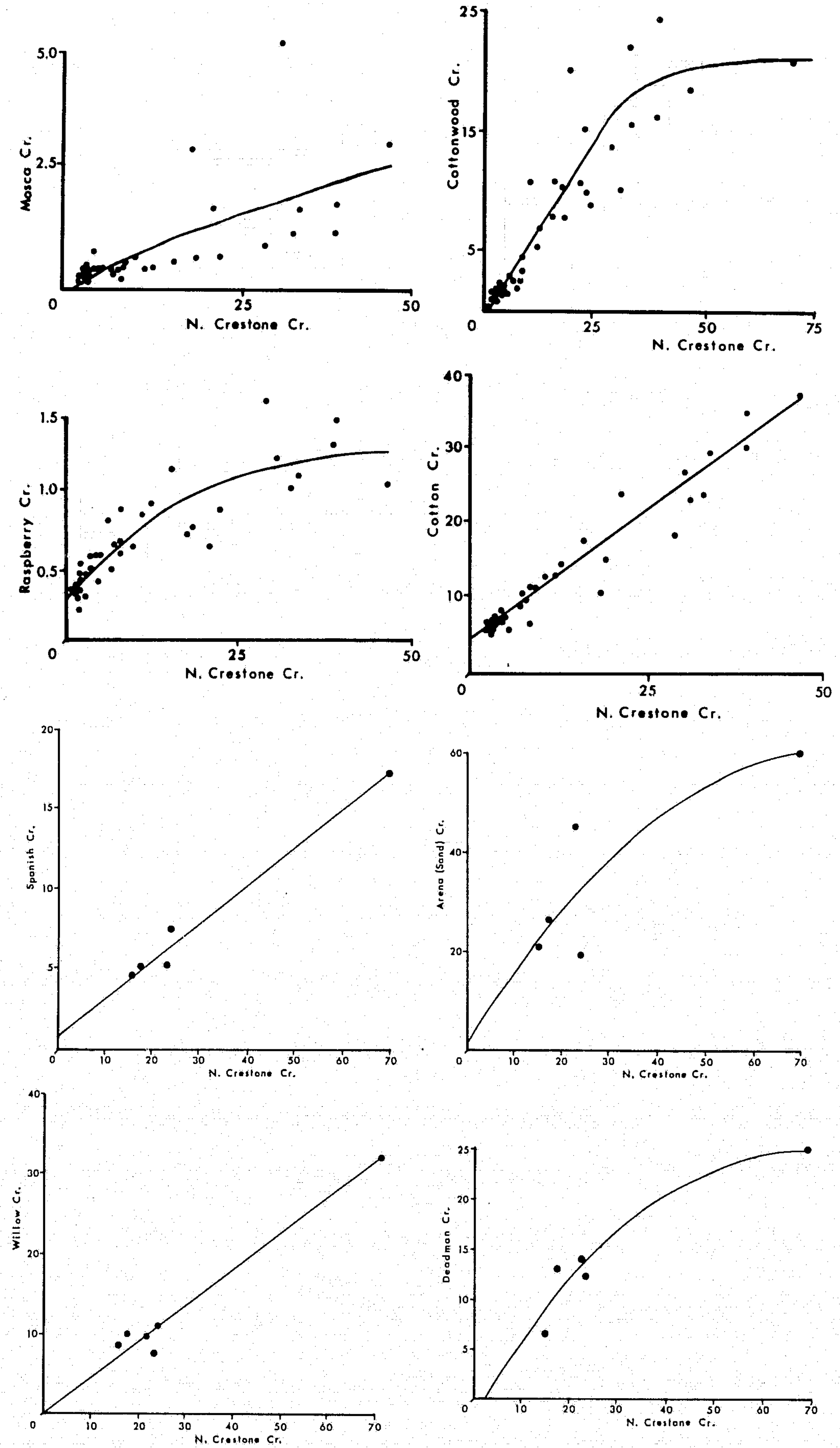


Figure 9: Stream discharge relations, Sangre de Cristo Mountains. All discharges in cubic feet per second.

an inflow-outflow study for the 1949-1952 period. Surface water inflow for that study included La Garita Creek and all irrigation canals at the point they crossed the southern ground water divide. During this period, total inflow, minus inflow from La Garita Creek, averaged 3.28 $(10^8)$ $m^3$ $(2.65(10^5)$ acre-ft).

GROUND WATER FLOW

A lack of information on transmissivity and hydraulic gradients in either the San Juan or Sangre de Cristo mountains eliminates any possibility of directly computing ground water flow from the mountain regions to San Luis Valley. Estimates of these terms from the water balance are given in Tables 2, 3, and 4 (p. 30-32). The ground water divides in the Sangre de Cristo and San Juan mountains coincide nearly everywhere with the surface water divides, and computer-generated, steady-state flow nets (Plate 5) of the mountain provinces indicate that the ground water divides act as ground water barriers throughout the geologic section.

Similarly, the southern ground water divide, where it is well-defined (Plate 6), acts as an effective barrier to ground water movement in the unconfined aquifer. Where the divide is not well-defined, the gradient is so low (on the order of 0.0006) that, using the estimate of transmissivity of Emery and others (1973), a relatively insignificant quantity of ground water inflow from the unconfined aquifer is computed (on the order of $10^5$ $m^3/yr$).

In the confined aquifer, there is no effective barrier to movement at the southern ground water divide, but gradients (Fig. 57, p. 145) are still relatively low (0.0002 to 0.0008). Again using the estimate of transmissivity of Emery and others (1973), one arrives at an estimate of ground water inflow from the confined aquifer south of the closed basin on the order of $1.0(10^7)$ $m^3$/yr.

## WATER BALANCE

Use of a water balance to examine the different components of basin inflow and outflow is based on the balance equation;

$$\Sigma O = \Sigma I + \Delta S$$

where $\Sigma O$ = Sum of all components of outflow.

$\Sigma I$ = Sum of all components of inflow.

$\Delta S$ = Change in storage.

In the San Luis Basin, average yearly change in storage is less than the accuracy of measurement (Emery and others, 1973) and can safely be ignored. The equality of inflow and outflow can be used to compute components of the water balance that cannot be computed directly. It should be noted that errors in the individual components of the balance compound themselves in the term computed using the equality of inflow and outflow.

In the water balances presented in Tables 2, 3, and 4 for

Table 2: Water balance, Sangre do Cristo Mountains. Precipitation data from U.S. Dept. of Commerce. Other data computed by this author using methods and values presented in this report.

INFLOW

PRECIPITATION

| Watershed | Area ($m^2$) | Period | Average Rate (m/yr) | Total ($10^6 m^3$/yr) | Proportion of Yearly Precip. (%) |
|---|---|---|---|---|---|
| Arena (Sand) | 6.1($10^7$) | May-Sept. | 0.31 | 18.74 | 42 |
| | | Oct.-Apr. | 0.43 | 25.95 | 58 |
| Cotton | 3.5($10^7$) | May-Sept. | 0.28 | 9.8 | 37 |
| | | Oct.-Apr. | 0.47 | 16.3 | 63 |
| Cottonwood | 1.7($10^7$) | May-Sept. | 0.28 | 4.77 | 37 |
| | | Oct.-Apr. | 0.47 | 8.06 | 63 |
| Deadman | 2.5($10^7$) | May-Sept. | 0.25 | 6.15 | 37 |
| | | Oct.-Apr. | 0.41 | 10.34 | 63 |
| Mosca | 9.5($10^6$) | May-Sept. | 0.21 | 1.95 | 51 |
| | | Oct. Apr. | 0.19 | 1.84 | 49 |
| N. Crestone | 2.8($10^7$) | May-Sept. | 0.29 | 8.0 | 38 |
| | | Oct. Apr. | 0.46 | 12.9 | 62 |
| N. Spanish | 8.3($10^6$) | May-Sept. | 0.26 | 2.13 | 36 |
| | | Oct.-Apr. | 0.46 | 3.79 | 64 |
| N. Zapata | 1.2($10^7$) | May-Sept. | 0.25 | 3.00 | 40 |
| | | Oct.-Apr. | 0.37 | 4.4 | 60 |
| Raspberry | 4.6($10^6$) | May-Sept. | 0.21 | 0.98 | 40 |
| | | Oct.-Apr. | 0.31 | 1.44 | 60 |
| S. Crestone | 1.2($10^7$) | May-Sept. | 0.23 | 2.77 | 37 |
| | | Oct.-Apr. | 0.39 | 4.65 | 63 |
| Willow | 1.6($10^7$) | May-Sept. | 0.29 | 4.65 | 38 |
| | | Oct.-Apr. | 0.47 | 7.55 | 62 |
| Sangre de Cristo Mts. | 8.54($10^8$) | May-Sept. | 0.26 | 222.0 | 39 |
| | | Oct.-Apr. | 0.40 | 344.0 | 61 |

GROUND WATER

NONE

OUTFLOW

| Stream | Stream Discharge ($10^6 m^3$/yr) | Evapotranspiration ($10^6 m^3$/yr) | Ground Water Flow ($10^6 m^3$/yr, Computed) |
|---|---|---|---|
| Arena | 11.6 | 18.1 | 15.0 |
| Cotton | 11.9 | 10.4 | 3.8 |
| Cottonwood | 5.3 | 5.0 | 2.0 |
| Deadman | 5.1 | 7.4 | 4.2 |
| Mosca | 0.7 | 2.8 | 0.5 |
| N. Crestone | 11.6 | 8.3 | 1.0 |
| N. Spanish | 2.9 | 2.5 | 0.5 |
| Raspberry | 0.6 | 1.4 | 0.4 |
| Willow | 5.6 | 4.7 | 1.9 |
| Total for Sangre de Cristo Mts. | 233.1 | 253.3 | 79.6 |
| % of total outflow | 41.2 | 44.7 | 14.1 |

Table 3: Water balance, San Juan Mountains. Precipitation data from U.S. Dept. of Commerce. Other data computed by this author using methods and values presented in this report.

## INFLOW

### PRECIPITATION

| Watershed | Area ($m^2$) | Period | Average Rate (m/yr) | Total ($10^6 m^3/yr$) | Proportion of Yearly Precip. (%) |
|---|---|---|---|---|---|
| Carnero | $3.03(10^8)$ | May-Sept. | 0.25 | 74.4 | 37 |
| | | Oct.-Apr. | 0.42 | 128.0 | 63 |
| Kerber | $9.84(10^7)$ | May-Sept. | 0.25 | 24.4 | 37 |
| | | Oct.-Apr. | 0.41 | 40.6 | 63 |
| La Garita | $1.58(10^8)$ | May-Sept. | 0.26 | 41.9 | 44 |
| | | Oct.-Apr. | 0.34 | 53.8 | 56 |
| Saguache | $1.54(10^9)$ | May-Sept. | 0.27 | 423.0 | 48 |
| | | Oct.-Apr. | 0.29 | 451.0 | 52 |
| Other | $9.70(10^8)$ | May-Sept. | 0.14 | 137.0 | 38 |
| | | Oct.-Apr. | 0.23 | 219.0 | 62 |
| Total | $3.07(10^9)$ | May-Sept | 0.23 | 700.0 | 44 |
| | | Oct.-Apr. | 0.29 | 892.0 | 56 |

### GROUND WATER

NONE

## OUTFLOW

| Watershed | Stream Discharge ($10^6 m^3/yr$) | Evapotranspiration ($10^6 m^3/yr$) | Ground Water Flow ($10^6 m^3/yr$) (computed) |
|---|---|---|---|
| Carnero | 9.7 | 89.9 | 102.8 |
| Kerber | 12.0 | 29.2 | 23.8 |
| La Garita | 10.8 | 46.9 | 38.0 |
| Saguache | 52.4 | 456.8 | 364.8 |
| Other | 0.0 | 287.7 | 68.3 |
| Total | 84.9 | 910.5 | 597.7 |
| % of total outflow | 5.3 | 57.2 | 37.5 |

Table 4: Water balance, San Luis Valley. Precipitation data from U.S. Dept. of Commerce. Other data from this author using methods and values presented in this report.

INFLOW

| Source | Flow ($10^8 m^3/yr$) | Proportion of total inflow (%) |
|---|---|---|
| Precipitation | 9.44 | 41.4 |
| Streamflow from Sangre de Cristo Mts. | 2.33 | 10.2 |
| Streamflow from San Juan Mts. | 0.85 | 3.7 |
| Inflow from irrigation canals | 3.28 | 14.4 |
| Ground water inflow from Sangre de Cristo Mts. | 0.80 | 3.5 |
| Ground water inflow from San Juan Mts. | 5.98 | 26.3 |
| Ground water inflow under southern ground water divide | 0.10 | 0.5 |
| Total | 22.78 | 100.0 |

OUTFLOW

| Source | Discharge ($10^8 m^3/yr$) | Proportion of total outflow (%) |
|---|---|---|
| Evapotranspiration: | | |
| from irrigated cropland | 12.8 | 56 |
| from irrigated pastureland and natural streamside vegetation | 4.8 | 21 |
| from undeveloped land with ground water 0-2 m from surface | 2.8 | 12 |
| from undeveloped land with ground water 2-4 m from surface | 1.5 | 7 |
| from undeveloped land with ground water >4 m from surface | 0.9 | 4 |
| Surface water | 0 | 0 |
| Ground water | 0 | 0 |
| Total | 22.8 | 100.0 |

the Sangre de Cristo and San Juan mountains and San Luis Valley, it can be seen that the three provinces are quite different with respect to the relative importance of the components of inflow and outflow. In both the Sangre de Cristo and San Juan mountains all inflow is from precipitation, most of which falls in the October-April period. Similarly, evapotranspiration accounts for roughly half of the outflow from the two mountain regions. The relative proportions of surface and ground water outflow is quite different in the two mountain provinces. In the Sangre de Cristo Mountains (Table 2), composed of fractured hydrologic basement rock, 41% of outflow is surface water outflow and only 14% is ground water outflow. In the San Juan Mountains (Table 3), consisting of volcanic rocks, ground water flow is more important, 37% of outflow, and stream flow accounts for only 5% of outflow, suggesting that the rock permeabilities of the two regions are markedly different.

San Luis Valley (Table 4) is the region of discharge for the northern San Luis Basin, with all recharging waters being discharged by evapotranspiration. Despite the low precipitation in the valley, it accounts for 41% of the inflow, with ground water inflow from the San Juan Mountains the next most important item. Because there is no potential gradient across the central surface drainage of the valley in either the unconfined (Plate 6) or the confined (Fig. 57, p. 145) aquifer, this central drainage acts as an effective barrier to east-west

movement across San Luis Valley. This means that inflow to San Luis Valley can be viewed as recharging two distinct areas, one east and one west of San Luis Creek. All inflow east of San Luis Creek is either in the form of precipitation (55%), or from the Sangre de Cristo Mountains as ground water flow (11%), or surface water flow (34%). Inflow west of San Luis Creek is composed of precipitation (36%), stream flow (5%), imported irrigation water (21%), and ground water (38%).

These components of inflow to San Luis Valley all represent potential sources of recharge to the aquifers. Whether or not the components actually recharge the aquifers is determined by their spacial relations to the flow systems of the valley and by the soil moisture balance. All ground water inflow from the Sangre de Cristo Mountains either discharges as springs at the base of the mountains or reaches the aquifers of San Luis Valley within the zone of recharge. Most of this inflow is a source of direct recharge to the valley aquifers. Seepage measurements (Appendix A) along streams originating in the Sangre de Cristo Mountains show that these streams nearly always disappear by seeping into the permeable alluvial fan sediments within the zone of ground water recharge, thereby contributing to recharge of the aquifers. The proportion of precipitation in San Luis Valley that reaches the aquifers depends upon the permeability of the sediments, the temperature of the soil, the soil

moisture, the vegetation, and the position within the flow system, although the proportion is believed to be small.

To define the flow systems as required above, and to study the movement of ground water within the basin, there must be a detailed understanding of the geologic relations within the basin.

## GEOLOGY

### HYDROSTRATIGRAPHY

Ground water flows from areas of high potential to areas of low potential. The subsurface distribution of elevation and pressure potential is governed by the position of the water table and the spacial distribution of permeability in the ground water basin. There is, therefore, considerable interest in the distribution and hydrologic properties of the geologic rock and alluvial units within the basin. Units here are grouped according to their hydrogeologic similarities. As the units are defined by their relative permeability, they may be described as aquifers, aquicludes, or aquitards. These terms are used as defined in Davis and DeWiest (1966). An aquifer is considered to be a saturated formation that stores and transmits water in sufficiently large quantities to be economically important, while an aquitard is a formation that stores water and transmits only enough water to be important in the study of regional migration of ground water. An aquiclude

is a formation that stores, but does not transmit significant ground water.

Heterogeneity and anisotropy become important in the study of natural geologic materials. A formation is defined as heterogeneous if its hydrologic properties vary from point to point (Davis and DeWiest, 1966) and anisotropic if its hydrologic properties vary with direction.

## HYDROLOGIC BASEMENT

The basement complex includes Precambrian schists, gneisses, and granite to granodiorite plutonic rocks, Paleozoic sandstones, quartzites, limestones, dolomites and shales, as well as upper Cretaceous to Oligocene intrusives of the Mount Blanca intrusive complex (Plate 2). More detailed descriptions of the rocks within this sequence are found in Knepper (1974), Peel (1971), and Karig (1964).

Distribution and lithology of the Paleozoic rocks within the basement sequence of the Sangre de Cristo Mountains (Plate 1) are strongly controlled by faulting contemporaneous with, and postdating, deposition, as well as by periods of erosion following deposition. One of the best examples is the distribution of the lower member of the Sangre de Cristo Formation, a conglomerate containing boulders up to 6 m (20 ft) in diameter, which varies in thickness from 0 to 915 m (3000 ft) in lateral distances of less than 5 km (3 mi). These thickness changes are related to a postulated Paleozoic fault, the Kerber-Crestone

Fault (Peel, 1971). A rapid coarsening of sediment is also noted towards this fault, which closely follows the present trace of the Sangre de Cristo and Villa Grove fault zones (Plate 1).

Within the San Juan Mountains, the distribution of the basement sequence is controlled by post-depositional faulting and erosion. Paleozoic rocks appear only in a block exposed by the Major Creek Fault Zone near Kerber Creek. Elsewhere in the San Juan Mountains, the Paleozoic rocks were not deposited because the region was topographically positive (the Uncompahgre Highland). Exposures of Precambrian plutonic and metamorphic rocks are found as erosional remnants in several areas north of Saguache Creek in the San Juan Mountains, though the author was unable to detect any outcrops of basement south of Saguache Creek. Field mapping was of a reconnaissance nature, so outcrops may exist, though Steven and others (1974) similarly did not map any basement exposures south of Saguache Creek. The lack of any basement exposures could be explained by a pre-Oligocene fault trending parallel to Saguache Creek or simply by a southward dip to the basement surface.

Basement depths within San Luis Valley are controlled almost entirely by Cenozoic normal faulting, varying from 1430 m (4700 ft) to 5029 m (16,500 ft). No Paleozoic sedimentary rocks are present within the valley because of the coincidence of the present valley position with part of the

Uncompahgre Highland (Peel, 1971). More detailed discussion of basement depths in the San Luis Valley is deferred to a later section.

Despite the presence of significant thicknesses of clastic deposits, permeability in the basement sequence is essentially of secondary fracture origin. Sandstones, siltstones, and conglomerates in the section are so well-compacted and well-cemented that intergranular permeability is insignificant. Micaceous sandstones of the Minturn Formation, for example, are nearly indistinguishable in hand specimen from schists. Karig (1964) documents extensive low-grade metamorphism of the Paleozoic rocks in the Sangre de Cristo Mountains. Samples of the Harding Sandstone, Sharpsdale Formation, and Sangre de Cristo Formation were selected as being typical of the Paleozoic sequence and were tested for permeability and porosity by Core Laboratories of Denver, Colorado. The intergranular hydraulic conductivities of both the Harding Sandstone and the Sangre de Cristo Formation were unmeasurable, less than $10^{-8}$ cm/sec, with porosities of 2.4% and 2.0%, respectively. The hydraulic conductivity of a sandstone sample from the Sharpsdale Formation was determined to be $10^{-8}$ (perpendicular to bedding) and 3.0 ($10^{-8}$) (parallel to bedding) cm/sec, with a measured porosity of 3.4%. In contrast, Davis and DeWiest (1966) suggest that hydraulic conductivities of fractured rock near the surface range from $10^{-6}$ to $10^{-2}$ cm/sec.

As no wells penetrate the basement complex, spring discharge

measurements are the only source of estimates of hydraulic conductivity. Using Darcy's Law;

$$Q = KAi$$

where Q = Discharge

K = Hydraulic conductivity

A = Cross-sectional area

i = Hydraulic gradient,

hydraulic conductivity can be determined for a known discharge, cross-sectional area, and hydraulic gradient. The latter term is the most difficult to determine in the absence of observation wells and must be estimated using either a flow net or by simply assuming a gradient of unity to determine the minimum permeability of the terrain. In general, because terrain slopes within the mountain are relatively steep (30°-45°), and because the shape of the water table often is a subdued replica of the terrain slope, gradients vary between 0.5 and 0.7, so an assumption of unity gradient is not grossly in error.

In the Sangre de Cristo Mountains, typical spring discharges vary from 0.063 liters/sec (1 gpm) from bedding-plane fractures with 1 m (3.28 ft) spacing to 0.75 liters/sec (12 gpm) from a 15 cm (6 inch) fracture zone. Estimated hydraulic conductivities in these two cases range from 4.0 ($10^{-3}$) cm/sec to 1.8 ($10^{-2}$) cm/sec, with assumed discharge areas of 1.5 and 4 $m^2$ respectively. All hydraulic conductivities estimated from spring discharge measurements in the Sangre de Cristo Mountains fell within this range. Agreement with published values, such

as those listed by Davis (1969), suggest that these are reasonable values for hydraulic conductivity on a local scale.

Regional hydraulic conductivity is not as high as the local conductivities given above because of the absence of fracture zones for tens of meters and the variability of joint and bedding-plane spacing. In tectonically disturbed zones, fracture zones typically have a spacing of 5-30 m (17-100 ft), producing a regional conductivity of roughly 1.0 $(10^{-4})$ - 5.0 $(10^{-4})$ cm/sec. Regional values of surface hydraulic conductivity are therefore estimated to be on the order of $10^{-5}$ to 5.0 $(10^{-4})$ cm/sec.

Hydraulic conductivity of the fractured basement complex depends more upon the tectonic and erosional environment than on rock type. Little evidence was noted in the field for a relationship between fracture permeability and rock type (Figs. 10-12), other than the existance of bedding plane fracturing as a source of permeability in some of the sedimentary rocks. It is important to note that there was little or no field evidence for modern enlargement of fractures by solution, even in limestone or dolomite rock types (Fig. 12). The steep western slopes of the Sangre de Cristo Mountains inhibit the development of thick soils, probably the most significant factor in the production of acidic ground water that dissolves carbonate rocks. Limestone caves developed on the east side of the Sangre de Cristo Mountains are associated with thick, organic-rich soils and were likely formed through solution

REPRODUCIBILITY OF THE
ORIGINAL PAGE IS POOR



Figure 10: Fracturing in Basement Harding Sandstone.

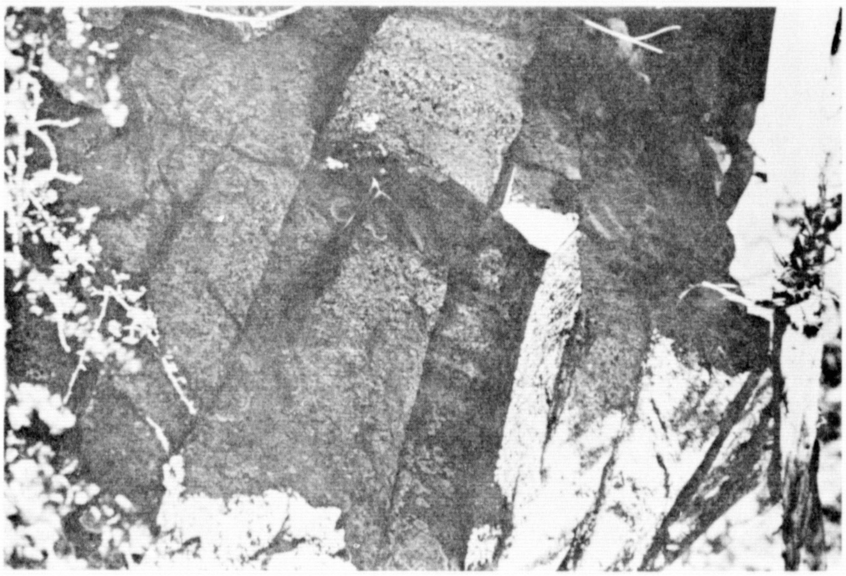

Figure 11: Fracturing in Basement Quartz Monzonite.

Figure 12:  Joint patterns in Manitou Dolomite.

REPRODUCIBILITY OF THE
ORIGINAL PAGE IS POOR

by acidic ground water that has infiltrated the soil zone.

An important consideration in estimating permeability in rocks with secondary fracturing is the change in permeability with depth, related to (1) closing of fractures due to stresses normal to the fracture plane, (2) a decrease in fracturing or an increase in fracture spacing with depth, (3) a decrease in the effectiveness of weathering with depth, or (4) a combination of the above. Certainly, closing of fractures due to increased stress at depth is a significant factor. Snow (1968a) demonstrates that permeability is proportional to the third power of the fracture opening. This will more strongly influence horizontal fractures than vertical fractures, as vertical stresses increase at approximately three times the rate at which horizontal stresses increase with depth. If horizontal fractures are significant avenues of transport of water from vertical fractures at one level, to vertical fractures at a lower level, the differential change in stress will produce an anisotropic permeability in the fractured rock, with horizontal permeability being greater than vertical permeability.

If fracturing caused by stress relief due to erosion is a significant cause of permeability, permeability also decreases with depth because of an increase in fracture spacing. Louis and Pernot (1972) found matching relationships between fracture permeability and stress in the laboratory and field, suggesting that a decrease in permeability with depth could be explained

solely by stress changes, without any effect of changing fracture spacing. Fracture orientations measured at the test site, though, show strong correlation with modern topography, indicating erosional stress relief as a mechanism of fracturing.

Work by Davis and Turk (Davis, 1969), Snow (1968b), and Louis and Pernot (1972) find consistant evidence of a relationship between permeability and depth of the form;

$$K = K_0 e^{-c\ell}$$

where K = Permeability at depth

$K_0$ = Surface permeability

c = Constant

$\ell$ = Depth.

## MESOZOIC ROCKS

The only known outcrop of Mesozoic rocks in the northern San Luis Basin is a small exposure of the Dakota Sandstone and Morrison Formation as an erosional remnant in T. 45 N., R. 5 E., sec. 9 (Plate 1). The Morrison Formation here consists of 9-15 m (30-50 ft) of mudstones, siltstones, and shales, while the overlying Dakota Sandstone consists of 21 m (70 ft) of fine to medium-grained quartz sandstone. The sandstone is well-cemented and has an intergranular hydraulic conductivity of 2.26 ($10^{-4}$) cm/sec (parallel to bedding) and 1.55 ($10^{-4}$) cm/sec (perpendicular to bedding). Fracture permeability likely increases the effective hydraulic conductivity somewhat. The

limited distribution of these units make their presence unimportant in terms of regional ground water flow.

## TERTIARY VOLCANIC AND INTRUSIVE ROCKS

Volcanic rocks within the northern San Luis Basin range in age from 34 m.y. to 15 m.y. (Anon, 1974) and in composition from basalt to rhyolite. Intrusives range in age from 64 m.y. to 32 m.y. and have a similar range in composition.

The oldest intrusives in the basin that post-date the Precambrian are a group of granitic intrusives in the Mount Blanca area that range in age from 50-64 m.y. and precede a period of intrusive activity dated at 31.8 ± 2.3 m.y. (Rio Alto Stock (T. 46 N., R. 11 E., sec. 17)) to 32.2 ± 0.8 m.y. (Blanca Peak Pluton). Cuttings from rocks interpreted as intrusive sills in a geothermal exploration well (T. 40 N., R. 12 E., sec. 32) were dated at 34.4 ± 1.4 m.y. These later dates on the east side of the basin correlate well with a major period of intrusive and extrusive activity on the west side of the basin that ranges in age from 34-31 m.y. Volcanic rocks of this age period are grouped together in the Conejos Formation.

The Conejos Formation is an extremely heterogeneous group of rocks, including volcanic flows, flow breccias, laharic breccias, air-fall tuffs, water-laid tuffs, and agglomerates (Plate 2). Sources for the volcanic rocks of the Conejos Formation are numerous and local. Therefore, while

subdivision and mapping of different lithologic types is possible on a local scale (Bruns, 1971), the difficulty in correlation between volcanic centers makes regional subdivision of the Conejos Formation nearly impossible. Volcanic centers of Conejos Formation age include the Summer Coon Center (Lipman, 1968) (T. 41 N., R. 6 E.), the Beidell Gulch (T. 43 N., R. 6 E.) and North Tracy Canyon (T. 44 N., R. 6 E.) intrusives, and the Bonanza volcanic center (Bruns and others, 1971) (T. 46 N., R. 8 E.). All four of these important centers lie along a remarkably straight northeast trend, paralleling the edge of San Luis Valley (Plate 1), suggesting structural control of the volcanic centers.

Overlying the Conejos Formation is a sequence of intermediate to silicic ash-flow tuffs, air-fall and water-laid tuffs, and local andesite flows, all dating from 26.5 to 30 m.y. (Plate 2). The ash-flow tuffs are much more extensive than local flows of the Conejos Formation and can be correlated on the basis of stratigraphic position, mineralogy, and texture. Ash-flow tuffs in the region may consist of single or compound cooling units. Each cooling unit consists of an unwelded top and bottom, with increasing degree of welding toward the center of the flow.

The youngest volcanic unit in the northern San Luis Basin is the Hinsdale Basalt, ranging in age from 4.7 to 23.4 m.y. This unit caps several plateaus in the San Juan Mountains, but because it consistantly lies above the water-table it

affects only infiltration rates to the underlying aquifers.

Distribution and thicknesses of the volcanic rocks are controlled by the quantity and energy of material erupted, the position of the source, and the topography of the land surface at the time of eruption. Thickness of volcanic flows and ash-flows can vary by several orders of magnitude between paleo-valleys and paleo-ridges. Water-laid tuffs are restricted entirely to paleo-lows. The effect of paleotopography is most noticeable where units of different stratigraphic levels are found at similar elevations, such as at Houghland Hill (T. 45 N., R. 6 E.), where ash-flow tuffs are found at lower elevations than the surrounding hills, composed of older, Conejos Formation flows. Ash-flow tuffs are thickest in calderas at their source. Steven and others (1974) present a map of the calderas of the San Juan Mountains. Of the ash-flows found within the basin, only the Fish Canyon and Bonanza Tuff have sources within the basin (La Garita and Bonanza calderas). The source calderas for the Nelson Mountain, Rat Creek, and Carpenter Ridge tuffs are near the western boundary of the basin, while the sources for the other tuffs are farther away.

The ash-flow tuffs are most significant in terms of regional ground water flow where they crop out at the western edge of San Luis Valley (Plate 1). The high permeability of these ash-flow tuffs provides a direct conduit for ground water flow to the deeper aquifers of the valley. Ash-flow tuffs crop out in several places along the edge of San Luis Valley, are

reported in several shallow wells near the edge of San Luis Valley, but are encountered in only one deep well in San Luis Valley. The Tennessee Gas Transmission (TENNECO) Number 1-B State Well (T. 41 N., R. 7 E., sec. 14) reports ash-flow tuff at depths of 646 m (2220 ft) and 722 m (2370 ft), with thicknesses of 10.7 m (35 ft) and 29 m (95 ft) respectively. Deep wells near the center and eastern edge of San Luis Valley do not show any sign of ash-flow tuffs, despite the presence of older lava flows.

Volcanics of the Conejos Formation are the most extensive rocks, and the most significant rocks in terms of ground water flow, constituting the porous medium of most of the ground water reservoir of the San Juan Mountains and continuing significant distances into the alluvial basin of San Luis Valley (Plate 3). Laharic breccias, flow breccias, and agglomerates are thickest near extrusive centers and thin rapidly away from their sources. The majority of volcanics encountered in wells in San Luis Valley are andesite to rhyolite flows which, because of the restriction of silicic flows to the 32-34 m.y. range, are believed to be correlative with the Conejos Formation.

Permeability of the Tertiary volcanic pile as a whole is extremely heterogeneous and strongly anisotropic. The existance of numerous springs upgradient of dikes and the stream seepage measurements on La Garita and Carnero creeks (Appendix A) indicate that the intrusives of the Conejos Formation act as

aquitards or aquicludes. At the other extreme, spring discharge measurements in areas of welded ash-flow tuff suggest permeabilities equal to, or greater than, those of the most permeable alluvium in San Luis Valley.

Fracture permeability is by far the most important source of permeability in the volcanic rocks of the basin. Table 5 shows measured values of intergranular permeability for typical volcanic rocks of the basin. Intergranular permeability for welded ash-flow tuffs is insignificant in all cases. Intergranular permeability of air-fall/water-laid tuffs and laharic breccias is low, but measurable.

Fracturing in volcanic rocks may be primary (related to the flow and cooling history of rock) or secondary (due to post-depositional changes in stress). Columnar jointing caused by cooling of the rock is the most obvious fracturing found (Fig. 13), but fracturing along flow layering is also an evident feature in surface outcrops (Fig. 14).

Primary fracture permeability is restricted to welded ash-flows, lava flows, and some flow breccias, while secondary fracturing is the only significant source of permeability in most flow breccias and agglomerates. Primary or secondary fracturing does not appear to be a significant source of permeability in laharic breccias (Fig. 15), water-laid or air-fall tuffs, or unwelded ash-flow tuffs, both because of the absence of a slow history of cooling and because of the fine-grained and ductile nature of the rock.

TABLE 5: Intergranular Hydraulic Conductivity

| Rock Type | Degree of Welding or Compaction | Hydraulic Conductivity (cm/sec) |
|---|---|---|
| Ash-flow tuff | Moderate | $<2.5(10^{-7})$ |
| Ash-flow tuff | Moderate | $<2.5(10^{-7})$ |
| Ash-flow tuff | Moderate | $<2.5(10^{-7})$ |
| Ash-flow tuff | Moderate | $<2.5(10^{-7})$ |
| Ash-flow tuff | Weak | $2.05(10^{-6})$ |
| Ash-flow tuff | Weak | $<2.5(10^{-7})$ |
| Ash-flow tuff | Weak | $<2.5(10^{-7})$ |
| Ash-flow tuff | Strong | $<2.5(10^{-7})$ |
| Ash-flow tuff | Strong | $2.6(10^{-5})$ |
| Water-laid tuff (Sandy) | Weak | $1.9(10^{-4})$ |
| Water-laid tuff (Silty) | Weak | $4.4(10^{-6})$ |
| Water-laid tuff | Weak | $6.9(10^{-5})$ |
| Tuffaceous sandstone | Moderate | $1.2(10^{-6})$ |
| Laharic breccia | Moderate | $2.6(10^{-5})$ |
| Laharic breccia | Moderate | $1.6(10^{-6})$ |
| Laharic breccia | Moderate | $1.6(10^{-5})$ |

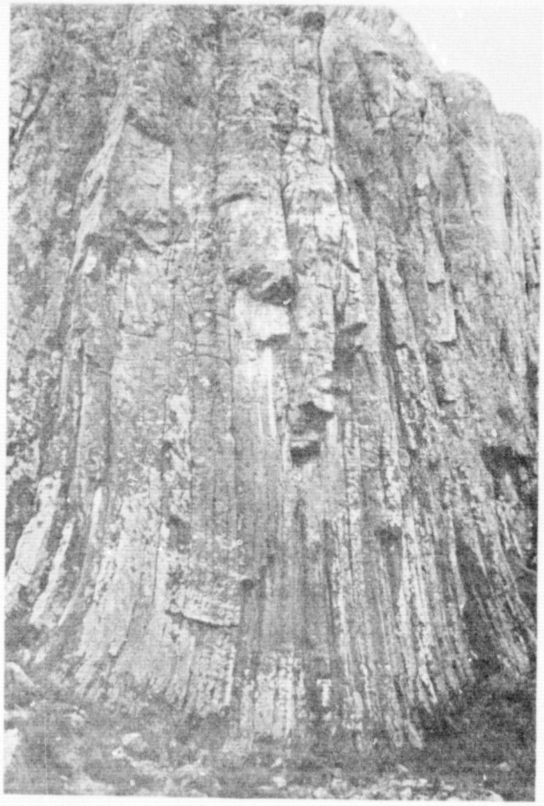

Figure 13: Columnar jointing, Conejos Formation flow.

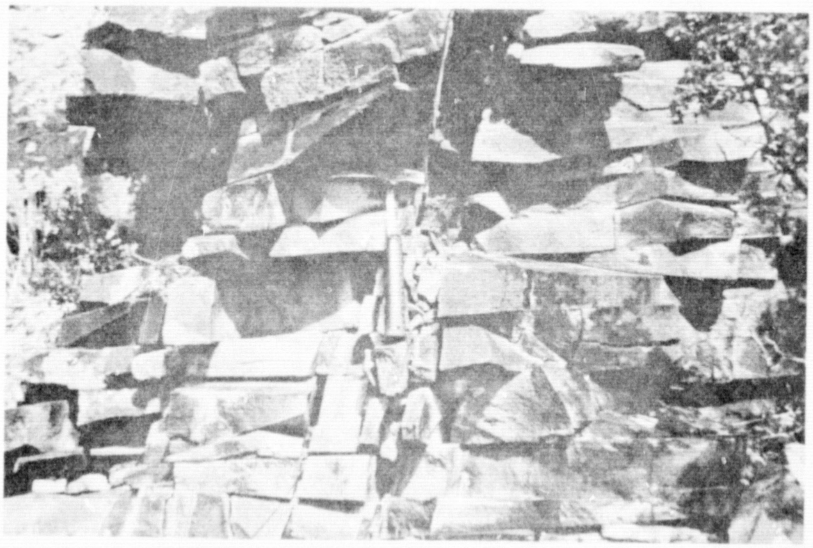

Figure 14: Primary fractures in andesite flow of the Conejos Formation.

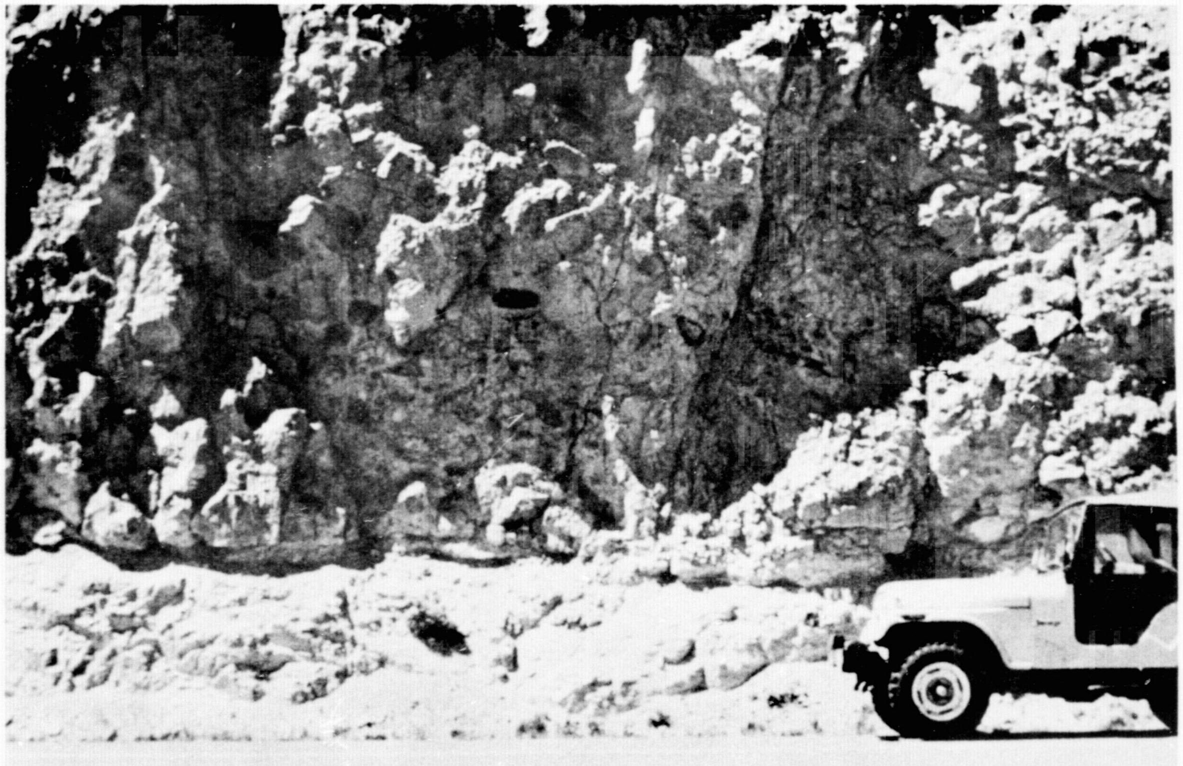

Figure 15:  Laharic breccia of the Conejos Formation.

REPRODUCIBILITY OF THE ORIGINAL PAGE IS POOR

In welded ash-flow tuffs, the degree of fracturing corresponds very closely to the degree of welding and therefore to permeability. The most densely-welded centers of ash-flow tuffs have the most pervasive fracturing. This is true for both primary and secondary fracturing, both because the densely-welded tuffs have had the slowest cooling history, and therefore ample time to form joints, and because the welded tuffs are the stiffest and most brittle members of the local stratigraphic section and fracture more extensively than the weak, ductile, unwelded tuffs. Winograd (1971) reports an identical conclusion from a review of the literature and field work in similar rock types in Nevada.

Very little information is available on the magnitude of fracture permeability of the volcanic rocks in the San Luis Basin. Emery and others (1973) consider the lava flows of the San Juan Mountains to be confining layers where they are present in San Luis Valley. The water budget, observations of a relatively flat water table in the San Juan Mountains, and measurements of spring discharges suggest otherwise. The most important information available on permeability of the volcanic rocks of the northern basin is a single specific capacity test on the municipal well of Saguache. This well is perforated for a 160 m (524 ft) interval, consisting of 95 m (311 ft) of lava flows and 65 m (213 ft) of laharic breccia and water-laid tuff, all of the Conejos Formation. A twenty-four hour test was conducted at the time of completion of the

well, with an average discharge of 675 gpm and a total drawdown of 82 ft (25 m). Using Jacob's approximation to the Theis nonequilibrium formula;

$$s = \frac{264Q}{T} \log \frac{0.3Tt}{r^2S}$$

where s = Drawdown in feet

Q = Discharge in gallons/minute

T = Transmissivity in gallons per day/foot

t = Time, in days

r = Distance between the pumped well and the observation well in feet (for the case of drawdown in the pumped well, r = radius of the well).

S = Storage coefficient,

transmissivity can be solved for iteratively, provided the discharge, drawdown, and storage coefficient are known. The storage coefficient for the rocks involved is unknown, so transmissivity is estimated for a storage coefficient of 0.1 and 0.01, giving a range of values. Davis (1969) suggests a value of 0.05 for fractured basalts as being typical, which falls into the range used. Using the values given above, transmissivity is calculated to range from 11,800 to 14,000 gpd/ft, giving a range of average hydraulic conductivity for the section of 1.3 $(10^{-3})$ - 1.6 $(10^{-3})$ cm/sec. These permeabilities, 2-4 orders of magnitude greater than the intergranular permeabilities of the volcanics in the basin, are

quite significant. In fact, they are comparable to permeabilities of the finer alluvial sands and gravels in San Luis Valley.

Even more striking, but less dependable estimates of the magnitude of fracture permeability in some of these rocks, are the large spring discharges from the welded ash-flow tuffs. Several springs flow from fractures in the Fish Canyon Tuff at Big Springs Picnic Ground (T. 44 N., R. 6 E., sec. 18) (Fig. 16), the largest of which flows at 0.014-0.04 $m^3$/sec (0.5-1.5 cfs), suggesting a hydraulic conductivity on the order of 5.0 ($10^{-2}$) cm/sec, as great as the most permeable alluvium in San Luis Valley.

Review of the work of Winograd and Thordarson (1975) and Winograd (1971) shows that these values are quite compatible with values measured by pump tests in similar rock types of the Nevada Test Site. They measured a range of average values from 6.0 ($10^{-4}$) to 4.0 ($10^{-2}$) cm/sec in sections containing tuff with a full range of welding.

The presence of unwelded tuff underlying and overlying the central, welded zone of ash-flow tuff produces a high degree of anisotropy in the ash-flow units. Horizontal permeability of the unit as a whole is the thickness-weighted average permeability of the section, while vertical permeability is, at most, only several times that of the least permeable rock type. Horizontal permeability is therefore several orders of magnitude greater than vertical permeability.

REPRODUCIBILITY OF THE
ORIGINAL PAGE IS POOR



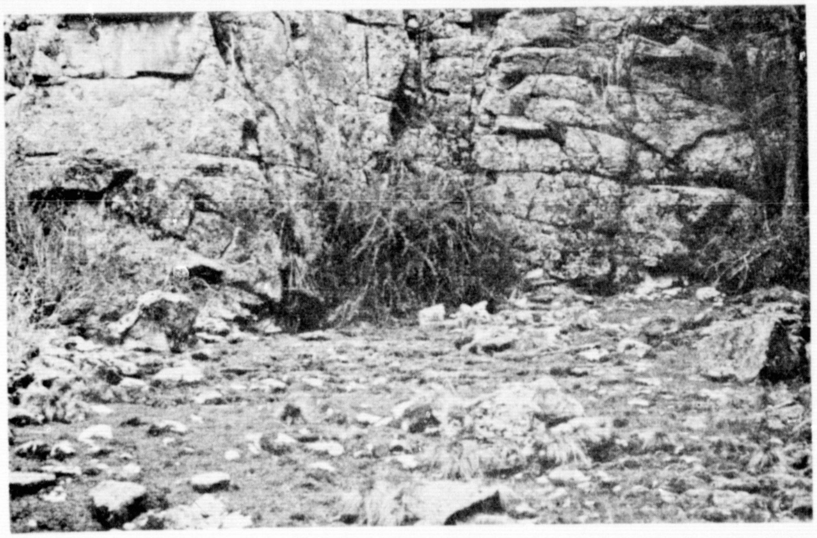

Figure 16: Area of spring discharge from fractures in Fish Canyon Tuff.

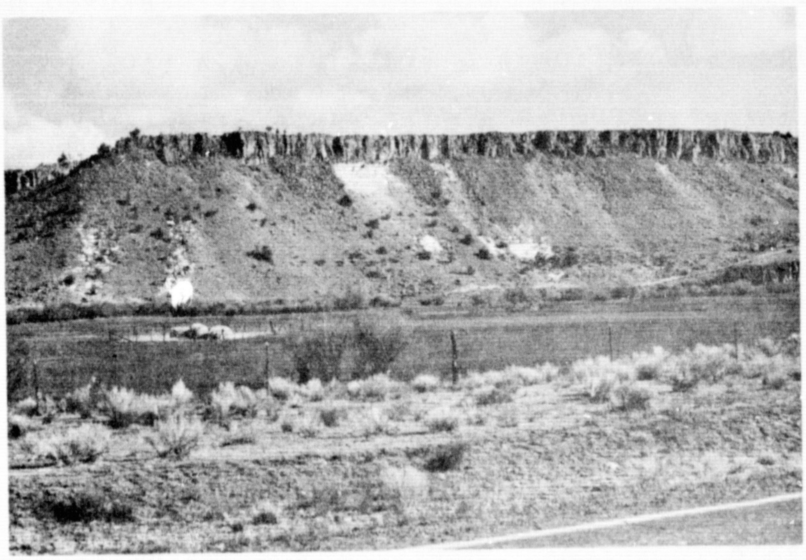

Figure 17: Welded Fish Canyon Tuff, capping the ridge, overlying unwelded air-fall/water-laid tuff and welded Sapinero Mesa Tuff.

The presence of air-fall and water-laid tuffs (Fig. 17), as well as the presence of unwelded ash-flow tuffs, produces the same effect for the volcanic section as a whole; with vertical hydraulic conductivity limited by the interstitial permeability of the air-fall/water laid tuffs (on the order of 5.0 $(10^{-5})$ cm/sec) and horizontal hydraulic conductivity being the weighted average of the column (on the order of $10^{-3}$ cm/sec).

## VALLEJO/SANTE FE FORMATION

Alluvial sedimentary rocks underlie, interfinger with, and overlie Tertiary volcanic rocks in San Luis Valley (Plate 2). The oldest sequence of these deposits include what has been described by Powell (1958) as the Sante Fe Formation and by Upson (1941) as the Vallejo Formation. Upson describes the Vallejo Formation as being dominantly red shale, siltstone, and sandstone, with some thick lenses of coarse conglomerate, believed to be Eocene or Oligocene in age because it conformably underlies volcanic flows correlated with the Hinsdale Basalt. Powell (1958) describes the Sante Fe Formation in San Luis Valley as conglomerate, sandstone, clay, and volcanic debris. The Sante Fe Formation was assigned by Powell to the Miocene-Pliocene.

Rocks of this sequence crop out in two localities within the northern closed basin. In the northernmost locality (T. 28 S., R. 73 W., sec. 17) approximately 450 m (1475 ft) of sedimentary rock crops out, but only 30 m (98 ft) is well-exposed.

Here, the section (Fig. 18) consists of conglomerates, fine to coarse-grained sandstones, and siltstones, all very angular, poorly-sorted, and well-consolidated, but poorly cemented. Conglomerates fill channels (Fig. 19) that indicate dominant south-southwest transport directions. In the second locality (Fig. 20) (T. 29 S., R. 73 W., sec. 24) the rock is finer-grained, dominantly maroon siltstone, interbedded with well-consolidated conglomerate similar to that described above. Strong oxidation is characteristic of the deposits in both localities, and pediment gravels overlie the Tertiary sedimentary rocks in both localities.

Recent evidence from the deepest wells in San Luis Valley suggest that the Vallejo and Sante Fe formations represent a single, relatively uninterrupted period of alluvial deposition from Paleocene through early Pliocene time. Analysis of palynomorphs from a 3048 m (10,000 ft) geothermal exploration well near the eastern edge of San Luis Valley (T. 40 N., R. 12 E., sec. 32) by Dr. K.A. Newman of Colorado School of Mines indicate a continuous succession of Paleocene through Holocene flora, as correlated with reference sections in the Western Uinta and Piceance Creek Basins. The well penetrated 550 m (1800 ft) of Pliocene through Recent sediment, 1280 m (4200 ft) of Oligocene through Pliocene sedimentary rock, 396 m (1300 ft) of Eocene sedimentary rock, and 526 m (1726 ft) of Paleocene sedimentary rock, bottoming at 3011 m (9880 ft) depth in alluvial sedimentary rock (Fig. 21). Deposits are

REPRODUCIBILITY OF THE
ORIGINAL PAGE IS POOR

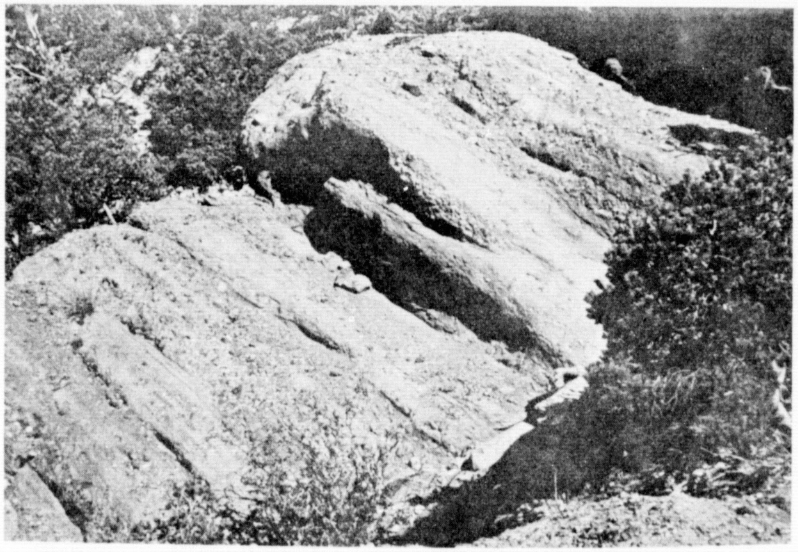

Figure 18: Outcrop of sandstone and conglomerate of the Vallejo/Sante Fe Formation at Urraca Canyon.

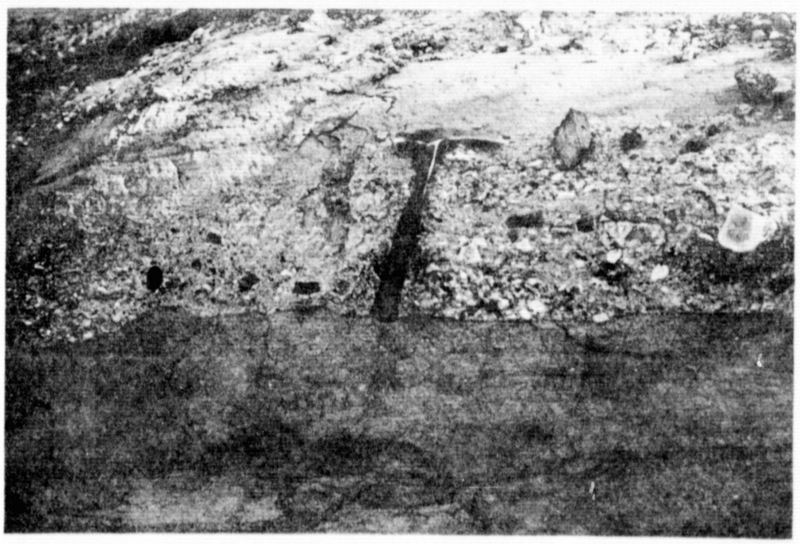

Figure 19: Channel-fill in Vallejo/Sante Fe Formation.

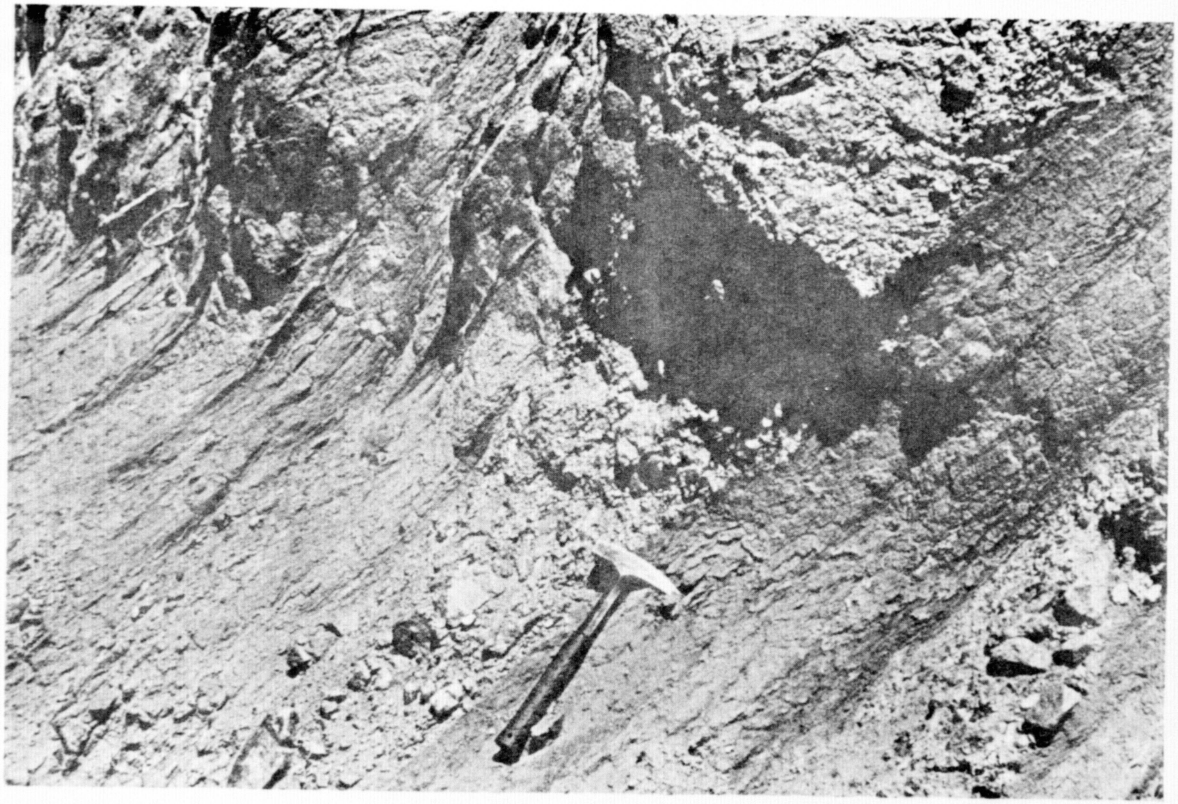

Figure 20: Fine-grained deposits of the Vallejo/Sante Fe Formation.

REPRODUCIBILITY OF THE ORIGINAL PAGE IS POOR

| Depth(m) | Age | Hydrogeologic Unit | Lithologic Description |
|---|---|---|---|
| 0-55 | Holocene ? | Eolian Sands | Very-fine to coarse-grained, angular to subrounded, frosted sand. |
| 56-550 | Pleistocene ? | Alamosa Formation | Blue-gray, soft, bentonitic clay with traces of interbedded, very-fine to coarse-grained, dark sand. |
| 551-610 | Pliocene | Sante Fe/ Vallejo Formation | Very-fine to coarse-grained, angular, white to orange sandstone, interbedded with red, brown, orange, and pink shales and conglomerates. |
| 611-1830 | Miocene ? Oligocene | | |
| 1831-2226 | Eocene | | |
| 2227-2591 | Paleocene | | |
| 2592-2758 | Oligocene | Tertiary Intrusive | Light gray, silicic, medium-crystalline igneous rock. |
| 2759-2804 | Paleocene | Sante Fe/ Vallejo Fm. | See Sante Fe/Vallejo Fm. above. |
| 2805-2896 | Oligocene | Tertiary Intrusive | See Tertiary Intrusive above. |
| 2897-3011 | Paleocene | Sante Fe/ Vallejo Fm. | See Sante Fe/Vallejo Fm. above. |

Figure 21: Cenozoic stratigraphy at the AMOCO geothermal exploration well.

described throughout the section as consisting of red siltstone, shale, sandstone, and conglomerate.

To determine the total thickness of pre-volcanic deposits at the position of the well, gravity data obtained by Gaca and Karig (1966) were reevaluated using density values obtained in the course of logging the well. Using the basin configuration, equation, and density values shown in Figure 22, gravity anomalies for each layer were computed. Density was assumed to be constant from the bottom of well to basement rock. Basement depth at the site of the test well, computed in this manner, is 3353 m (11,000 ft), suggesting a maximum of 1524 m (5000 ft) of pre-volcanic alluvial fill at this position in the basin.

Examination of other deep wells in San Luis Valley indicates that the thickness of the pre-volcanic section is variable and dependent upon structural control. The TENNECO 1-B State Well (T. 41 N., R. 7 E., sec. 14), which penetrated granitic gneiss at 3024 m (9920 ft) depth, encountered 677 m (2220 ft) of sedimentary rock, described as maroon mudstone and siltstone, with thin beds of fine to coarse-grained sandstone, and occasional conglomerate, between the lowermost lava flow and the basement. Originally interpreted as Pennsylvanian Sangre de Cristo Formation by the drillers, this author, because of lithologic similarity to the Vallejo Formation, and because the well site was part of the Uncompahgre Highland during Paleozoic time, believes that these rocks are pre-volcanic

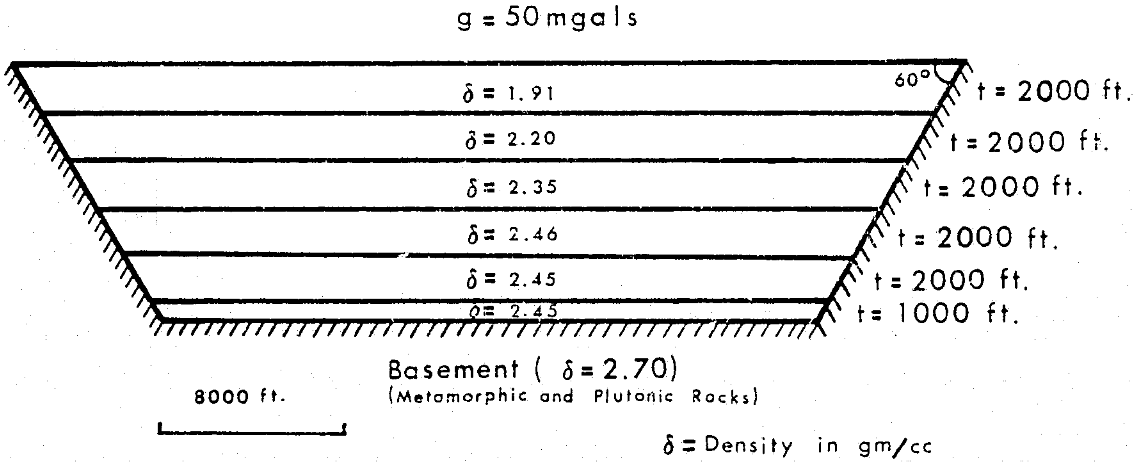


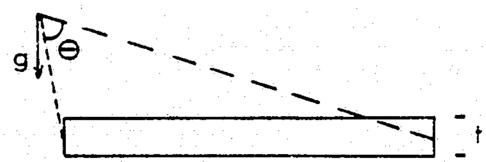


$g = 4.07\ \Theta\ \sigma\ t$

g = gravity anomoly in mgals.

$\Theta$ = angle in radians.

$\sigma$ = density contrast in gm/cc.

t = thickness in kilo feet.

Figure 22: Gravity model and equations used to compute Bouger anomaly (T. 40 N., R. 12 E.). Equation from Nettleton (1942).

Tertiary alluvial deposits. The AMERADA 1-F State Well (T. 39 N., R. 10 E., sec. 16) penetrates basement at 1430 m (4700 ft) depth, and interpretation of electric and sonic logs suggests a maximum of 530 m (1740 ft) of pre-volcanic sedimentary rock, the thickness of section below the last identifiable lava flow. The structural relation of these thickness changes will be discussed in more detail in a later section, but it should be noted that the AMERADA well overlies a gravity high (Gaca and Karig, 1966), while the other wells overlie gravity lows on the east and west sides of San Luis Valley.

The thickness of the entire Vallejo/Sante Fe Formation is similarly highly variable. The maximum gravity anomaly determined by Gaca and Karig (1966) is approximately 19 km (12 mi) north of the AMOCO geothermal test well (T. 41 N., R. 11 E.) and is a 60 mgal low. Using the densities of the test well and the same approach as above, the maximum thickness of deposits in San Luis Valley is computed to be 5029 m (16,500 ft), as opposed to 9754 m (32,000 ft) arrived at by Gaca and Karig using an assumed sediment density of 2.37 gm/cc. Of this 5029 m of sediment, approximately 610 m (2000 ft) is of Pliocene through Holocene age, while the remaining 4419 m (14,500 ft) is Vallejo/Sante Fe Formation deposits and volcanic rocks. On the west side of San Luis Valley, in the TENNECO 1-B State Well, approximately 131 m (430 ft) of Pliocene through Holocene sediment was penetrated, with the remaining 2892 m (9490 ft) drilled in Vallejo/Sante Formation

deposits and volcanic flows. In the AMERADA 1-F State Well total section thickness was 1433 m (4700 ft), with nearly 200 m (650 ft) of Pliocene through Holocene sediment and 1233 m (4050 ft) of Vallejo/Sante Fe Formation.

The Vallejo/Sante Fe Formation everywhere unconformably overlies older rocks. The contact between the Vallejo/Sante Fe Formation and the overlying Alamosa Formation is delineated by the change from the characteristic oxidized state of the older rock to the reduced state of the overlying sediment. The relation between the Vallejo/Sante Fe Formation and the overlying sediments of the Alamosa Formation is difficult to determine, as it is nowhere observable in the field. Significant dip to the older rocks where they do crop out, however, suggest that horizontal younger sediment unconformably overlies the older Tertiary sedimentary rock.

Permeability of the Vallejo/Sante Fe Formation is highly heterogeneous and strongly anisotropic. Hydraulic conductivity of a surface sample of Conejos Formation fluvial sandstone interbedded with andesite flows was determined to be 6.3 $(10^{-3})$ cm/sec (parallel to bedding) and 3.9 $(10^{-3})$ cm/sec (perpendicular to bedding), with a porosity of 27.4%. A second sample, taken from outcrop on the east side of San Luis Valley, was determined to have a hydraulic conductivity of only 1.9 $(10^{-4})$ cm/sec (parallel to bedding) and 3.3 $(10^{-5})$ cm/sec (perpendicular to bedding), with a porosity of 20.1%. These rocks are likely representative of the range of permeabilities

for coarse-grained, near-surface, Vallejo/Sante Fe Formation. Interbedded finer-grained material will decrease the average permeability and increase the degree of anisotropy.

Porosity, and therefore permeability, decreases with depth in the Tertiary section. Density values for the sedimentary rock encountered in the AMOCO 1-32 State Well (T. 40 N., R. 12 E., sec. 32) suggest that porosities range from 17% at the top of the section to 7% at the bottom. Study of electric logs from the same well show similar results, porosities of coarse-grained sedimentary rock averaging 11% and composing 10-25% of the section. An average value of horizontal hydraulic conductivity might, therefore, be on the order of 5 ($10^{-5}$) cm/sec, with vertical hydraulic conductivity as low as $10^{-6}$ - $10^{-7}$ cm/sec.

## ALAMOSA FORMATION

The uppermost blue clay of a series of interbedded clays and sands of Plio-Pleistocene age divides much of San Luis Valley into a lower, confined aquifer and an upper, unconfined aquifer (Plates 2-5). Powell (1958) assigned the clays and sands to the Alamosa Formation and, because of the difficulty of differentiating these sediments from overlying Holocene sediments, included Holocene sediments in the Alamosa Formation. Siebenthal (1910) limited the Alamosa Formation to sediments below the first persistant clay layer. For the purposes of this report, the Alamosa Formation is restricted

to those sediments between the Vallejo/Sante Fe Formation and the top of the first blue clay encountered in a drill hole.

State of oxidation or reduction is extremely important in identification of the Alamosa Formation. Both clays and sand in the Alamosa Formation are characteristically in the reduced state and described by water-well drillers as blue, gray, or green. Clays, sands, and sandstones above and below the Alamosa Formation are characteristically red, brown, or yellow, because of oxidation. As noted above, the Alamosa Formation unconformably overlies the older Vallejo/Sante Fe Formation. Younger sediments conformably overlie the Alamosa Formation.

The type section (Siebenthal, 1910) of the Alamosa Formation is an exposure along the Rio Grande River, south of Alamosa, called Hansen Bluff (T. 36 N., R. 11 E., sec. 11). Siebenthal (1910) described the section as consisting of drab joint clay, fine-coarse, drab-black sand, and olive-green, sandy joint clay. A visit to the section by the author revealed a heterogeneous section of green to blue clays interfingering with fine-grained, dark sands. Individual beds have little lateral continuity, with frequent sand-filled channels disrupting clay beds. The reduced nature of the clays, the presence of fresh-water ostracods (Siebenthal, 1910) in the clays, and the fine-grained nature of the sands evidence a lacustrine or swamp environment of deposition for the clays, with sands being deposited in channels eroded through the clays during periods

of relatively low water level. The presence of natural gas in parts of the confined aquifer also tends to support this type of model. Analysis of pollen by Dr. K.A. Newman of Colorado School of Mines, dating of ostracods reported by Siebenthal (1910), and dating of vertebrate fossils reported by Powell (1958) all confirm the Plio-Pleistocene age of the Alamosa Formation.

The degree of communication between the upper unconfined aquifer and the lower confined aquifer is determined by the thickness and spacial extent of the clays of the Alamosa Formation and by the effective vertical hydraulic conductivity of the clays. Previous workers (Siebenthal, 1910; Powell, 1958; Emery and others, 1973) have used the extent of flowing wells as a direct measure of the extent of the clays. Evaluation of basin ground water flow systems with a steady-state, finite-difference model (discussed later) and analysis of trends in water chemistry (also discussed later), however, indicate that the limit of flowing wells does not correspond to the limit of the clays throughout the valley.

The availability of logs of numerous artesian wells along the western edge of San Luis Valley allows a reasonably accurate determination of thickness and spacial extent of the Alamosa Formation clays. This information is not available, however, for the eastern edge of San Luis Valley, and other data must be used to interpret the lateral extent of the clays. In general, where well logs do exist, a picture emerges of a decreasing

number of clay beds and decreasing thickness of clay beds toward the western edge of the valley. For much of the western edge of San Luis Valley, there is only one blue clay, which pinches out against coarse-grained alluvial material or volcanic flows and increases in thickness toward the center of San Luis Valley. On the east side of San Luis Valley, the maximum known thickness of the Alamosa Formation is 555 m (1820 ft) (T. 40 N., R. 12 E.). The thickening of the formation from zero on the west side of the valley to 555 m on the east side appears to be continuous. On a local scale, continuity of the clays appears to be much greater along the western edge of San Luis Valley than along the eastern edge. Clays toward the eastern boundary of the valley appear to be a series of discontinuous beds, interrupted by sands, while correlation of individual clays in western San Luis Valley is comparitively good.

Transmissivity of the confined aquifer in the northern San Luis Valley (Fig. 23) ranges from 100,000 gpd/ft to over 1,200,000 gpd/ft, corresponding to a range in average hydraulic conductivity of 3.15 $(10^{-3})$ cm/sec to 3.8 $(10^{-2})$ cm/sec. Vertical hydraulic conductivity is much more difficult to determine. Emery and others (1975), using a water budget of the unconfined aquifer and assumptions of an average hydraulic gradient across the clays of the Alamosa Formation, obtained a value of 2.20 $(10^{-5})$ cm/sec. A second approach, utilizing a non-steady-state digital model, with different values of

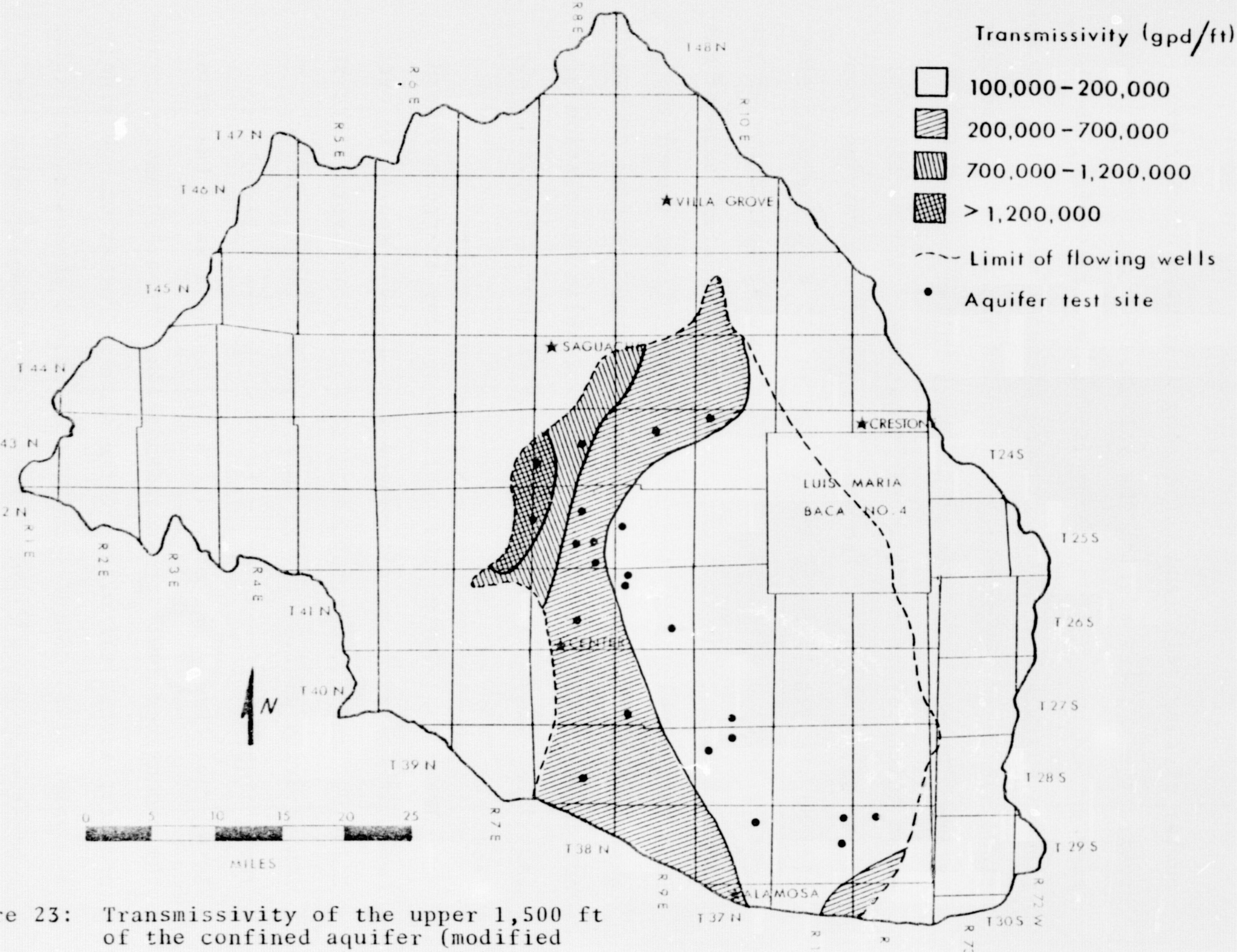


Figure 23: Transmissivity of the upper 1,500 ft of the confined aquifer (modified from Emery and others, 1973).

vertical hydraulic conductivity tried until a match with field piezometric levels was achieved, obtained a value of 2.1 $(10^{-5})$ cm/sec. It should be noted, however, that in the water budget method ground water inflow from both the San Juan and Sangre de Cristo mountains was assumed to be insignificant, an assumption that is clearly unjustified if the water budgets presented earlier in this report are even approximately correct. In the digital model, one value of vertical hydraulic conductivity was assumed for the entire northern closed basin of San Luis Valley, even where the clays are not present. Both errors would tend to produce a higher value of hydraulic conductivity than may exist.

This author used a steady-state digital model of selected cross-sections across the northern San Luis Basin, adjusting the vertical conductivity of the Alamosa Formation clays until a best match with field piezometric measurements was achieved. Using this method, two values were arrived at for different parts of the basin. In the western part of the basin, a vertical hydraulic conductivity value of 1.0 $(10^{-6})$ cm/sec produced the best match, while in the eastern part of the basin a value of 7.0 $(10^{-6})$ produced the best fit with observed piezometric values. It is believed that the difference between the two values is justified, as examination of well logs on the western side of San Luis Valley indicate a much greater continuity of clay beds than is observed on the eastern side.

## PLEISTOCENE-HOLOCENE SEDIMENTS

The youngest deposits in northern San Luis Basin include Pleistocene-Holocene alluvial fans, glacial moraine, eolian sands, pediment gravels, landslide deposits, and stream channel deposits.

### Alluvial Fans

A series of coalescing alluvial fans borders both the Sangre de Cristo and San Juan mountains in San Luis Valley and has been subdivided into four ages based on maximum topographic height above modern streams, extent and slope of the fan surface, degree of dissection of the fan surface, and sequences of intersecting distributaries (Plate 2). The sequence of alluvial fans follows the subdivision given by Knepper (1973) for the northern extremity of San Luis Valley and is similar to the sequence mapped by Limbach (1975) for a selected portion of the Arkansas Valley. Cyclic climatic variations within the Pleistocene, identical to the variations outlined by Scott (1963) for the Front Range of Colorado, are believed to be responsible for the age sequence of fans. This cycle involves; 1) downward stream cutting during the coldest and wettest period of the cycle, 2) sideward stream cutting and lateral erosion of older alluvial fans during a warming and drying period, 3) deposition of younger alluvial fans during a period of increased warmth and aridity, and 4) wind erosion

and deposition during the warmest and driest part of the cycle. This climatic cycle produces a sequence of fans, with older fans standing at greater elevations than younger fans and distributaries of older fans being interrupted by younger fan deposits.

In general, the alluvial fan deposits range in grain size from cobble to fine silt and clay (Appendix A), and, according to Folk's (1968) sorting criteria, all of the deposits are poorly to very-poorly sorted (Fig. 24).

While relative ages are discernable based on the criteria given above, absolute ages for the units are based on correlation with work elsewhere in the state. Van Alstine (1969) identified nine levels of terrace gravels in the upper Arkansas Valley and dated several of the deposits using ash-fall horizons. Limbach (1975) mapped a sequence of alluvial fans similar to those found in San Luis Valley and correlated these deposits with the gravels of Van Alstine.

The oldest alluvial fan found in San Luis Valley stands approximately 21 m (70 ft) above modern stream level and has a characteristic caliche layer (Fig. 25) near the surface (this report and Limbach, 1975). This fan is tentatively correlated with gravel unit 4 of Van Alstine (1968), which is Illinoian in age and stands 21 m above modern stream level.

The two intermediate-age fans in San Luis Valley, standing 14 m (40 ft) and 3.7 m (12 ft) above modern stream level, appear to correlate with the Bull Lake and Pinedale age gravels

REPRODUCIBILITY OF THE
ORIGINAL PAGE IS POOR

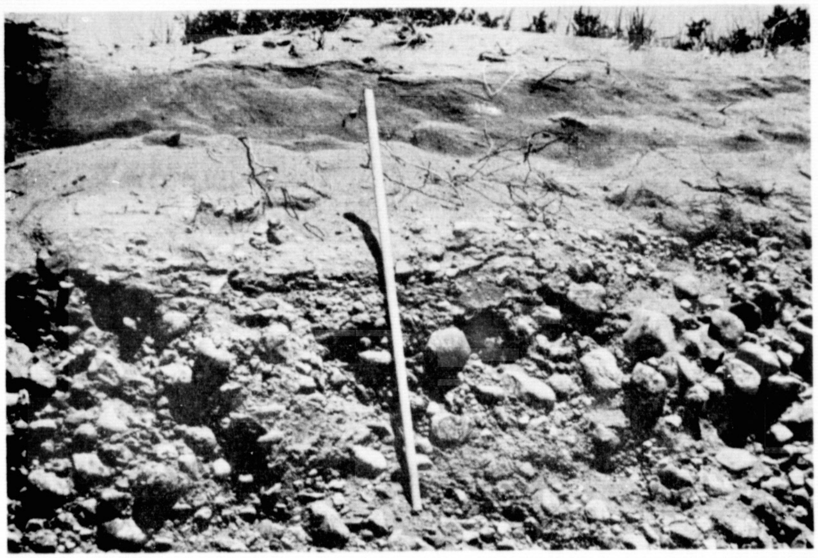

Figure 24: Eolian sands overlying gravels of $Qf_3$. Stick is 5 ft in length.

Figure 25: Caliche-cemented gravels of $Qf_1$.

of Van Alstine. Scott (1970), describes these alluvial fans, near Villa Grove, as Bull Lake and Pinedale outwash fans.

Small alluvial cones, mapped as the youngest alluvial fan, found at the mouths of small canyons and at the toes of older, trenched alluvial fans, are presently in equilibrium with modern streams and are therefore Holocene in age.

Permeability of the alluvial fans is very high, but extremely variable. Their position in the recharge zone at the edge of San Luis Valley suggests that rates of stream seepage into the alluvial fans might be very high, as is observed (Appendix A). Streams entering San Luis Valley from the Sangre de Cristo Mountains commonly lose most of their water to the alluvial fans within the first several kilometers, and many streams disappear into the alluvium within the first kilometer of flow. Rates of seepage loss on the west side of San Luis Valley are less rapid, not because of lower permeability, but because of lower subsurface hydraulic gradients and more restricted, local, zones of recharge.

Four methods were used to estimate permeability of the alluvial fans; 1) computation of permeability from grain-size analysis, 2) determination using a constant head permeameter, 3) computation based on stream seepage losses, and 4) pump tests. Each method has advantages and disadvantages, and results from the methods vary widely.

Estimation of permeability from grain-size analysis is based on an empirical formula given by Krumbein and Monk (1942).

Their formula, determined for glacial and glacio-fluvial sediments, is;

$$K = 0.760\mu_G^2\ e^{-1.31\sigma_\phi}$$

where K = Hydraulic conductivity (cm/sec)

$\mu_G$ = Geometric mean grain diameter, which is equivalent to the graphic mean of Folk (1968), in millimeters.

$\sigma_\phi$ = Phi standard deviation of grain sizes of Folk (1968).

Though the mean permeabilities determined by this method vary (Appendix A), there is considerable variation within the alluvial fans, and, at the 80% significance level, there is no statistical difference between the means of the different fans. The mean of all hydraulic conductivities for all four alluvial fans (18 samples) is 1.35 ($10^{-1}$) cm/sec.

Determinations of permeability using a constant head permeameter were somewhat higher (Appendix A). The oldest alluvial fan has a significantly (80% level) lower hydraulic conductivity than the second oldest unit, with means of 1.0 ($10^{-1}$) cm/sec and 2.35 ($10^{-1}$) cm/sec respectively, but there is no statistically significant difference between $Qf_1$, $Qf_3$, and $Qf_4$ or between $Qf_2$, $Qf_3$, and $Qf_4$. The mean hydraulic conductivity of all four alluvial fans (17 samples) is 1.70 ($10^{-1}$) cm/sec.

Problems with both the above methods are inherent in the physical process of sampling. The hydraulic conductivities determined by the two methods are those of a selected bed at a selected location, by no means representative of the range

of permeabilities found within that alluvial fan. Probably more important, the process of removing the sample changes the degree of compaction of that sample. This is particularly evident in the permeameter determinations, where pore pressure decreases the grain-grain stress, and the density of the sample was decreased considerably. Piping became a problem with some of the specimens.

Of the four methods used to estimate permeability of the alluvial fans, stream seepage measurements and pump tests were the only methods that integrate a significant volume of the fan being measured. Hydraulic conductivity can be estimated using stream seepage measurements by applying Darcy's Law to the seepage loss along a measured length of stream with a relatively constant, known, wetted perimeter and a known subsurface hydraulic gradient. For a shallow stream and a deep (>30 m) water table, a hydraulic gradient of 1.0 can be assumed with very little error. Hydraulic conductivities determined by this method (Appendix A) are much lower than those determined by either of the two previous methods. Again, there is no statistically significant (80% level) difference between the means for the three different fans tested. No measurements were taken for the oldest fan unit, because no active streams flow over that unit. The mean hydraulic conductivity of the three fans (16 measurements) is 3.9 $(10^{-3})$ cm/sec. Problems with this method are the assumption of a unit hydraulic gradient and errors in stream discharge, length,

and wetted perimeter. The narrow range (1.29 ($10^{-3}$) - 6.7 ($10^{-3}$) cm/sec) of values measured for $Qf_3$ (10 measurements) suggests that the method is at least internally consistant. This method measures only the vertical permeability of the medium.

Three pump tests were conducted near Crestone, Colorado, all within the second youngest alluvial fan, $Qf_3$. Transmissivities ranged from 2,400 gal/day/ft to 11,600 gal/day/ft (Appendix A), corresponding to a range in hydraulic conductivity of 3.8 ($10^{-3}$) to 2.8 ($10^{-2}$) cm/sec. Emery and others (1973) report a range of transmissivity for the unconfined aquifer, composed of coalescing alluvial fans of all ages, of 5000 - 255,000 gal/day/ft, corresponding approximately to a range of hydraulic conductivities of 1.8 ($10^{-3}$) to 6.2 ($10^{-2}$) cm/sec. Wilson (1965) reports the results of several pump tests in undivided alluvial fans of the closed basin of San Luis Valley. Hydraulic conductivities computed from these tests (26 samples) range from 1.8 ($10^{-3}$) to 2.2 ($10^{-1}$) cm/sec, with a mean of 5.0 ($10^{-2}$) cm/sec and a standard deviation of 3.4 ($10^{-3}$) cm/sec.

These data suggest considerable variation in permeability of the alluvial sediments, variation that is statistically unrelated to age of deposition. It is apparent that variations in degree of sorting and grain-size within an alluvial fan are as important as, or more important than, variations between alluvial fans. The low to moderate permeabilities encountered in wells near Crestone suggest that the poor degree of sorting

near the mountain front is more important in decreasing the permeability than is the finer grain-size found away from the mountain front.

Results of stream seepage measurements are relatively consistant with those of pump tests, particularly if one assumes that seepage tests measure vertical hydraulic conductivity. Results from permeameter tests are overly high, probably because of problems of sample density. Though the mean of all computations based on grain-size analysis is also relatively high, the mean hydraulic conductivity of the most widespread alluvial fan, $Qf_3$, is only 1.7 $(10^{-2})$ cm/sec, which agrees to an order of magnitude with the pump tests.

## Glacial Moraines

Lateral moraines are found within both the San Juan and Sangre de Cristo mountains, while end moraines are found only in two locations in the Sangre de Cristo Mountains. Glacial lake deposits behind a terminal moraine are found at Willow Creek Park, in the Sangre de Cristo Mountains. Peterson (1971) reports five stages of Wisconsinian glaciation on the east flank of the Sangre de Cristo Mountains, and Knepper (1973) and Limbach (1975) describe deposits from four stages of glaciation in the upper Arkansas Valley. Only two stages of glaciation are evidenced in terminal moraine deposits on the west flank of the Sangre de Cristo Mountains. Nested

terminal moraines are found on Willow Canyon, south of Crestone, and an excellent example of a closed terminal or recessional moraine is found at the mouth of South Zapata Canyon. Elsewhere glaciation is evidenced by lateral moraines, numerous cirques, and rock glaciers. No attempt was made to establish the ages of lateral moraines, and only relative ages were assigned to the nested moraines of Willow Canyon because of the incomplete record of glaciation.

Morainal deposits are unsorted with abundant fine rock-flour clogging the interstices of coarse sand to cobble-size material. The only available data on permeability of these sediments are from grain-size analyses and permeameter tests, with the same problems as stated above. Only two samples were taken because of the lack of unweathered outcrops. Permeameter tests yield a mean hydraulic conductivity of 1.7 ($10^{-1}$) cm/sec (Appendix A), but piping of fine-grained material was excessive in both samples, and the values are likely high by 1-2 orders of magnitude. Computations based on grain-size analysis yields a mean of 1.7 ($10^{-2}$) cm/sec, probably much closer to the real value. Morainal deposits are regarded as low-moderate permeability aquifers in both the Sangre de Cristo and San Juan mountains.

Eolian Sands

Active transverse, parabolic, and longitudinal dunes (Johnson, 1971) are present in and near Great Sand Dunes National Monument, and stabilized parabolic dunes are found overlying fluvial deposits (Fig. 24, p. 74) north and south of the Monument. The eolian deposits are 55 m (180 ft) thick at the site of the AMOCO test well (T. 40 N., R. 12 E., sec. 32) and as thick as 300 m (980 ft) at Great Sand Dunes National Monument, where transverse dunes rise 244 m (800 ft) above the valley floor.

Mean grain diameter (Appendix A) ranges from fine to medium sand size, and sorting ranges from moderately-well to poorly sorted, by Folk's (1968) classification. The high proportion of heavy minerals in the eolian sand and the prevailing northeast wind direction indicate that the source of the sand is alluvial material derived from the San Juan Mountains. The presence of biotite and hornblende inclusions in feldspar grains in samples of stabilized dunes, but not in samples of active dunes, suggests a component of locally-derived material in the stabilized deposits north and south of the Monument.

The only information available on the permeability of the eolian sands is from three stream seepage measurements and permeameter and grain-size analyses of six and seven samples, respectively. The mean hydraulic conductivity as determined by permeameter tests is 4.0 ($10^{-2}$) cm/sec, significantly (80% level)

lower than the means of all alluvial fans determined by the same method. The mean of the hydraulic conductivities computed using grain-size analysis is 1.0 ($10^{-2}$) cm/sec, not differing significantly from the means of the alluvial fans determined by the same method. The mean of the conductivities determined using stream seepage measurements is 2.0 ($10^{-3}$) cm/sec, significantly (80% level) lower than the conductivities of $Qf_3$ and $Qf_2$.

From these determinations, it is concluded that the permeability of the eolian sands is lower than that of alluvial fan deposits because of the finer grain size. Vertical hydraulic conductivity is on the order of 2.0 ($10^{-3}$) cm/sec, with horizontal hydraulic conductivity being nearly an order of magnitude greater, on the order of 1.0 ($10^{-2}$) to 4.0 ($10^{-2}$) cm/sec.

## Pediment Gravels

Pediment gravels are present at four localities along the eastern border of San Luis Valley, and remains of gravels occur throughout the San Juan Mountains.

Thin pediment gravels overlie Precambrian metamorphic rocks in the vicinity of Poncha Pass (T. 48 N., R. 8 E.). These gravels are absent in many places, and only the planar surface of the basement rock provides evidence of pedimentation. The pediment gravels lie approximately 61 m (200 ft) above modern stream level. A small outlier of Conejos volcanic rock

was reported by Knepper (1973) to overlie this same surface 5 km (3 mi) south of Poncha Pass. This surface is therefore postulated to be pre-Oligocene in age.

Well-rounded cobbles of reworked Paleozoic(?) sandstone and conglomerate overlie a beveled surface on the ridge north of Cotton Creek, at the edge of San Luis Valley (T. 45 N., R. 11 E., sec. 20). These gravels deposits, below the scale of the hydrogeologic map, are believed to be pediment gravels, but could be remains of an alluvial fan. The gravels lie approximately 24 m (80 ft) above modern stream level and correlate well with Van Alstine's (1968) gravel unit 4 and $Qf_1$ of San Luis Valley. The surface is therefore believed to be Illinoian in age.

Pediment gravels cap outcrops of Vallejo/Sante Fe Formation at both Urraca Canyon (T. 28 S., R. 73 W.) and in the vicinity of Ikes Creek (T. 29 S., R. 72 W.). Gravels at both locations lie 24 m (80 ft) above the modern stream level and correlate with the oldest alluvial fan of the valley. The age of the underlying sedimentary rock is unknown, though estimated to be Paleocene-Pliocene in age. Pedimentation is believed to be Illinoian.

Pediment gravels everywhere overlie the water-table and are less than 1.5 m (5 ft) thick. Their occurrence affects ground water flow only by affecting infiltration rates.

## Landslide Deposits

Steven and others (1974) mapped a large area of landslide deposits in the vicinity of Table Mountain (T. 43 N., R. 2 E.) The landslides appear to be controlled by a thick zone of unwelded Wason Park Tuff overlying Carpenter Ridge Tuff. No information is available on either the hydraulic characteristics or the effect on ground water flow of the landslide deposits.

## Holocene Stream Deposits

Modern stream deposits are found throughout the basin and are contemporary with the youngest alluvial fan deposit. These deposits are mapped only where they are of large enough extent to be discriminated at the scale of the geologic map. As the modern streams are generally reworking older alluvial material, the permeability is controlled by that of the older material.

# GEOLOGIC STRUCTURE

Geologic structure affects ground water flow in three important ways; 1) by changing the relative positions of aquifers and aquitards, 2) by controlling sedimentation, and 3) by changing the permeability of the medium. In the northern San Luis Basin, faulting that changes the relative position of aquifers and aquitards is of little importance in terms of regional ground water flow. In the San Juan Mountains,

separations along faults are relatively small, and ground water flow patterns are disrupted only on a local scale. In the Sangre de Cristo Mountains, fracture permeability controls ground water flow and the rock units are relatively homogeneous with respect to fracture permeability. Offset of beds by faulting is therefore unimportant, though, as will be discussed later, the faulting itself certainly cannot be neglected.

## CONTROL OF SEDIMENTATION

Interpretation of the Bouger gravity map (Fig. 26) and examination of the hydrogeologic map of the basin (Plate 1) indicate that San Luis Basin is strongly dominated by a series of north trending horsts and grabens (Fig. 27). The Sangre de Cristo Mountain Range is a horst bounded on the west by the Sangre de Cristo Fault Zone, which also forms the eastern boundary of a pronounced gravity low. A linear gravity high lies along the center of San Luis Valley, with a second gravity trough west of the central horst. Outcrops of basement rock are found at the northern extremity of the central horst, north of Saguache Creek (Plate 1). Well information confirms considerable variation in basement depth corresponding to the gravity anomalies first described by Gaca and Karig (1966).

As discussed previously, Peel (1971) presents evidence that suggests that the major bounding faults of the basin, the Sangre de Cristo and Villa Grove fault zones, have been active at least since Pennsylvanian time. Movement on the postulated

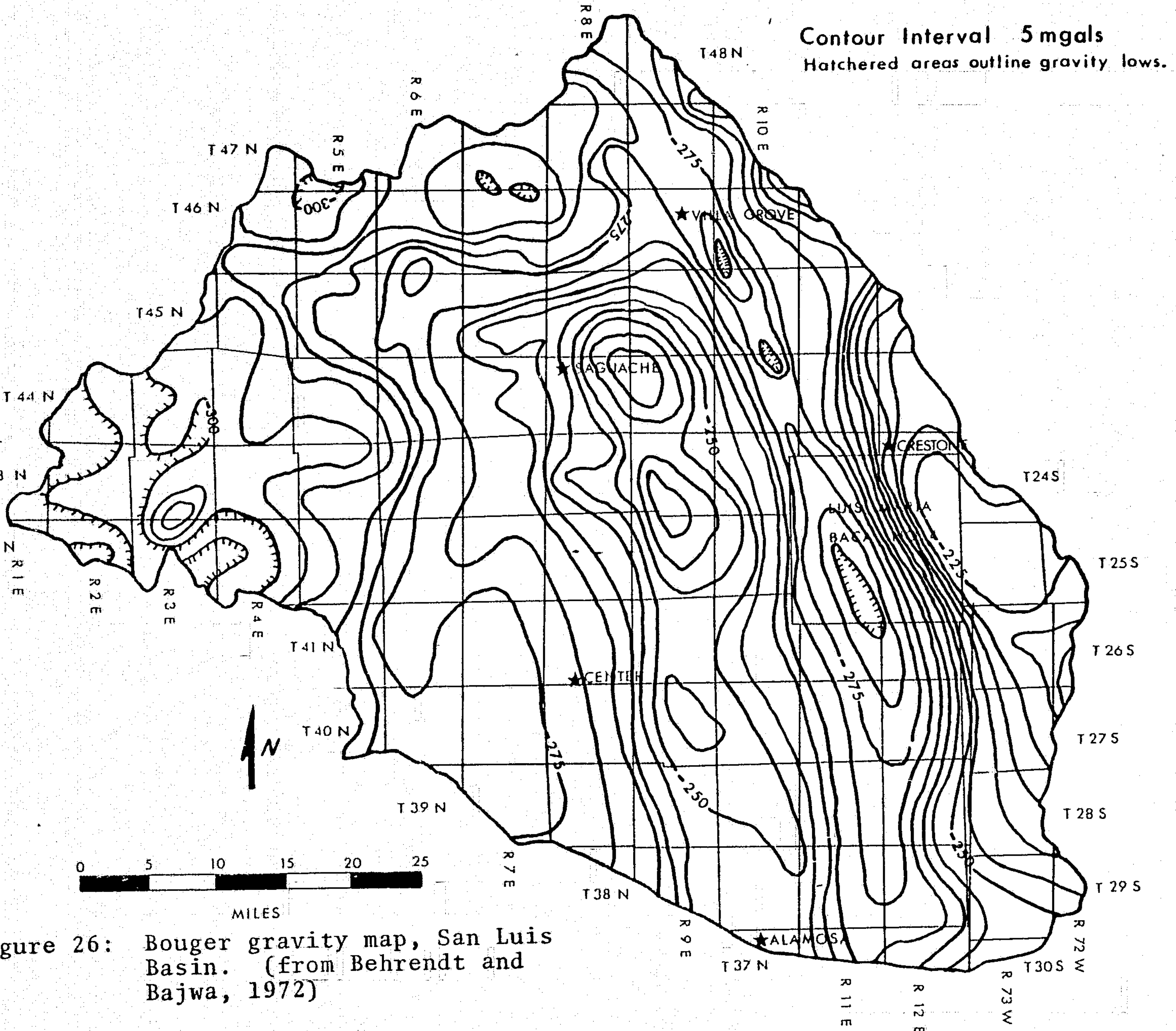


Figure 26: Bouger gravity map, San Luis Basin. (from Behrendt and Bajwa, 1972)

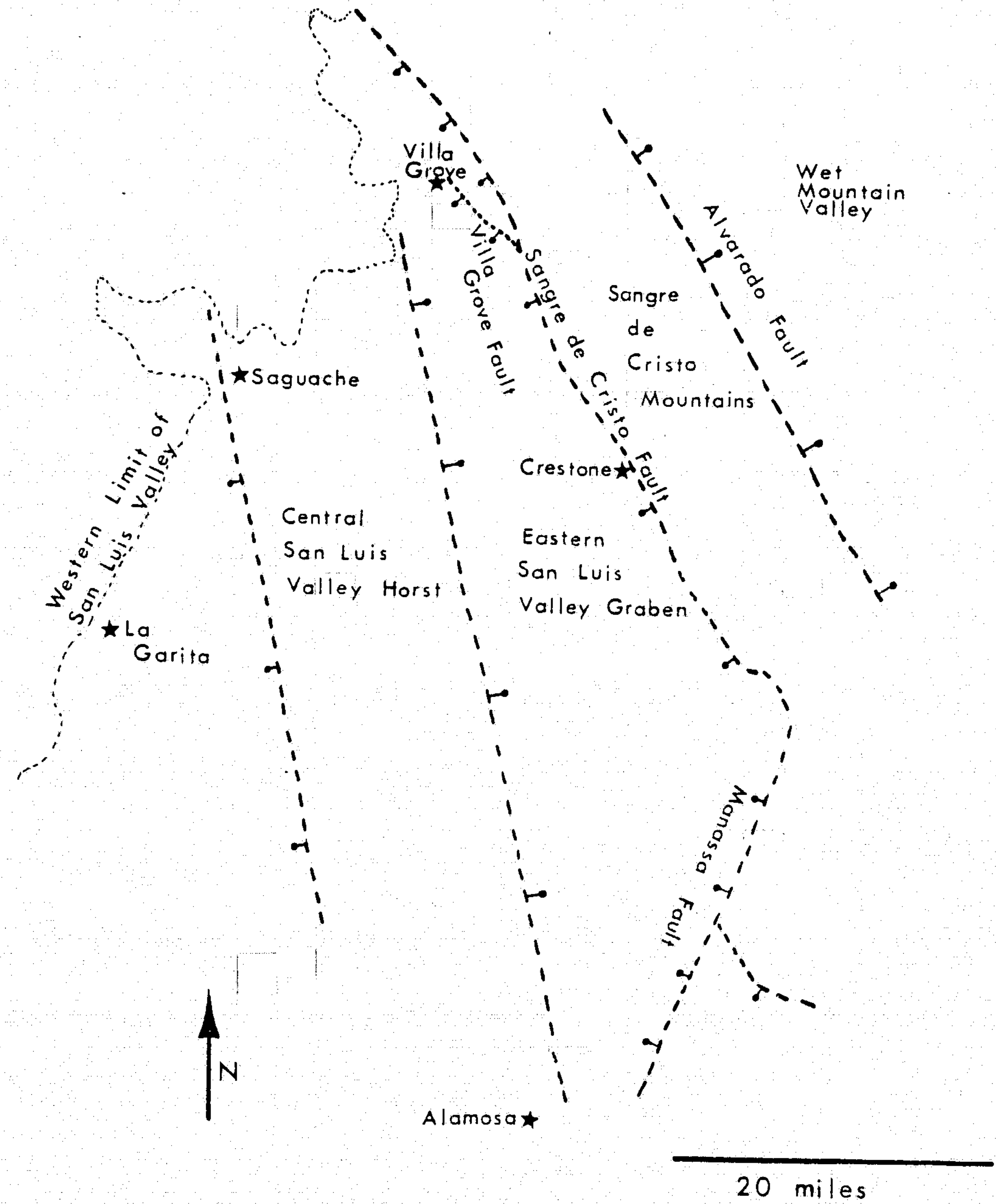


Figure 27: Simplified structure map showing Cenozoic normal faults in the vicinity of San Luis Basin. Bar and ball located on downthrown side of fault.

fault, the Crestone-Kerber Fault, was opposite the normal fault separation seen today along the Sangre de Cristo and Villa Grove fault zones, but the position and trend of the Paleozoic fault is nearly identical with surface expression of the two Cenozoic fault zones. An examination of Figure 28, based on deep well logs and gravity measurements, suggests that the Sangre de Cristo Fault has continued to affect sedimentation through the Cenozoic, and the central horst, which may or may not have been active in the Paleozoic, exerts similar controls over sediment thicknesses. The Vallejo Formation is thickest in the two grabens and thin or non-existant over the central horst. The thickness of the Vallejo Formation shown overlying the central horst is only the thickness of the section below the last lava flow identifiable on the electric logs of the AMERADA 1-F State Well and is given only as the maximum thickness of the Vallejo Formation. The very noticeable change in thickness of the Vallejo Formation between the east and west side of San Luis Valley suggests that the Sangre de Cristo Fault may have been an active normal fault as early as Paleocene time, as opposed to the Miocene age commonly given (Chapin, 1971) for the beginning of normal fault activity. Thicknesses of deposits over the central horst may have been controlled by either erosion or faulting contemporaneous with sedimentation. The relatively uniform increase in thickness of the Alamosa Formation from west to east implies that thickness was controlled by movement

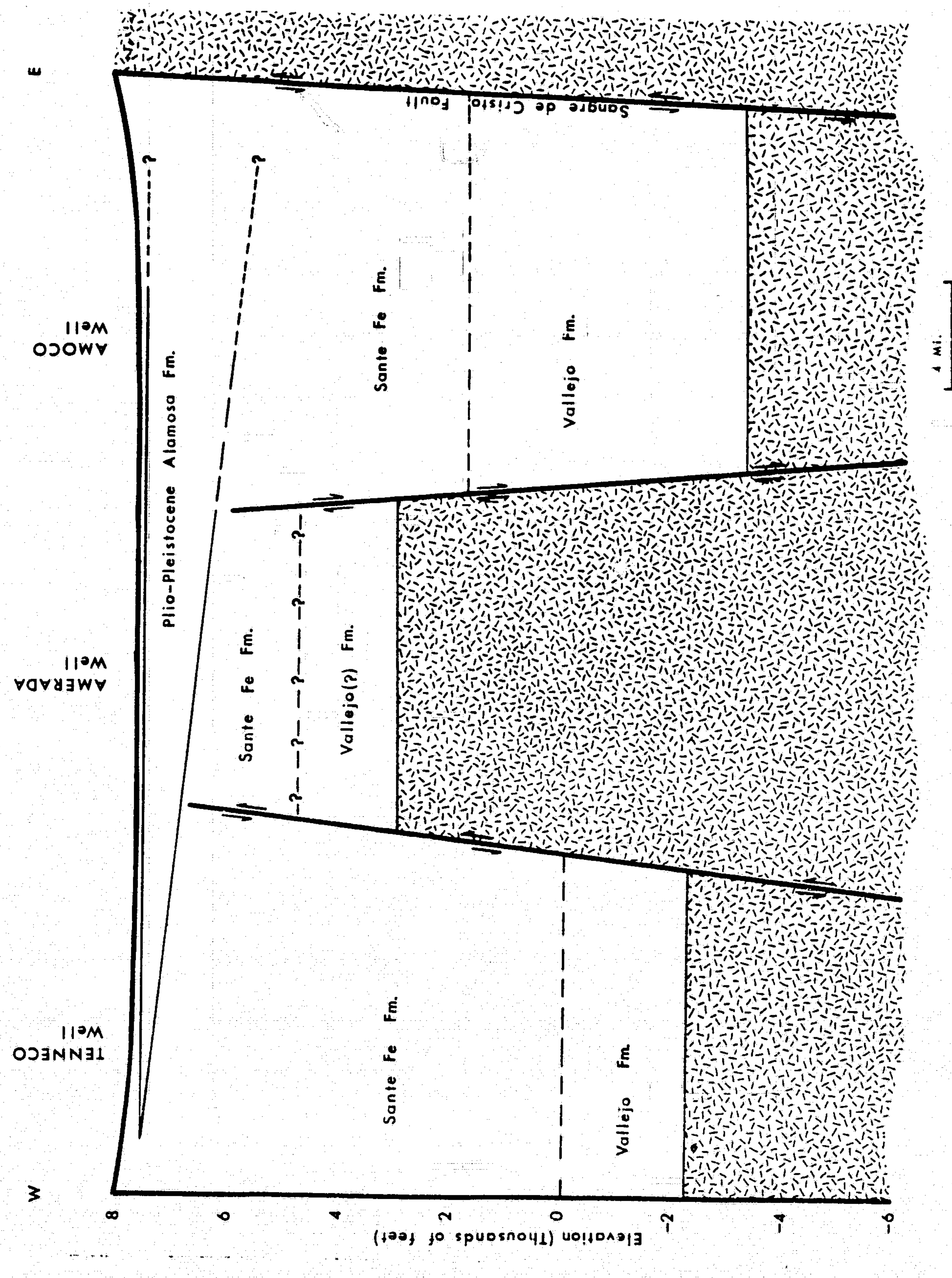


Figure 28: Generalized cross-section across San Luis Valley.

along the Sangre de Cristo Fault Zone contemporaneous with sedimentation, and that movement of the central horst had ceased by late Pliocene time. There is no identifiable offset of the lacustrine clays by the faults bounding the central horst.

Normal faulting continued in San Luis Valley to Holocene time, as evidenced by numerous fault scarps offsetting alluvial fan deposits along the Sangre de Cristo, Manassa, and Villa Grove fault zones (Figs. 29, 30). Fault scarps offset all ages of alluvial fans in the valley but not the most recent stream deposits. A general increase in fault scarp height is observed with increase in alluvial fan age, suggesting repeat motion along the same fault. Though fault scarp height is a function not only of fault offset but also climate, length of time between periods of faulting, and alluvial fan texture (controlling slope stability), it can nevertheless be used as an estimate of fault activity. A plot (Fig. 31) of cumulative fault scarp height versus the minimum age of faulting (taken as the age of deposition of the next youngest alluvial fan) shows a concave upward curve of increasing height with age in the last 10,000 years. The concave upward nature of the curve implies that fault offsets have been decreasing in magnitude through late Pleistocene and Holocene time. That the San Luis Valley may be more stable with time is also suggested by the total lack of historic seismicity in the vicinity (Hadsell, 1968) and by the anomolously low level of

REPRODUCIBILITY OF THE
ORIGINAL PAGE IS POOR

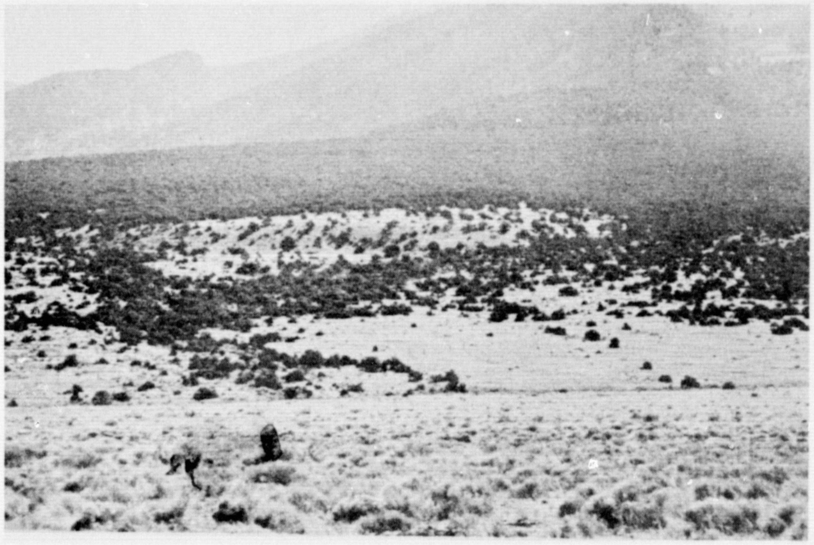

Figure 29: 10 m high fault scarp, north of Urraca Canyon.

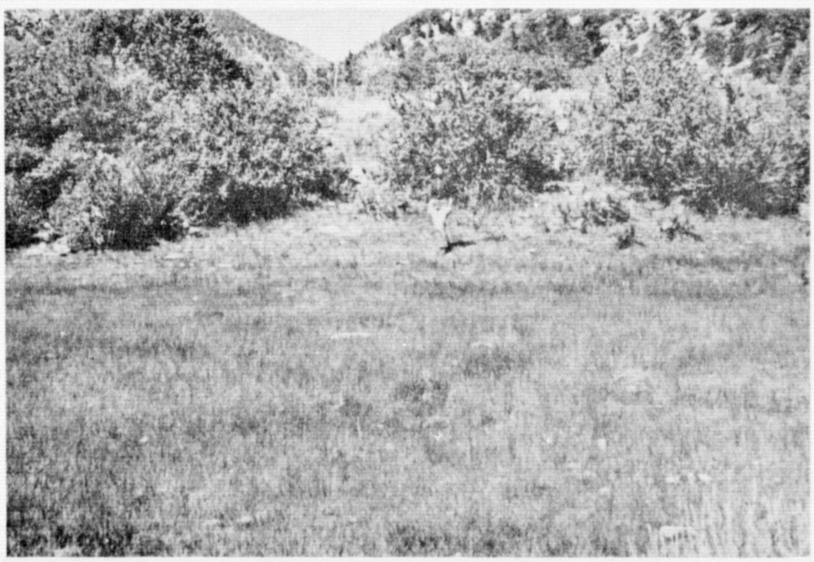

Figure 30: Dense vegetation associated with springs discharging along Sangre de Cristo Fault Zone.

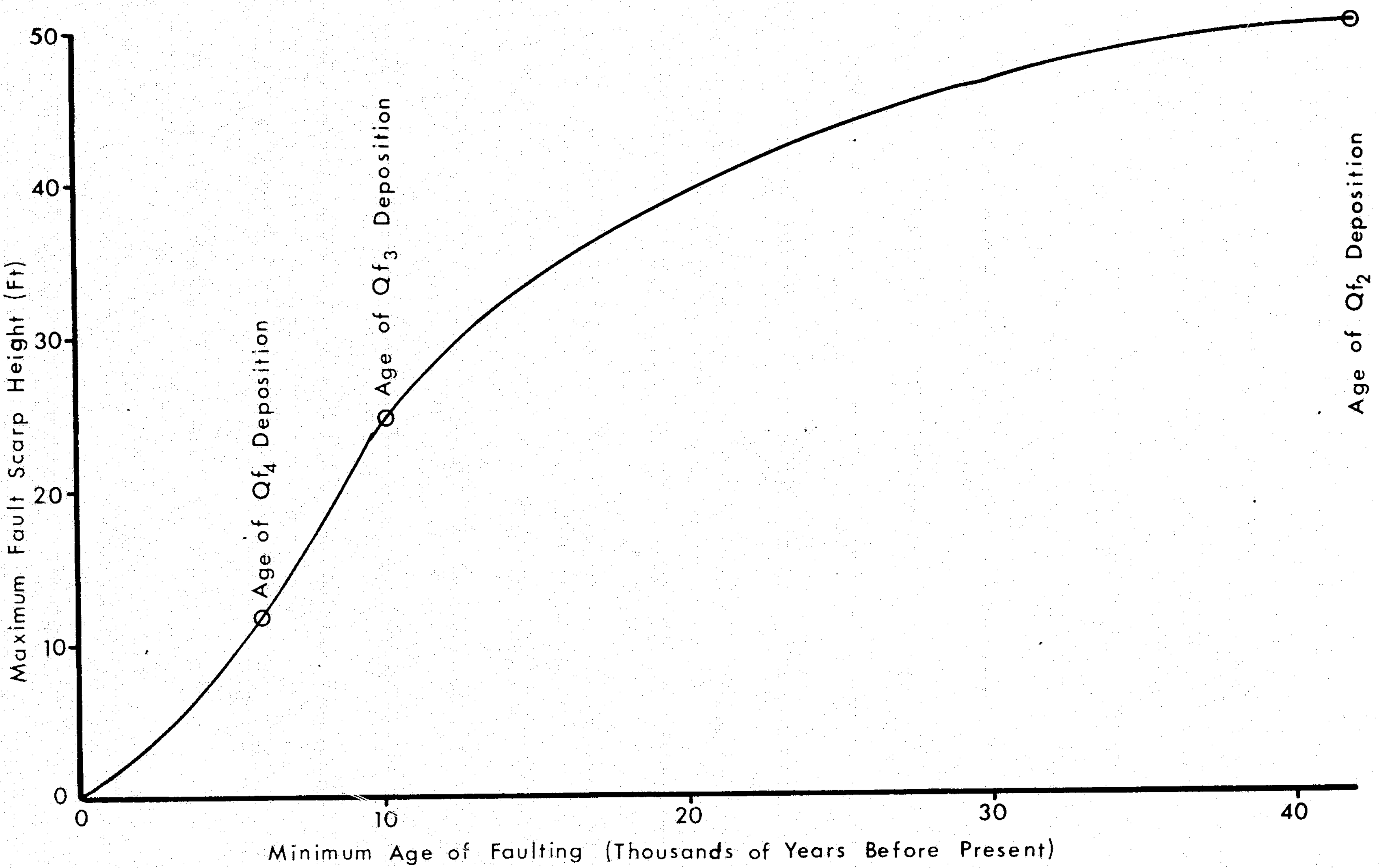


Figure 31: Relations between alluvial fan age and maximum fault scarp height.

micro-seismic activity reported by Keller and Adams (1976).

## ANALYSIS OF STABILITY

Because of the evidence of relatively recent faulting, and the possibility of increasing stability, it is important to know what changes of stress have occurred as a result of geologic and hydrologic processes. One approach to this problem was proposed by Snow (1972) for the evaluation of possible reservoir-induced seismicity. This method involves the computation of changes in effective stress due to sedimentation, erosion, and changes in pore pressure and using Mohr's failure criteria to evaluate the computed stress changes relative to those necessary for failure. Haxby and Turcotte (1976) demonstrate that thermal stresses are of the same order of magnitude as stresses induced by the weight of rock being added or removed from a region and therefore also need to be taken into account.

In the San Luis Valley, the lacustrine clays of the Alamosa Formation serve as an excellent datum plane; the elevation of the water table and the land surface is approximately known, and the Sangre de Cristo Fault was active at the time of deposition. Since deposition of the uppermost blue clay, two processes have continued more or less continuously; deposition of sediment and a rise of the water table. Today the water table at the Sangre de Cristo Fault is 300 m (980 ft) above the elevation of the highest lacustrine clay, and the land surface at the Sangre de Cristo Fault is 421 m (1380 ft)

above the elevation of that clay. Changes in effective stresses due to the weight of deposited sediment are compressional and are given by the formula (Snow, 1972);

$$\Delta\sigma_v = \gamma\Delta h$$

$$\Delta\sigma_h = \frac{\nu}{1-\nu}\ \gamma\Delta h$$

where $\Delta\sigma_v$ = Change in vertical effective stress.

$\Delta\sigma_h$ = Change in horizontal effective stress.

$\gamma$ = Unit weight of the sediment.

$\Delta h$ = Thickness of deposited sediment.

$\nu$ = Poisson's ratio.

For the case of the deposition of 421 m of sediment (density = 2.2 gm/cc) the change in vertical effective stress in the basement (Poisson's ratio = 0.30) is 1316 psi (92.5 kg/cm$^2$) and in horizontal effective stress is 564 psi (39.6 kg/cm$^2$). Change in effective stress due to a rise in the water table is tensional in nature and of a magnitude;

$$\Delta\sigma_v = \Delta\sigma_h = \gamma\Delta h$$

where $\Delta\sigma_v$ and $\Delta\sigma_h$ are as above.

$\gamma$ = Unit weight of water.

$\Delta h$ = Rise of the water table.

For a rise of 300 m, the change of both horizontal and vertical effective stress is -425 psi (-29.9 kg/cm$^2$).

An increase in temperature induced by sedimentation will produce compressional stresses. The magnitude of these stresses

are given by (Haxby and Turcotte, 1976);

$$\Delta\sigma_V = 0$$

$$\Delta\sigma_h = \frac{E\ \alpha\ \Delta T}{1 - \nu}$$

where $\Delta\sigma_V$ = Change in vertical effective stress.

$\Delta\sigma_h$ = Change in horizontal effective stress.

E = Young's Modulus of Elasticity.

$\alpha$ = Coefficient of thermal expansion.

$\Delta T$ = Temperature change.

$\nu$ = Poisson's ratio.

Haxby and Turcotte show that, if surface temperatures and geothermal gradients remain constant, an approximation to the change in temperature induced by sedimentation and erosion can be made using the thickness of the deposited or eroded blanket and the geothermal gradient. For example, in a region with a gradient of 25°C/km, deposition of 1 km of sediment would raise the temperature by 25°C. Using this geothermal gradient (a conservative estimate for San Luis Valley) a Young's Modulus of 5.0 ($10^6$) psi (Krynine and Judd, 1957), a coefficient of thermal expansion of 8.0 ($10^{-6}$) (Clark, 1966), and a Poisson's ratio of 0.30, deposition of 421 m (1380 ft) of sediment increases the horizontal effective stress by 180 psi (12.6 $kg/cm^2$). The total change in vertical effective stress due to the weight and thermal effect of sediment deposition and the pore pressure effect due to a rising water table is

891 psi (62.6 $kg/cm^2$) compression, and the change in horizontal effective stress is 319 psi (22.4 $kg/cm^2$), also compressional.

To understand the relationship these stress changes have to changes in stability of the Sangre de Cristo Fault, we use the graphical Mohr's envelope of failure, based on Mohr's criteria of failure, as seen in Figure 32. Failure occurs when the circle defined by the maximum and minimum stresses reaches tangency (Fig. 32a) with the line defined by;

$$\tau = c + n \tan \phi$$

where $\tau$ = Shear stress across the plane of failure.

$c$ = Cohesion of the surface (= 0 for a fault with previous movement).

$n$ = Normal stress across the plane of failure.

$\phi$ = Angle of internal friction

Figure 32b shows the original stress configuration at an arbitrary depth along the Sangre de Cristo Fault, along with the stresses induced by subsequent changes. The stresses induced by the geomorphic processes since Pleistocene time tend to move Mohr's circle away from the envelope of failure, thereby increasing the stability of the fault zone.

This type of analysis, however, gives only the direction that geomorphic changes tend to affect the stress distribution. The underlying assumption in using the elastic response to sedimentation processes is that lateral strain is zero, a condition that is not strictly met in San Luis Valley. Movement along the Sangre de Cristo Fault has occurred since deposition of the lacustrine clays, so some of the horizontal stress has

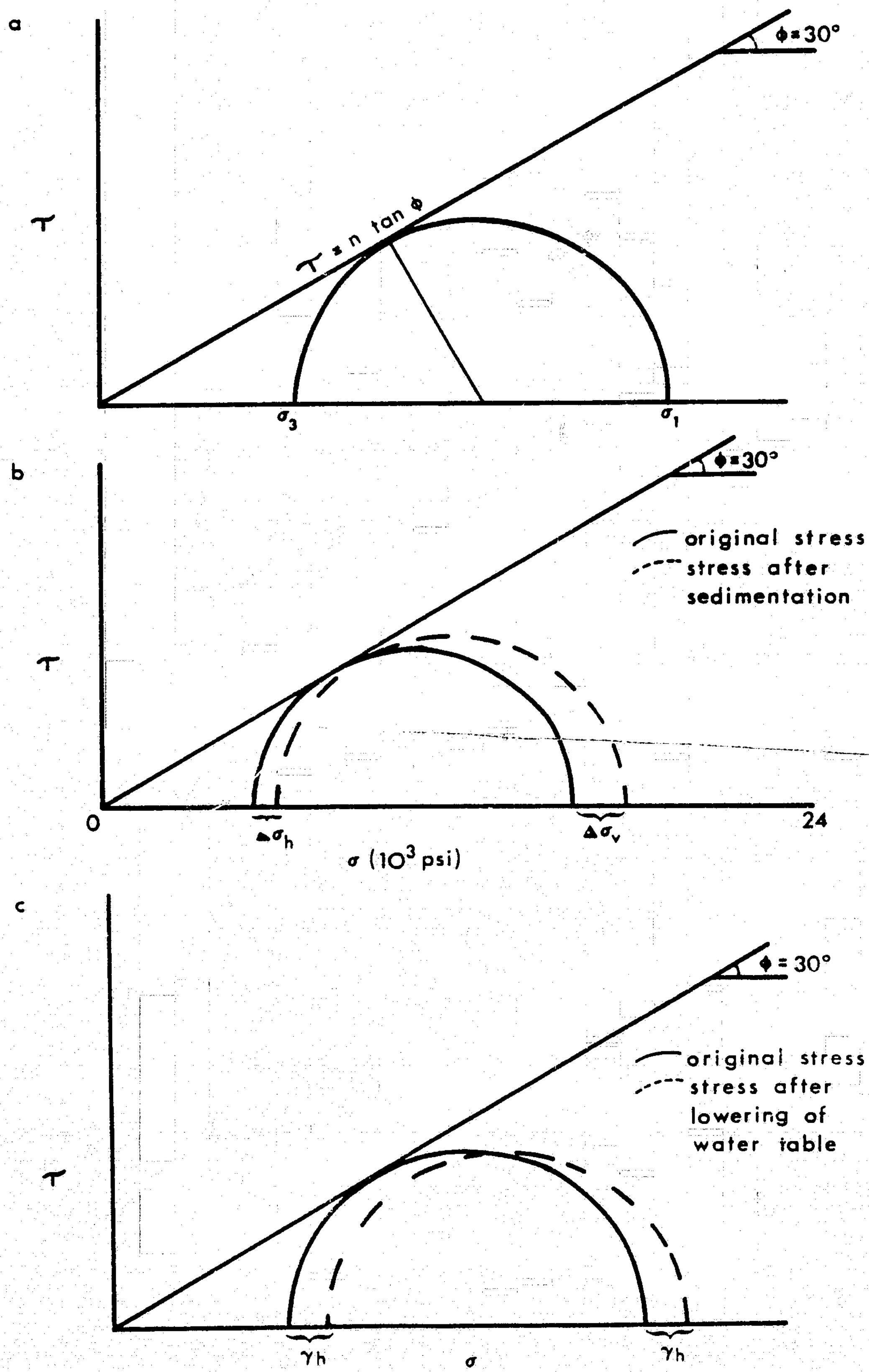


Figure 32: Mohr's Criteria of Failure, a) Stress conditions at tangency. b) Changes in stress due to sedimentation and water table rise. c) Changes in stress due to decreasing ground water levels.

been relieved by extensional movement in the crust. Perhaps more important, this analysis does not take into account changes in stress distribution due to tectonic stresses. The analysis does indicate, however, that modern processes are tending toward stability. The youngest alluvial fan has been offset by the Sangre de Cristo Fault, so activity continued at least to within 5000 years ago. It is likely that water table elevations were much higher in the wetter Pleistocene than today. Progressive decrease in water table elevation alone tends to make the valley more stable with respect to fault activity. The effective stress law is;

$$\sigma_e = \sigma_T - p$$

where $\sigma_e$ = Effective (or grain-to-grain) stress.

$\sigma_T$ = Total stress.

p = Pore pressure.

A decrease in pore pressure (lowering of the water table) increases effective stress equally in all directions and, as seen in Figure 32c, increases stability. Recent lowering of the water table and piezometric surface in San Luis Valley tend to continue this trend. The analysis indicates therefore, that if extensional tectonic stresses have relaxed, the hydrologic and sedimentologic changes tend toward increased stability of the normal faults in San Luis Valley.

## CONTROL OF PERMEABILITY

As discussed previously, secondary fracturing is the only source of permeability in the rocks found in the Sangre de Cristo Mountains. Fracturing is related to faulting, to folding, and to stress relief by erosion of rock and melting of Pleistocene glaciers and shows little identifiable relation to rock type. Fracturing is found parallel and perpendicular to fold axes and along bedding planes in folded areas. Numerous springs are associated with bedding plane fractures, dominantly in the coarse clastic and conglomeratic Permian-Pennsylvanian rocks. Slippage along bedding planes in these rocks juxtaposes bedding-plane irregularities caused by pebble to cobble-size clasts that are more resistant to fracturing than the surrounding matrix. This juxtaposition of bedding-plane irregularities produces open fractures of moderate permeability.

Faulting plays an important role in increasing the frequency and permeability of fractures in the Sangre de Cristo Mountains, though, in most cases, major faults themselves tend to be relatively impermeable. Faults with significant displacements frequently are filled with fault gouge, particularly those faults that have experienced high stresses normal to the failure surface, such as reverse faults. Another cause for the relative impermeability of major faults is infilling with secondary veins. The Sangre de Cristo Fault may be good example of this, with quartz mineralization and old mining prospects found frequently along the trace of the

fault. Numerous cold water springs are found along the trace of this fault, suggesting that it represents a barrier to ground water flow due to the development of gouge, secondary mineralization, or a combination of the two.

Subsidiary fractures associated with major faults, but without significant displacement and no fault gouge development, are significant conduits of ground water. These subsidiary fractures generally have the same strike as the controlling faults, but dips may vary widely from that of the controlling fault. Using the strikes of major faults as a directional criterion, permeability associated with faulting is dominantly oriented northwest.

Important fracturing in the Sangre de Cristo Mountains is caused by relief of stress due to erosion. These fractures are oriented parallel to the modern drainages and thus serve as the major conduits for ground water recharge from the Sangre de Cristo Mountains to San Luis Valley. Fracturing may be caused either by relief of lithostatic stresses by erosion of deep canyons, or by relief of residual stresses stored in the elastic rock medium from early tectonic events.

Fracture permeability in the San Juan Mountains is dominantly primary, but secondary fracturing increases the permeability of primary fractured rock masses and may be the only source of permeability in rocks such as flow breccias and agglomerates. Faults in the San Juan Mountains are all normal faults, and separations are small. Maximum separation on the

Sheep Creek Fault (T. 45 N., R. 5 E.), the most pervasive and significant fault in this hydrologic region, is on the order of 90 m (300 ft). There is no evidence that faulting of this magnitude acts as a barrier to ground water movement because of the development of fault gouge, both because of the low stresses perpendicular to the failure surface in a normal fault environment and because of the small displacements of these faults. Fracturing is more intense in the vicinity of faults, and faults are therefore areas of increased permeability in the competant brittle volcanic rocks of the San Juan Mountains.

Several types of information suggest that faults in the alluvium of San Luis Valley elevate ground water levels upgradient of the fault. Cold springs are associated with the Sangre de Cristo Fault, not only in basement rock, but more commonly in alluvium. Wychgram (1972) identified several portions of the Villa Grove Fault Zone as areas of increased soil moisture upgradient of fault scarps. Stream seepage measurements along Willow Creek showed anomolously low seepage rates upstream of a segment of the Sangre de Cristo Fault, possibly because of an elevated water table upgradient of the fault scarp. Wells drilled at Great Sand Dunes National Monument have much shallower ground water levels upgradient of the Sangre de Cristo Fault than downgradient (Fig. 33).

There are four possible explanations for the effect of the Sangre de Cristo and Villa Grove fault zones upon ground

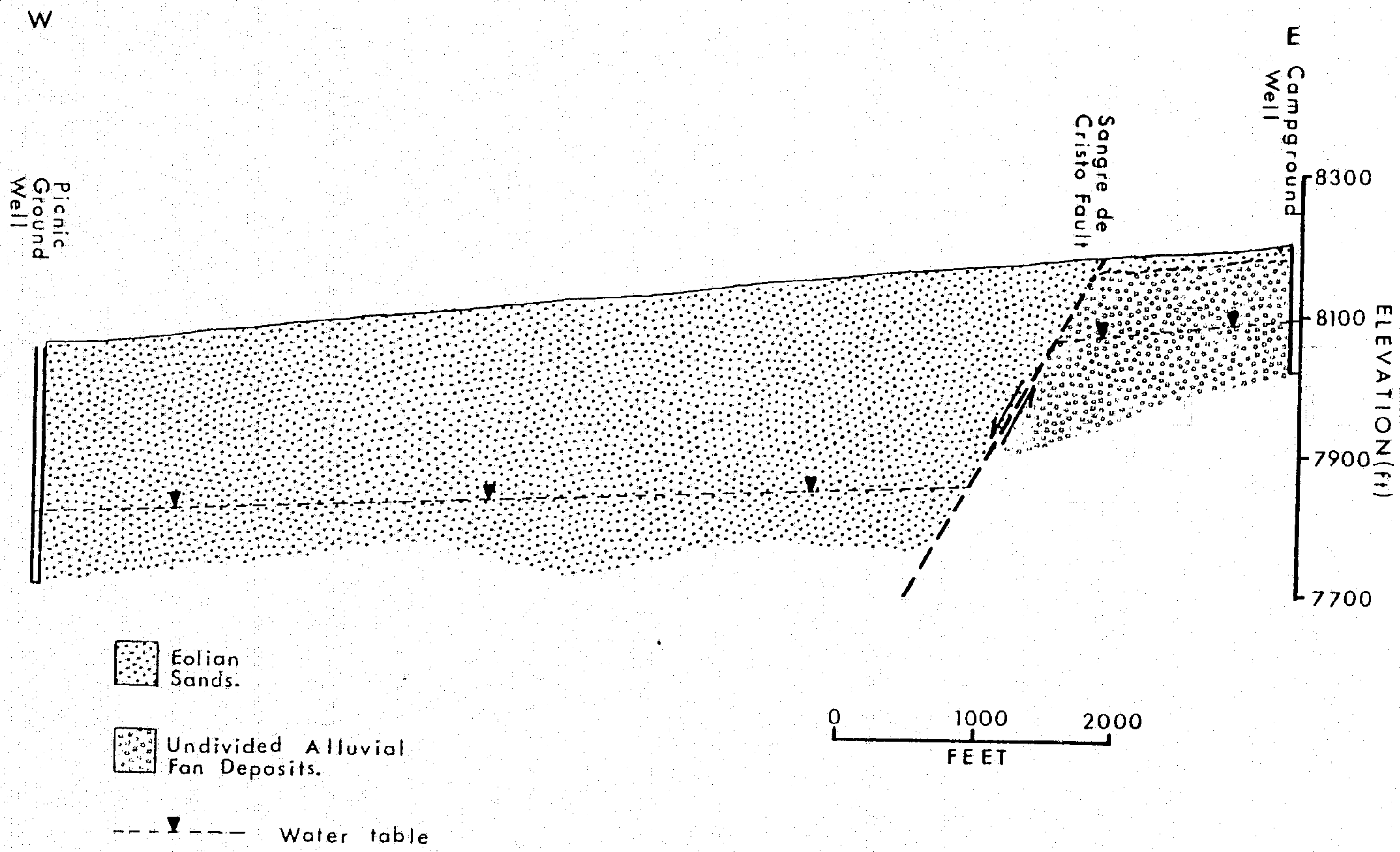


Figure 33: Hydrogeologic cross-section within Great Sand Dunes National Monument.

water levels; 1) upwelling of confined water along the fault zones, 2) juxtaposition of impermeable beds downgradient of the fault against permeable beds upgradient of the fault, 3) ground water cascading from an area of shallow basement rock to an area of deep basement rock, and 4) development of gouge along the fault zone, ponding ground water upgradient of the fault.

Both ground water chemistry (discussed later) and piezometric data (Plate 5) show that the source of water for the cold springs along the Sangre de Cristo Fault is shallow, unconfined water, so upwelling of confined water along the fault is not a viable mechanism. Though stratigraphic control is not sufficient to completely discount juxtaposition of aquifers and aquitards across the fault, no thick sequences of clay are known in the vicinity of any of the fault scarps, other than the Alamosa Formation clays. To juxtapose these clays against aquifers upgradient of the fault scarps, fault motion would have to be opposite that implied by surface and subsurface geologic and geophysical data. At Great Sand Dunes National Monument eolian sands and fluvial gravels are present to significant depths near the fault, eliminating juxtaposition of aquifers and aquitards as a mechanism for this site.

Cascading of ground water from areas of shallow basement to areas of deep basement likely accounts for some of the springs along the Sangre de Cristo Fault, particularly where its trace is very near the mountian/valley boundary. A gravity

profile (Fig. 34a) across the fault trace at Great Sand Dunes National Monument shows the flexture of the gravity curve located over the fault scarp, indicating that the surface scarp represents the trace of the fault, and that basement rock is relatively shallow upgradient of the fault.

In other areas in San Luis Valley, most notably along the Villa Grove Fault Zone, cascading of water over a basement step is not likely to be the explanation of shallow ground water upgradient of faults. Two gravity profiles (Fig. 34b, c) across different parts of the Villa Grove Fault Zone show steep gravity slopes both upgradient and downgradient of the fault zone, suggesting that basement rock is relatively deep above and below the fault. Though the gravity profiles show that there is significant basement relief across the fault scarp, the deep basement upgradient of the fault makes cascading of water over a basement scarp an unlikely explanation for a sharp change in ground water depth.

Williams (1970) documented extensive development of gouge along faults in the alluvium of Owens Valley in California. Surface outcrops of faults, the texture of the alluvial material, and the occurrence of shallow ground water upgradient of the fault scarps are very similar to that of San Luis Valley, and it is believed that gouge along faults in San Luis Valley is similarly ponding ground water. This mechanism also likely contributes to shallow ground water levels in areas where basement rock is shallow upgradient of the fault.

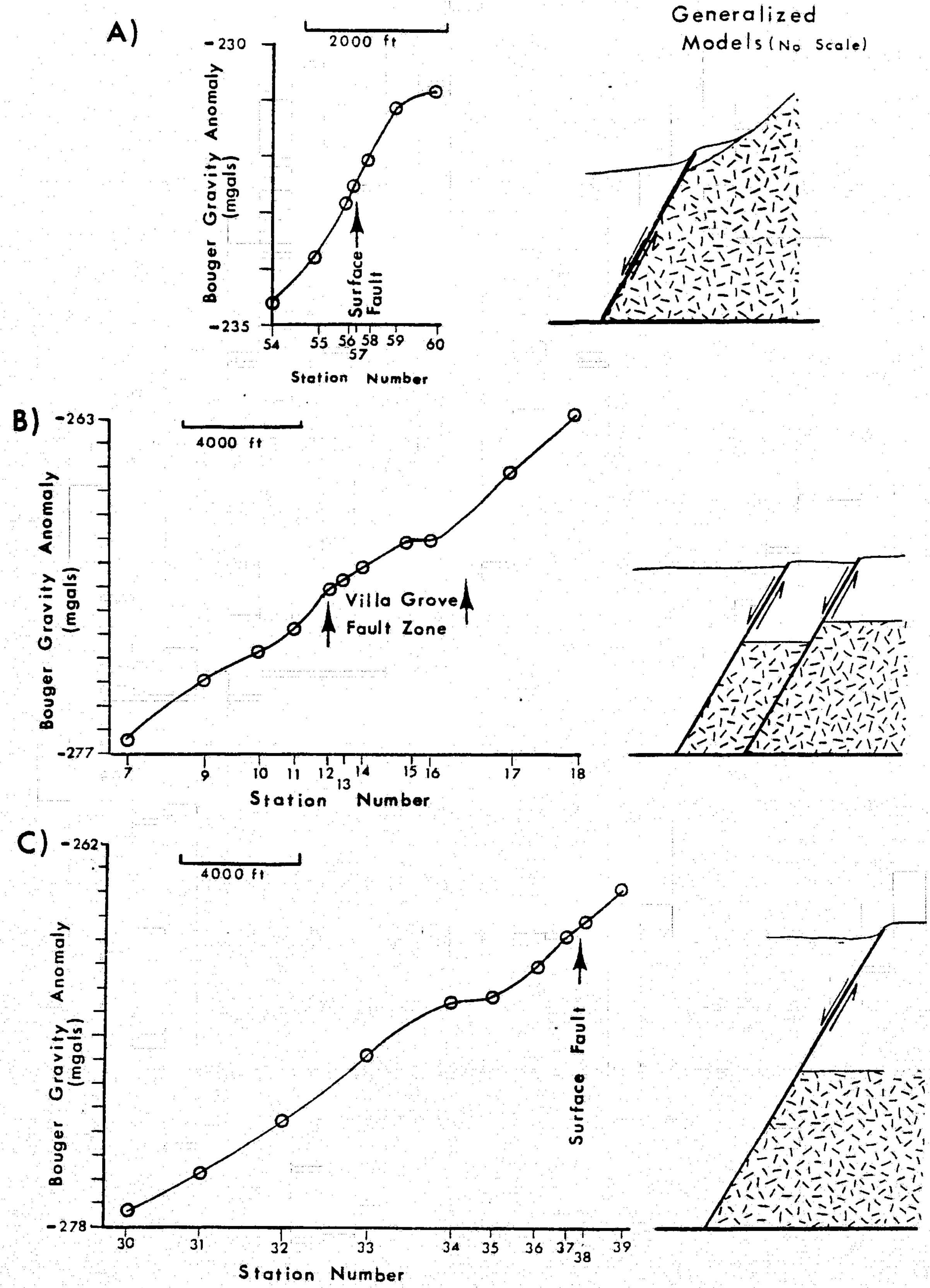


Figure 34: Gravity profiles across major faults, San Luis Valley. Stippled pattern in models represents basement rock, while blank areas represent valley-fill sediments. See Plate 8 for location of stations.

GEOLOGIC HISTORY

Knepper (1974) outlines seven stages in the tectonic development of a region that includes the northern third of the closed San Luis Basin: 1) Precambrian deformation, metamorphism, and plutonism. 2) Tectonic quiescence through Mississippian time. 3) Block faulting in Permian and Pennsylvanian time. 4) Mesozoic subsidence and sediment deposition. 5) Folding, faulting and igneous intrusion during the late Mesozoic to early Tertiary Laramide orogeny. 6) Volcanic activity in the Oligocene. 7) Uplift during the Cenozoic. Using this framework, we can follow the history of the northern San Luis Valley that is of importance to the hydrogeology of the basin.

Early Paleozoic time (through Mississippian time) was a period of relative tectonic quiet, dominated by marine sedimentation in the areas now occupied by the Sangre de Cristo Mountains and portions of the San Juan Mountains (near Kerber Creek). The position now occupied by San Luis Valley and the southern San Juan Mountains either was an upland at this time, and did not receive sediment, or sediment was later eroded. Permian and Pennsylvanian time was one of uplift of the Uncompahgre Highland west of a fault that parallels the Sangre de Cristo and Villa Grove fault zones. Thickness and facies of sediment deposited north and east of this boundary fault was strongly controlled by the fault.

There is little or no evidence for interpreting Mesozoic history in the basin. It is likely that areas that formed the Uncompahgre Highland in Paleozoic time continued to remain high through much of the Mesozoic. Limited outcrops of Cretaceous shoreline deposits (Dakota Sandstone) suggest that the northwestern part of the basin may have received marine and coastal non-marine sediment. Extensive compaction and cementation of Paleozoic sediment is the most significant early Mesozoic event in terms of hydrogeology.

The end of the Mesozoic and beginning of the Tertiary was a period of crustal compression, producing folds and reverse faults in the Sangre de Cristo Mountains and igneous intrusion in the area of Mount Blanca.

Cenozoic history of the basin is dominated by extensional tectonics and vulcanism. Though Epis and Chapin (1975) show abundant evidence for a broad Paleocene-Eocene erosional surface north and east of the San Luis Basin, there is little evidence for such a surface in the basin. An outlier of Oligocene volcanic rock overlies the pediment surface near Poncha Pass, suggesting such an erosional surface, and Knepper (1974) has suggested that Hayden Pass may be part of this surface. The presence of a thick, fault-controlled, pre-volcanic section within San Luis Valley indicates that San Luis Valley had its inception during the time period that an erosional surface was forming elsewhere. Knepper (1974) presents evidence that, in Miocene to Pliocene time, the upper

Arkansas Graben and the San Luis Graben were separated by a topographic barrier a short distance north of Villa Grove. This author believes it consistant with geologic evidence that the Villa Grove Fault Zone was that barrier, and that any Paleocene-Eocene erosional surface was restricted to regions north of the Villa Grove Fault, with deposition of clastic debris occurring south of the Villa Grove Fault Zone.

Oligocene through Miocene time was marked by some intrusive activity in the Sangre de Cristo Mountains and San Luis Valley and by extensive volcanic and associated intrusive activity in the San Juan Mountains. Lipman and others (1970) summarize the volcanic history of the San Juan Mountains as a succession of early intermediate lava flows and flow breccias followed by more silicic ash-flow tuffs and finally by the youngest flows, a bimodal association of basalt and rhyolite. Welding of the ash-flow tuffs and jointing of the lava flows and welded ash-flow tuffs have produced fracture permeabilities on the same order of magnitude as the intergranular permeabilities of the alluvial fill of San Luis Valley.

Normal faulting in the San Luis Basin has continued to the Holocene, at least along the Sangre de Cristo Fault. Movement of a central horst in San Luis Valley ceased prior to deposition of Plio-Pleistocene lacustrine clays. Sediment deposition continued to be controlled by normal faulting to Pleistocene time. Deposition of Pleistocene-Holocene alluvial fans appears to have been controlled more by climate than tectonic activity.

## WATER CHEMISTRY

The composition of ground water is a function of the composition of the water recharging the aquifers, the length of time the water is in contact with the porous medium, the mineral composition of the porous medium, and the temperature and pressure of the ground water. As such, the water chemistry is important both in terms of the quality of water with respect to the intended use and as a tracer of ground water movement.

To obtain information on both of the above aspects of ground water chemistry, 123 samples were collected of surface and ground water from San Luis Basin to augment 141 analyses chosen from Emery and others (1972). Temperature and pH of each sample collected by this author was measured at the time of collection using either a thermister probe or a standard mercury thermometer and a battery-operated pH meter. The samples were analyzed for the eight major anions and cations, plus flouride, iron, and silica within 10 and usually within 5 days of collection. Specific conductance of each sample was also determined at this time using a laboratory conductance meter.

Concentrations of sodium and potassium ions were determined using a flame photometer, calibrated with standards of sodium and potassium. Silica, iron, sulphate, and flouride were determined by colorimetric methods. Concentrations of all other ions were determined titrametrically. Chemical analyses for the samples collected by this author, as well as

those used from Emery and others (1972) are given in Appendix B. The locations of the samples used in this study are shown in Plate 7.

## GENERAL DESCRIPTION

Although many schemes for the chemical classification of water exist, one of the most commonly used is the Piper diagram. On the Piper diagram, water is plotted according to the relative abundance of 6 groups of major cations and anions. Water can then be classified by its hydrochemical facies (Back, 1966) by the region within which it plots (Fig. 35). Classification is based only on relative proportions of the major anions and cations and does not contain information about the quantity of dissolved solids. Several authors (Back, 1966; Charron, 1969) have related changes in hydrochemical facies to direction of ground water flow, length of flow path, the length of time the water is in contact with the porous medium, and the chemical composition of the porous media. Chebotarev (1955) presented abundant evidence for a change in ground water types away from the source of recharge. He found that most surface and ground water near its source of recharge is calcium bicarbonate type. Away from the source of recharge there is a change in anion facies of;

$$HCO_3 \rightarrow HCO_3 + Cl \rightarrow Cl + HCO_3 \rightarrow Cl + SO_4 \text{ or } SO_4 + Cl \rightarrow Cl,$$

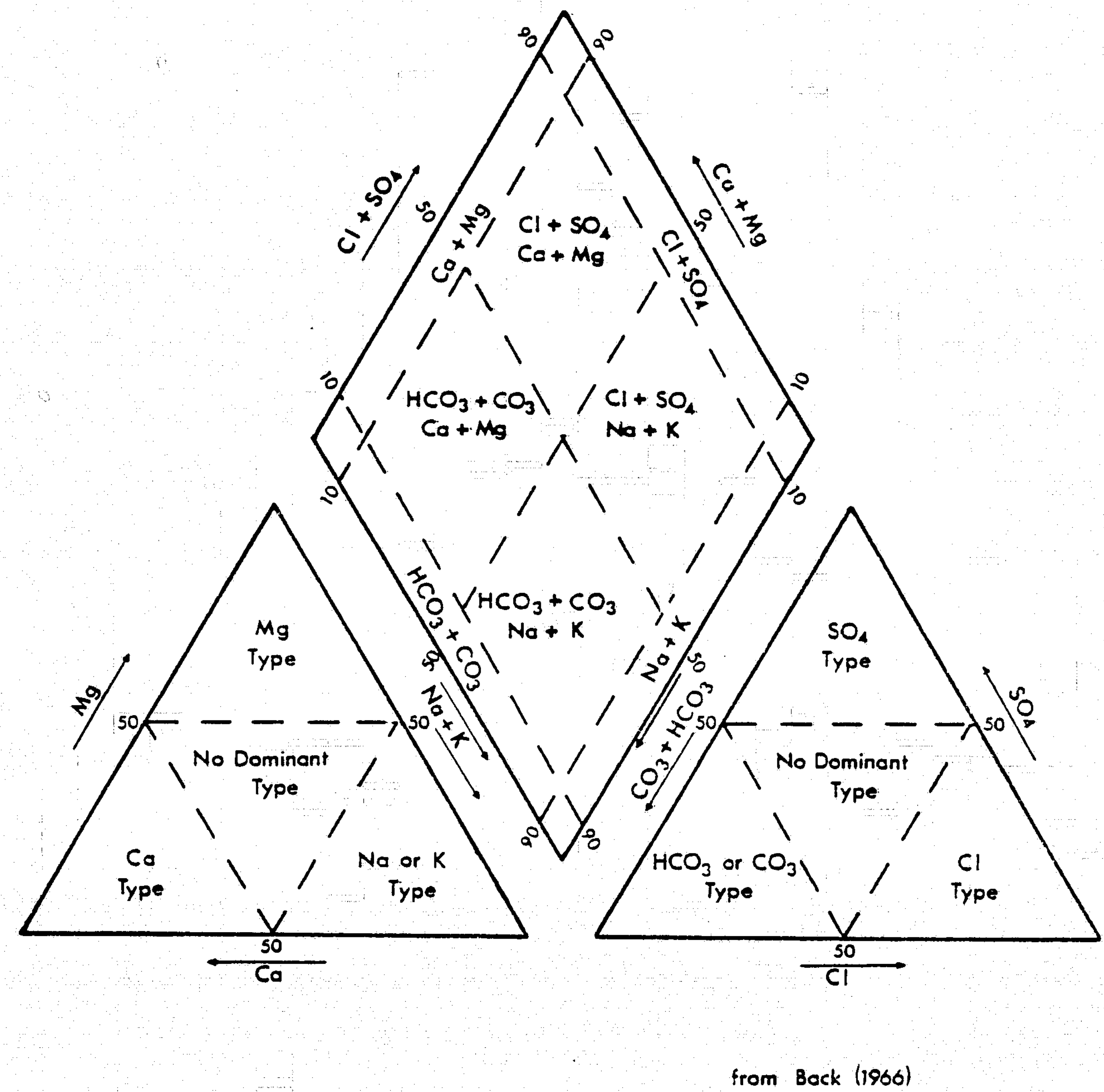


Figure 35: Piper diagram, showing compositions of hydrochemical facies. Compositions plotted by % epm.

and a change in cation facies of;

$Ca + Mg \rightarrow Ca + Na \rightarrow Na + Ca \rightarrow Na + K$.

Ground water therefore tends to change from calcium bicarbonate type water to water approaching the composition of sea water. Changes of this sort are similarly observed in the San Luis Basin.

Surface water in both the San Juan and Sangre de Cristo mountains is dominantly calcium bicarbonate (Figs. 36, 37). Surface water in the San Luis Valley varies from calcium bicarbonate to sodium sulfate type water, depending upon the distance from the valley perimeter and the source of the water. In the unconfined aquifer, (Fig. 38) although the major anion is usually bicarbonate, the dominant cation can be either calcium or sodium, suggesting that the cation chemistry is much more sensitive to changes along the flow path than is anion chemistry. Sodium type water is more common in the confined aquifer (Fig. 39) than in the unconfined aquifer and surface water. There is proportionately less sulfate in water samples of the confined aquifer than in the unconfined aquifer, suggesting either that the increase in sodium is due to some mechanism other than gradual change along the flow path, or that sulfate concentration is being buffered.

Comparison of Piper plots from different environments indicates that there are relatively regular changes from one flow system to another, particularly notable in changes in the dominant cation. Surface water is calcium bicarbonate, while

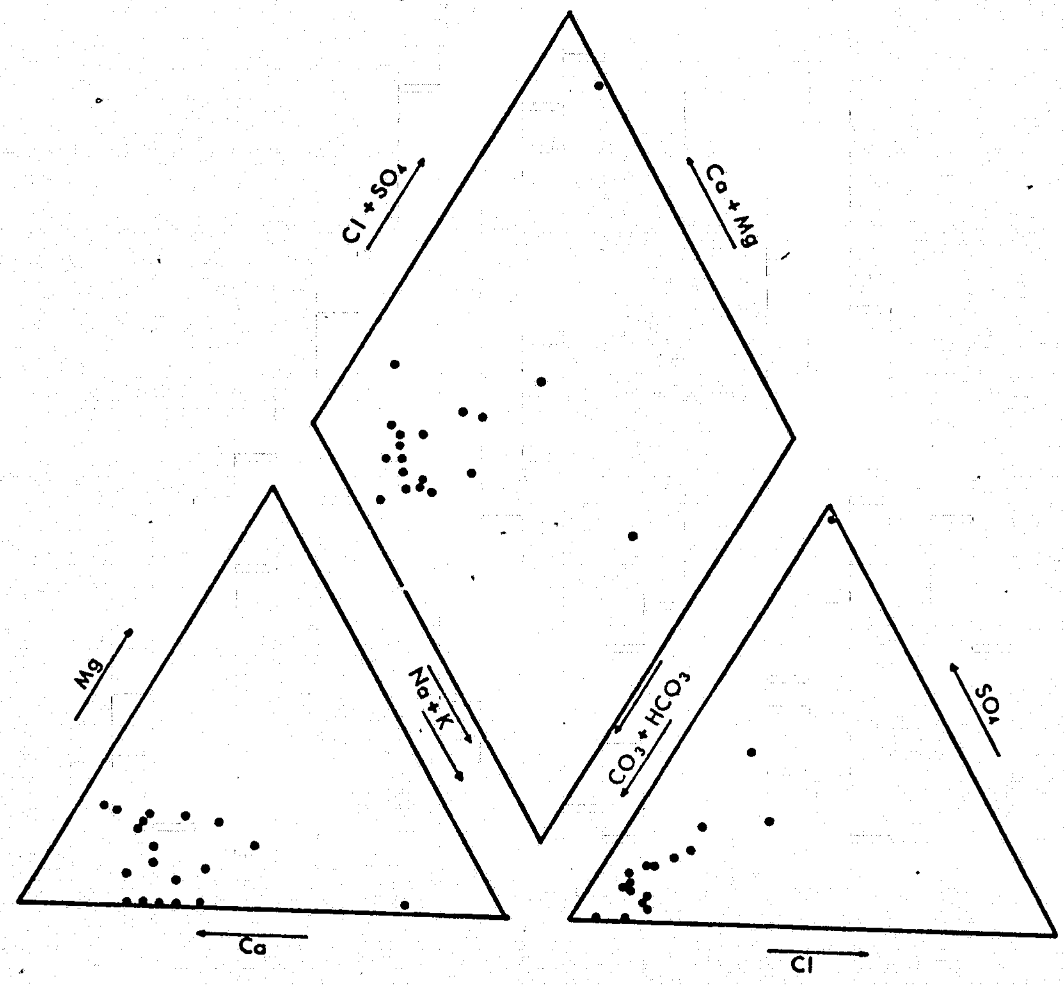


Figure 36: Surface water, San Juan Mountains (18 samples).

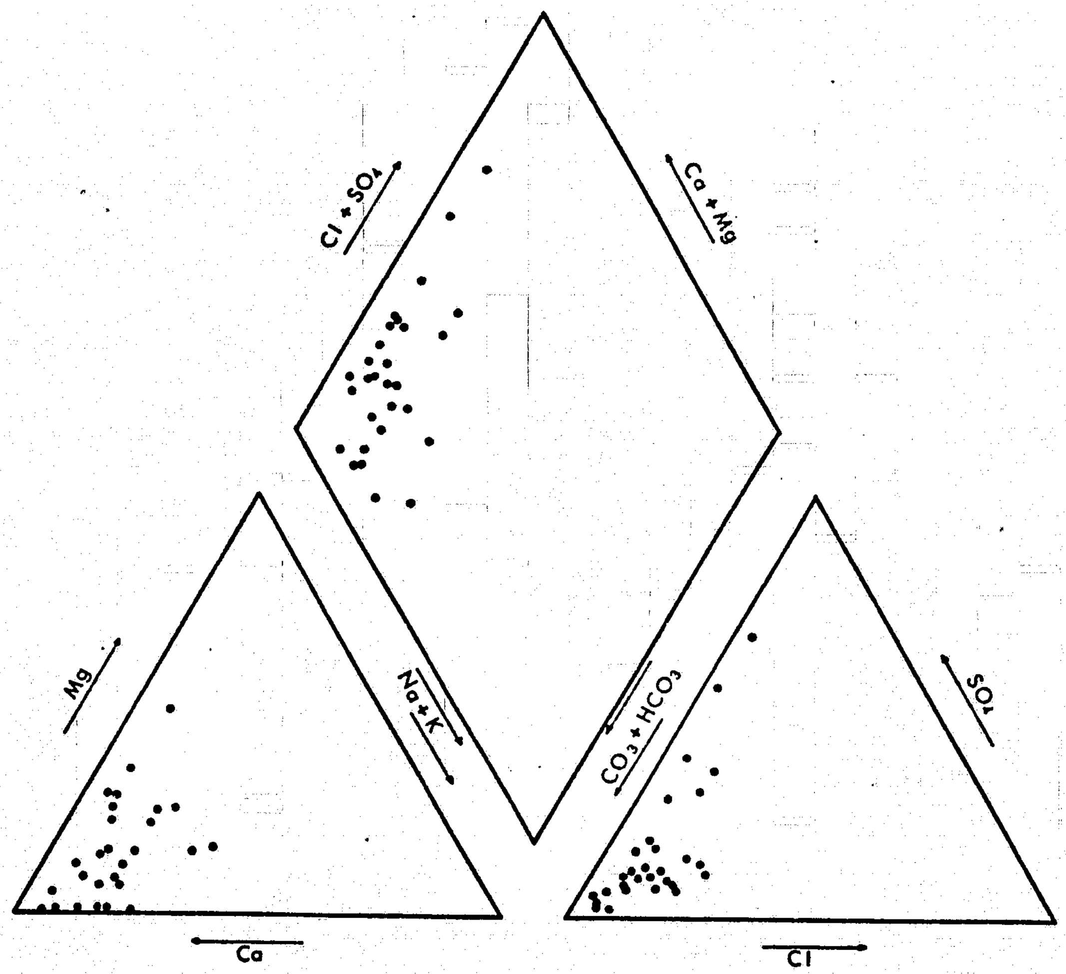


Figure 37: Surface water, Sangre de Cristo Mountains (29 samples).

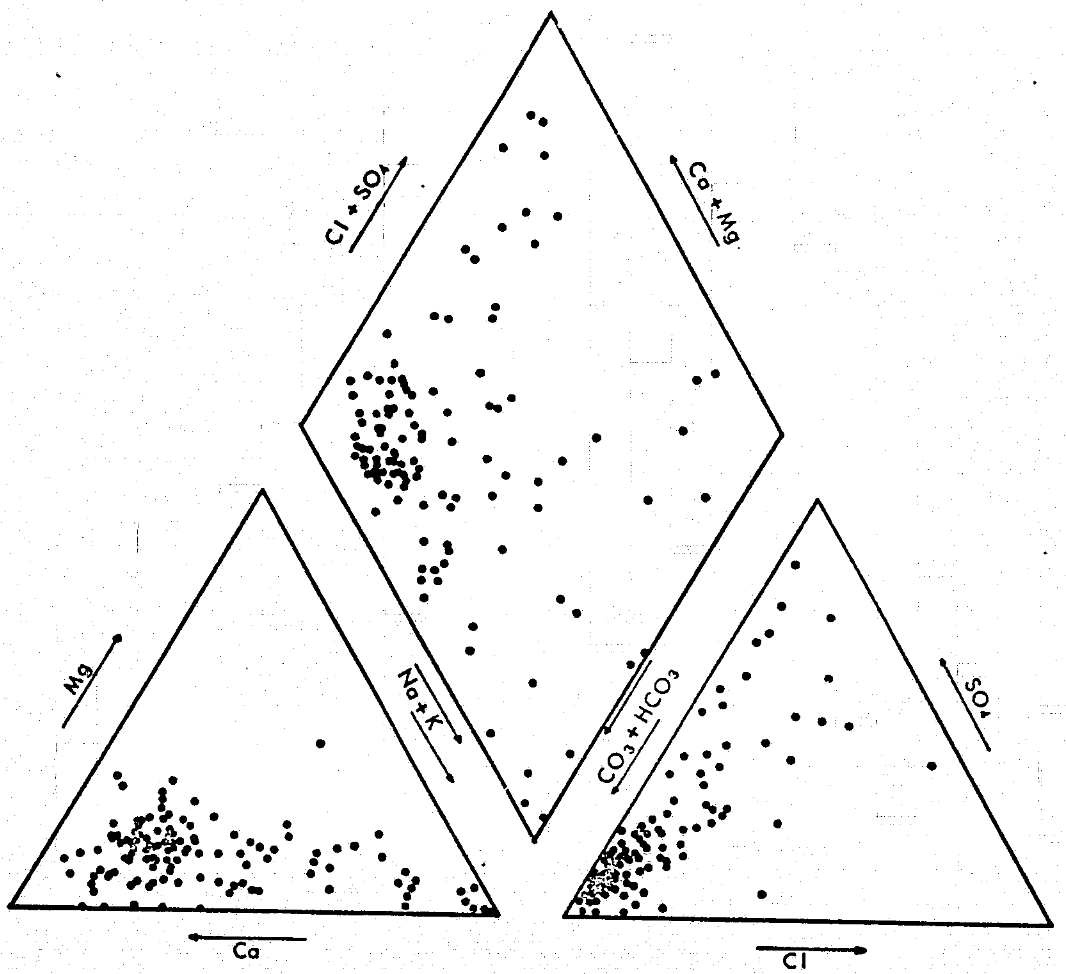


Figure 38: Water from unconfined aquifer, San Luis Basin (122 samples).

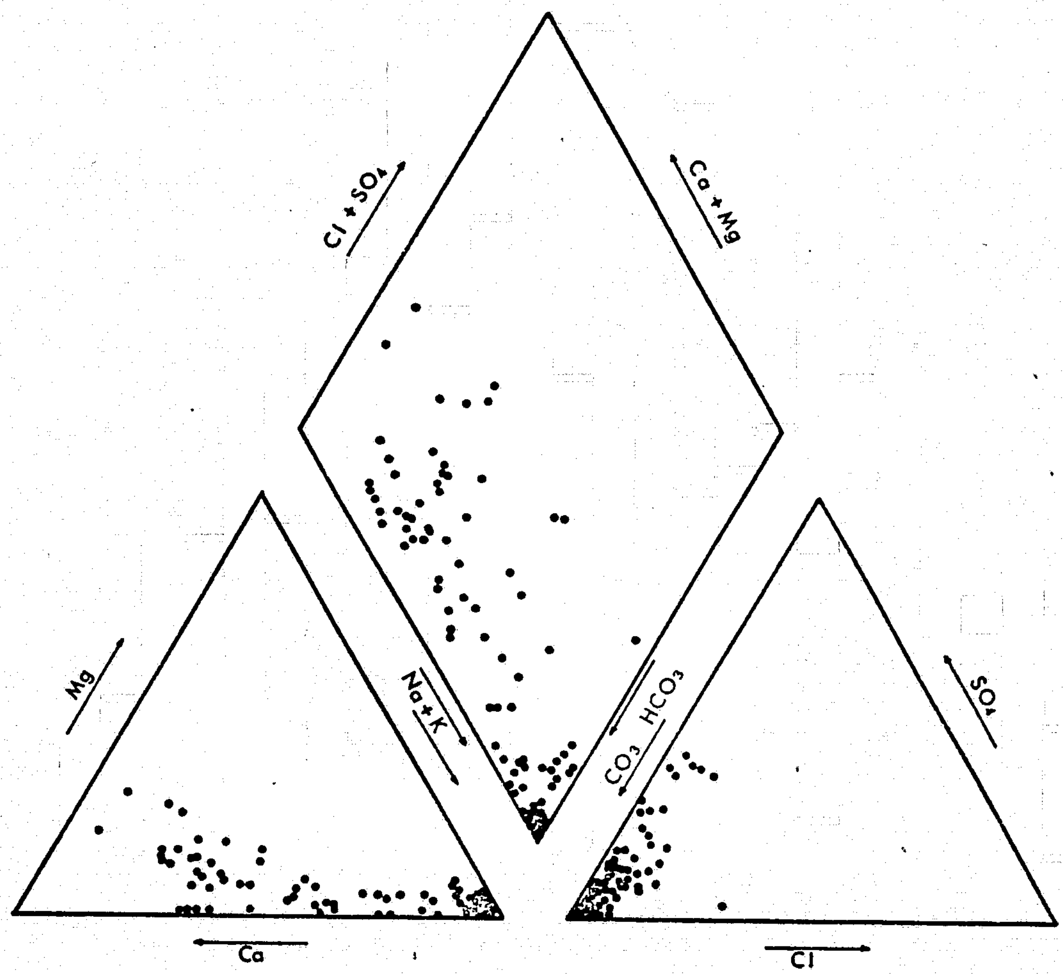


Figure 39: Water from confined aquifer, San Luis Basin (98 samples).

shallow ground water is a mixed assemblage of calcium or sodium bicarbonate, with some sulfate waters found. The deepest waters in the basin, those of the confined aquifer, are more sodium enriched than surface or shallow ground waters. This succession suggests a constant increase in the relative concentration of sodium as water flows from the surface to depth. An example of the use of this concept of hydrochemical facies is in attempting to find the source of water for the numerous springs along the Sangre de Cristo Fault. As noted previously, these springs may be from either shallow ground water from the Sangre de Cristo Mountains or from deep confined ground water flowing upward along the fault zone. A comparison of the distribution of water types from the surface springs (Fig. 40) and from the confined aquifer (Fig. 39) shows very little similarity. Water from the surface springs is calcium bicarbonate or calcium sulfate, similar to the water types of the unconfined aquifer, indicating a shallow origin for the spring water.

## WATER QUALITY

Quality of water for drinking and irrigation is a function of both absolute and relative concentrations of dissolved ions. The distribution of total dissolved solids is shown in Figures 41 and 42, for shallow and deep water, respectively. Most of the water in both aquifers is suitable for general household use as well as irrigation (less than 500 ppm (Davis and DeWeist,

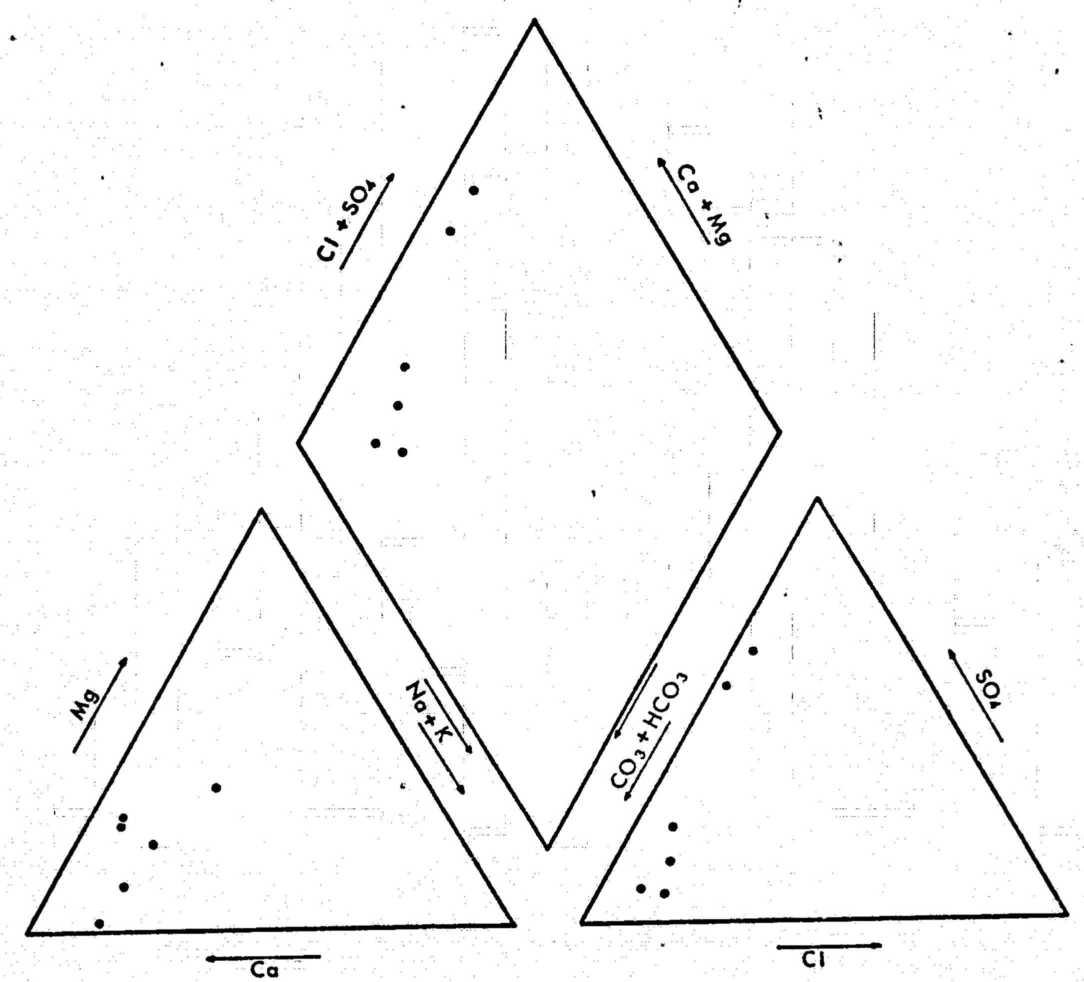


Figure 40: Water from springs along Sangre de Cristo Fault (6 samples).

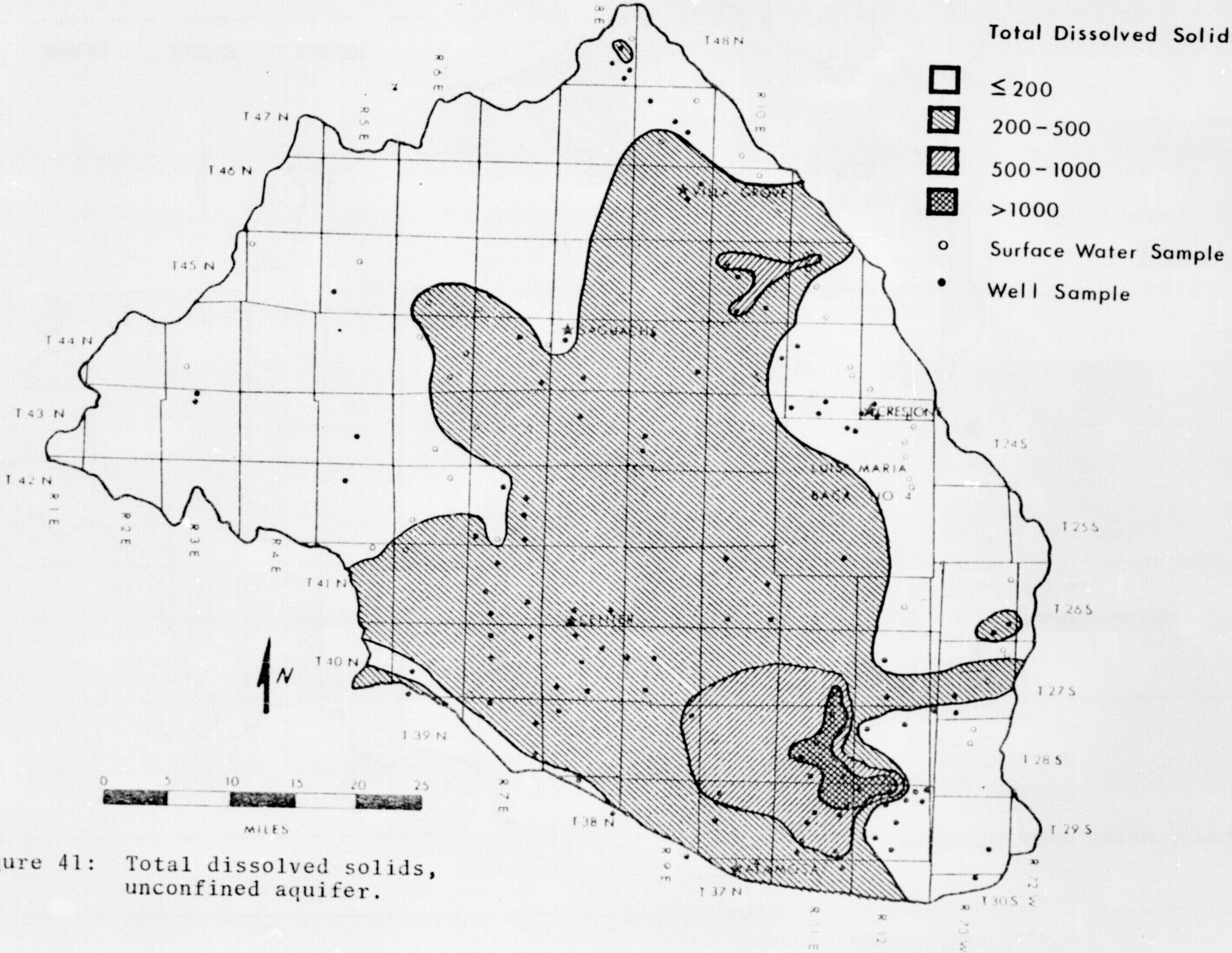


Figure 41: Total dissolved solids, unconfined aquifer.

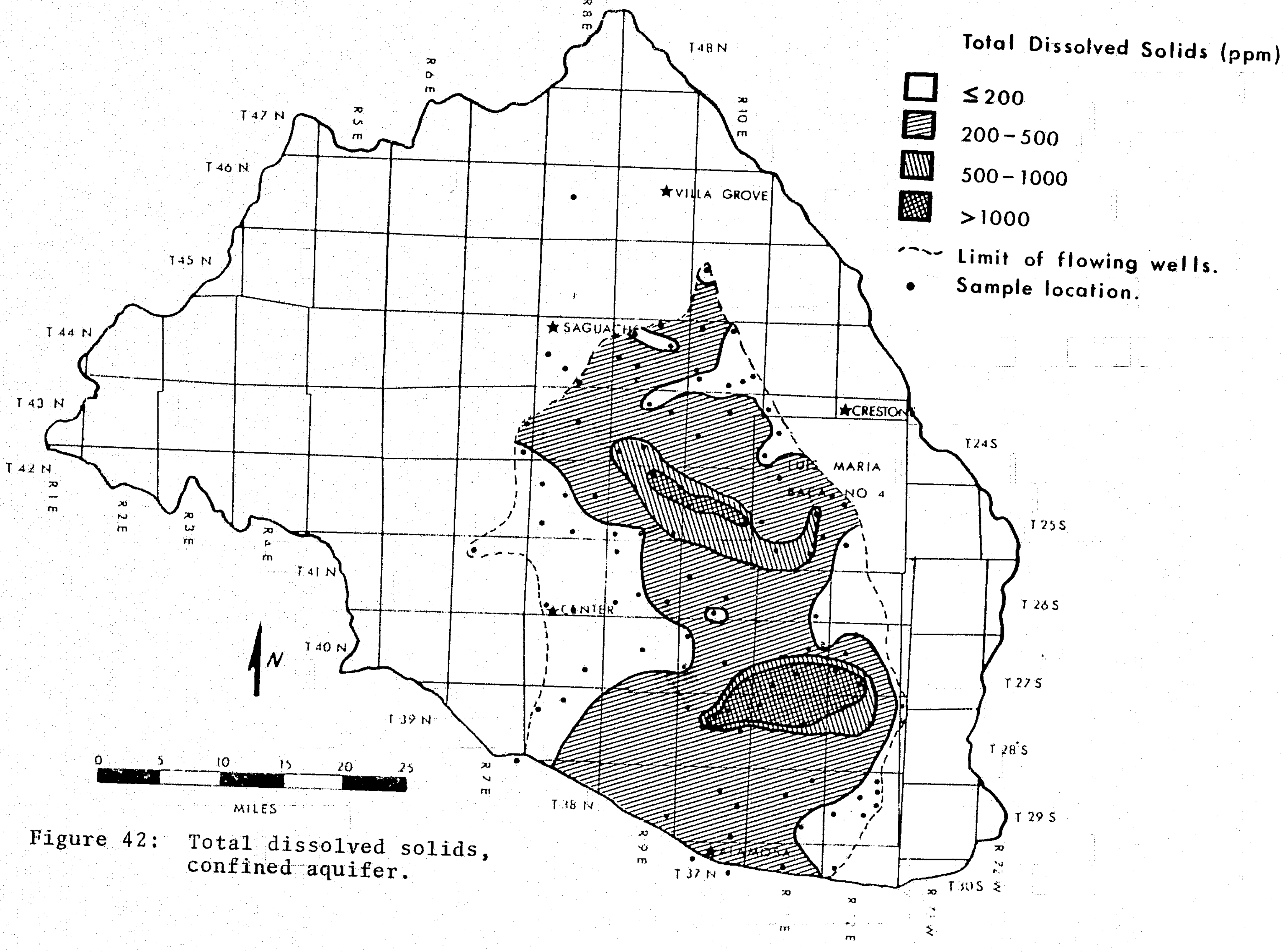


Figure 42: Total dissolved solids, confined aquifer.

1966, p. 121)). High concentrations of dissolved solids are found in both aquifers in the sump area of San Luis Valley due to concentration by evapotranspirative discharge. In the vicinity of the town of Center, total dissolved solids concentrations are higher in the unconfined aquifer than in the confined aquifer because of irrigation.

A property of water that is of considerable interest for household use is hardness, conventionally expressed as ppm of calcium carbonate. Water hardness decreases the effectiveness of soap and results in incrustation of metal well screens and pipe fittings. Water that has a hardness of less than 50 ppm is considered to be soft, while water sometimes requires softening with concentrations between 50 and 150 ppm. 150-300 ppm concentrations usually need water softeners for washing purposes, and concentrations over 300 ppm nearly always require water softening for household uses (Johnson, 1966, p. 68). Hardness is rarely a problem with water from the confined aquifer (Fig. 44), while water in the unconfined aquifer (Fig. 43) is excessively hard in several areas. The low degree of hardness in the confined aquifer is related to the processes of hyperfiltration and ion exchange in the clay membranes of the aquifer. The most extensive areas of hard water in the unconfined aquifer are caused by evapotranspirative discharge of shallow ground water. Less extensive areas appear to correlate with regions of outcropping carbonate rocks in the Sangre de Cristo Mountains.

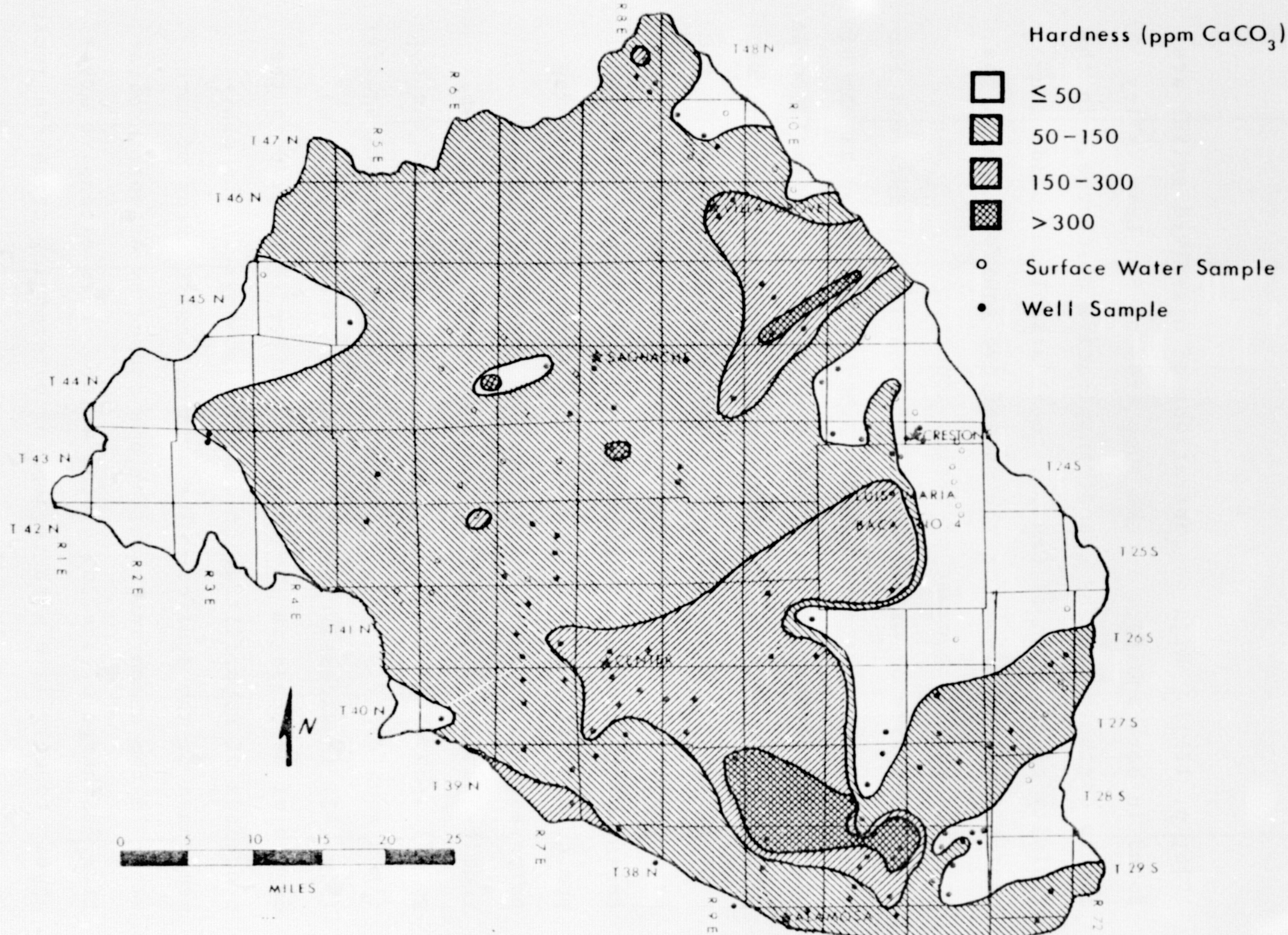


Figure 43: Water hardness, unconfined aquifer.

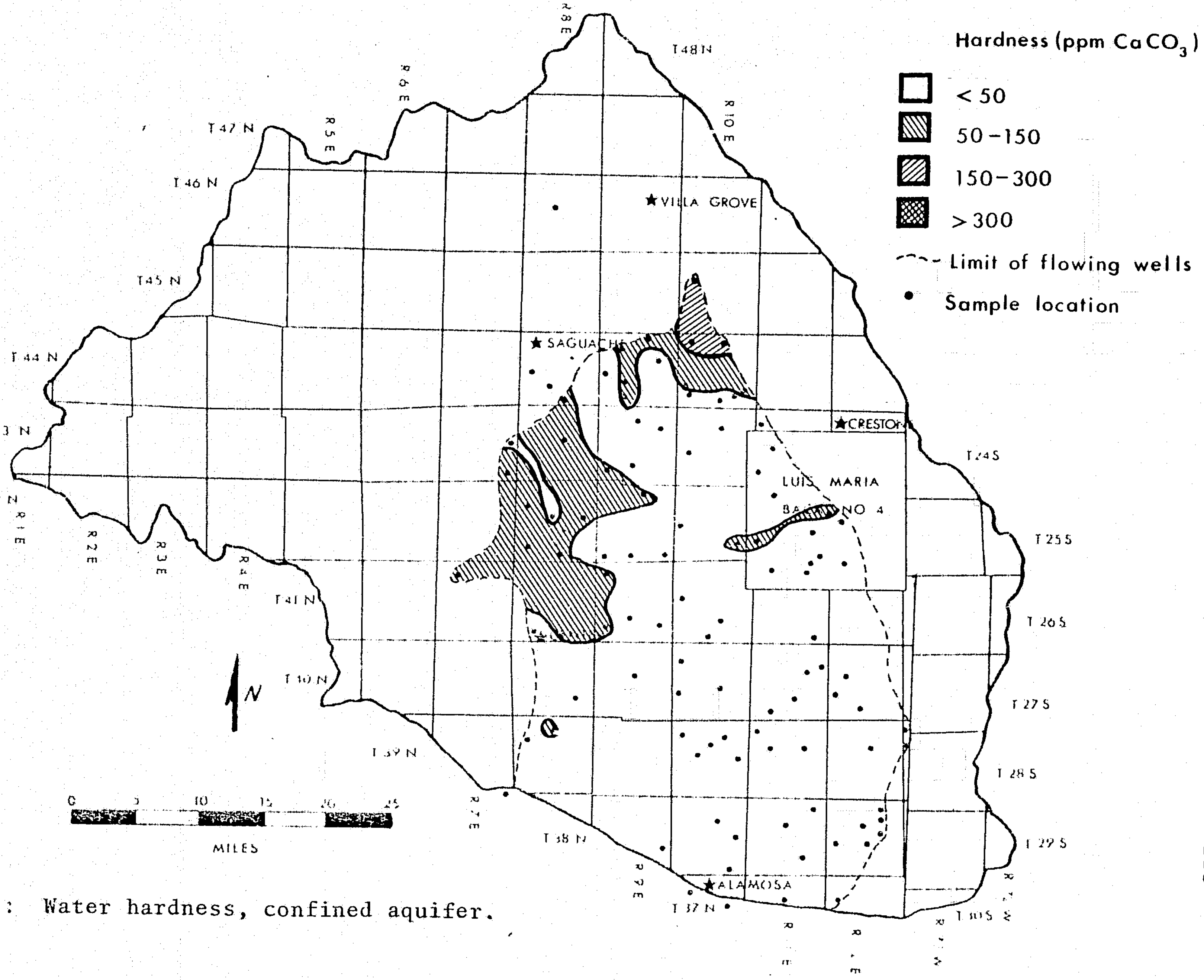


Figure 44: Water hardness, confined aquifer.

REPRODUCIBILITY OF THE ORIGINAL PAGE IS POOR

Problems with excessively high concentrations of flouride (Fig. 45a) in the confined aquifer and nitrate (Fig. 45b) in the unconfined aquifer are also encountered in San Luis Valley. Emery and others (1973) consider flouride concentrations above 1.3 ppm to be over the recommended limit for drinking water in San Luis Valley, while concentrations of nitrate in excess of 45 ppm can lead to nitrate poisoning when used for drinking. Glanzman (1972) extensively discusses flouride in the confined aquifer of San Luis Valley.

Problems caused by concentrations of sodium in irrigation water are present in San Luis Valley. The U.S. Salinity Laboratory has devised a classification scheme (Fig. 46) based on the specific conductance and sodium adsorption ratio of the water. The sodium adsorption ratio is defined by;

$$SAR = \frac{Na}{\sqrt{\frac{Ca + Mg}{2}}}$$

where the concentrations of all ions are expressed as milliequivalents per liter.

Using this scheme, a water sample is classified under two properties, sodium hazard, which is a function of both sodium adsorption ratio and specific conductance, and salinity hazard, a function of specific conductance. Problems of sodium hazard in the unconfined aquifer (Fig. 47) are encountered only in the sump area and are due to high rates of evapotranspirative discharge. Sodium hazard is more widespread in

a) Flouride Hazard, Confined Aquifer.

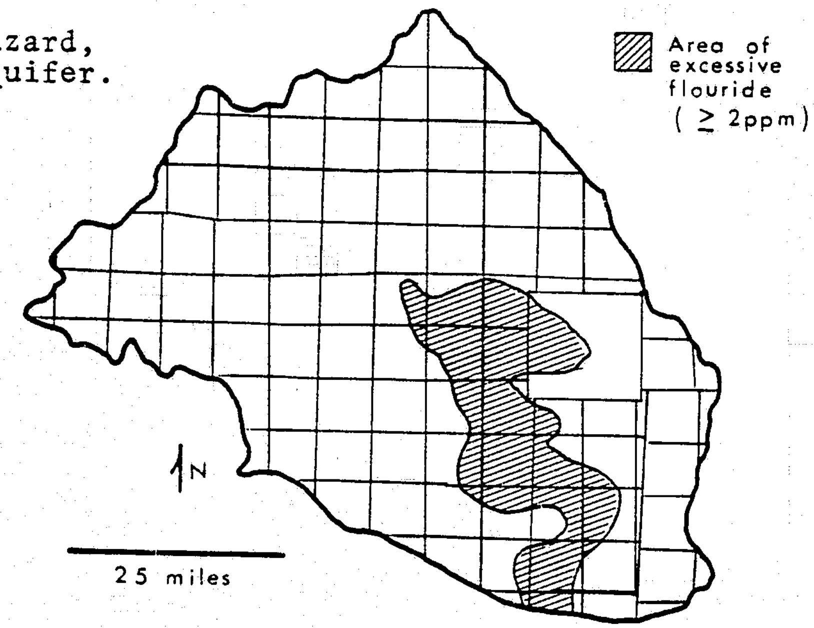


from Emery and others, 1973

b) Nitrate Hazard, Unconfined Aquifer.

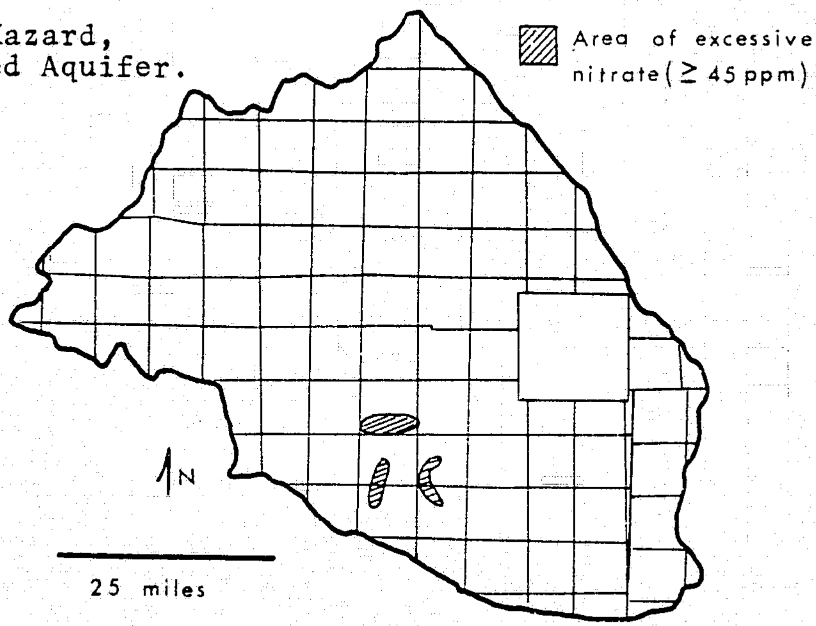


from Emery and others, 1973

Figure 45

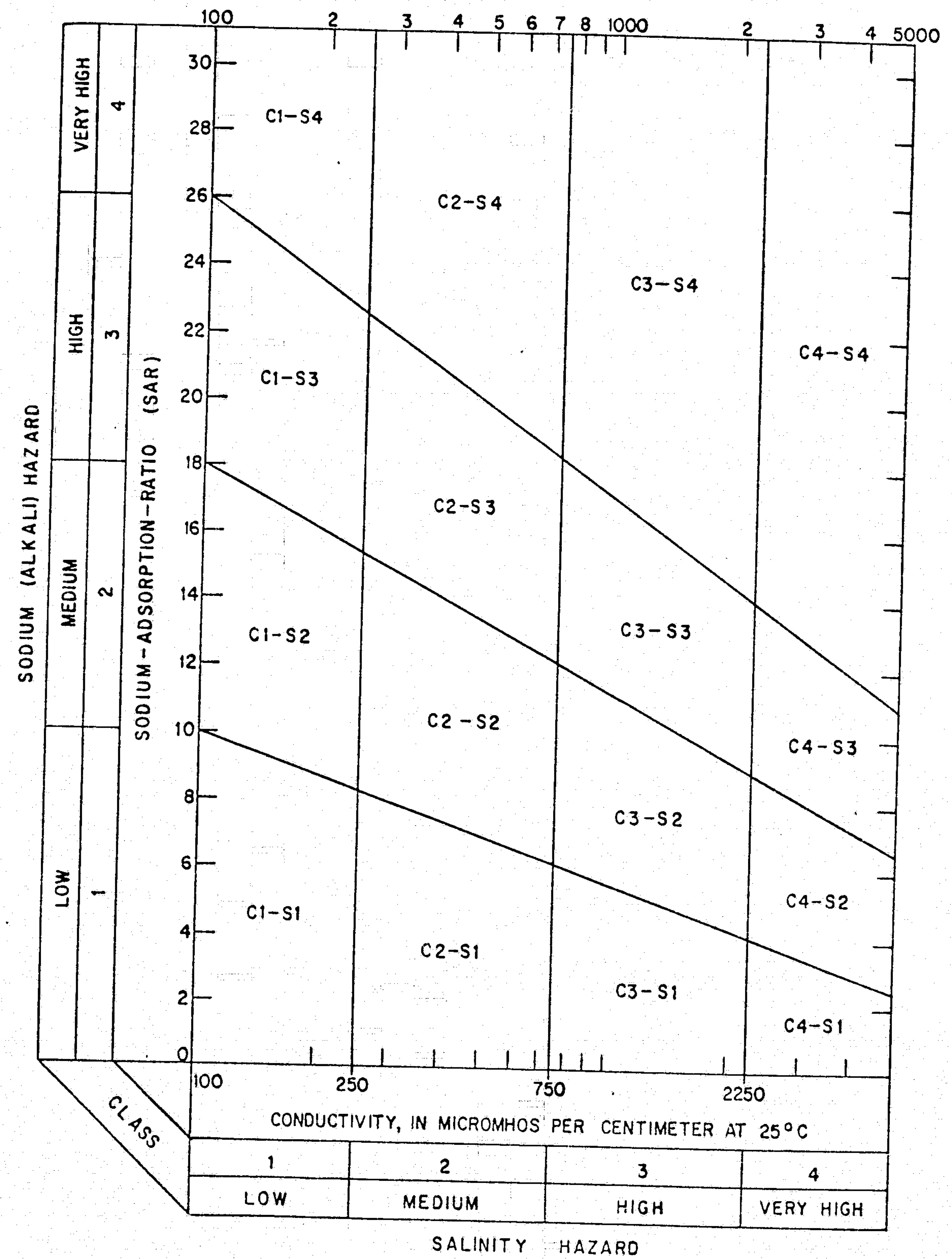


Figure 46: Classification of irrigation water (from U.S. Salinity Laboratory, 1954).

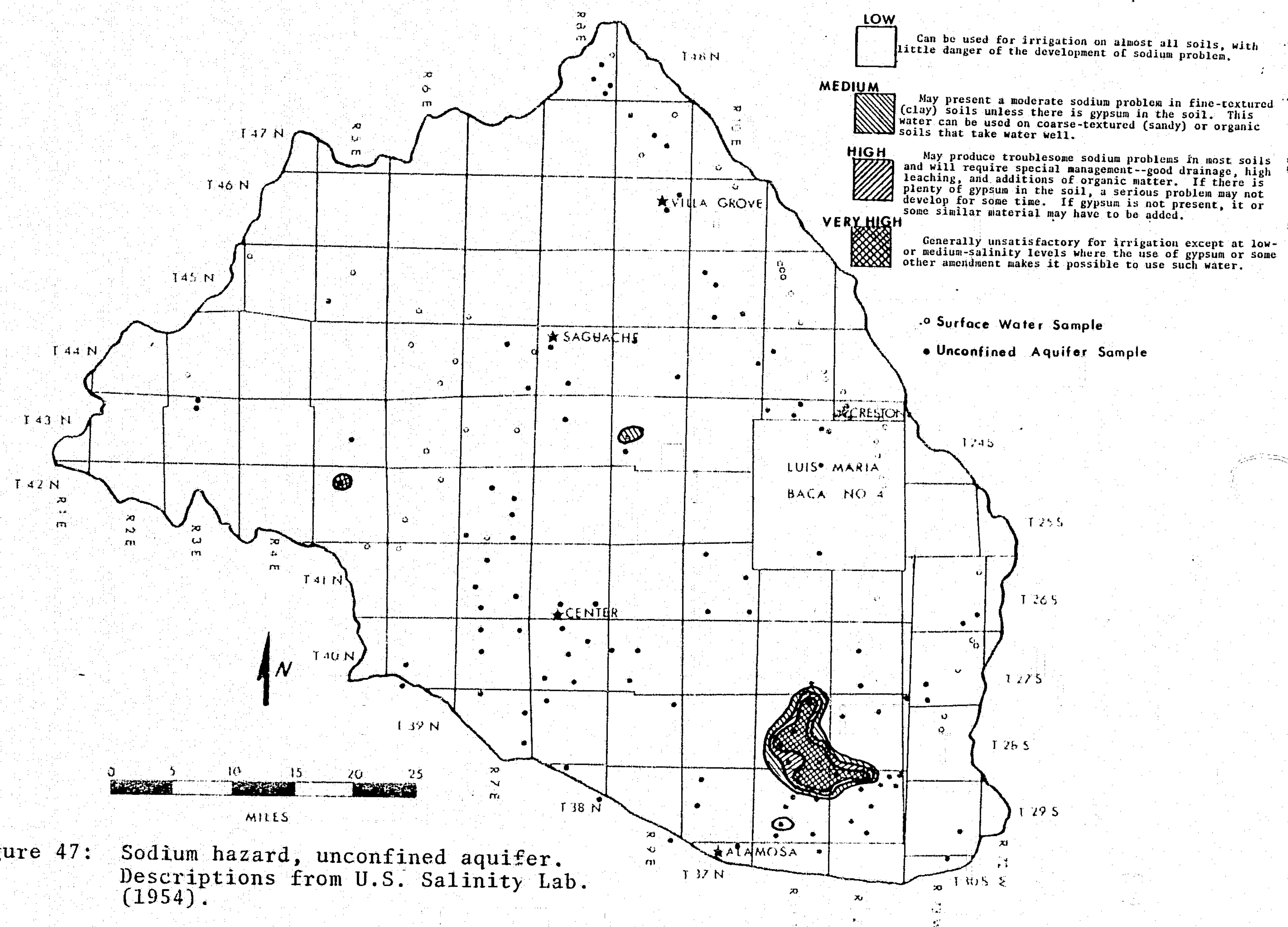


Figure 47: Sodium hazard, unconfined aquifer. Descriptions from U.S. Salinity Lab. (1954).

the confined aquifer (Fig. 48) because of hyperfiltration and ion exchange in the clay beds.

Salinity hazard (Figs. 49, 50) problems are similarly distributed, with serious problems in the unconfined aquifer restricted to the sump area, while much more widespread problems exist in waters of the confined aquifer.

## USE IN TRACING FLOW

The pattern of changes in ground water chemistry across a basin can be a valuable tool in delineating directions of flow and sources of ground water recharge. It has already been seen (Figs. 49, 50) that specific conductance increases towards the center of the basin in both the confined and unconfined aquifers in San Luis Valley. As specific conductance increases with increasing total dissolved solids and with increasing proportion of sodium ions, it might be expected that the increase in specific conductance to the center of the basin parallels a flow of ground water toward the center of the basin. A brief view of the water table contours (Plate 6) and the piezometric map of the confined aquifer (Fig. 57, p. 145) verifies that ground water in both aquifers does flow from the valley margins to the center of the basin.

A more refined view of the changes in chemistry through the basin uses changes in relative proportions of the major anions and cations, thereby reducing some of the effects due to changes in ground water temperature and pressure associated

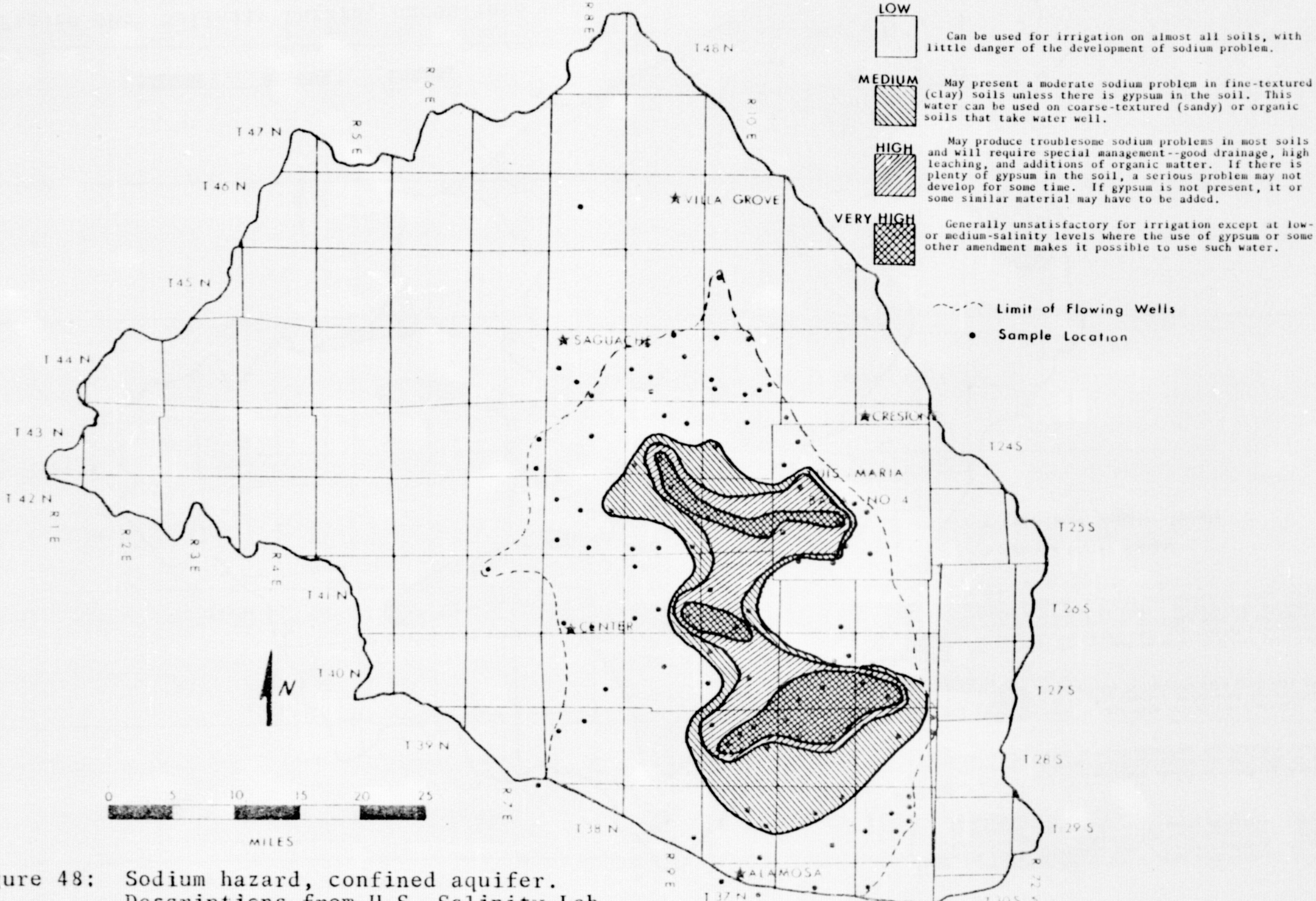


Figure 48: Sodium hazard, confined aquifer. Descriptions from U.S. Salinity Lab. (1954).

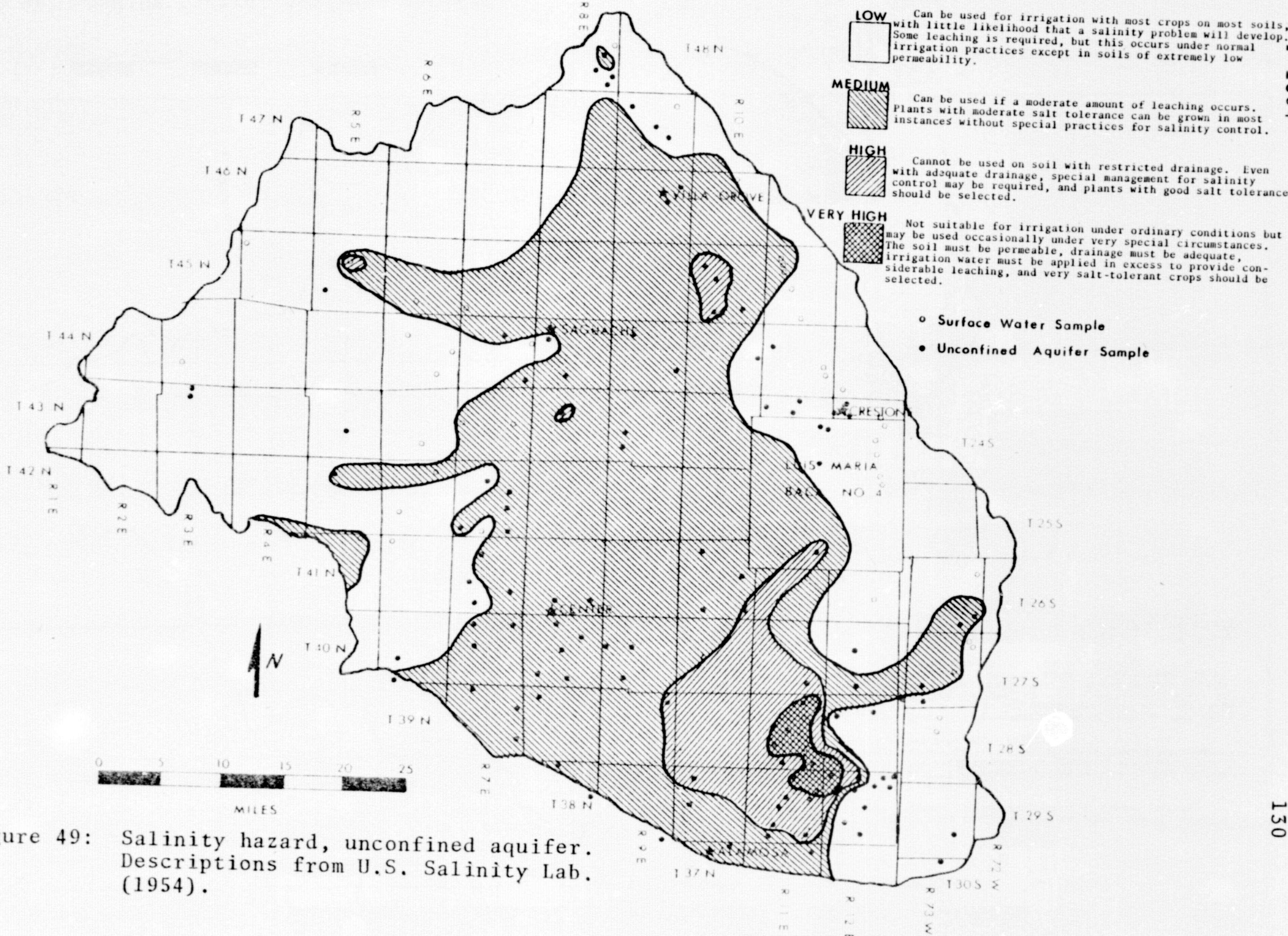


Figure 49: Salinity hazard, unconfined aquifer. Descriptions from U.S. Salinity Lab. (1954).

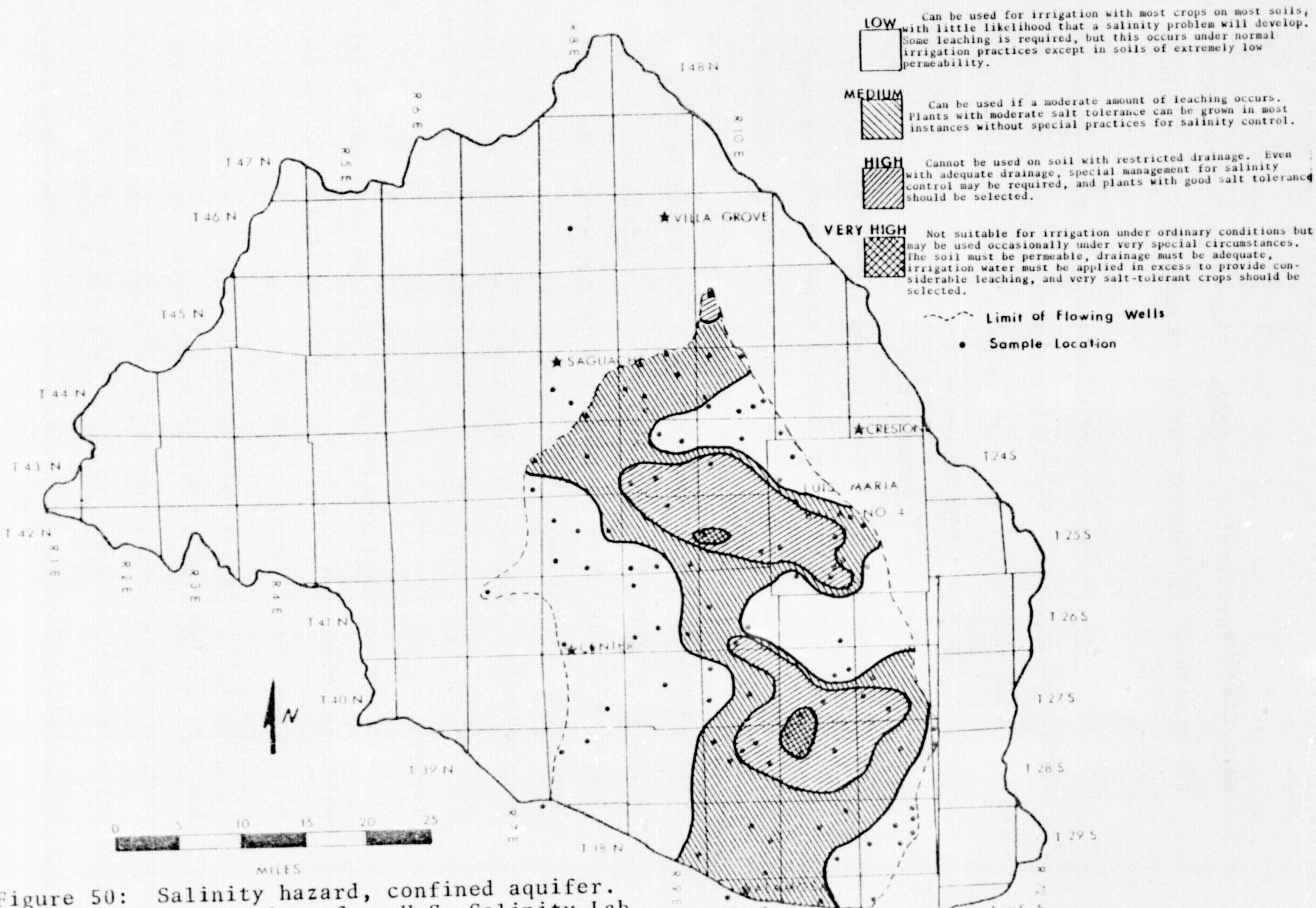


Figure 50: Salinity hazard, confined aquifer. Descriptions from U.S. Salinity Lab. (1954).

with differing sampling depths. The most obvious way of using these data is by mapping the hydrochemical facies across the basin.

As noted in the earlier discussion of water types in the unconfined aquifer, calcium bicarbonate type water predominates. It can be seen (Fig. 51) that calcium bicarbonate water is found at the outer boundaries of the basin, with water progressively changing to sodium bicarbonate, sodium sulfate, and sodium chloride to the center of the unconfined aquifer. Using the sequence of Chebotarev (1955), these changes suggest a pattern of ground water flow from the outer boundaries inward to the sump area of San Luis Valley. An extensive area of calcium sulfate water southeast of Villa Grove is related to a region of mineralization and calcium sulfate hot spring activity (Valley View Hot Springs) in the Sangre de Cristo Mountains. Field investigation of a second area of calcium sulfate water southwest of Saguache showed that it is similarly related to mineralization and alteration of the rocks in the region.

In the confined aquifer (Fig. 52), calcium bicarbonate water is found near the limit of flowing wells, with sodium bicarbonate water found almost exclusively in the interior portion of the region, again suggesting ground water flow to the interior portion of the artesian basin. An interesting feature to note is the lack of calcium bicarbonate water near portions of the eastern boundary of flowing wells, while calcium bicarbonate water occupies large areas along the western

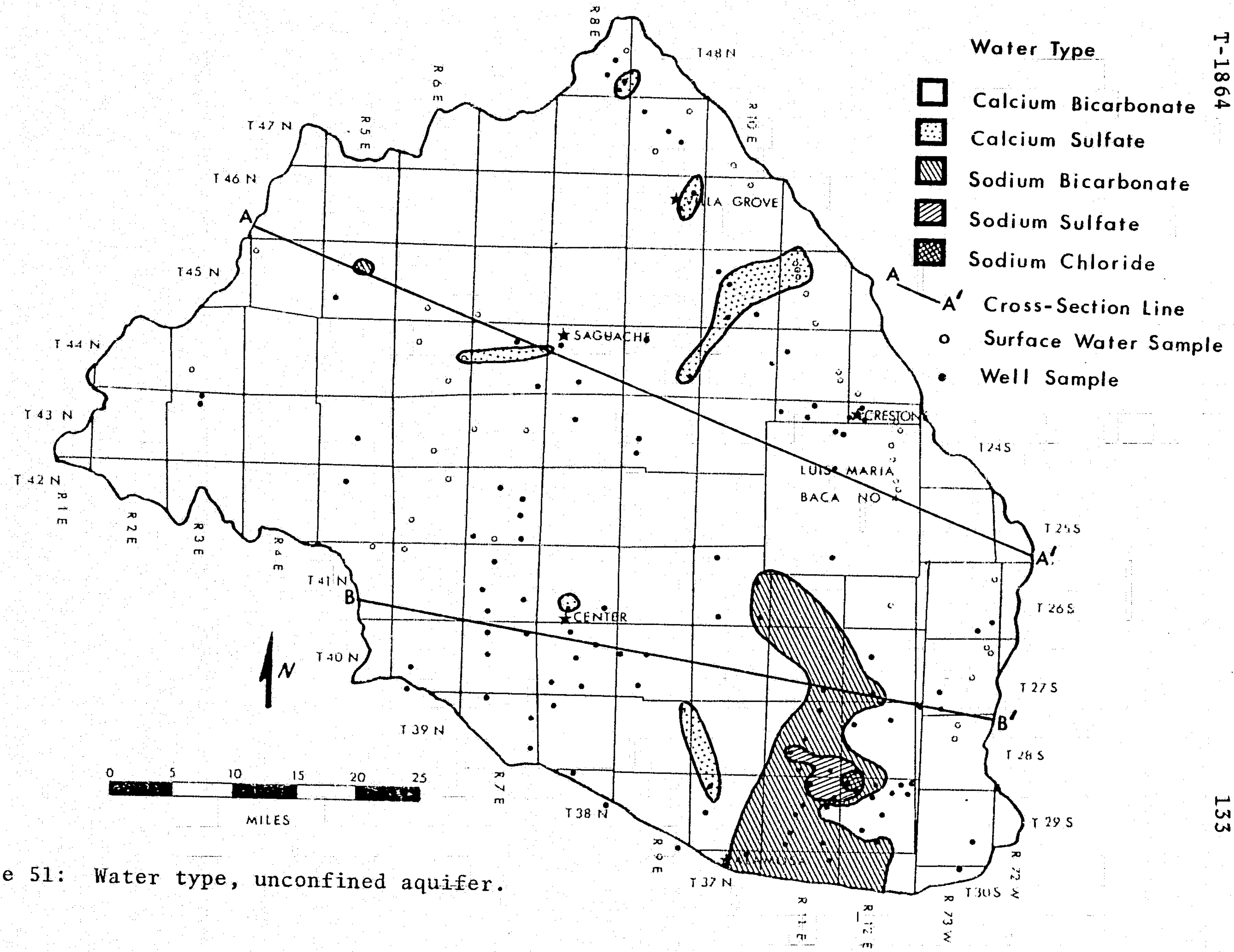


Figure 51: Water type, unconfined aquifer.

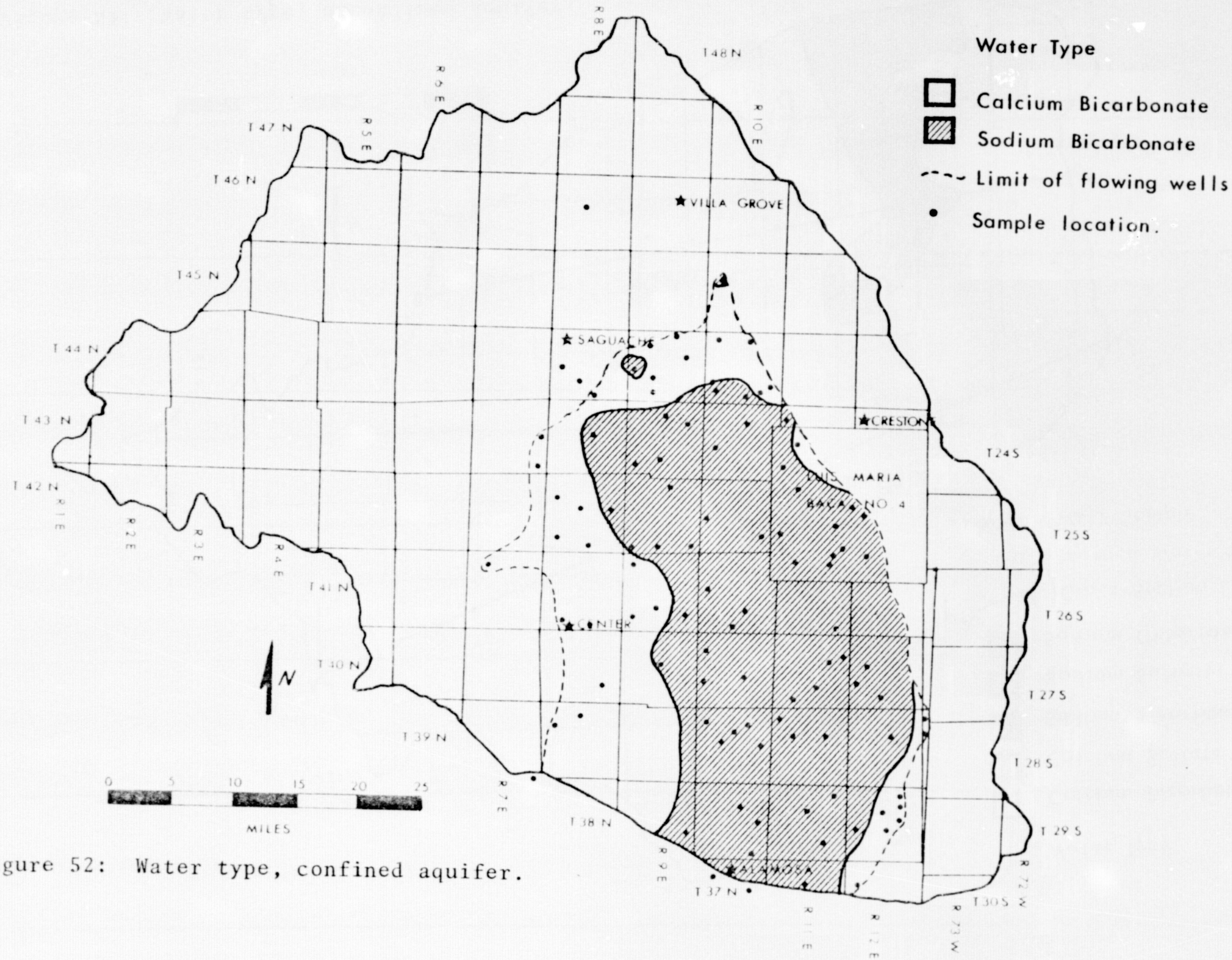


Figure 52: Water type, confined aquifer.

limit of flowing wells. Three possible explanations for this apparent inconsistancy are; 1) there is more calcium in the water recharging the aquifer from the west than from the east, 2) evaporite deposits could exist along the eastern boundary of the valley, increasing the relative concentration of sodium rapidly along the east side of the valley, and 3) the process of hyperfiltration and ion exchange is particularly active along the eastern edge of San Luis Valley.

The map of water types in the unconfined aquifer (Fig. 51) indicates that relative proportions of sodium and calcium in waters recharging the confined aquifer are roughly the same on the east and west sides of the basin. A map showing the distribution of calcium/sodium ratios in the unconfined aquifer (Fig. 53) shows even more strongly that, if anything, there is more calcium in the waters on the east side of the basin.

The second possibility given above is discounted on the evidence that no evaporite deposits have either been observed in the field or encountered in any drill holes in San Luis Valley.

The process of hyperfiltration, the selective adsorption of one ion over another during flow through semi-permeable membranes, has been recognized for some time (DeSitter, 1947; Berry, 1959). Most recently, Kharaka and Berry (1974) and Kharaka (1975) present field and laboratory data on the relative retardation of specific ions in flow through semi-permeable membranes. In general, divalent ions, such as calcium, were

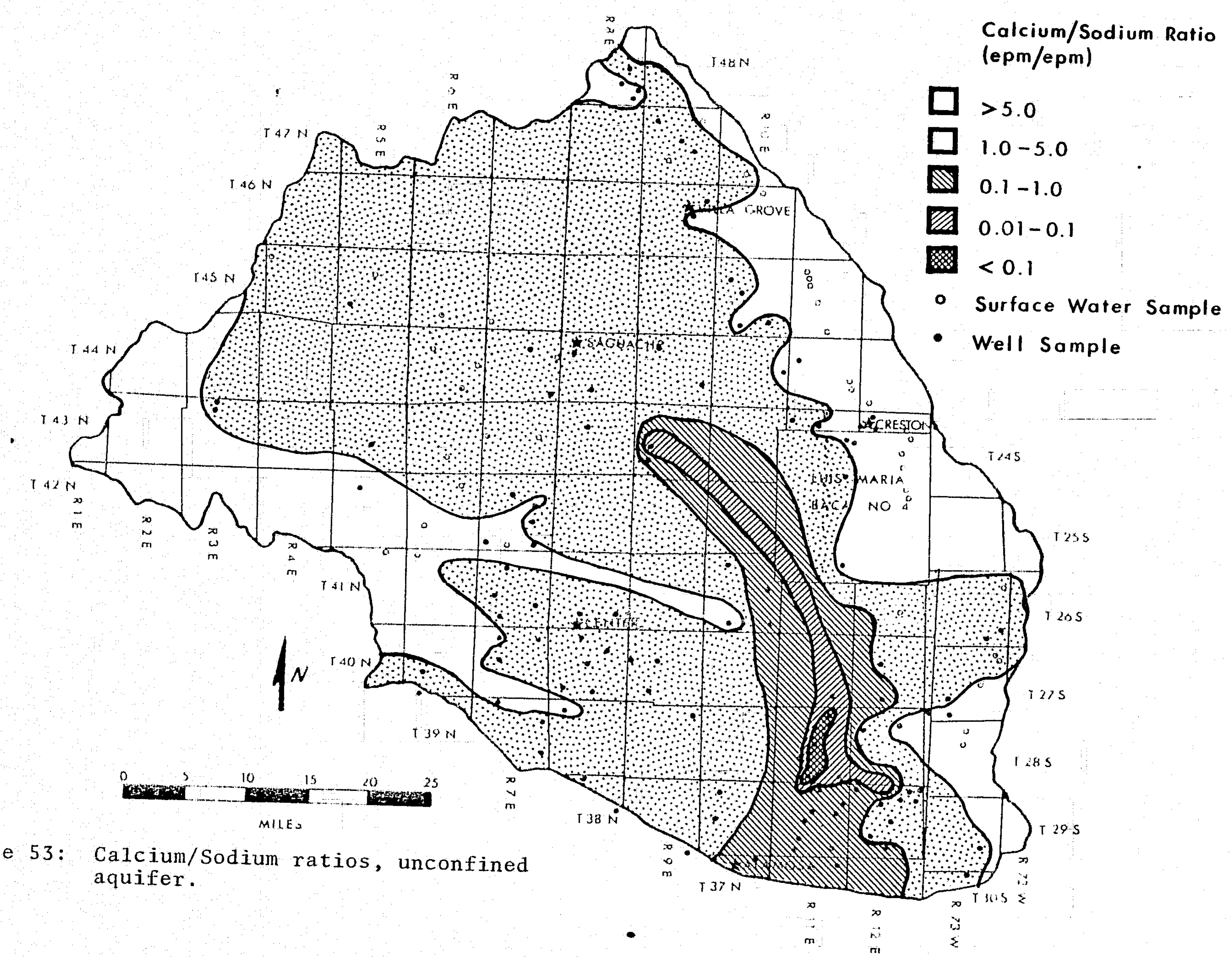


Figure 53: Calcium/Sodium ratios, unconfined aquifer.

found to be more effectively retarded than monovalent ions, such as sodium. The difference in water types along the eastern and western boundaries of flowing wells may therefore be related to differences in the types of geologic materials encountered in the flow path.

Figure 54 more effectively shows the variation in the relative concentrations of calcium and sodium ions in waters of the confined aquifer. It should again be noted that calcium/sodium ratios are much higher along the western limit of flowing wells than along the eastern. If hyperfiltration and ion exchange are the mechanisms for the selective increase in sodium, then more clays must be encountered during the path of ground water recharge to the eastern part of the confined aquifer than to the western part. The most obvious source of clays is the blue lacustrine clays that constitute the confining layers for the confined aquifer, and it is suggested that much of the recharge to the eastern part of the confined aquifer follows a path <u>through</u> the confining clays, whereas recharge to the western part of the confined aquifer involves direct hydraulic connection between the confined and unconfined aquifers. Subsurface stratigraphic control on the west side of San Luis Valley is adequate to define a pinch-out of lacustrine clays, but subsurface evidence on the extent of the lacustrine clays on the eastern side of San Luis Valley is totally lacking. Emery and others (1971) have simply assumed a pinch-out of clays at the eastern limit of flowing wells,

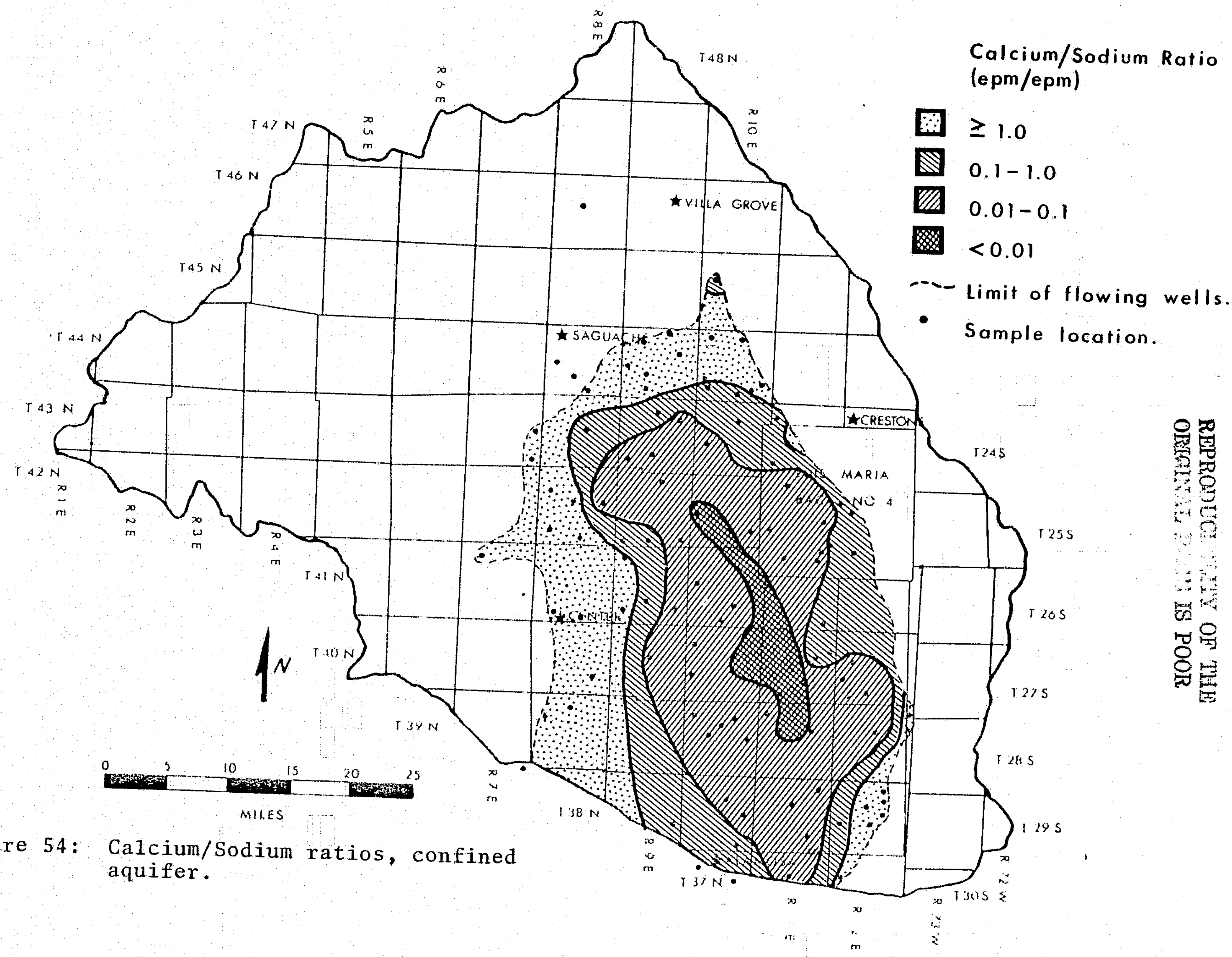


Figure 54: Calcium/Sodium ratios, confined aquifer.

REPRODUCIBILITY OF THE ORIGINAL PAGE IS POOR

but both the chemical evidence and the gradual eastward thickening of the entire clay series suggest that the clays may extend much farther east than the eastern limit of flowing wells, possibly even terminating against the Sangre de Cristo Fault. Results from a steady-state digital ground water flow model (discussed in more detail later) indicate that the shape of the piezometric surface is changed negligibly by varying the eastern limit of the clays from 0 to 3.0 km (0-2 mi) from the Sangre de Cristo Fault.

Figure 55 shows schematic cross-sections of two areas of the basin fitting two different recharge models and the geochemical evidence supporting the models. The positions of the cross-sections are shown in Figure 51 (p. 133). More accurate cross-sections, showing depths of sampling, cannot be drawn because most of the older artesian wells are uncased or tap aquifers at several depths. Water samples of the confined aquifer are therefore composite samples of several depths, all of which are unknown.

Cross-section AA' shows the model of recharge through clays, that is, where the lacustrine clays extend to the Sangre de Cristo Fault. In both water type (a) and calcium/sodium ratio (c) there is an abrupt discontinuity between the confined and unconfined aquifers, particularly noticeable along the east side of San Luis Valley. Recharge through clays along this eastern boundary is suggested by the abrupt change of calcium/sodium ratios of greater than 5.0 in the unconfined

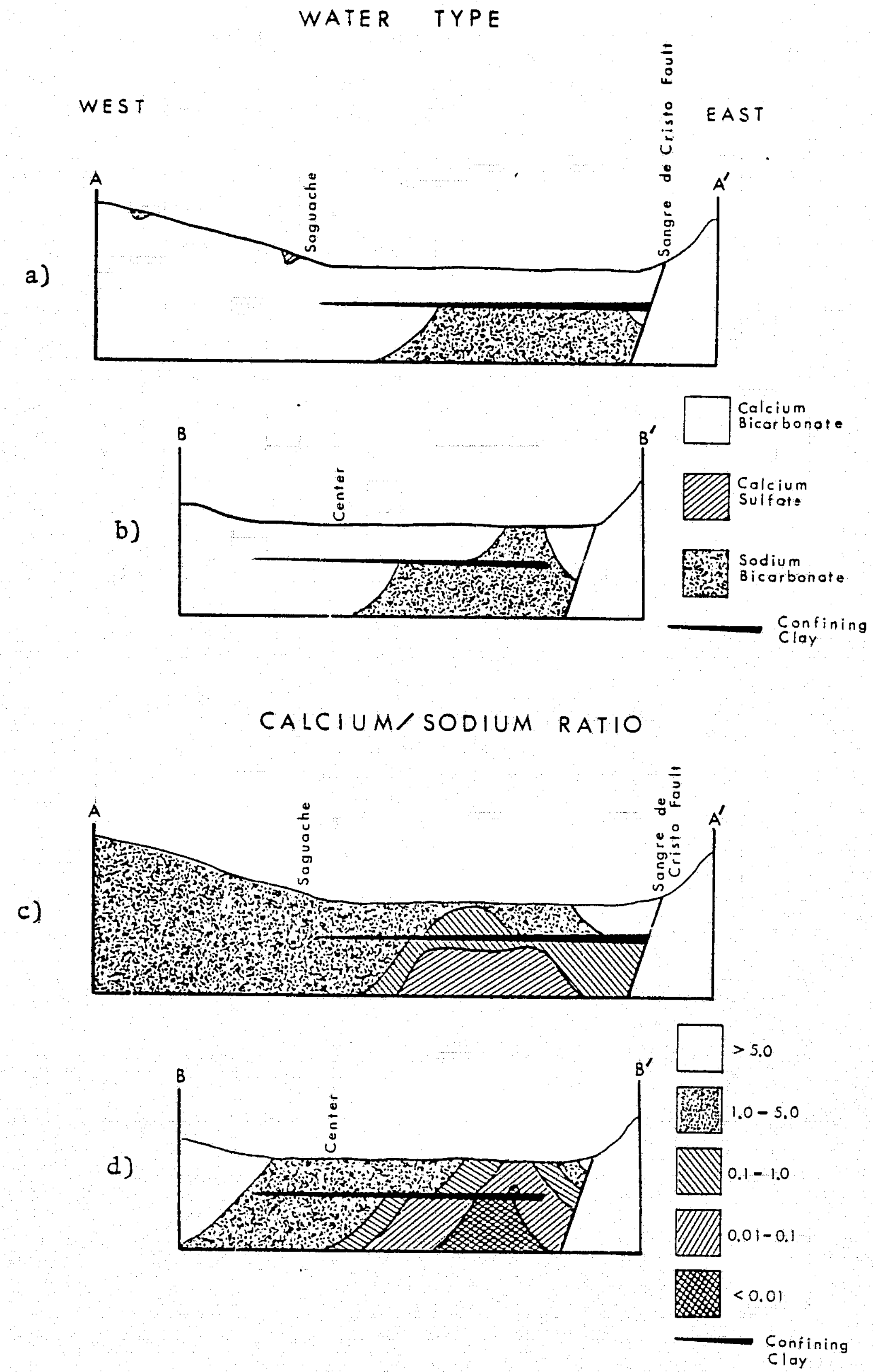


Figure 55: Schematic hydrochemical cross-sections, San Luis Valley.

aquifer to 0.1-1.0 in the confined aquifer across the confining clays.

The second model, exemplified by section BB', is one in which the confining clays end well before the Sangre de Cristo Fault (Fig. 55b, d) and there is continuity between the two aquifers, particularly well-shown by the chemical continuity along the eastern side of San Luis Valley.

Where subsurface stratigraphic evidence is lacking, the geochemistry of water in the confined aquifer can therefore be used to estimate the extent of the confining clays. Such a map, a compilation of stratigraphic and geochemical evidence, showing the lateral distribution of the lacustrine clays that separate the confined and unconfined aquifers is presented in Figure 56.

## GROUND WATER FLOW

### GENERAL DESCRIPTION

Ground water moves from positions of high energy to positions of low energy in response to potential gradients. For the purposes of this discussion, the only potentials considered are elevation and pressure potential. Other potentials which may be important in the San Luis Basin, but which are ignored because of a lack of data, are chemical and thermal potentials. A chemical potential gradient is produced when waters of differing salinities are separated by a semi-

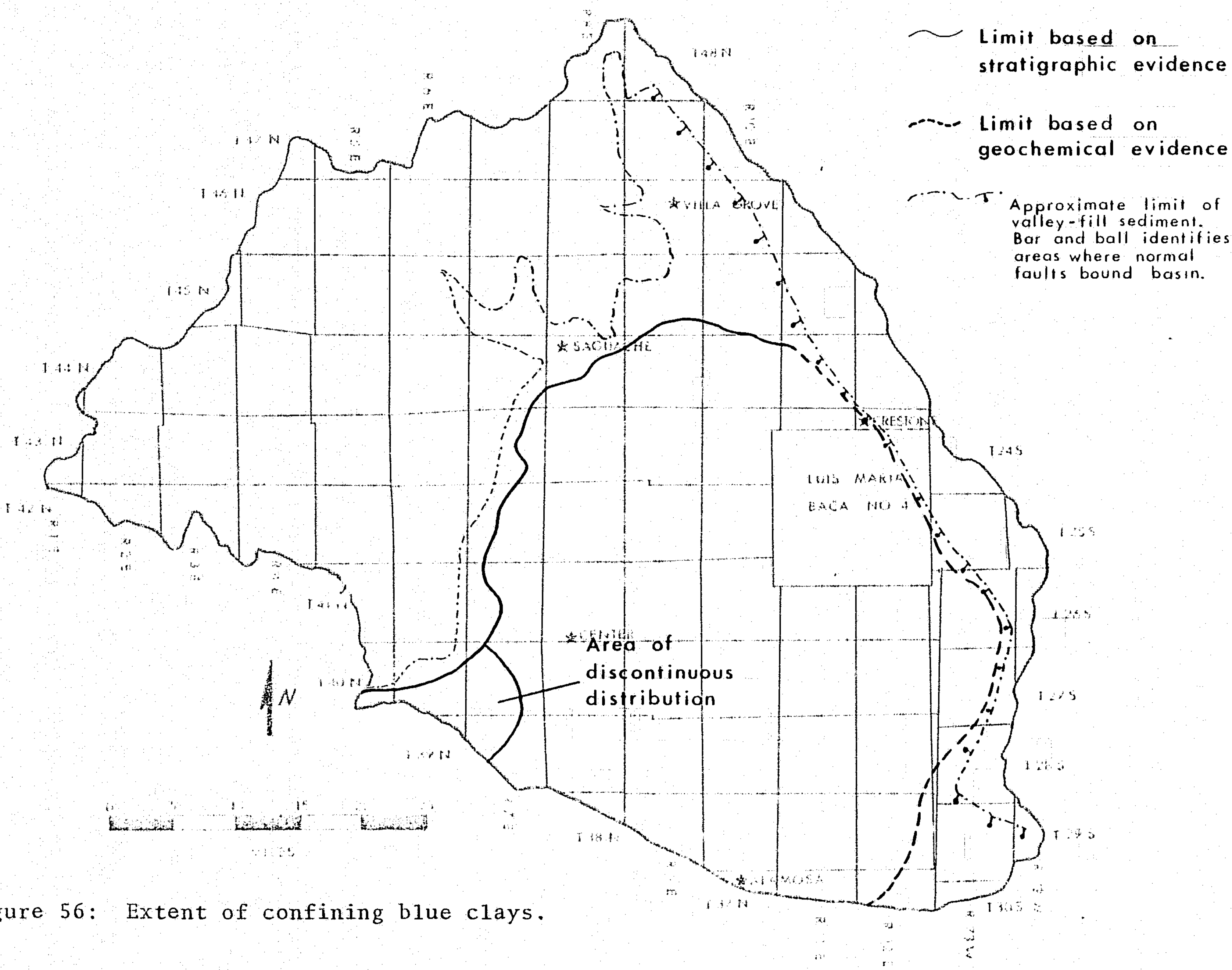


Figure 56: Extent of confining blue clays.

permeable membrane, such as the lacustrine clays in San Luis Valley. Experimental evidence indicates that chemical osmotic potential may be as high as 12-15 psi (0.84 to 1.1 kg/cm$^2$) for every 1000 ppm difference in total dissolved solids from one side of the membrane to the other (Domenico, 1972), with the potential tending to move water from low salinity areas to high salinity areas. For the San Luis Basin, potential gradients due to this salinity contrast vary from 0 to 0.07, while pressure and elevation potential gradients across the confining clay beds vary from 0.03 to 0.95. Significant chemical osmotic potentials are present in only isolated portions of the basin and may tend to move water from the confined to the unconfined aquifer or visa versa (Figs. 41, 42, p. 119, 120).

Potentials due to thermal gradients also may be important within the basin, particularly in explaining Valley View Hot Springs (T. 46 N., R. 10 E., sec. 36) and Mineral Hot Springs (T. 45 N., R. 9 E., sec. 12), but geologic, hydrologic and geophysical data are almost entirely lacking.

If it can be assumed that the hydraulic conductivity of the rocks composing the basin is isotropic in the horizontal plane, an assumption not contradicted by evidence from the San Luis Basin, ground water can be said to flow perpendicular to equipotential contours for individual aquifers. A contour map of the water table (Plate 6) therefore accurately shows the direction of ground water movement in the unconfined aquifer

and, similarly, a piezometric map (Fig. 57) shows the direction of ground water movement in the confined aquifer. Unless horizontal flow is assumed, however, the manner of data-gathering precludes the use of either of these maps in more than a general model. In a basin that has a significant vertical component of ground water motion, great care must be taken to obtain well level measurements from the same aquifer. Relatively little error is introduced in the unconfined aquifer by neglecting the vertical component of motion, but significant error is likely in the piezometric map because of the lack of control over the aquifer whose potential is being measured. Therefore, though the shape of the piezometric surface is generally correct, the values of piezometric head have a considerable range of uncertainty.

Even a cursory look at the water table and piezometric map reveals similarity of patterns of ground water flow in the two aquifer systems. Ground water flows from the outer limits of the basin towards the sump area of San Luis Valley. The area of central discharge in both aquifers is coincident with the major surface drainages of the valley, San Luis Creek and Saguache Creek. South of the point that Saguache Creek joins San Luis Creek, San Luis Creek acts as an effective barrier to ground water movement in both aquifers, as there is no potential gradient across the drainage. North of Mineral Hot Springs, San Luis Creek is again the surface drainage controlling ground water flow. Between Mineral Hot

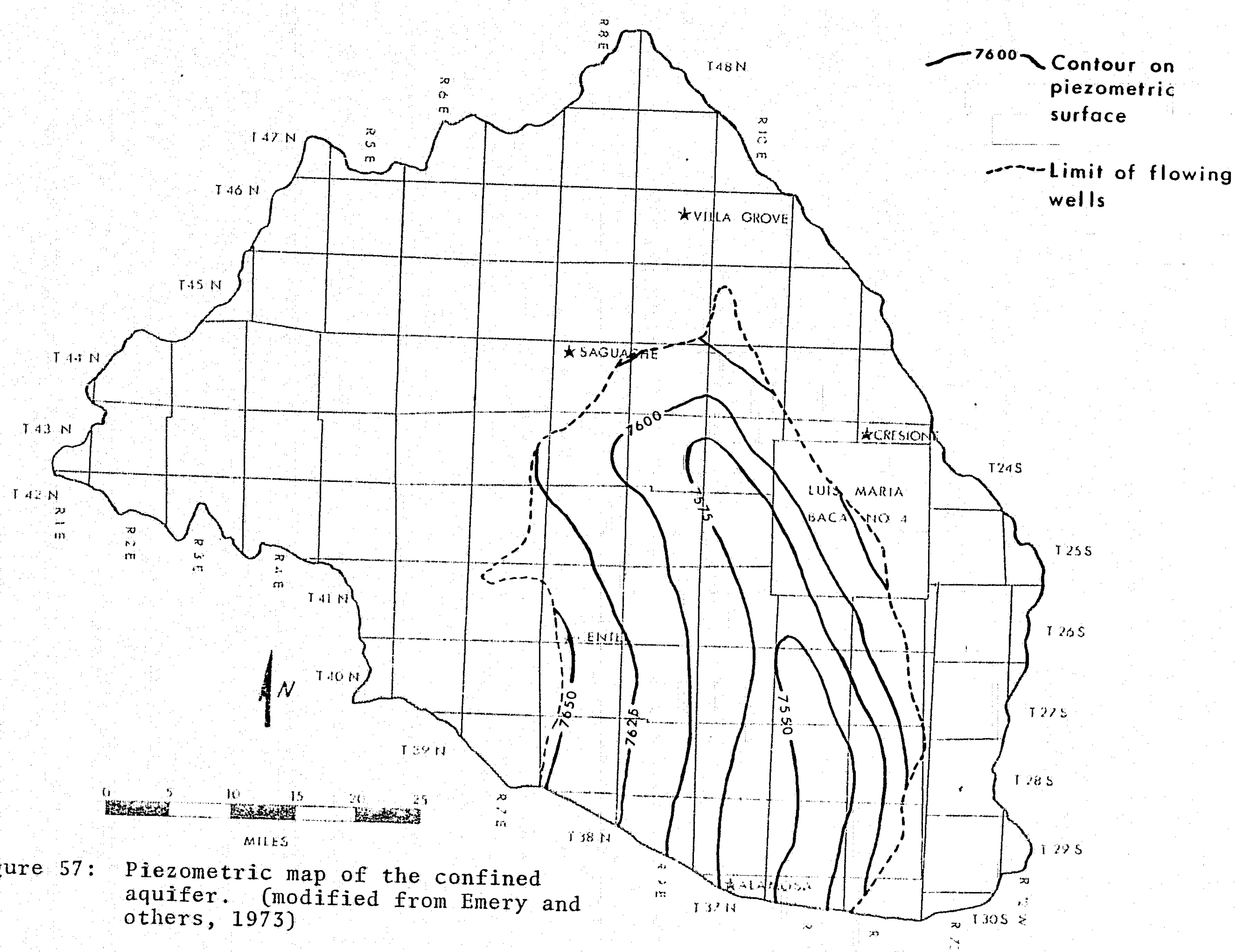


Figure 57: Piezometric map of the confined aquifer. (modified from Emery and others, 1973)

Springs and the junction of Saguache and San Luis creeks, the central area of ground water discharge trends northwest, again acting as a barrier to ground water movement in both aquifers.

Numerous irregularities are noticeable on the surface of the water table, related to losing and gaining reaches of streams and irrigation canals. One of these irregularities, the southern ground water divide, is coincident with a surface divide and forms a boundary to ground water flow in the unconfined aquifer, effectively producing a closed drainage basin. The coincidence of the topographic high and the ground water divide is produced by irrigation and surface water diversion across the divide. Even in areas where the divide is not well-defined, however, ground water flow is, by coincidence, dominantly parallel to the divide in both the unconfined and confined aquifers, and potential gradients across the divide are very low.

All available evidence, such as position of springs, gaining versus losing reaches of streams, and well levels, indicate that the ground water divides at the extremeties of the basin are coincident with surface water divides.

While directions of ground water flow in the horizontal plane can be obtained using equipotential contours on the water table or piezometric surface, the types of flow systems involved and the position of ground water recharge areas can be obtained only by considering the third dimension, the vertical component of flow.

The vertical component of ground water flow is controlled by the shape of the water table and by the underlying geology. Tóth (1963) introduced a system of classifying flow systems in a homogeneous, isotropic medium based on the spacial relations of recharge and discharge areas (Fig. 58). By this classification, a regional ground water flow system is one in which the recharge area lies at the regional ground water divide, and the discharge area is located at the major drainage of the basin. A local flow system is one where the recharge and discharge areas are adjacent. For the purposes of this discussion, the definitions of recharge and discharge areas are those of Mifflin (1968), Freeze (1969), and Freeze and Witherspoon (1966, 1967, 1968). A ground water recharge area (Fig. 59) is an area characterized by decreasing potential with depth and, therefore, a downward component of ground water motion. A zone of ground water discharge is characterized by increasing potential with depth and an upward component of ground water motion. The zones of ground water recharge and discharge are separated by a zone of lateral flow or a hinge line characterized by constant potential with depth and horizontal ground water flow.

To study the vertical component of ground water motion and the distribution of recharge and discharge areas within the basin, a steady-state, two-dimensional computer model, based on programs presented by Freeze (1969), was employed. The model involves the finite-difference solution of the

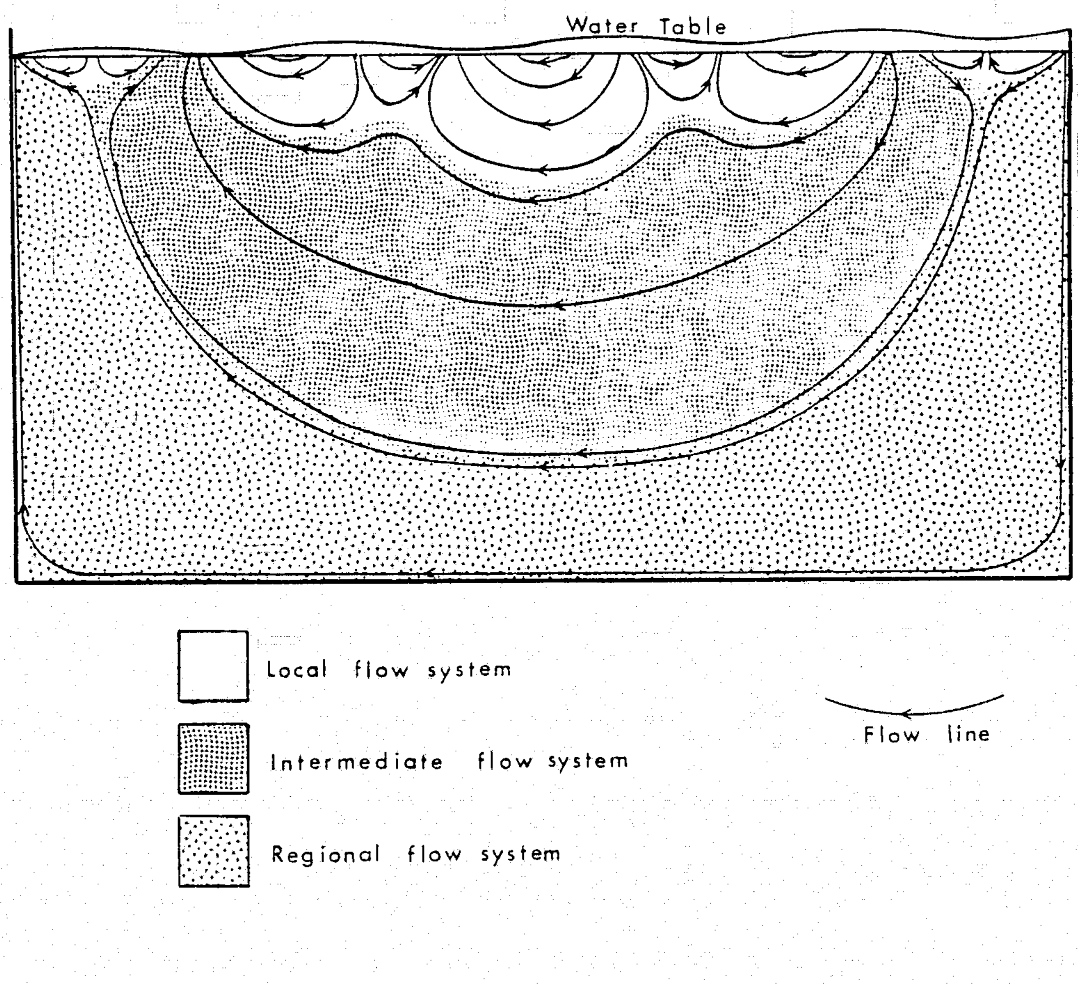


Figure 58: Basin flow systems (modified from Tóth, 1963).

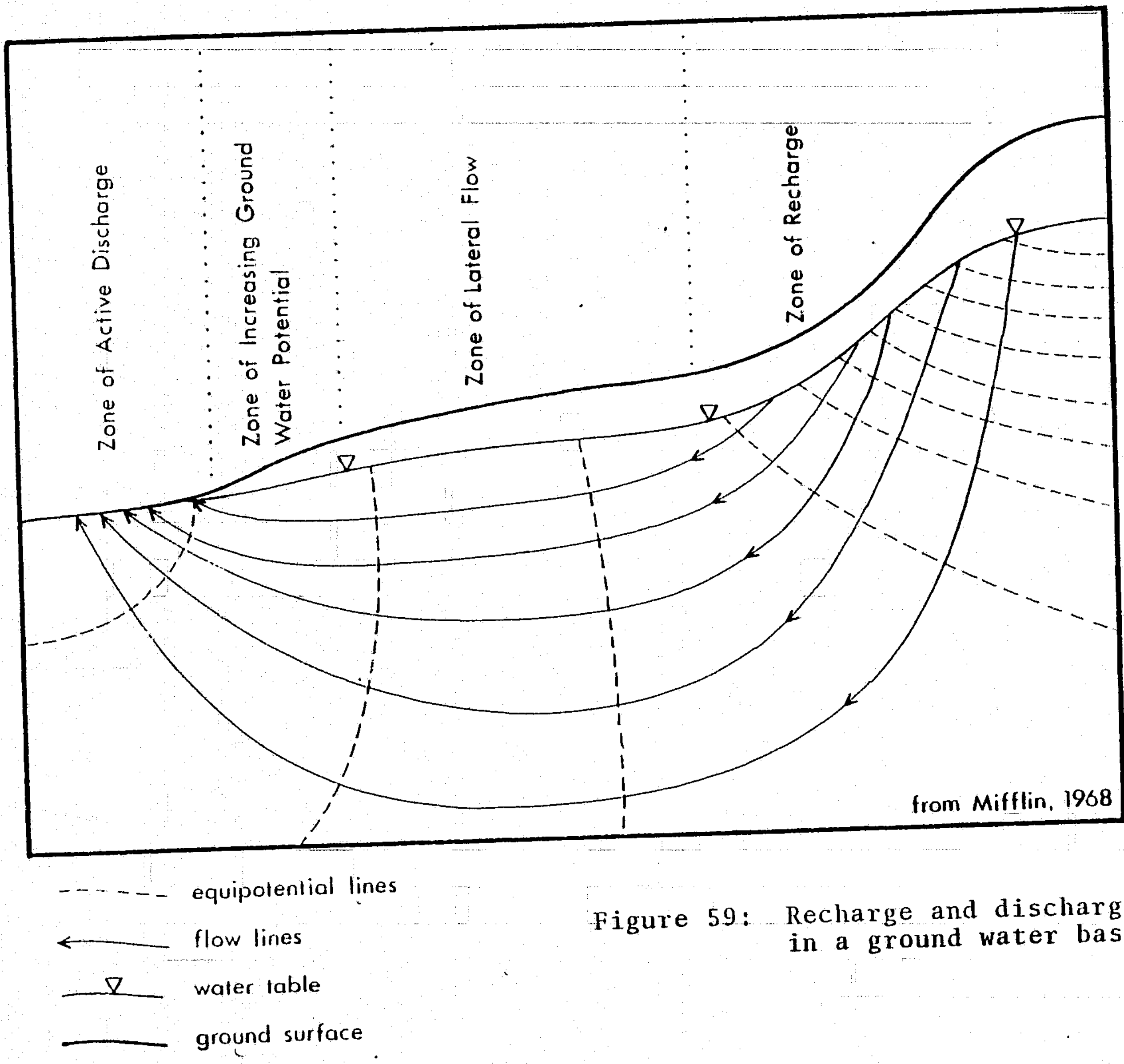


Figure 59: Recharge and discharge in a ground water basin.

expression;

$$\frac{\partial}{\partial x}[K(x,z)\frac{\partial\phi}{\partial x}] + \frac{\partial}{\partial z}[K(x,z)\frac{\partial\phi}{\partial z}] = o$$

where x,z = Horizontal and vertical coordinates, respectively.

K = Hydraulic conductivity.

$\phi$ = Ground water potential.

The model allows for anisotropy and inhomogeneity relative to the horizontal and vertical planes. Where geologic units were dipping, and the principle coordinates of permeability were not either horizontal or vertical, the horizontal and vertical components of permeability were determined using the expression (Bear, 1972, p. 140).

$$K_x' = \frac{K_x + K_z}{2} + \frac{K_x - K_z}{2} \cos 2\theta$$

$$K_z' = \frac{K_x + K_z}{2} - \frac{K_x - K_z}{2} \cos 2\theta$$

where $K_x'$, $K_z'$ = Hydraulic conductivity in the transformed planes.

$K_x$, $K_z$ = Hydraulic conductivity in original planes.

$\theta$ = Angle between the two coordinate systems.

Other assumptions of the model are steady-state, two dimensional flow and impermeable boundaries at the ground water divide, at the major drainage of the basin, at the base of the geologic section, and at the water table. The presence of impermeable boundaries at the ground water divides and major drainage of San Luis Valley has previously been discussed.

Freeze (1969) shows that the flow configuration of a basin is relatively insensitive to the depth of a basal impermeable boundary. The steady-state assumption is justified if annual fluctuations in the water table are small relative to the saturated thickness of the section. In the case of San Luis Basin, fluctuations of the water table are on the order of 0.075% of the saturated thickness of the section and no long-term decline in storage can be demonstrated (Emery and others, 1973), justifying the assumption of steady-state ground water flow.

As in most finite-difference approximations, a major limitation on the accuracy of the model is the grid spacing used, as defined by the size of the problem and the computer storage limitations and cost. For the problems in the San Luis Basin, where anisotropy and heterogeneity were important, a maximum grid size of 90 X 100 matrix points could be used. The grid spacing in the vertical direction, where variation was most rapid, was set at 100 ft (30.5 m), while the horizontal grid spacing varied from 2000-3500 ft (610-1067 m), depending upon the length of the cross-section. The results, plotted as equipotential lines on selected cross-sections, are shown in Plate 5, while directions of ground water flow, as determined using the computer model, are shown on the geologic cross-sections of Plates 3 and 4. Because of the contrast between horizontal and vertical permeabilities, ground water flow is not perpendicular to equipotential lines. To

determine the direction of flow, a method developed by Liakopoulos (1965) and described by Freeze (1969) was used. The method involves drawing an ellipse of the dimensions shown in Figure 60, drawing a vector perpendicular to the equipotential line to the border of the ellipse, drawing a line tangent to the ellipse at the intersection of the ellipse and the previous line, and finally, drawing the flow line perpendicular to the tangent to the ellipse.

## FLOW IN THE SANGRE DE CRISTO MOUNTAINS

Because ground water flow is restricted to fractures that are distributed in a relatively homogeneous manner, flow in the Sangre de Cristo Mountains is largely controlled by irregularities in the shape of the water table. Freeze (1969) examined the effect of water table configuration on ground water flow and found that irregularities in the water table produce local and intermediate flow systems, while a constantly sloping water table produces a single regional flow system. Of the three hydrologic provinces, local flow systems are most important in the Sangre de Cristo Mountains, where the shape of the water table is controlled by the surface topography, both because of the orographic effect of the mountains on precipitation patterns and because of the relation between permeability and depth. Consequently, flow in the Sangre de Cristo Mountains is dominated by local recharge at ridge crests, local discharge to stream valleys, and generally

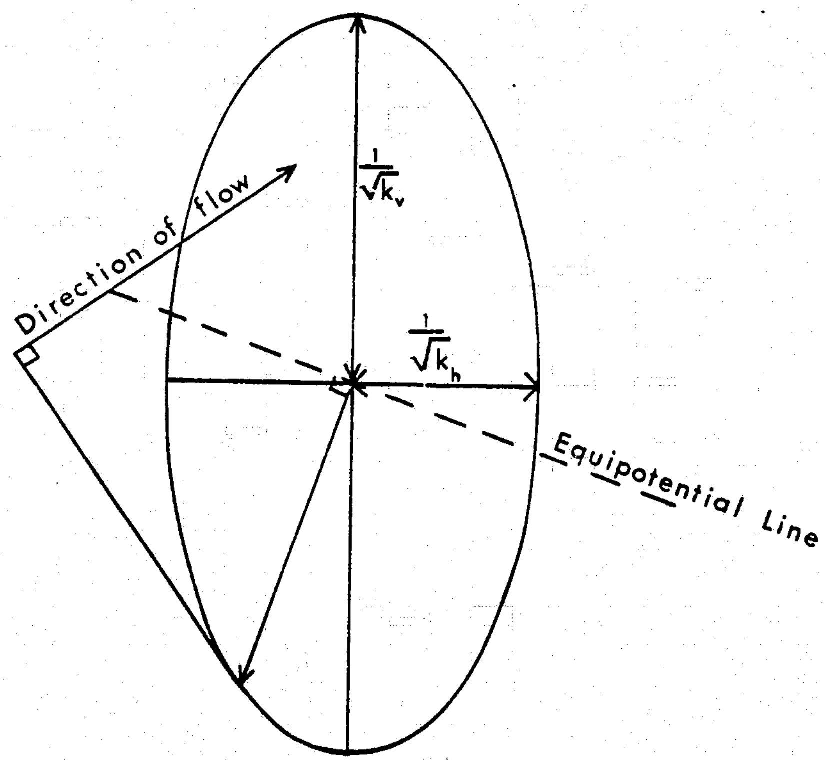


Figure 60: Ellipse used to determine direction of ground water flow in an anisotropic media.

high gradients with strong vertical components. Where alluvial deposits overlie the basement rock, flow is dominantly horizontal in the more permeable sediments and more vertical in the less permeable basement rock. Hydraulic gradients increase rapidly towards the Sangre de Cristo Fault, where gradients closely approach 1.0 across the fault.

## FLOW IN THE SAN JUAN MOUNTAINS

The permeability of the volcanic rocks in the San Juan Mountains is high and nearly constant with depth, producing a relatively flat water table. Because of the relative flatness of the water table and the anisotropic nature of rock permeability in the San Juan Mountains, local flow systems are rare. Instead ground water flow is controlled by both larger scale fluctuations in the water table and by the geology. In general, the flow systems found are regional systems, recharging at the Continental Divide and discharging to San Luis Valley, and intermediate flow systems that discharge to the major drainages present within the mountains.

Geology exerts the strongest control over ground water flow of all factors in this region. Extreme anisotropy (horizontal to vertical permeability ratios as high as 1000 for the ash-flow sequences and as high as 150 for the Conejos Formation) produces a strong component of ground water motion parallel to bedding. Ground water flow is therefore dominantly near-horizontal within this hydrologic region. The high degree

of anisotropy in this region is most apparent where flow lines are at only small angles to equipotential lines.

Ground water recharge and discharge occurs over roughly equal areas in the San Juan Mountains. Though recharge areas associated with ground water mounds are found to produce intermediate flow systems near San Luis Valley, ground water discharge associated with the regional system begins west of the edge of San Luis Valley. Flowing wells should not, therefore, be unusual in the volcanic province both because of increasing potential with depth and because of the degree of anisotropy of the rocks. The only known deep well in the volcanics is, in fact, a flowing well (T. 46 N., R. 8 E., sec. 17).

In contrast to the horizontal flow of ground water in the volcanic aquifers, flow in the air-fall/water-laid tuff aquitards is dominantly vertical and is generally directed toward more permeable units. Alkali Spring (T. 45 N., R. 5 E., sec. 9), at the contact of the tuff aquitard and more permeable Dakota Sandstone, is likely of such origin. The high dissolved solids content is probably caused by a flow path through tuffs of relatively low permeability, containing abundant soluble minerals.

## FLOW IN THE SAN LUIS VALLEY

The types of ground water flow found in specific portions of the San Luis Valley depend on the position within the regional flow system and the assumptions regarding permeability,

anisotropy, and distribution of the hydrogeologic units. The shape of the water table determines the position of the impermeable boundary at the center of the basin, as shown by the coincidence of the central lows in the piezometric surface of the confined aquifer and the water table of the unconfined aquifer. Local flow systems may exist where influent streams produce ground water mounds, but these local flow systems do not appear on east-west cross-sections.

Flow in the Vallejo/Sante Fe Formation is considered to be relatively simple in the ground water flow models shown because of a lack of detailed information about the texture or variability of the unit. On the east side of San Luis Valley, ground water in the Vallejo/Sante Fe Formation has a downward component of motion from the Sangre de Cristo Fault to 6 km (3.7 mi) west of the fault and an upward component from that point to the central drainage divide. The degree of anisotropy dictates that ground water flow is nearly horizontal except near boundaries and where flow is toward more permeable conduits of ground water. Conduits of this type are abundant on the west side of San Luis Valley, where volcanic flows and ash-flows are interbedded with the less-permeable sedimentary rock. In this situation, flow in the sedimentary rock has a strong vertical component, flowing upward or downward to the volcanic flows, where the flow-lines are refracted parallel with bedding planes in the volcanic flows.

Hydraulic gradients in the Vallejo/Sante Fe Formation vary with position in the flow system and direction of flow. Gradients are higher where flow is near-vertical than in areas of horizontal flow, averaging about 0.12 in the vertical direction and 0.008 in the horizontal direction, corresponding to ground water velocities of 0.12 m/year for horizontal flow and 0.04 to 0.4 m/year for vertical flow.

Flow in the interbedded ash-flows found within the valley is consistantly down-dip, nearly parallel with bedding. Flow within the less-permeable flows of the Conejos Formation, similarly found interfingering with the alluvial fill of San Luis Valley, is strongly affected by the anisotropy of the volcanic rocks, but the vertical component of flow is more important than in the welded ash-flows. Gradients in both volcanic units increase toward the land surface, ranging from 0.0016 to 0.032 for the ash-flows, and from 0.05 to 0.01 for the lava flows. Corresponding ground water velocities are 2.6 to 5.04 m/year for the flows of the Conejos Formation and 26.4 to 522.8 m/year for the welded ash-flow tuffs.

Modeling of the confined aquifer was generalized because of the relatively large vertical matrix spacing. Except where beds were known to be thicker, the interbedded sands and clays of the Alamosa Formation were modeled as consisting of alternating 100 foot thick beds with continuous distribution from the eastern to the western extent of clay. This approximation produces some errors, but does yield usable information

regarding the general pattern of ground water flow in the confined aquifer. The major error is the assumption of continuity of very discontinuous clay beds. In estimating vertical permeability by matching theoretical piezometric slopes with real piezometric slopes, this approximation yields a permeability that takes into account both vertical flow through clay and vertical flow in areas where the clay is discontinuous. As has been noted previously, the vertical permeability estimated by the model for the western half of the basin, where the clay is relatively continuous on a local scale, is lower than that estimated for the eastern half of the basin, where the clays are discontinuous on a local scale.

Ground water flow in the confined aquifer consists of vertical flow in the confining clays and near-horizontal flow in the interbedded sands. The importance of the vertical component of flow in the sands of the confined aquifer depends upon the position within the flow system, becoming important near the central drainages and the Sangre de Cristo Fault and relatively unimportant elsewhere. Decreasing potential with depth (recharge) in the sands of the Alamosa Formation is encountered only along the eastern side of San Luis Valley. Hydraulic gradients within the sands range from 0.004 to 0.048, corresponding to a velocity range of 7.44 to 68.8 m/year.

Ground water flow in the confining clays is vertically upward through all of the western half of the basin and most of the eastern half. Whether vertical downward ground water

flow through the clays occurs in the basin at all depends upon the eastward extent of the confining clays. Plate 5 shows two cross-sections of the eastern edge of San Luis Valley, one with the lacustrine clays extending to the Sangre de Cristo Fault and a second with the clays ending 1.8 km (1.14 mi) west of the fault. The flow patterns are nearly identical in the two sections, differing only in whether downward flow in the recharge zone is through clays or sands. Study of the plots of theoretical piezometric heads in Appendix A shows that varying the eastward extent of the confining clays has little effect on piezometric heads in the confined aquifer.

Hydraulic gradients across the confining clays vary throughout the valley from 0.03 to 0.95, and ground water velocities vary from 0.02 to 1.3 m/year.

Ground water flow in the unconfined aquifer is near-horizontal nearly everywhere in San Luis Valley, except near the central drainages, where a vertical upward component of motion becomes important, and near the Sangre de Cristo Fault, where a vertical downward component of motion becomes important. Ground water potential increases slightly with depth (discharge zone) in the unconfined aquifer everywhere west of San Luis Creek and east of the creek to 1.8 km (1.14 mi) west of the Sangre de Cristo Fault. Hydraulic gradients range from 0.01 to 0.1, with ground water velocities ranging from 15.8 to 35.0 m/year.

GROUND WATER RECHARGE

Study of the flow nets for the areas marginal to San Luis Valley confirms the conclusions drawn about the sources of recharge to the aquifers of San Luis Valley. The paths and sources of ground water recharge are quite different on the west and east sides of San Luis Valley. On the west side of the valley, recharge from ground water flow through the volcanic rocks of the San Juan Mountains is dominant. It is, in fact, the only source of recharge to the confined aquifer on the west side of the valley. The existance of increasing potential with depth in the unconfined aquifer at the western valley margin suggests that infiltration of surface water is of importance only in local flow systems where flow is directed perpendicular to the east-west cross-sections shown and of negligable importance as a regional ground water recharge source. This model is supported by the ground water chemistry, with generally higher total dissolved solids found in the unconfined aquifer on the west side of San Luis Valley than on the east.

In contrast to this model, ground water recharge is of a quite different nature on the east side of San Luis Valley. Streamflow entering the valley from the Sangre de Cristo Mountains is abundant, and ground water flow is of lesser significance. Streamflow infiltrating to the unconfined aquifer within the first 1.8 km of flow recharges that aquifer. The unconfined aquifer recharges the confined aquifer along

the eastern edge of the valley for the same distance from the Sangre de Cristo Fault. Therefore, the recharge to the aquifers of the eastern part of San Luis Valley comes from hidden ground water recharge from the Sangre de Cristo Mountains, streamflow that infiltrates into the alluvial fans within the first 1.8 km of flow, and limited precipitation near the Sangre de Cristo Mountains. In addition, for streamflow or precipitation to reach the confined aquifer, it must infiltrate into the alluvial fan sediments within the easternmost 1.16 km (0.72 mi) of the valley. Changes in local stratigraphy and water-table configuration will change this dimension somewhat, but in general it can be said that recharge to the confined aquifer east of San Luis Creek occurs along a relatively narrow strip bordering the Sangre de Cristo Mountains.

Whether or not the confining clays extend to the Sangre de Cristo Fault affects the flow patterns only slightly, but does change the sediment type the water flows through. What is more important is that the eastern or western limit of flowing wells (previously assumed to be the limit of the confining clays) <u>does not</u> coincide with the limits of the ground water recharge areas. In other words, all ground water east of the eastern limit of flowing wells does not recharge the confined aquifer. Wells located west of the narrow (1.8 km) recharge strip along the Sangre de Cristo Mountains do not affect either the unconfined or confined aquifer in a way significantly different from wells located in the center of

San Luis Valley, because the flow regimes are the same.

## HOT SPRINGS ACTIVITY AND GEOTHERMAL POTENTIAL

Evidence related to the heat sources for, and the controls over, hot springs in the basin is sparse. Hot springs appear to be restricted to areas of complex structural intersection. Valley View Hot Springs (T. 46 N., R. 10 E., sec. 36) are near the intersection of the Sangre de Cristo and Villa Grove fault zones. Mineral Hot Springs (T. 45 N., R. 9 E., sec. 12) are near the intersection of the Major Creek Fault Zone (Knepper, 1974) and the eastern boundary fault of the central horst of San Luis Valley. It is not clear whether the hot springs are controlled by the major faults, by subsidiary fractures, or by a combination of the two.

The temperatures of the spring discharge vary widely, from 27-37°C at Valley View Hot Springs and from 32-60°C at Mineral Hot Springs (Pearl and Barrett, 1976). Silica geothermometry of water samples from Mineral Hot Springs suggests reservoir temperatures of 98-100°C (Pearl and Barrett, 1976), with lower temperatures indicated for Valley View Hot Springs.

Water from Valley View Hot Springs is calcium sulfate type and total dissolved solids content is less than 200 mg/1, possibly suggesting relatively shallow circulation. The relatively high proportion of sulfate in the water is unusual for surface water in the Sangre de Cristo Mountains,

but may simply be due to mineralization of rocks in the vicinity. Water from Mineral Hot Springs is sodium sulfate type (Pearl and Barrett, 1976). The dominance of the sodium cation is not unusual for waters found within the zone of ground water discharge of San Luis Valley, but the high proportion of sulfate in the water is again unusual. The water chemistry does not indicate whether ground water feeding Mineral Hot Springs has been subjected to more than the usual ground water circulation patterns.

There are two probable heat sources of sufficient strength to generate hot spring activity. Because San Luis Basin is an area of extensional tectonics, it may also be an area of crustal thinning and elevated geothermal gradients. A second potential source of heat is the Tertiary intrusives found in the Sangre de Cristo and San Juan mountains and San Luis Valley. Geothermal gradients are high in San Luis Valley. Temperature measurements in the AMOCO geothermal exploration well indicate a gradient of 41°C/km, while a normal continental gradient is on the order of 25°C/km. The source of the Tertiary sills encountered in this well is unknown.

There is some evidence, such as the alignment of several intrusives in the San Juan Mountains along a line that parallels the edge of San Luis Valley and the occurrence of quartz veins along the Sangre de Cristo Fault, to suggest structural control on the emplacement of intrusives. This author feels that this structural control of intrusives may be the cause for the

apparent control of structure on the location of hot springs. The anomalous occurrence of high proportions of sulfate in hot spring water may, in fact, represent juvenile water contribution to the ground water circulation system.

## SUMMARY

Analysis of the water budget, the geology, the hydrochemistry, and the modeled ground water flow patterns in the San Luis Basin are all consistant in suggesting that the basin can be divided into three distinct, but hydrologically interconnected regions. The Sangre de Cristo Mountain Range, consisting of fractured basement rock, is a region of relatively low, depth-dependent permeability. Secondary fracturing is more related to tectonic and erosional environment than to rock type. Major faults with significant displacement tend to be barriers to ground water motion, while subsidiary fractures are important conduits of ground water. This province is one of high rates of surface water runoff and low rates of ground water flow.

The San Juan Mountain Range is a region of moderate to high permeability caused by primary and secondary fracturing of volcanic rocks. Extreme anisotropy characterizes the sequence of interbedded flow and welded ash-flow aquifers and laharic breccia, flow breccia, and unwelded tuff aquitards. The range of permeabilities in the San Juan Mountains is similar to the range in San Luis Valley, and there is little or no

hydrologic discontinuity between the two regions. In contrast to the Sangre de Cristo Mountains, the San Juan Mountains are characterized by low rates of surface water runoff and high rates of ground water flow.

The geology of San Luis Valley is dominated by Cenozoic faulting and fault control of sedimentation. Development of gouge along fault zones and significant relief to the basement surface affects ground water levels in the vicinity of faults, with shallow ground water levels and springs often found upgradient of major faults. The San Luis Valley is a region of intergranular permeability and ground water discharge. Ground water recharge to the western San Luis Valley is primarily from ground water flow in the volcanic rocks of the San Juan Mountains. Ground water recharge to the eastern valley is primarily from seepage of surface water into the upper parts of the alluvial fans bordering the eastern edge of the valley. Hydraulic continuity between the unconfined and confined aquifers of the valley is suggested by ground water chemistry, digital modeling, and coincidence of the boundaries and shapes of the water-table and piezometric surface. Ground water chemistry suggests that recharge to the confined aquifer along the eastern edge of the valley is through the confining clays for much of the strip. Neither the limit of flowing wells nor the limit of blue clays in San Luis Valley has any special significance in defining the limit of ground water recharge to the confined aquifer.

## REMOTE SENSING INVESTIGATIONS

The use of remotely sensed data was an integral and necessary part of this study, both from a standpoint of the time allowed to complete the ground water investigation and in terms of the completeness of the investigation. During the course of three summers of field work, approximately 2900 square kilometers were either mapped without any prior geologic mapping or examined in detail where previous mapping covered the area. In addition, 3700 square kilometers, chiefly within the interior portion of San Luis Valley, were studied in a reconnaissance fashion, while only 1170 square kilometers, about 15% of the basin, were studied only briefly or not at all, in areas where geologic mapping was of sufficient detail and accuracy for the present study.

More important is the increased accuracy obtained by using all the available tools in the study of ground water flow in the basin. Most of the surface faulting in San Luis Valley would, for example, be overlooked without the view afforded by aerial photography. Similarly, the synoptic view of aerial photography has, in several instances, led to revised interpretations of field-gathered geologic data.

# VISIBLE AND NEAR-VISIBLE SENSING

## DISCRIMINATION OF HYDROGEOLOGIC UNITS

Successful discrimination of rock and alluvial units depends on two features; 1) tonal or color difference and 2) differences in the geomorphic expression. Use of the first feature depends upon differences in the reflectance spectra that are detectable with the photographic system being used. Use of the second feature depends on the ground resolution of the photographic system.

## REFLECTANCE

In general, spectral reflectance differences between hydrogeologic units in the San Luis Basin are less important in photo-interpretation than differences in geomorphic expression. This is due to two causes; 1) the similarity of the shape of the spectral reflectance curve for most units found in the basin and 2) the effect of soil and vegetative cover in obscuring tonal differences between hydrologic units.

Spectral reflectance measurements by Raines and Lee (1975) in sedimentary rocks with as much chemical variation as is found in the sedimentary rocks of the Sangre de Cristo Mountains demonstrate that the spectral reflectance curves in the 400-1000 nanometer region are not statistically different in shape, although the absolute magnitude of reflectance may vary between rock types. Qualitative evaluation of photography

confirms the uniformity of rock colors in the Sangre de Cristo Mountains. In limited regions, absolute reflectance can be used to discriminate some rock types, such as limestones and dolomites of high reflectance from dark schists, but thick forest cover and the development of soils tend to decrease reflectance contrasts.

Reflectance differences between Quaternary deposits are generally unimportant or nonexistant, as the deposits are chemically similar, and reflectance differences depend only on post-depositional weathering and the growth of vegetation. Though these latter factors, such as the preferential growth of vegetation on the younger alluvial fan shown in Figure 65 (p. 177), can sometimes be used locally to discriminate between deposits, the relations are not areally consistant and cannot be used with confidence. Only the active dunes, with characteristically sparse vegetation, can be discriminated from other Quaternary deposits on the basis of reflectance, but the development of vegegation on stabilized dunes even negates this application in mapping eolian sands.

Areas of fresh rock outcrop in the San Juan Mountains are the only areas where reflectance contrasts between rock units are useful. Absolute reflectance differences between fresh outcrops of air-fall tuff and intermediate to basic flows are, for example, easily observable on photography over the region. To obtain more quantitative estimates on rock reflectance differences in this province, and to determine

whether the conclusions of Raines and Lee (1975) were valid for volcanic as well as sedimentary rocks, reflectance measurements within thirteen filter passbands were taken using the instruments and techniques described by Raines and Lee (1974).

The thirteen filter passbands within which rock reflectances were measured extend from the blue through the near-visible infrared spectral regions (Fig. 61). Rock types are grouped into four categories, (1) Fish Canyon Tuff (quartz latite ash-flow), (2) Carpenter Ridge and Sapinero Mesa tuffs (rhyolite ash-flows), (3) intermediate lava flows and flow breccias, and (4) air-fall/water-laid tuffs and laharic breccias. As was qualitatively observed on the photography, absolute band reflectance differences are significant between the volcanic units (Fig. 62). The air-fall tuffs have the highest reflectance in all bands, while the intermediate lava flows consistantly have the lowest. There is no significant (80% confidence level) difference between the reflectances of the quartz latite and rhyolite ash-flows. There are no crossovers in reflectance, that is, units with a higher reflectance in one band maintain a high reflectance throughout. The reflectance of all the the rock types increases with increasing wavelength. This suggests that there are no significant departures from spectral reflectance curves for sedimentary rocks.

To examine the shape of the spectral reflectance curves in relative terms, band reflectances can be recomputed as normalized reflectance by dividing bandpass reflectances by

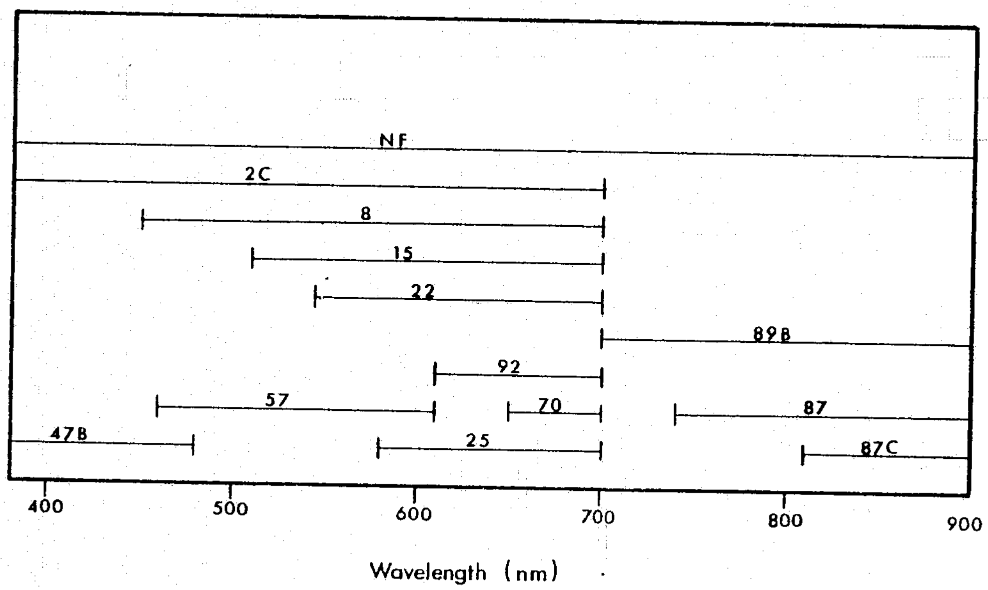


Figure 61: Filter passbands used for reflectance measurements. Infrared light is excluded from all bands except the NF, 89B, 87, and 87C with an infrared cut-off filter.

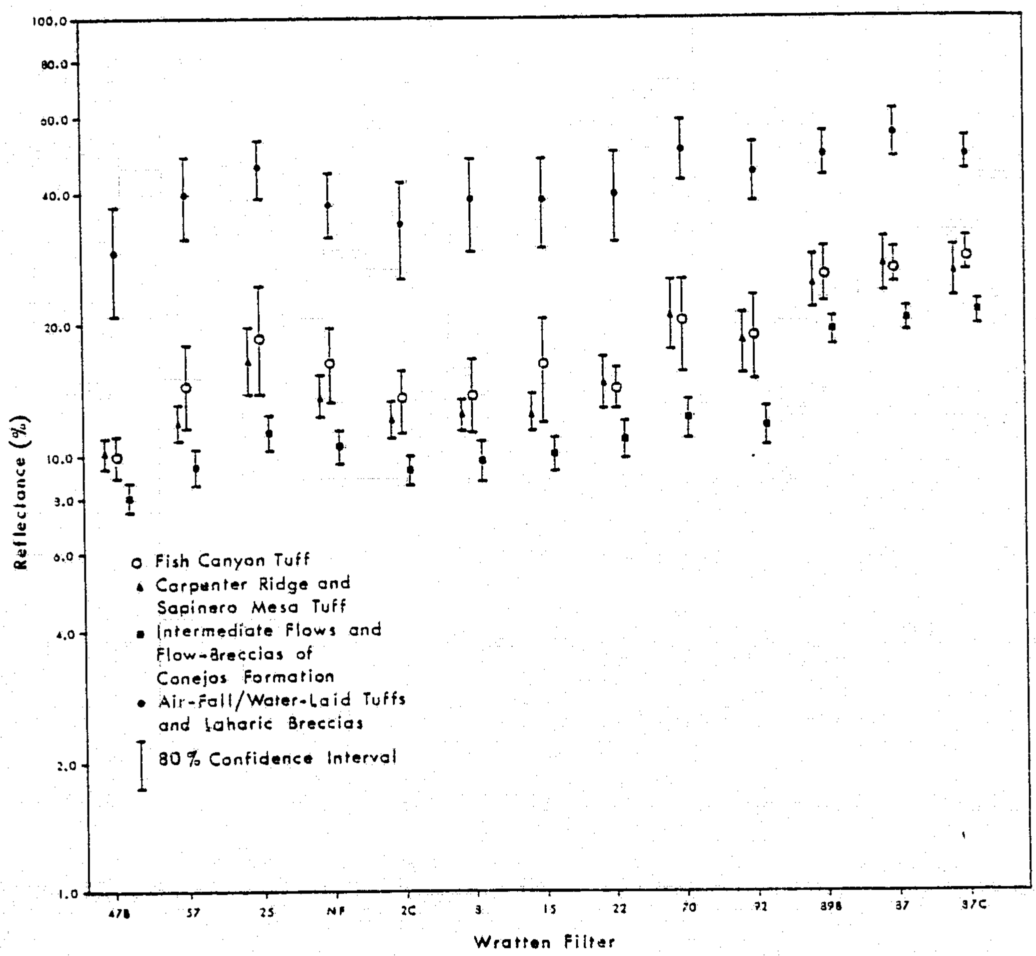


Figure 62: Absolute band reflectance, volcanic rocks.

the reflectance for the entire spectral region of interest (the NF filter). This removes the effect of absolute reflectance, and plots of normalized reflectances (Fig. 63) show only differences in the shape of the spectral reflectance curve. Raines and Lee (1975) found, using normalized reflectance values, that there is no significant (95% confidence level) difference between the mean normalized reflectance among sedimentary rock types. Plots of normalized reflectance for volcanic rocks (Fig. 63) show little to no significant (80% confidence) difference between rock types. The conclusions at the 95% confidence level are identical to those for sedimentary rocks; that is, the shape of the spectral reflectance curve is the same for all rock types, only the absolute magnitude of reflectance changes from rock to rock. This further implies that the reflectance of a rock in any spectral region can be predicted by knowing the reflectance in any one spectral region.

The reflectance differences noted above for outcrops of volcanic rocks are diminished considerably with the development of soil cover and growth of vegetation. Soils throughout the volcanic province are a relatively uniform, clay-rich, brown silt. Reflectance differences between parent rock-types are not transferred to the soils developed on them. Reflectance is therefore a useful photo-interpretive key only for exposed outcrops and generally is not usable for areas with any soil development.

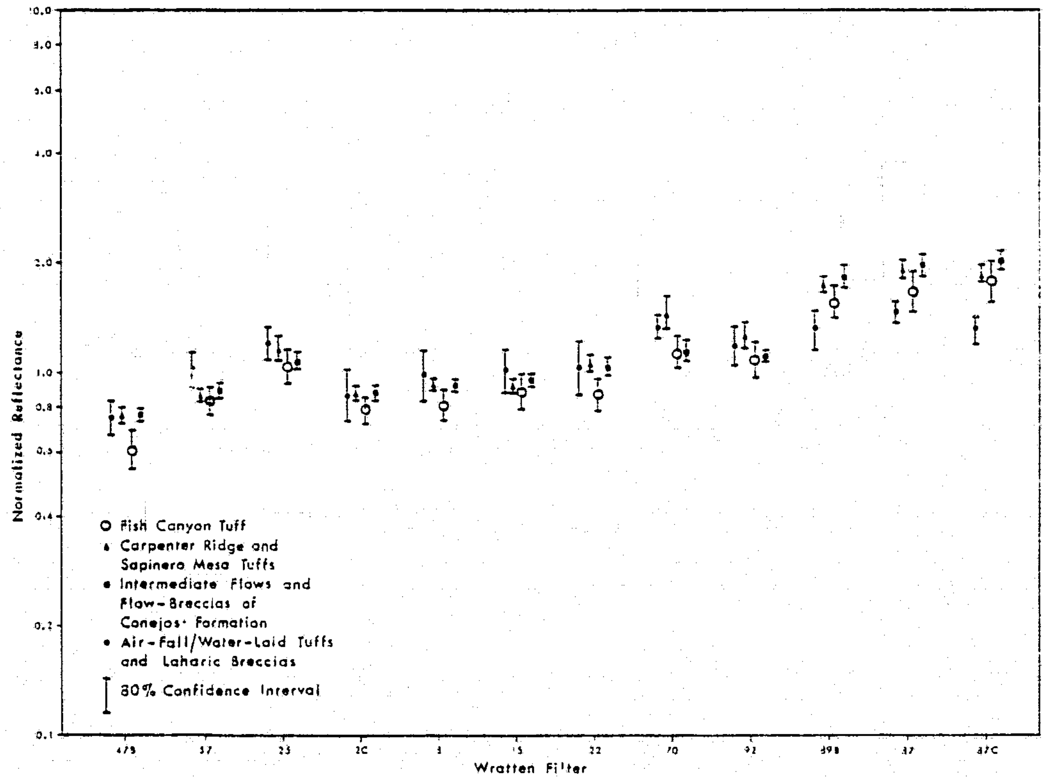


Figure 63: Normalized band reflectance, volcanic rocks.

Vegetation, with only one exception, similarly decreases the reflectance contrasts found between rock outcrops in the San Juan Mountains. The exception to this is the Fish Canyon Tuff, which is favored by pinyon pine and juniper (Fig. 64). In regions where the growth of these trees is not governed by elevation, their disturbution is often restricted to soils developed on the Fish Canyon Tuff.

## RESOLUTION

Geomorphic expression of hydrogeologic units, and therefore the ground resolution of the film-camera system, is the most important parameter dictating the success of photo-interpretation in all hydrologic provinces. In the Precambrian-Paleozoic rock complex of the Sangre de Cristo Mountains, where variation in hydrologic properties between rock types is minimal, rock discrimination is also minimal. The high degree of cementation and induration of the sedimentary rock sequence, together with the strong foliation of the metamorphic rocks, minimize variations in outcrop resistance and surface drainage characteristics and similarly minimize variation in permeability. A similarity in hydrologic properties is therefore associated with a similarity in geomorphic expression in this province.

In the San Luis Valley, surficial units are mapped primarily on the basis of relative elevation and drainage pattern. The degree to which the surficial units can be subdivided,


REPRODUCIBILITY OF THE ORIGINAL PAGE IS POOR

Figure 64: Aerial photograph showing selective growth of pinyon pine trees on Fish Canyon Tuff (Tfc). Contact between Fish Canyon Tuff and Conejos Formation (Tc) is indicated by dashed line. Approximate scale 1:12,000.

therefore, depends almost entirely on the ground resolution of the system (Fig. 65). On LANDSAT imagery (1:1,000,000 scale) and Skylab S190A photography (1:700,000 scale), small-scale alluvial drainage patterns generally are below the resolution capability of the system and, therefore, there is little or no discrimination between surficial units. There is, however, adequate resolution to define a general contact between bedrock and alluvium. Well-developed alluvial drainage patterns are within the resolution limits of the Skylab S190B system (1:475,000 scale), and alluvial fans can be subdivided for most of the valley. Eolian sands can also be discriminated from other Quaternary deposits at this scale. For a thorough subdivision of the Quaternary units described in this study, aircraft photography at a scale of 1:110,000 is the minimum scale necessary, although photography at twice that scale (1:55,000) is preferred. For this reason, the combined acquisition of small-scale photography with the RC-8, 6-inch focal-length lens and larger scale photography with the Zeiss, 12-inch focal-length lens is the most efficient system this author has seen for studies of this nature.

Photo-interpretation of the volcanic rocks of the San Juan Mountains is similarly largely dependent upon the geomorphic expression of the unit, and geomorphic expression is strongly correlative with hydrogeologic properties. The most permeable rocks, the fractured ash-flow tuffs and intermediate flows, are characterized by relatively high resistance to

REPRODUCIBILITY OF THE
ORIGINAL PAGE IS POOR

a)

b)

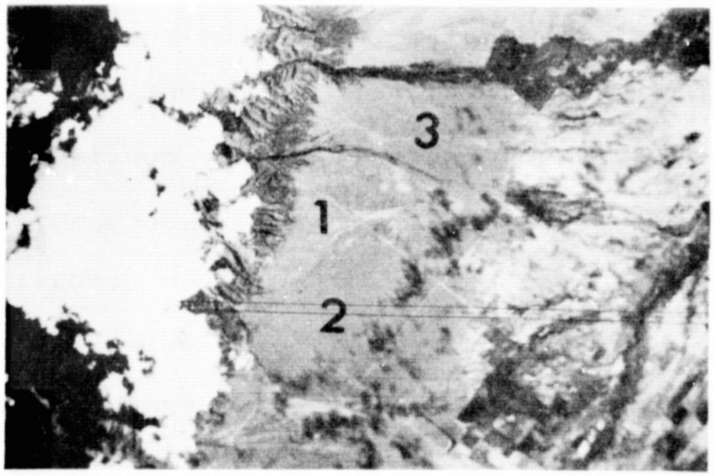


c)

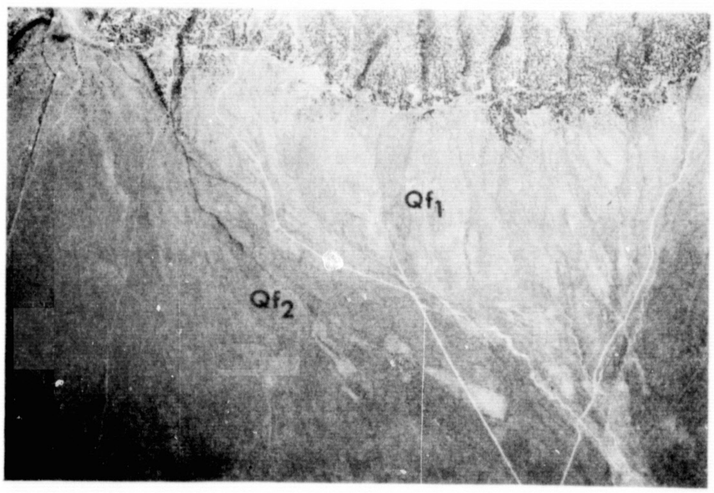


Figure 65: Effect of photo resolution on discrimination of alluvial units. a) Skylab S190A. North to upper left. Scale 1:300,000. b) Skylab S190B. North to bottom 1 = $Qf_1$, 2 = $Qf_2$, 3 = $Qf_3$. Scale 1:170,000. c) Aircraft photography. North to left. Scale 1:44,000.

erosion and coarse drainage patterns. The least permeable units, the unwelded ash-flow tuffs, the air-fall/water-laid tuffs, and the laharic breccias, occupy the slopes of plateaus, characteristically have little resistance to erosion, and have a much finer drainage network. Intrusives can be discriminated only where they are associated with dikes.

Photography of a scale of 1:110,000 or larger is required for more than minimal mapping within the volcanic terrain of the basin. Even with large-scale (1:18,000) photography, however, field work is necessary for any confidence to be placed on the resulting interpretation. Because of the control pre-existing topography exerts on the depositional patterns of volcanic units, correlation between units over large, uncontrolled areas is tenuous. Frequent points of control, or areas where the stratigraphic units are known and can be identified, are therefore a necessity in the volcanic terrain. Photography is used most efficiently in volcanic rocks when photo-interpretation is done in the field and immediately precedes field checking and mapping. The scale of the photography should therefore be dictated by the use of photography in the field as a base map. This is in sharp contrast to both the San Luis Valley and Sangre de Cristo Mountains, where the most efficient use of photography involved photo-interpretation of large areas prior to field work, and where field work consisted primarily of field checking questionable areas.

## GEOLOGIC STRUCTURE

Successful mapping of hydrologically significant geologic structure, primarily fractures, is based on both the spectral and spacial sensitivity of the photographic system. Whereas the spectral sensitivity of the film is relatively unimportant in rock discrimination because of the lack of color differences between rock units, the use of vegetation as an indicator of hydrologically significant fracturing is an important application of remote sensing to ground water studies. The most obvious example of this in the San Luis Basin is its use in mapping the Sangre de Cristo and Villa Grove fault zones. The ponding of ground water and occurrence of springs along these fault zones has been discussed previously. The heavy growth of phreatophytic vegetation in areas of spring discharge and shallow ground water produces areas of high photo-infrared reflectance following the trace of fault zones. The largest areas of ground water ponding are visible on Skylab S190A color-infrared photography, while the smaller areas require much larger scales ($\geq$1:55,000) to be resolved. The use of color-infrared film is clearly an advantage in mapping these vegetation anomalies. Some of the structures, such as parts of the Villa Grove Fault Zone near Villa Grove, would only be marginally mappable without the presence of dense vegetation along linear trends.

The detection of geologic structures that are only geomorphically expressed is dependent only upon the system ground

resolution. The scale of the structure that is mappable varies from the ability to map a generalized Sangre de Cristo Fault on Skylab S190A photography (Fig. 65a, p. 177) to the ability to map relatively small fractures on large-scale aircraft photography (Fig. 66). The lack of necessary resolution is a serious drawback to Skylab S190A photography when used to delineate the Villa Grove Fault Zone, for example, where it is expressed only as a series of fault scarps offsetting alluvial fans. Delineation of the fault zone is not possible at this scale, although on larger-scale photography it is visible as a zone of fault scarplets (Fig. 67). In this specific example, as well as in all mapping in the basin, the low sun-angle photography allows the interpreter to view geomorphically-expressed features without the use of stereo viewing. Stereo-viewing of standard photography at the same scale delineates the fault zone equally well.

Mapping of geologic structures using photography is strongly biased toward near-vertical fractures, because these fractures are best expressed on vertical photos. The well-expressed, vertical joints of Figure 66b are part of a set of orthogonal fractures, in which a near-horizontal joint orientation is well-expressed at the outcrop. Mapping of fractures only from photography has the potential, therefore, of producing an incorrect view of the distribution of fracturing, which may influence a hydrogeologic interpretation. Another bias inherent in mapping of fractures from photographs, particularly

REPRODUCIBILITY OF THE
ORIGINAL PAGE IS POOR



a)

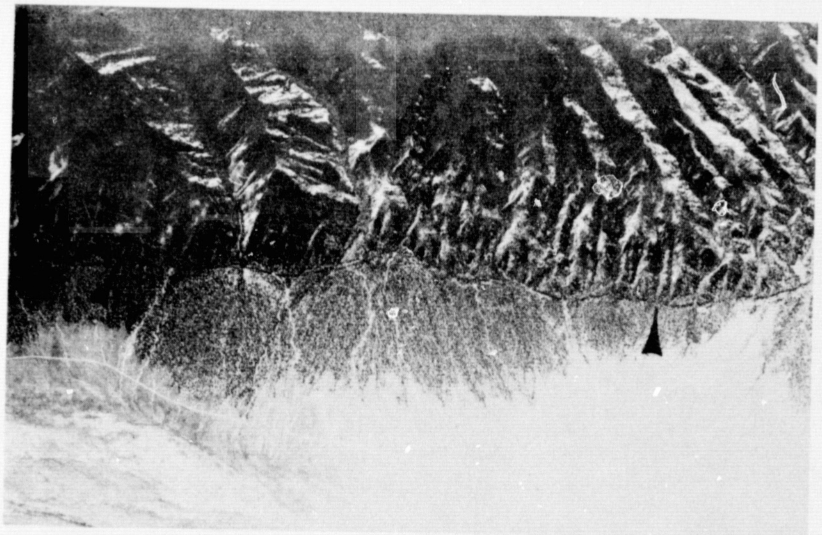

b)

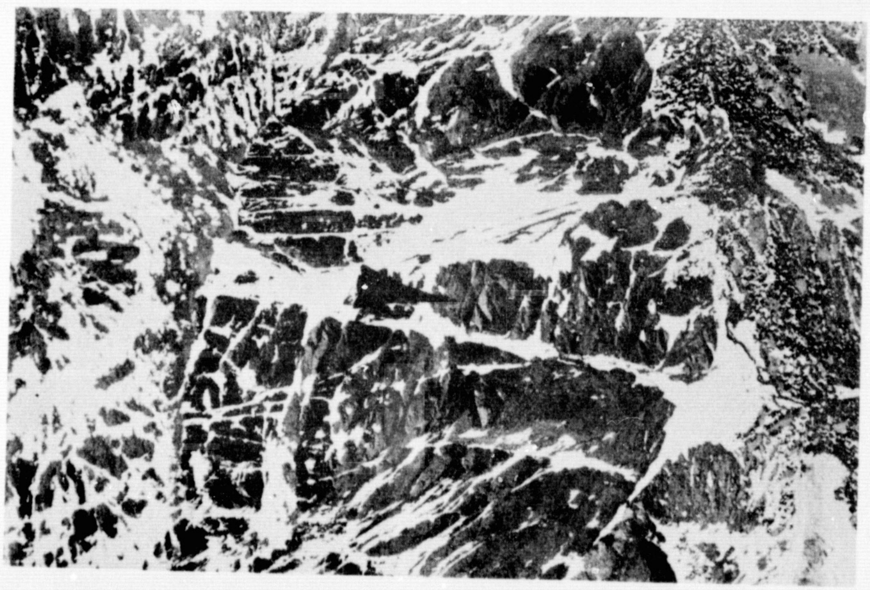

Figure 66: Effect of photo resolution on structural mapping. a) Medium-altitude aircraft photography with scarps of the Sangre de Cristo Fault indicated. North to left. Scale 1:50,000. b) Low-altitude aircraft photography with basement fractures indicated. Scale 1:12,000.

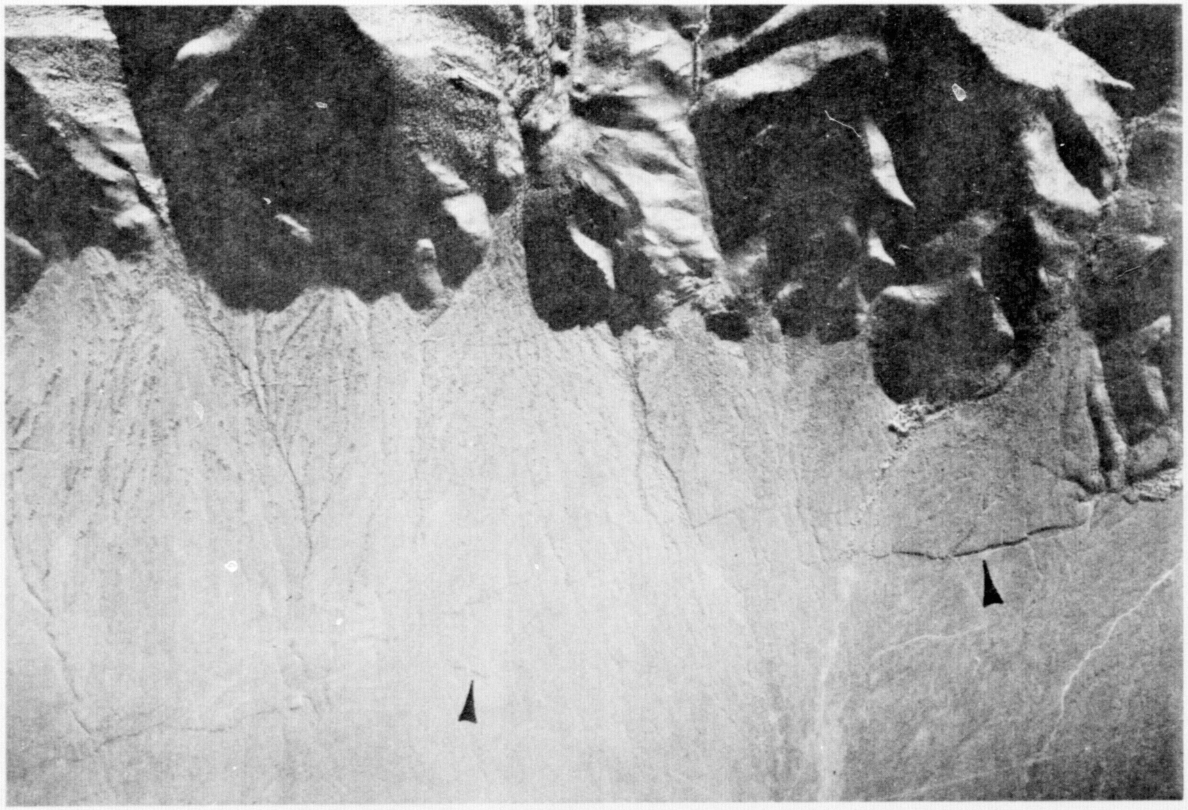

Figure 67: Low sun angle photograph, showing fault scarps (indicated by arrows) of the Villa Grove Fault Zone. Approximate scale 1:62,500.

REPRODUCIBILITY OF THE ORIGINAL PAGE IS POOR

small-scale photographs, is the bias produced by the geomorphic expression of faults. Faults with the greatest displacement generally are the best-expressed faults, as well as the faults with the best development of fault gouge and therefore the least permeable faults. The use of photointerpretation to map fractures is, therefore, inherently biased toward the least permeable fractures.

Faults not expressed geomorphically, or by alignments or anomalous growths of vegetation, must be mapped on the basis of the distribution of stratigraphic units. The ability of a photographic system to provide information useful for the interpretation of this class of structures depends only on the ability of the system to discriminate rock units. Ground resolution is therefore again the most important factor influencing the usefulness of the sensor.

## SOIL MOISTURE

Variation of reflectance of soils with varying soil moisture has been noted for some time. Attempts have been made to map soil moisture variations using empirically derived relations between moisture content and reflectance of individual soils. Success at this on a broad scale - i.e., the ability to relate reflectance to soil moisture for all soils, has broad implications. The relation between evapotranspirative rates and ground water depth given earlier (Fig. 8, p. 25), is a second order relation, caused by a

relation between soil moisture and evapotranspirative rates. The ability to remotely determine soil moisture could be used both as a way to estimate ground water depth and as an important data input for the estimation of evapotranspirative discharge.

These schemes are unpractical if a region has numerous soil types and if an empirical relation must be determined for each soil type. Direct measurement of ground water depths in this case would take less time than repetitive measurements of soil moisture and reflectance for every soil type. Recently, Piech and Walker (1974) presented some evidence that soil moisture not only decreases the absolute reflectance of soils, but also changes the shape of the spectral reflectance curve, decreasing the blue-band reflectance more than reflectances in other bands. If consistant, this property would allow estimation of soil moisture for all soils using multiband photography and minimal laboratory work. To test this for soils in the San Luis Valley, band reflectance measurements were taken for varying moisture contents of eight soils, and normalized reflectances were computed by dividing by the no-filter (NF) band reflectance.

The results (Fig. 68) contradict the conclusions of Piech and Walker (1974). Even at the 80% confidence level, there is no significant difference between the mean normalized reflectance of dry soils and soils with widely varying moisture content. The narrow confidence intervals for the moist soils

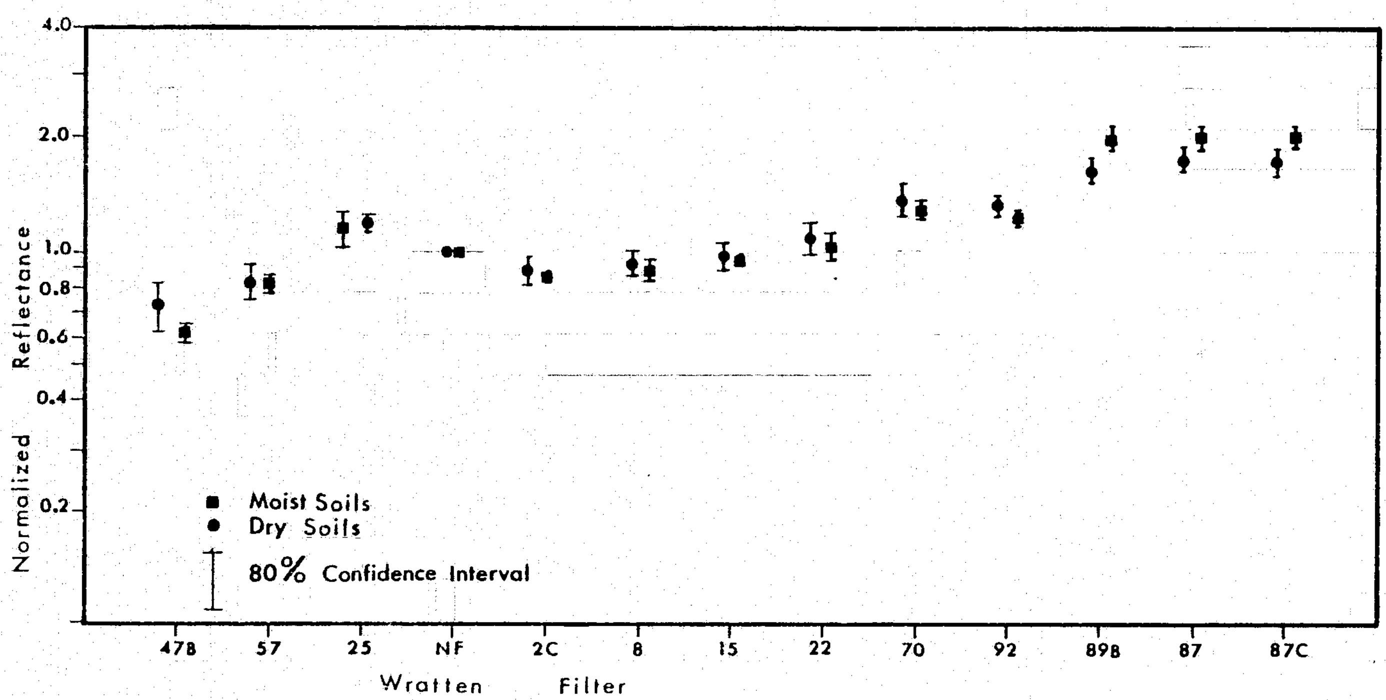


Figure 68: Normalized reflectance, dry and moist soils.

further suggests that there is little variation within the moist soils group. The conclusion of this author is that there is no significant change in the shape of the spectral reflectance curve for varying soil moisture, and therefore soil moisture cannot be related to reflectance for all soils by a general expression using some change in the spectral reflectances within the 400-900nm region.

Use of reflectance to quantitatively determine soil moisture must therefore involve the determination of a separate relation of soil moisture versus reflectance for each soil, as shown in Figure 69 for the eight soils sampled from San Luis Valley. Although most of the curves show a general decrease in reflectance with increasing soil moisture, the details vary considerably, and, even for soils of similar texture, separate relations must be determined for each soil.

## GROUND WATER DEPTH

Two approaches were followed in an attempt to determine ground water depth and quality using photographic sensors. The first approach consists of determining the relationship between vegetation type and density and ground water depth and then defining the minimum contrast between vegetation zones that is identifiable on photography. The second approach is an attempt to relate saline soils, which appear as light areas on photographs, to ground water depth and quality.

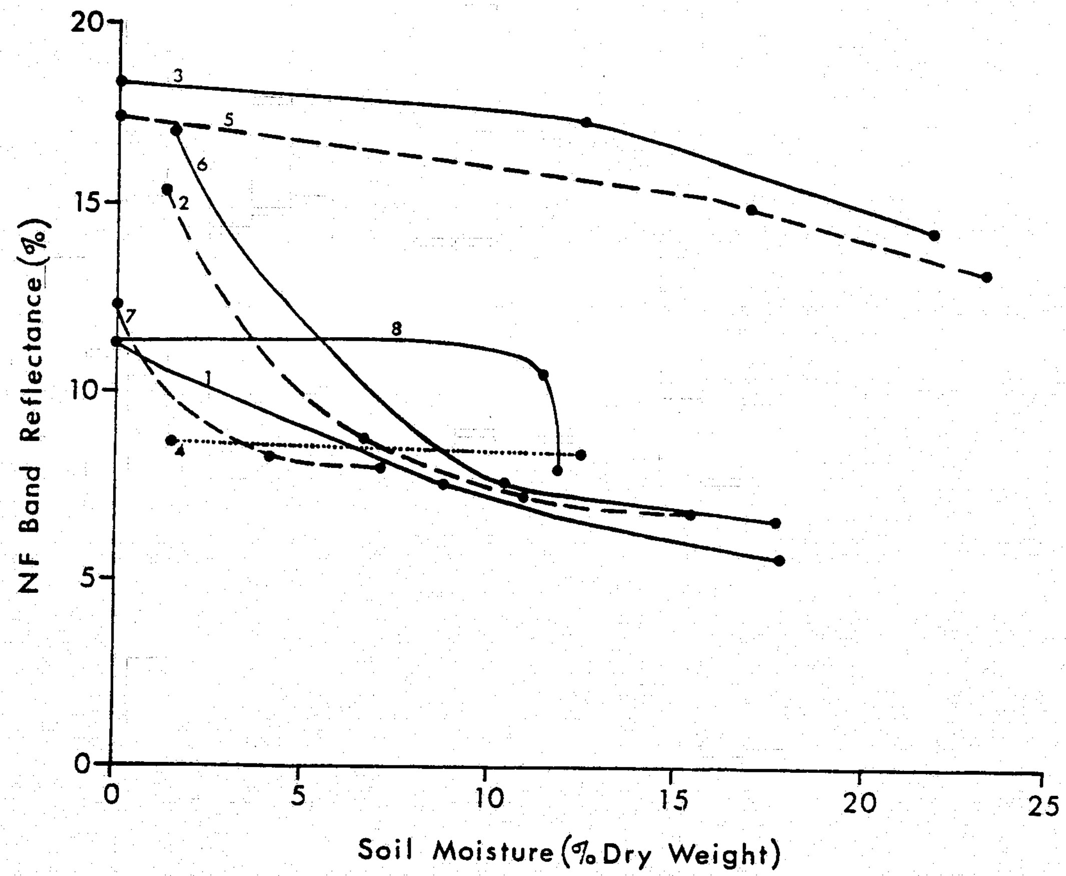


Figure 69: No-filter reflectance as a function of soil moisture. Numbers on plot refer to sample numbers (see Appendix C for description).

## VEGETATION INDICATORS

Several relations were observed between vegetation type and ground water depth in San Luis Valley. Thick stands of narrowleaf cottonwood trees are found where the water table is less than five meters from the surface, while thin stands of narrowleaf cottonwood are restricted to the immediate vicinity of perennial streams. An excellent example of the correlation between the growth of cottonwood trees and depth to saturated sediments is found at the town of Crestone (Fig. 70), where stands of cottonwood outline a region of shallow perched ground water, while xerophytic vegetation is found where ground water is deep (9-100 m).

Narrowleaf cottonwood trees are restricted to areas of good water quality, while growths of willow, which have an identical relation to ground water depth, are restricted to only areas of moderate to good water quality. The dark areas within San Luis Valley on the band four (green) LANDSAT mosaic of the basin (Fig. 2, p. 4) are primarily areas of narrowleaf cottonwood and willow. At this scale, there is no distinction possible between areas of shallow water table and areas of saturated stream-bank sediments. At larger scales (1:55,000), it is sometimes possible to discriminate between the two situations.

The density of rabbitbrush, greasewood, and saltbush can sometimes, but not consistantly be correlated with ground water depth. Figure 71 shows an excellent example of the

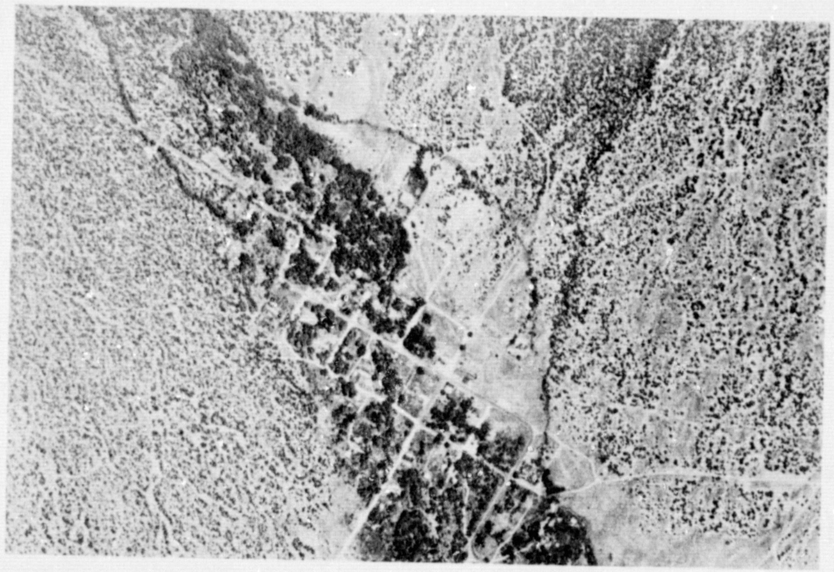

Figure 70: Aerial photograph of Crestone, showing narrowleaf cottonwood trees in areas of shallow ground water and other vegetation (brush & pinyon pines) in areas of deeper ground water. Approximate scale 1:15,000.

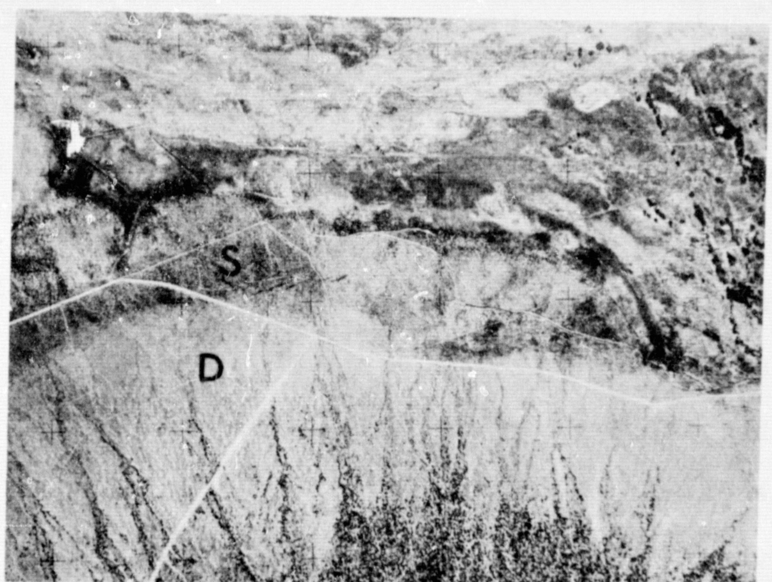


Figure 71: Aerial photograph, showing dense rabbitbrush in areas of shallow ground water (S) and xerophyte grasses in areas of deep ground water (D). Approximate scale 1:50,000.

control exerted by ground water depth on vegetation density. In this area, sparse growths of xerophytic grasses and shrubs are found where the water table is greater than 9 m (30 ft) deep, while very dense growths of rabbitbrush and greasewood are found where the water table is within 9 m of the surface. Where such a contrast or gradation of vegetation types or densities is observed, interpretation of ground water depth can be done confidently, but the reverse is not necessarily true; absence of dense rabbitbrush does not always indicate deep ground water.

Wiregrass and other succulent grasses and rushes and sedges commonly are found in areas where the water table is less than one meter from the surface, and periodically reaches the surface, and in areas of spring discharge.

Other vegetation, such as scrub oak, rock spirea, and gooseberry is found in areas of increased soil moisture, often related to shallow ground water. Vegetation found upgradient of the Villa Grove Fault Zone near Villa Grove is scrub oak, growing in an area where soil moisture is as high as 3.5% in a region where normal soil moistures vary from 0.6 to 2.0% (Wychgram, 1972).

Of the above relations, only the cottonwood/willow and the scrub oak assemblages can be used at satellite-scale resolution, because of the high photo-infrared reflectance of these deciduous vegetation types. Comparison of the land use map compiled from interpretation of Skylab S190A color-infrared

photography (Fig. 7, p. 23) and a ground water depth map (Fig. 72) shows a strong correlation between very shallow ground water (<2 m) and stream-associated vegetation. The correlation breaks down where agricultural practices have eliminated the natural vegetation or where the water quality is poor. This is the limit of estimation of ground water depth at this resolution. Density variations within brush-type vegetation are not observable with available satellite resolution, nor are areas of wiregrass or other succulent grasses associated with shallow ground water and springs.

High-altitude aircraft color-infrared photography (1:110,000) has sufficient resolution to detect sharp variations in vegetation densities, such as that seen in Figure 71 (p. 189), and large to moderate-size areas of succulent grasses. Intermediate (1:55,000) to large-scale (1:20,000) photography is required to use more subtle vegetation density variations as ground water depth indicators and to detect succulent grasses associated with small springs.

Vegetation indicators must be interpreted with care. As with the other indicators, their presence often suggests shallow ground water, but shallow ground water is often present without the vegetation indicator. Because of the high photo-infrared reflectance of deciduous vegetation, color-infrared film contains information, important in the mapping of vegetation, that is not present in other films. Although stereo viewing is not an absolute necessity, as it

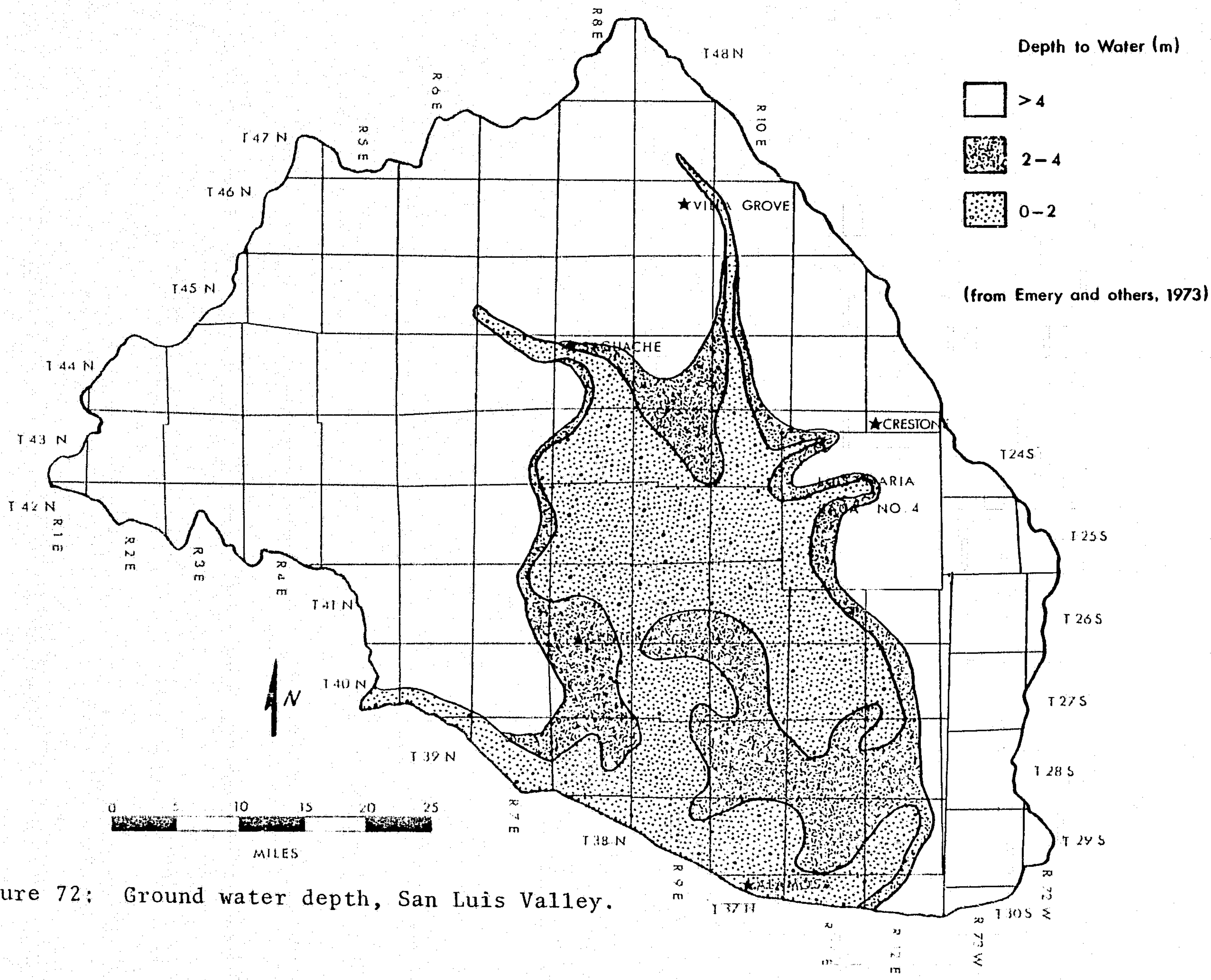


Figure 72: Ground water depth, San Luis Valley.

is in geologic interpretation, it greatly aids the interpretation, particularly in discrimination of trees from brush and grass.

## SALINE SOIL INDICATORS

Possible relations between saline soil and ground water depth were first observed on LANDSAT imagery and studied in more detail on Skylab 3 S190A photography (Fig. 73). The distribution of saline soils was mapped from S190A photography (Fig. 74) and was studied to determine its relation to ground water depth, quality, and direction of flow. Reflectances of dry saline soils, and moist and dry non-saline soils, were measured to determine the best method for isolating the saline soils on photography.

Comparison of the interpreted soil salinity (Fig. 74) with ground water depth (Fig. 72, p. 192) shows that saline soils develop only where the ground water is relatively shallow, but that saline soils are not present everywhere the water table is near the surface. Saline soils are not present, or are masked, in areas of agricultural land use, as seen when the saline soils distribution is compared with the vegetation/land use map (Fig. 7, p. 23). Overhead irrigation in agricultural areas tends to rinse the soil free of heavy surface accumulations of salts and, at the same time, the agricultural crops tend to hide soils at the resolution of satellite photography.

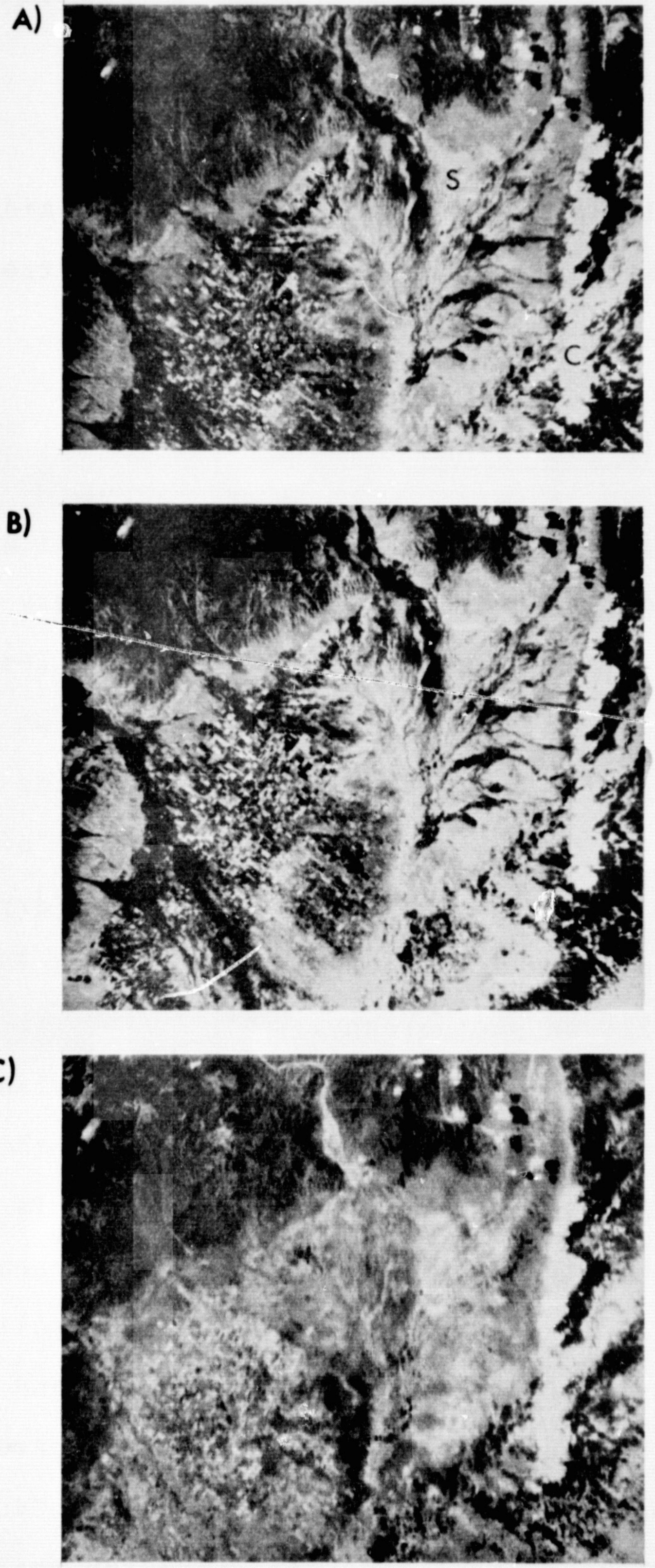


REPRODUCIBILITY OF THE
ORIGINAL PAGE IS POOR

Figure 73: Skylab multiband photographs, showing saline soils (labeled S in 73a) as areas of high reflectance in San Luis Valley. Clouds (labeled C in 73a) also appear as areas of high reflectance, as do areas of deciduous vegetation in 73c. A) Green band, B) Red band, C) Photo-infrared band. North is to the upper right. Approximate scale 1:1,500,000.

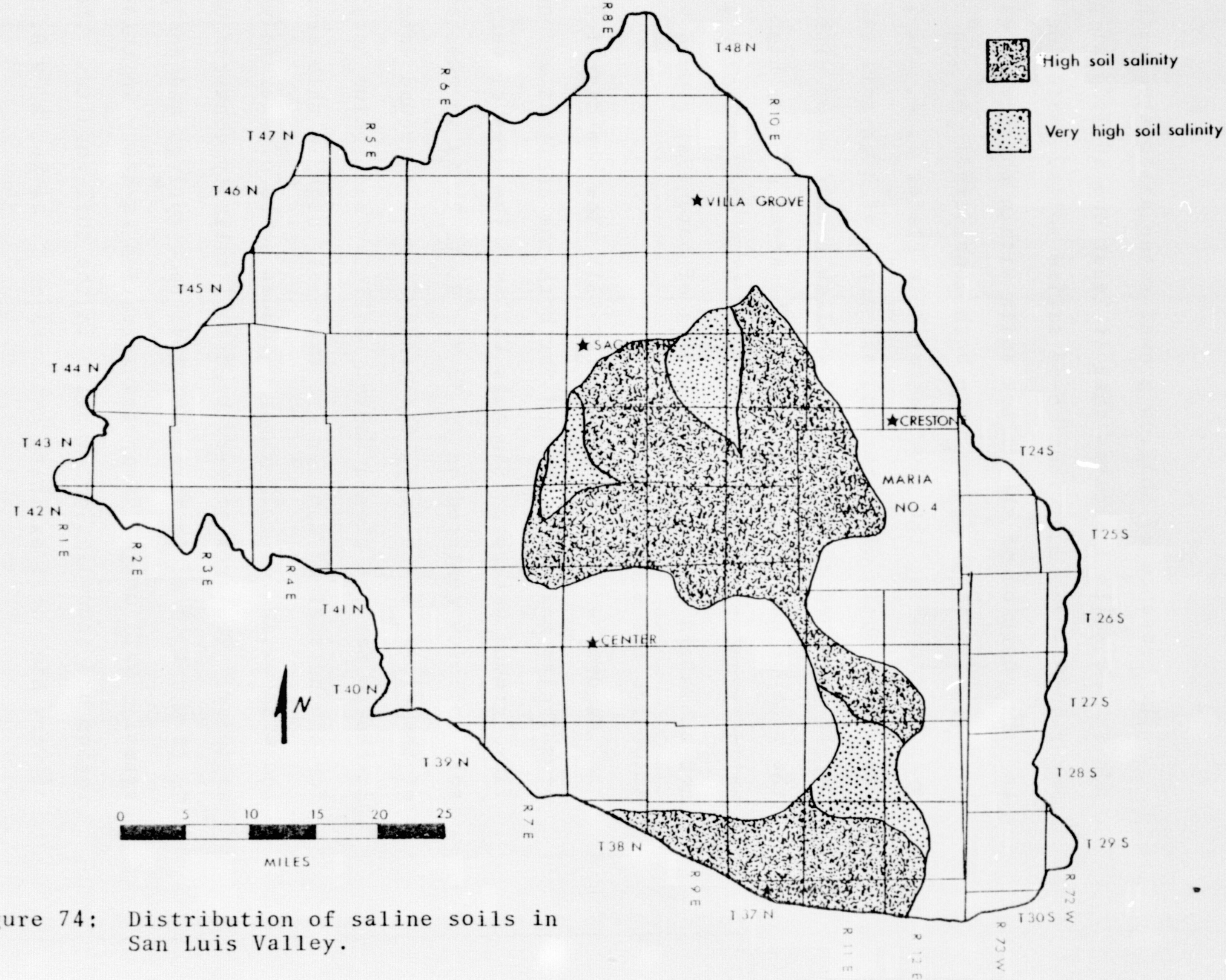


Figure 74: Distribution of saline soils in San Luis Valley.

The presence of shallow ground water associated with non-saline soils indicates that at least one additional parameter limits the distribution of saline soils. Water quality and the position of the saline soils within the ground water recharge/discharge system were both considered. As can be seen by comparing the flow patterns in Plates 3, 4, and 5 with the saline soils distribution, all areas of high soil salinity can be represented as areas of shallow ground water within the zone of potential discharge. The areas of very high soil salinity and the eastern boundary of high soil salinity are not explained by even a combination of potential ground water discharge and shallowness.

Figures 47 through 50 (p. 127-131) show the distribution of salinity and sodium hazard for both the confined and unconfined ground waters of San Luis Valley. The area of very high soil salinity centered on T. 39 N., R. 11 E. is in the center of the closed basin sump, the central area of ground water discharge for the closed basin. Salinity and sodium hazards for the unconfined aquifer are extremely high in this area and evaporation of this water produces soils of extremely high salinity. The area of very high soil salinity centered on T. 43 N., R. 8 E. is a region of surface springs and heavy artesian well usage. Evapotranspiration is heavy in this region and accumulation of salts in the soil results. The area of very high soil salinity centered on T. 44 N., R. 9 E. is one where evaporation from the water table (at a depth of 2-4 m)

is minimal, but artesian wells are used heavily and evaporation from accumulated surface water is substantial. The westward flexture of the soil salinity boundary near the southern boundary of the Luis Maria Baca No. 4 correlates well with areas of relatively high water quality in both the unconfined and confined aquifers.

Areas of high soil salinity appear to correlate relatively well with areas of shallow, discharging ground water that contain at least a moderate concentration of salts. The use of soil salinity in the interpretation of ground water depth appears to be more dependable than vegetation, if interpreted with care. With this in mind, examination of the spectral reflectance of the saline soils was undertaken to attempt to better delineate these soils.

Saline soil reflectances were measured in the field only, while dry and moist non-saline soil reflectances were measured in both the laboratory and field. The saline soils are dominantly very fine-grained silts and clays, while the non-saline soils range from clay through wind-blown sands, organic-rich peats, and cobble-strewn alluvium.

Figure 75 shows the normalized band reflectance plots for dry saline soils compared with moist and dry non-saline soils. Only the 47B (blue) band, the 2C (minus UV) band, and the 89B, 87B, 87C (photo-infrared) bands show significant separations at the 80% confidence interval. Saline soils having a high average reflectance show a reduced slope of increased reflectance

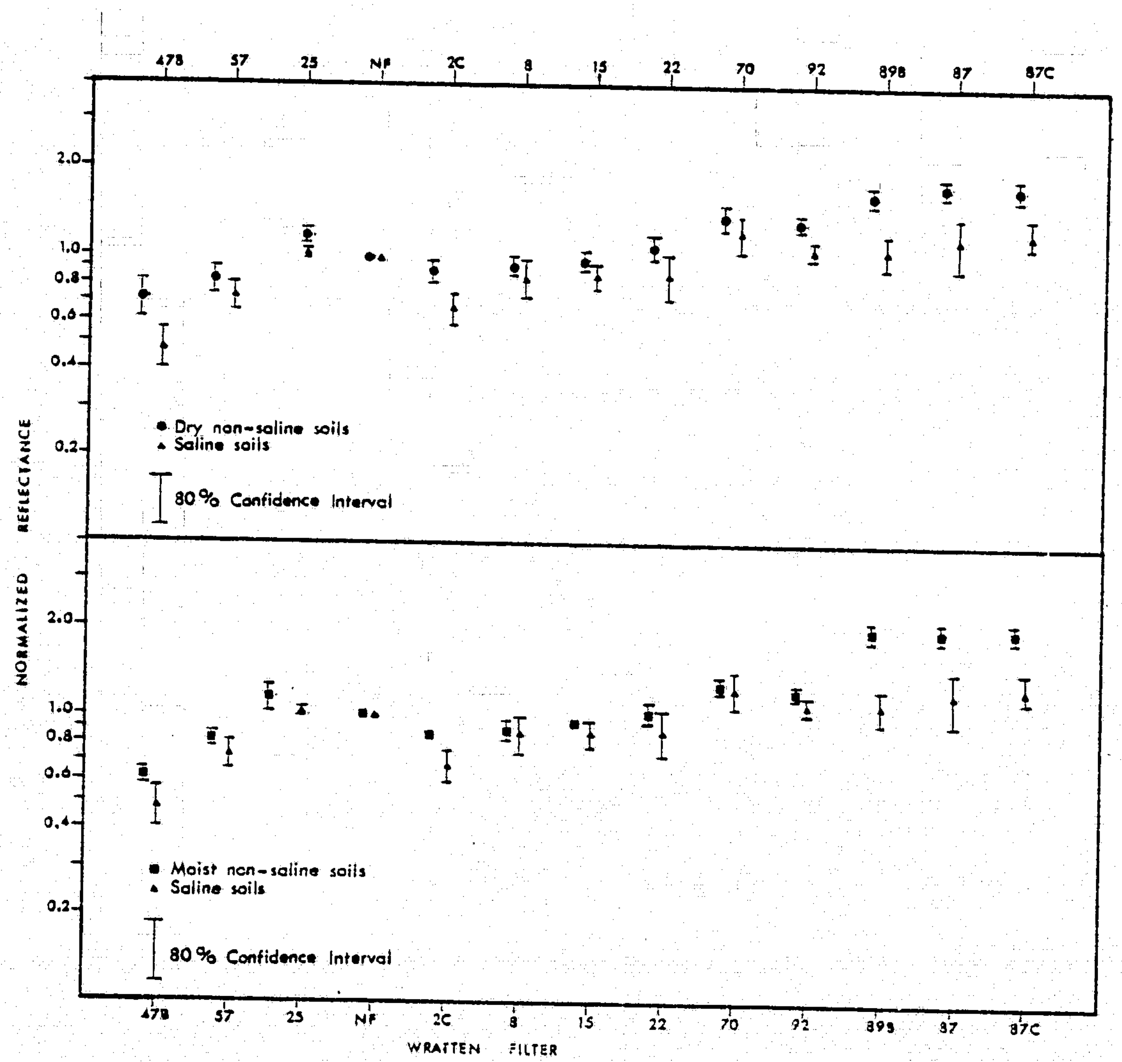


Figure 75: Normalized band reflectance, dry saline and non-saline soils.

towards the infrared region. These observations indicate that ratioing may help increase the contrast between high reflectance units, such as saline soils, and soils having the usual range of intermediate reflectances. This has not been tested in application.

A plot of absolute band reflectances for dry non-saline and saline soils is shown in Figure 76. There is significant (80% confidence level) separation of the means in all bands, with the greatest separations found in the green, red, and no-filter bands. These observations agree with the subjective evaluation of Skylab S190A photography (Fig. 73), where the infrared band shows lower contrast between saline and non-saline soils.

In general, the presence of saline soil more reliably indicates shallow ground water than do vegetative indicators, but saline soils are also dependent upon the position within the regional flow system and ground water quality. In addition, saline soils are resolvable at satellite resolution.

## THERMAL-INFRARED SENSING

Thermal infrared scanners measure the radiometric temperature of the ground, which is a function of atmospheric absorptance and scattering of the radiation and the spectral exitance of the surface. The spectral exitance of the surface is, in turn, a function of the ground temperature, the spectral

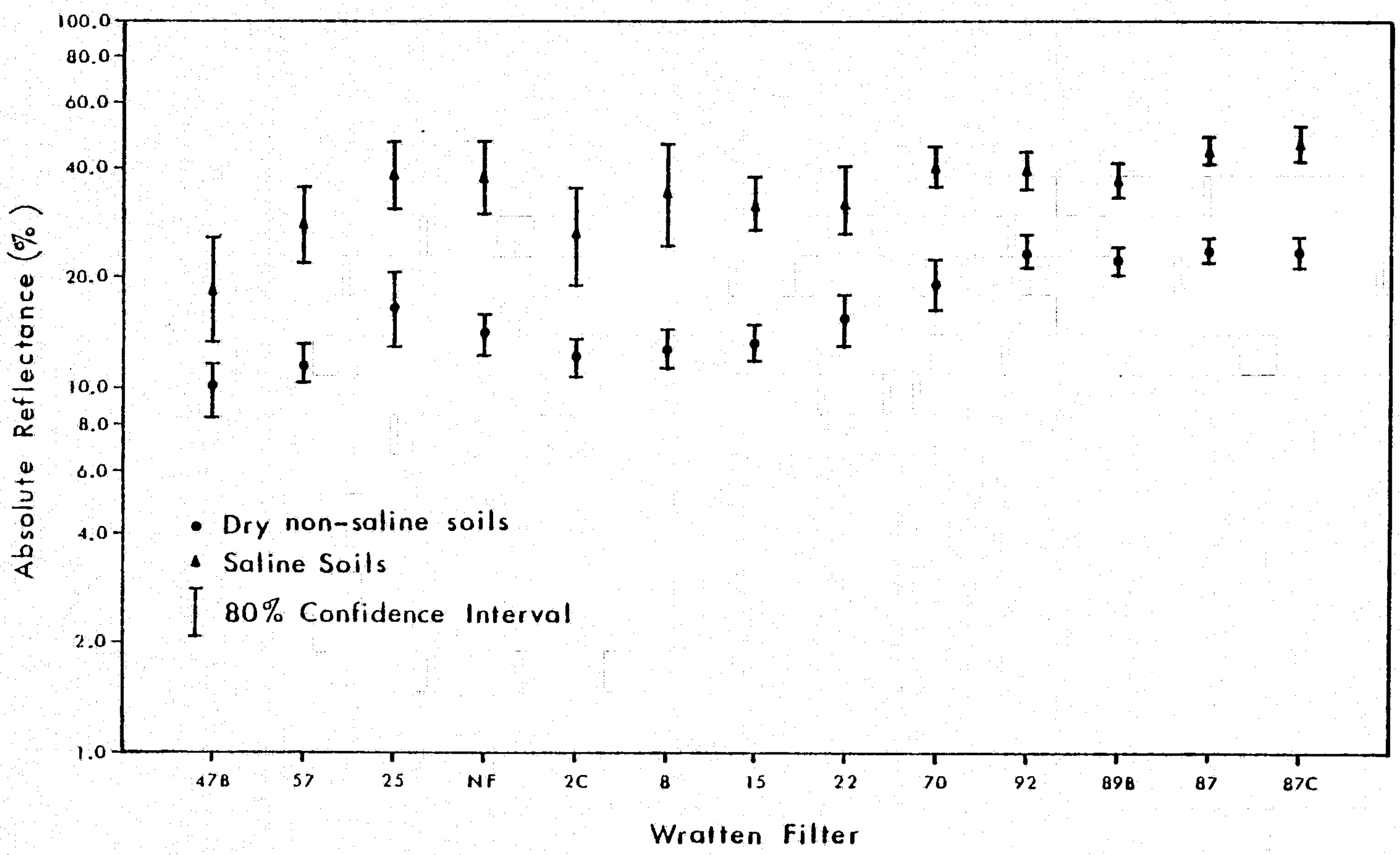


Figure 76: Absolute band reflectance, dry saline and non-saline soils.

emissivity of the ground, and the spectral region under consideration. As atmospheric effects are generally constant across the field covered by an image, the patterns in a thermal infrared image, in which film density is inversely proportional to radiometric temperature, primarily record variations in spectral emissivity and ground temperature.

Variations in spectral emissivity among geologic materials are relatively small, with the 8-14μm emissivity sometimes varying from 0.90-0.95, but more commonly remaining near 0.95 (Watson, 1975). To further decrease the significance of error in the spectral emissivity term, it should be realized that spectral emissivity not only affects the radiometric temperature of a soil, but also the surface temperature of the soil through radiative heat transfer, with the two effects acting in opposite directions. Materials with low emissivities have increased soil temperatures because of low rates of radiative heat loss, but decreased radiometric temperatures, and the two effects nearly cancel. Errors produced, therefore, by simplifying assumptions of spectral emissivity are low, and it can safely be said that radiometric temperatures recorded by thermal scanners are primarily a function of surface temperature.

If one-dimensional heat flow is assumed, the equation governing the soil temperature is;

$$\frac{\partial u}{\partial t} = \alpha \frac{\partial^2 u}{\partial x^2}$$

where $u(x,t)$ = Temperature, as a function of position and time.

$\alpha$ = Thermal diffusivity.

The boundary condition at the surface of the earth is governed by the necessary equivalence of the heat flow into or out of the system by surface processes to the conductive heat flow beneath the surface. The heat flow at the surface is the sum of radiative heat loss and absorptance of solar and sky radiation.

$$q_s = R_{solar} + R_{sky} - R_r$$

where $q_s$ = Surface heat flow.

$R_{solar}$ = Solar radiation absorbed by the surface.

$R_{sky}$ = Sky radiation absorbed by the surface.

$R_r$ = Radiative heat loss from the surface.

$$q_d = K \frac{\partial u}{\partial x}$$

where $q_d$ = Conductive heat flow at depth.

K = Thermal conductivity.

u = Temperature.

x = Vertical coordinate direction.

The upper boundary condition is therefore determined by;

$$q_d = q_s$$

$$K \frac{\partial u}{\partial x} = R_{solar} + R_{sky} - R_r$$

$$\frac{\partial u}{\partial x} = \frac{1}{K} \left( R_{solar} + R_{sky} - R_r \right)$$

Two different lower boundary conditions have been used by various authors. Kahle and others (1975) use a zero heat flux condition at 25 cm depth, a condition that requires temperatures above and below the 25 cm boundary to be equal. As this condition was not met for any of the temperature determinations in San Luis Valley, a different boundary condition is favored by this author, one of diurnally constant temperature at one meter depth, or;

$$u(L,t) = C$$

where C = Constant.

L = 1 meter.

t = time.

This boundary condition can be justified by considering the expression given by Carslaw and Jaeger (1959) for the amplitude of diurnal temperature variation at depth for a material with periodic temperature fluctuations at the surface;

$$A(x) = A_0 e^{-x\sqrt{\pi/P\alpha}}$$

where $A(x)$ = Amplitude of temperature fluctuation at depth.

$x$ = Depth (cm).

$A_0$ = Amplitude of temperature fluctuation at the surface.

$P$ = Period of fluctuation at surface (seconds).

$\alpha$ = Thermal diffusivity of the material ($cm^2$/sec).

For the maximum diurnal variation in surface temperature observed in San Luis Valley (40°C), and the maximum thermal diffusivity

measured for soils with a realistic soil moisture (0.008 $cm^2/sec$), the temperature variation at one meter depth is 0.05°C, or about 0.1% of the surface temperature variation.

Variations in the temperature of the earth's surface are, therefore, primarily due to variations in the thermal properties of the surface, the subsurface distribution of heat sources and sinks, the absorbed solar flux on the surface (as controlled by topography, meterologic factors, and solar reflectance), and the flux from a radiating sky. Because the heat flow equation and its upper boundary condition contain thermal diffusivity and thermal conductivity separately, each combination of the two terms define the diurnal temperature cycle, with all other variables held constant. The solution of the one dimensional heat-flow problem by Jaeger and Johnson (1953) in a semi-infinite medium shows that surface temperature is directly proportional to the solar absorptance of the surface and inversely proportional to the thermal inertia of the surface, where;

$$\beta = \sqrt{K\rho c}$$

where $\beta$ = Thermal inertia.

$K$ = Thermal conductivity.

$\rho$ = Density.

$c$ = Specific heat.

It can be seen, by considering that;

$$\alpha = \frac{K}{\rho c}$$

where $\alpha$ = Thermal diffusivity.

$K, \rho, c$, are as defined previously,

that, by simple algebraic manipulation;

$$\beta = K/\sqrt{\alpha}$$

While a single combination of thermal conductivity and diffusivity define a temperature cycle, they also define a value of thermal inertia. Finally, comparison of diurnal temperature cycles generated by a finite-difference model of one-dimensional heat flow with a radiative upper boundary and a constant-temperature lower boundary (discussed in more detail later) suggests that any combination of thermal conductivity and diffusivity that yields the same value of thermal inertia also produces the same diurnal temperature cycle. Thermal inertia and solar absorptance (or 1- solar reflectance) are therefore the two terrain properties that control the diurnal temperature variation in areas where the topographic effect on insolation can be ignored. Thermal inertia is inversely proportional to the amplitude of surface temperature variations, while variations in solar reflectance change the absolute magnitude of surface temperatures without strongly affecting the shape of the diurnal temperature curve. Increased solar reflectance lowers temperatures throughout the diurnal cycle (Watson and others, 1971).

## DISCRIMINATION OF HYDROGEOLOGIC UNITS

Discrimination of hydrogeologic units on thermal-infrared imagery is possible only when variations in thermal inertia and/or solar reflectance are great enough to produce detectable variations in their radiometric temperature. Several researchers (Rowen and others, 1970, Wolfe, 1971, Watson and others, 1971) have concluded that pre-dawn thermal-infrared imagery shows the maximum tonal contrast between geologic materials, both because topographic influences have been minimized, and because differential rates of cooling have maximized temperature differences at this time. Thermal imagery acquired over parts of the basin does show hydrogeologically significant capabilities in rock discrimination.

Discrimination between units within the basement complex of the Sangre de Cristo Mountains is nonexistant, both because of the low contrast in thermal and reflective properties and because of tree cover, which adds considerable "noise" to the image. Similar problems of tree-cover hinder interpretation of imagery in the San Juan Mountains. In addition, though considerable temperature contrast would be expected between the dense, fractured aquifers and the less-dense aquitards, covering of slopes with talus of dense rock eliminates any significant temperature contrast. Although the dense talus may be only 10-50 cm thick, it is sufficient to thermally mask any underlying material.

Thermal-infrared imagery does have considerable capability in discriminating hydrogeologically significant Quaternary deposits in San Luis Valley. The greatest thermal contrast in the basin occurs between the basement rock and the Quaternary deposits in the valley (Fig. 77) and between the eolian sands and some of the alluvial fans (Fig. 78). Where the contacts can be seen on the imagery, they are sharp and delineate a boundary not based simply on interpreted drainage patterns, but on physical changes in the material. Particularly significant is the ability to discriminate between geologic materials of similar spectral reflectances but varying densities, related to contrasting porosities.

## SOIL MOISTURE

Moisture changes in soils result in both a change in thermal inertia and a change in spectral reflectance. To determine the effect of varying soil moisture on the thermal properties of soils of San Luis Valley, an apparatus was designed to measure thermal diffusivity of wet and dry soils. The apparatus (Fig. 79) consists of a simple planar heat source (a hotplate) and a sample box, insulated on five sides and heat-conductive on one end. Soil temperatures at known distances from the heat source are measured at successive time intervals. The one-dimensional transient heat flow equation, given previously, applies, so that if temperatures are measured at points $x_1$, $x_2$, and $x_3$ from the heat source, each point

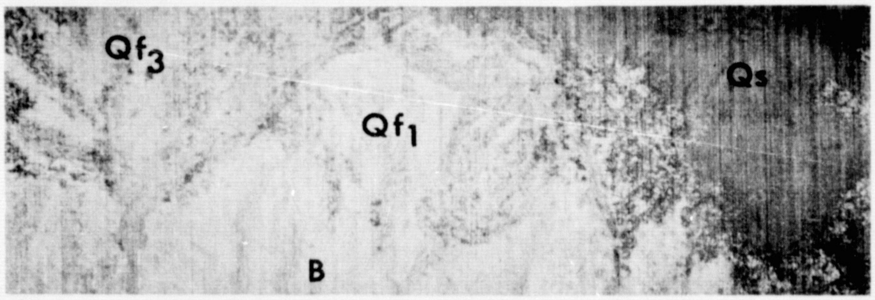


Figure 77: Pre-dawn thermal-infrared image, showing radiometric temperature contrast between eolian sands (Qs) and basement rock (B).

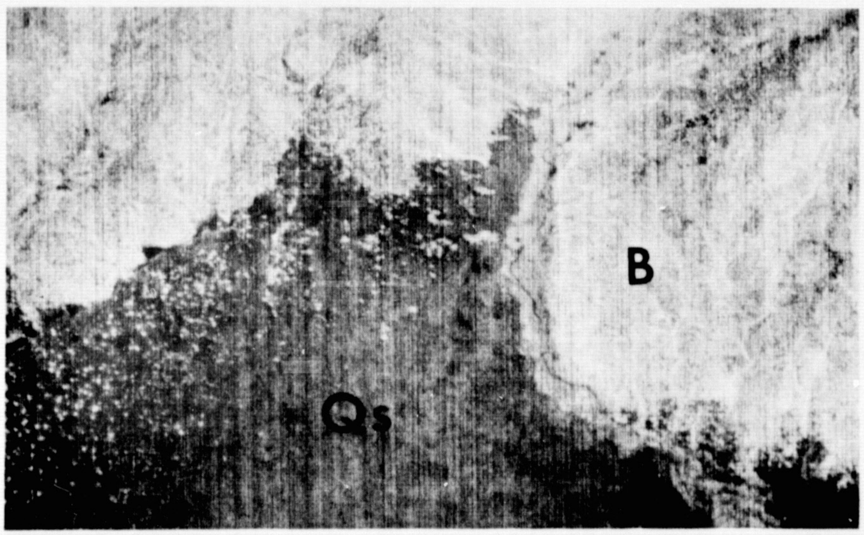


Figure 78: Pre-dawn thermal-infrared image, showing temperature contrasts between surficial units (Qs, $Qf_1$, $Qf_3$).

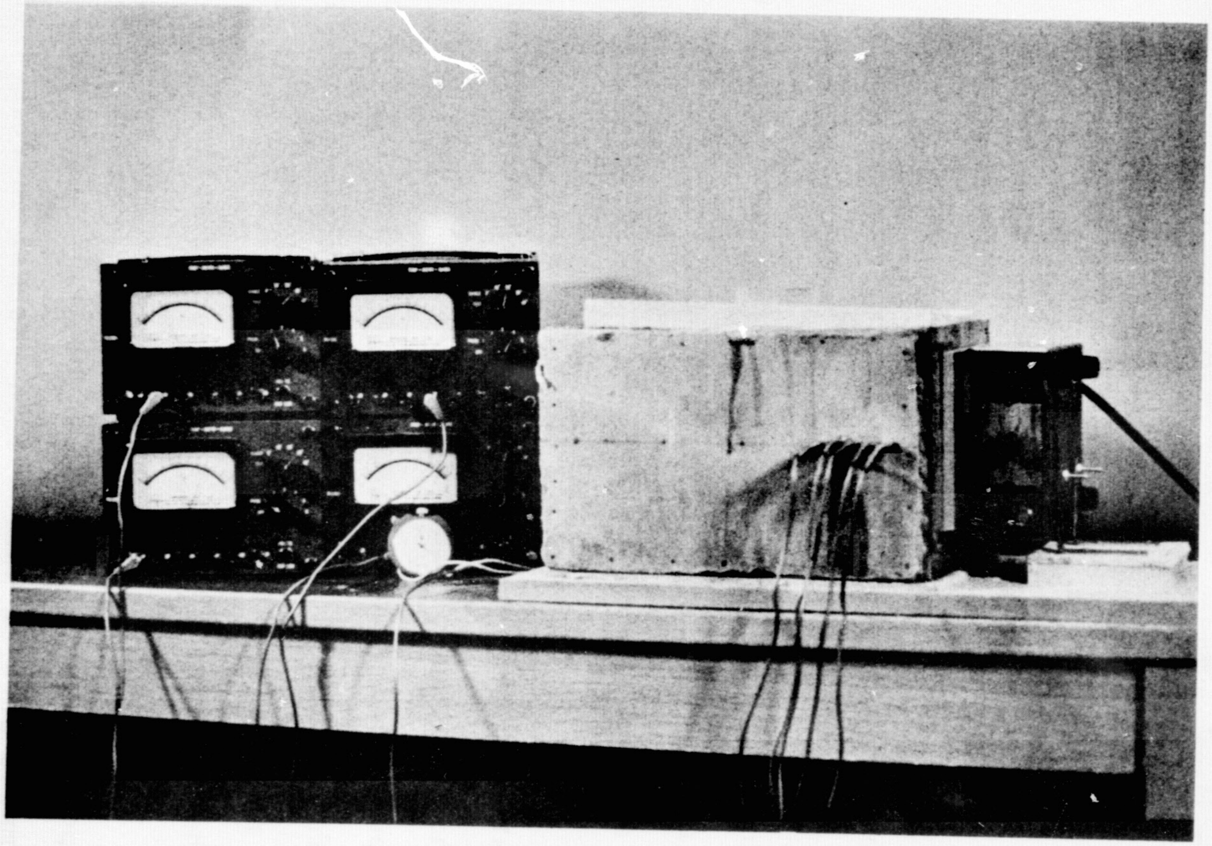

Figure 79: Apparatus used to determine thermal diffusivity of soil samples. Instruments are, from left to right; bank of thermister bridges, sample box with thermister probes inserted, and vertically mounted hotplate.

REPRODUCIBILITY OF THE ORIGINAL PAGE IS POOR

separated by distance $\Delta x$, then

$$\frac{\partial^2 u}{\partial x^2} = \frac{(u_1 - u_2) - (u_2 \cdot u_3)}{\Delta x^2}$$

where $u_{1,2,3}$ = temperature at $x_1$, $x_2$, $x_3$.

The quantity $\frac{\partial u}{\partial t}$ can be measured at point $x_2$, and

$$\alpha = \frac{\partial u}{\partial t} \Big/ \frac{\partial^2 u}{\partial x^2} = \frac{\Delta u_2}{\Delta t} \Big/ \frac{(u_1 - u_2) - (u_2 - u_3)}{\Delta x^2}$$

Thermal conductivity and thermal inertia can be computed using measured values of thermal diffusivity, density, and moisture content and assumed specific heat values for mineral material and water.

The instrument was tested on a sample of standard Ottawa Sand, for which values of thermal conductivity have been previously published (Woodside and Messmer, 1961). The test was successful, with values of thermal conductivity varying between 1.1 mcal/cm-sec-°C in the dry state to 7.7 mcal/cm-sec-°C in the saturated state, corresponding well to the change from 1.0 to 8.0 mcal/cm-sec-°C in the dry and saturated states, respectively, determined by Woodside and Messmer (1961).

All samples show an increase in thermal inertia with moisture content (Fig. 80) and a decrease in reflectance with increasing moisture content (Fig. 69, p. 187).

To determine the effects of these changes on the diurnal temperature cycle, and to compare these effects with those of

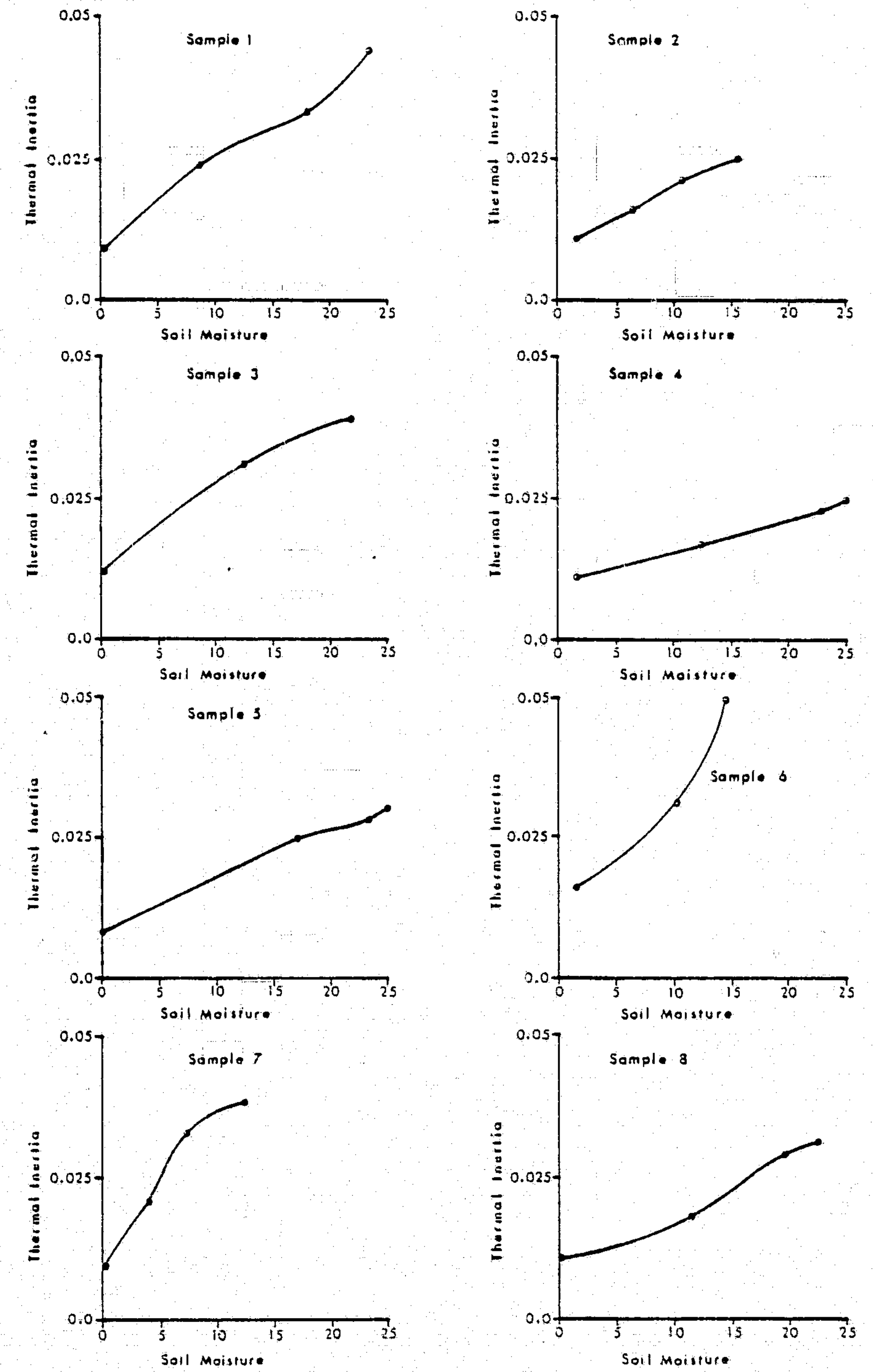


Figure 80: Relationship between soil moisture and thermal inertia for eight soils. For brief description of soils, see Appendix C.

varying ground water depth (discussed in next section), a computer program was written to solve the one-dimensional, transient heat flow equation with appropriate boundary conditions using finite-difference techniques. In more detail, the upper boundary condition is given by

$$\frac{\partial u}{\partial x}(o,t) = \frac{1}{K}((1-r)S + \varepsilon_{sky}\sigma T^4_{sky} - \varepsilon\sigma(u(o,t))^4)$$

where K = Thermal conductivity.

$(1-r)S$ = Solar radiation absorbed by the surface.

S = Solar radiation.

$(1-r)$ = Solar absorptance of the surface.

r = Solar reflectance of the surface.

$\sigma$ = Stephan-Boltzman constant.

$\varepsilon_{sky}\sigma T^4_{sky}$ = Total sky radiation absorbed by the surface.

$\varepsilon_{sky}$ = Sky emissivity (assumed to be 1.0).

$T_{sky}$ = Sky temperature that would, using the above expression, produce the same absorbed sky radiation as that observed.

$\varepsilon\sigma(u(o,t))^4$ = Total radiative heat loss from the surface.

$\varepsilon$ = Spectral emissivity of the surface.

$u(o,t)$ = Temperature of the surface.

The nighttime solar radiation is zero, while the daytime solar radiation is given by (Watson, 1975);

$$S = S_c CM(z) \cos z$$

where $S_c$ = Solar constant.

$C$ = Transmittance of clouds (0.1-0.5 (Sellers, 1965)).

$M(z)$ = Atmospheric attenuation = $1.0-0.2\sqrt{\sec z}$

$\cos z = \cos\lambda \cos\delta \sin\omega t + \sin\lambda \sin\delta$

$\lambda$ = Latitude.

$\delta$ = Solar declination.

$t$ = Time of day (measured from sunrise).

$\omega$ = Diurnal angluar velocity ($\pi$/time between sunrise and sunset).

For each point in time, the upper boundary can therefore be reduced to an expression of the form;

$$\frac{\partial u}{\partial x} = C_1 u^4 + C_2$$

where $C_1$ = Constant (varying between $1.3(10^{-8})$ and $2.6(10^{-7})$ °C/cm-°K$^4$ for the conditions assumed).

$C_2$ = Time dependent constant (varying between 0.3 and 285 °C/cm for the conditions assumed).

$u$ = Surface temperature (°K).

This can be solved iteratively using the Newton Method. Solution using this method requires a "first-guess" for the surface temperature and the temperature immediately below the surface. For this program, the "first-guess" used was the surface temperature at the previous time step, and the temperature below the surface was that of the previous time step, introducing some delay in the response of the model to rapid changes in solar flux. This technique converged after only 2-3 iterations. The heat flow system was then bounded

by known temperatures at the surface and base of the system, and the intermediate temperatures could be solved using the Crank-Nicolson equation and implicit solution techniques.

The program was tested by comparing theoretical diurnal temperature curves with measured diurnal temperature curves. The transmittance of the clouds and the sky temperature were two factors that could not be measured, but were adjusted as input variables until a best match with the measured temperature was achieved. Soil temperatures were measured over the diurnal cycle in San Luis Valley at five stations under widely varying meteorologic conditions. Adjustments in cloud transmittance and sky temperatures to obtain the best match between real and theoretical temperatures were logical and correlated well with observed meteorologic conditions. Modeled effective sky temperature varied between 265°K and 275°K, with high temperatures corresponding to nights with heavy cloud cover and low temperatures corresponding to evenings with little or no cloud cover and steady winds (increasing heat loss from the surface by convection). The cloud transmittance factor varied between 0.3 and 0.45, with low values corresponding to cloudy days and high values corresponding to relatively clear days.

The matching values of cloud transmittance and sky temperature were used as constant values throughout the diurnal cycle, whereas weather in the San Luis Valley varies considerably during a diurnal cycle. The values used could therefore

only be average values, and the matches obtained were only general matches, not taking into account fluctuations of cloud cover, wind, and other variables. This is illustrated in Figure 81, the measured and theoretical diurnal temperature curves for the first field station (D1, Plate 8). Curve matches in the late afternoon are relatively poor, because this is the time that heavy thunderstorms typically move into San Luis Valley, resulting in a rapid cooling of the land surface in the valley. The theoretical and measured curves match very well through the nighttime period, when radiative cooling is dominant. The rise of temperature at sunrise is closely matched by the theoretical curves until about 12:00 noon, where the theoretical curve falls behind the measured temperatures, both because the average cloud transmittance used was less than the real transmittance at this time of the day and because of the delay in the model for reasons explained above. The match at 10 cm depth is much better than at the surface because atmospheric variations not taken into account by the model tend to be damped out at this depth.

The curves for this first station are typical of the other stations. The match between theoretical and measured temperature cycles was consistantly better at 10 cm than at the surface, so these values were used to obtain the correct values of sky temperature and cloud transmittance. Once a best fit was achieved, these values were used to determine the theoretical effect of varying soil moisture and ground water

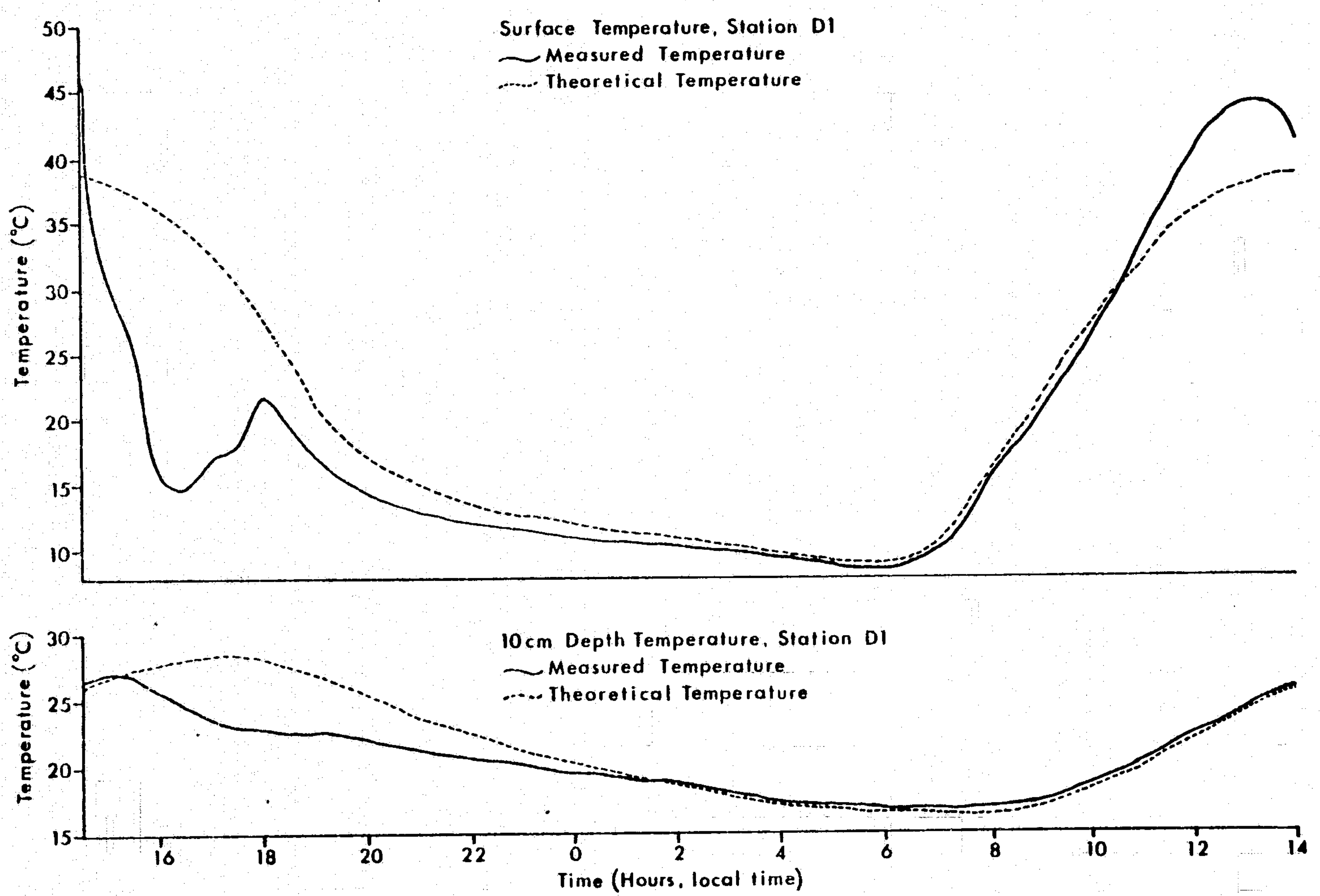


Figure 81: Theoretical and measured diurnal temperatures, station D1.

depth (described in following section) upon the diurnal surface temperature cycle.

Increasing soil moisture causes a simultaneous decrease in solar reflectance and increase in thermal inertia. The first effect produces an overall rise in the surface temperature, affecting the peak daytime temperature more strongly than the nighttime temperature (Watson and others, 1971), while the second effect decreases the amplitude of temperature variation and increases the time delay between peak insolation and peak surface temperature. Increasing the soil moisture therefore changes the absolute magnitude as well as the amplitude of diurnal variation of the surface temperature (Fig. 82). Average surface temperature changes irregularly with increasing soil moisture (Fig. 83), because of variations in the relative rates of change in solar reflectance and thermal inertia with soil moisture. Much more consistant, however, is the decrease in the amplitude of temperature variation with increasing soil moisture (Fig. 84), as well as the decrease in maximum temperature (Fig. 84) and increase in minimum temperature (Fig. 84) with increasing soil moisture. Keeping all other variables, such as sediment type, constant, knowledge of the amplitude of diurnal temperature variation to within 0.5°C (the typical minimum temperature contrast detectable with a thermal-infrared scanner) allows the determination of soil moisture to within 0.4%. Thermal-infrared imagery acquired only during the pre-dawn hours should, by this model, allow the determination of soil moisture to within 1.5%.

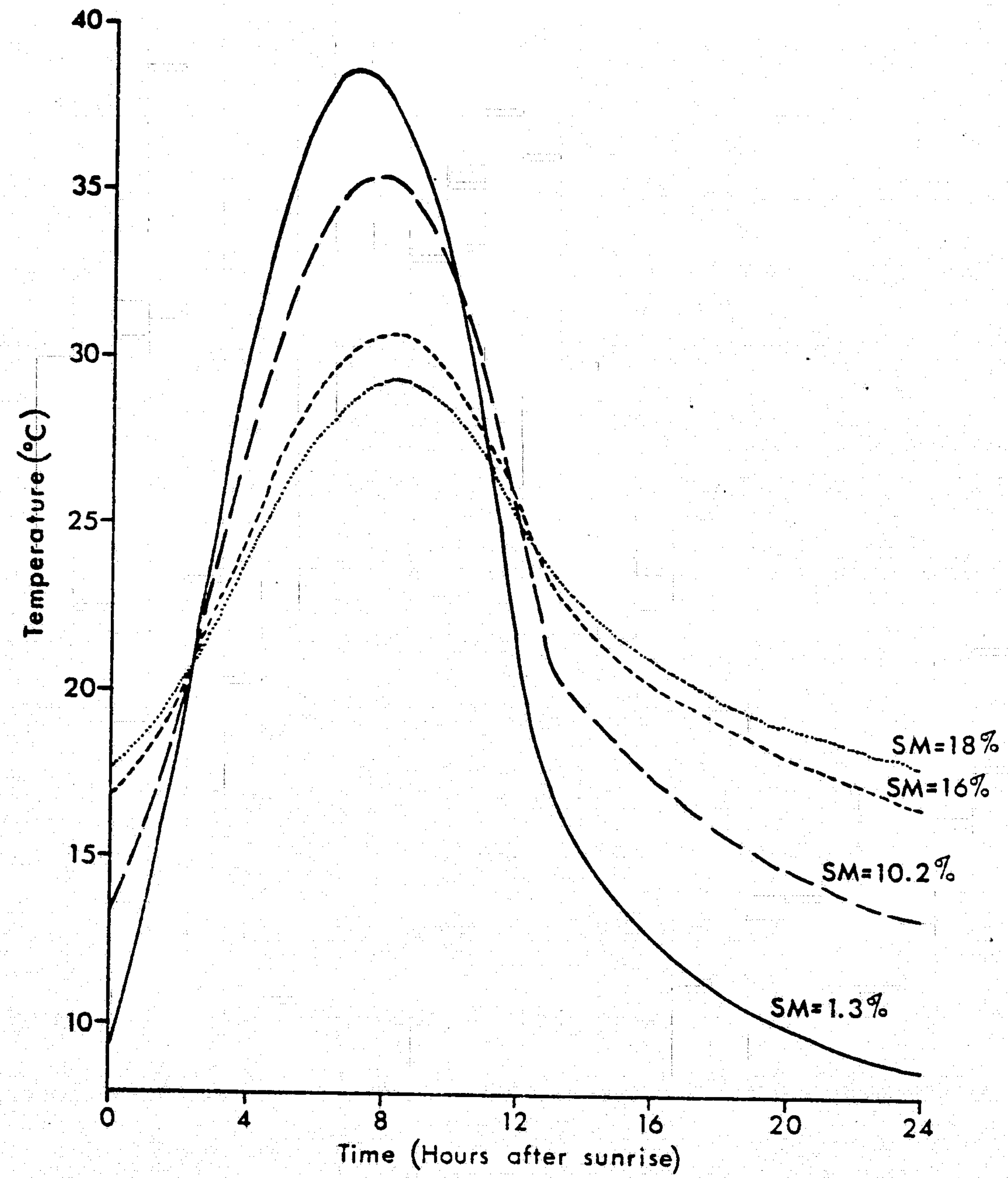


Figure 82: Theoretical effect of soil moisture on diurnal temperatures for Station D-1.

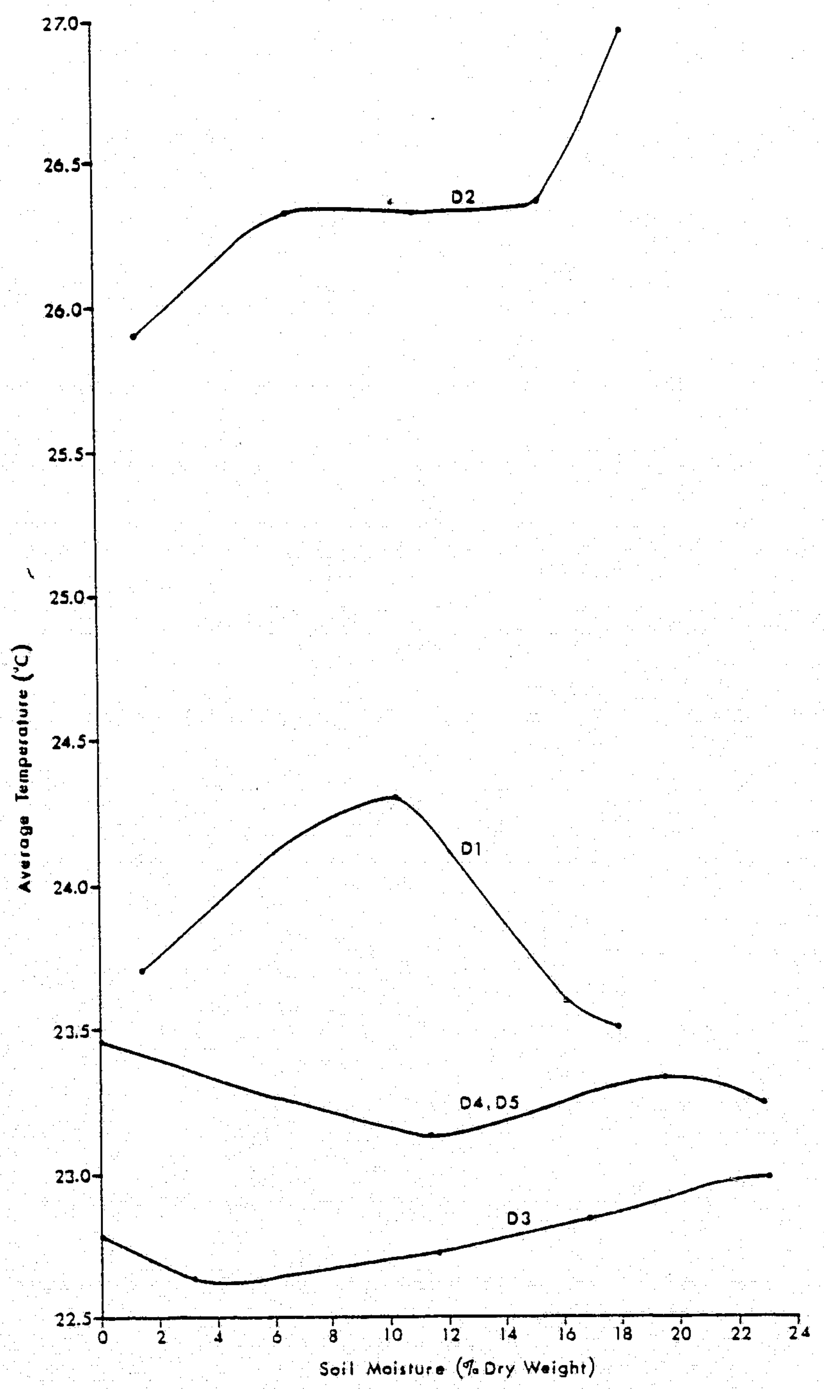


Figure 83: Theoretical relation between soil moisture and average temperature.

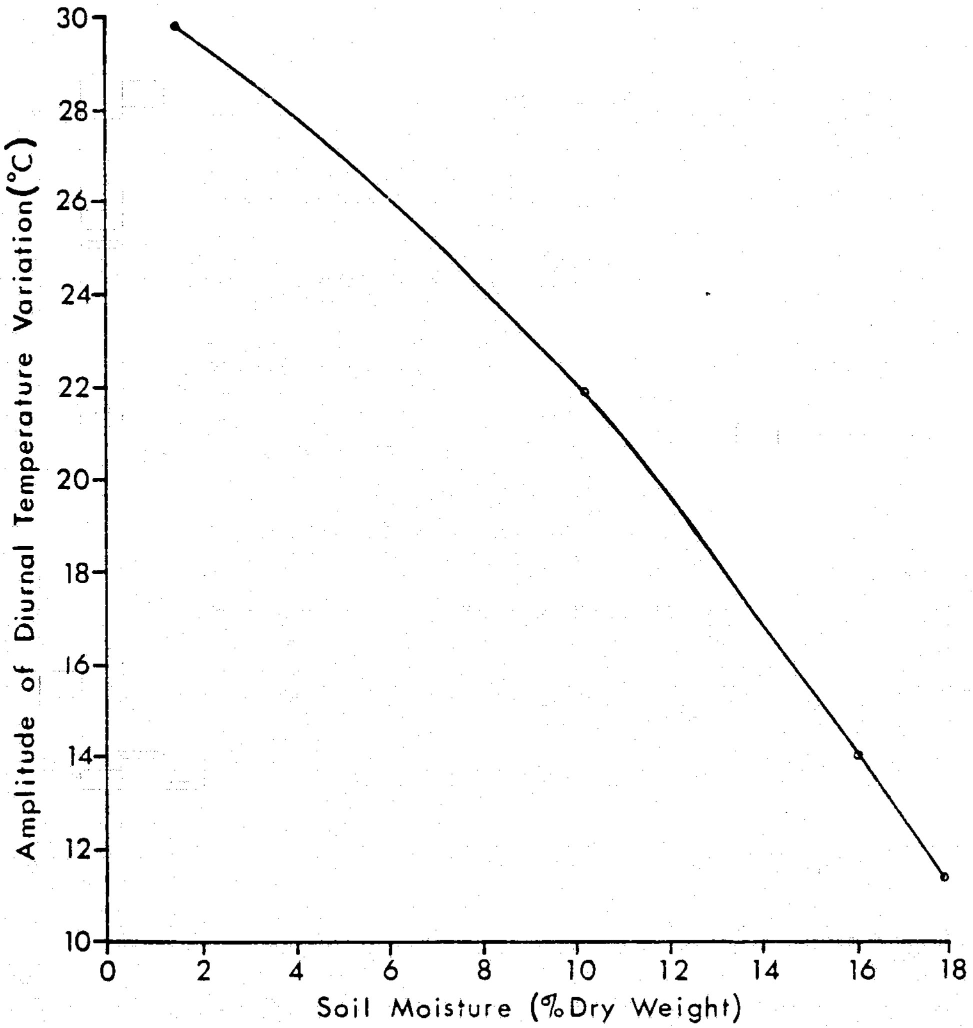


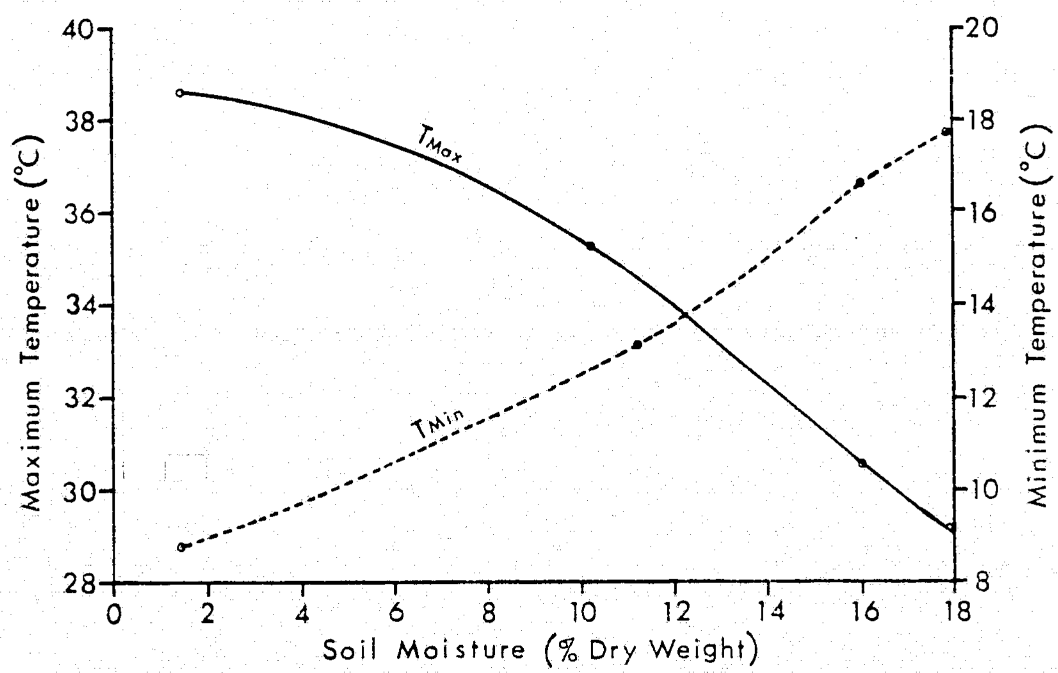


Figure 84: Theoretical relations between temperature variation, minimum temperature and maximum temperature and soil moisture for Station D-1.

It is important to note, however, that the temperature - soil moisture relations predicted by the theoretical model are opposite those commonly observed on thermal imagery for predawn hours. Areas of high soil moisture, in general, are areas of lower temperature throughout the diurnal cycle than areas of low soil moisture. The process not taken into account by the theoretical model is the loss of heat through evaporation from moist soils. This process decreases the absolute magnitude of temperatures throughout the cycle, without significantly affecting the amplitude of diurnal temperature variation. Temperature at a single point in space and time is therefore not simply a function of the thermal properties of the surface, but is also a function of the rate of evaporation. This decreases the usefulness of thermal imagery for estimating soil moisture from a single temperature measurement, but should not affect estimation of soil moisture using the maximum and minimum temperatures during the diurnal cycle. One further refinement of this would be the use of computer-generated thermal inertia maps, as described by Watson (1975) and Kahle and others (1975), which involves eliminating reflectance effects by acquiring daytime spectral reflectance data along with day and night thermal-infrared imagery. Radiometric temperatures are then reduced to relative temperatures by shifting the temperatures of high-reflectance surfaces up and those of low-reflectance surfaces down. A thermal inertia map can then be generated using day-night temperature differences

adjusted for reflectance. Topography (affecting local insolation) is a major factor unaccounted for by this analysis, but where this is relatively unimportant the technique can yield a map showing the variations in surface material and moisture content.

It is obvious from the above discussion that soil moisture cannot be separated from other variations that affect thermal inertia, such as variation in surface material. Soil moisture can therefore be determined only where the dry thermal inertia and the relation between thermal inertia and soil moisture have been previously determined. Variations in thermal inertia amongst soils in the same general environment are not as great as variations in spectral reflectance, however, so crude estimates can still be made. The multiple correlation coefficient between soil moisture as the dependent variable and the second degree polynomial of wet and dry thermal inertia for all samples tested was found to be 0.81, with a standard error of estimate of 5% soil moisture. It is, therefore, suggested that changes in soil moisture from one period of measurement to another can be estimated to within 5% by determining radiometric temperatures once during the day and once at night.

Perhaps even more promising, but totally untested, is use of both the determined thermal inertia and the absolute day and night temperatures to estimate evaporation rates. As noted above, evaporation should not change the amplitude of

diurnal temperature variation, but will shift the absolute magnitude to lower temperatures with increasing rates of evaporation. Determination of this shift should therefore allow the estimation of evaporation rates.

## GROUND WATER DEPTH

Two publications, Myers and Moore (1972) and Chase (1969), claim detection of shallow aquifers using thermal-infrared imagery, based on theory presented by Cartwright (1968a, 1968b). The potential of this technique was examined by this author using shallow subsurface temperature measurements along profiles in San Luis Valley, measurement of surface and shallow subsurface temperatures for a complete diurnal cycle at five stations in San Luis Valley, and theoretical modeling of one-dimensional heat flow using the finite-difference techniques described above.

Cartwright (1968a) assumes steady-state, one-dimensional heat flow between an aquifer and the surface. Because an aquifer is saturated with a fluid in motion, heat transfer is both conductive and convective, producing an extremely high "effective" thermal inertia of the aquifer. The aquifer, with nearly constant temperature throughout the year, therefore acts as a heat sink during the summer and as a heat source during the winter. To determine the temperature at some depth below the surface, we examine the steady-state heat flow equation;

$$\frac{d^2u}{dx^2} = 0$$

subject to the boundary conditions;

$$u(L) = T_a$$

$$u(o) = T_s$$

where $u$ = Temperature.

$x$ = Depth below the surface.

$T_a$ = Aquifer temperature.

$T_s$ = Mean diurnal surface temperature.

$L$ = Depth to aquifer.

Integrating the differential equation twice, and using the boundary conditions to solve for the constants of integration, we arrive at the expression;

$$u(x) = x\left(\frac{T_a - T_s}{L}\right) + T_s$$

Cartwright demonstrated considerable success in defining the extent and depth of aquifers in glacial terrain by measuring temperatures below the depth of diurnal temperature variation, thereby generating interest among investigators of remote sensing capabilities and resulting in claims of detection of shallow (1.5-4.5 m (Myers and Moore, 1972)) aquifers using thermal imagery. Quiel (1975), on the other hand, claims that aquifers cannot be detected unless they are within the depth of diurnal temperature variation, failing to recognize that aquifers can produce a temperature effect within the zone of

diurnal temperature variation without being that shallow themselves. The questions critical to this problem include:

1) Is there a consistant relation between subsurface soil temperature and ground water depth?
2) Can a temperature effect at the base of the zone of diurnal temperature variation be transmitted as a detectable effect at the land surface, where diurnal temperature variations are extreme?
3) How do these temperature effects affect the shape of the diurnal temperature curve?

To answer the first question, 61 temperature measurements were made at 70 cm depth along profiles with varying ground water depth (Plate 8). The data from these profiles were analyzed for significant relations between ground water depth and shallow subsurface temperature, both for individual profiles and for all measurements. The results using all measurements were dissappointnng, with a correlation coefficient of only 0.25 between ground water depth and temperature and a multiple correlation coefficient of only 0.41 between the dependent variable temperature and the second degree polynomial of ground water depth. This suggests that, if relations do exist in San Luis Valley between temperature and ground water depth, the relations are not consistant. This may be because of other significant heat sources, such as geothermal, because of varying ground water temperature, or simply because the steady-state heat flow assumption is not justified.

Results were better when the data were segregated into groups by geographic area. Correlation coefficients ranged foom 0.11 to 0.64, with multiple correlation coefficients between temperature and the second degree polynomial of ground water depth varying between 0.34 and 0.82. In both cases, the worst correlations occur on profiles near the Luis Maria Baca Grant #4 and Great Sand Dunes National Monument, and the best correlations were north and south of these areas. The areas of poor correlation are both areas of eolian sand and of active geothermal exploration interest, suggesting that either heat sources are masking ground water effects, or surface variation in thermal properties are important.

The problem of transference of subsurface temperature effects to the surface was approached both by using the computer model described above, with the lower boundary temperature determined by ground water depth, and by measurement of the diurnal temperature cycle at the surface, and 10,20,30,50 and 70 cm depth, as well as air temperature, for five stations in San Luis Valley (Plate 8). The five stations were distributed along two temperature/ground water depth profiles, with ground water depth varying from greater than 30 m to less than 2 m. Unfortunately, equipment was not available to record data from all five stations during the same time period, and meteorologic conditions varied considerably during the five consecutive diurnal cycles. Ground water depth correlates poorly with surface temperatures, as do thermal

properties. In general, surface and near-surface temperatures correlate best with air temperature, while the deeper subsurface temperatures correlate best with the thermal properties of the test sites. Data from these stations were therefore used primarily to calibrate the theoretical model.

Because of the inconsistancy in the relations between ground water depth and subsurface temperatures in San Luis Valley, the theoretical model was used to determine the feasibiiity of thermal-infrared detection of shallow aquifers only under the best possible circumstances, that is, using the regression relation with the greatest multiple correlation coefficient. That relation, that of the northernmost profile, is;

$$T = 14.95 + 0.315\ d - 0.00295\ d^2$$

where T = Temperature at 70 cm depth (°C).

d = Ground water depth (m).

This relation was then adjusted to compute temperature at the 1 m depth lower boundary, using known ground water temperatures and a steady-state heat flow assumption, and surface diurnal temperature curves (Fig. 85) were generated by the model, holding other variables constant, for each station.

Variations in ground water depth do not significantly affect the shape of the surface diurnal temperature curve (Fig. 85), but do shift the curve up or down in absolute magnitude. In other words, the amplitude of diurnal temperature variation

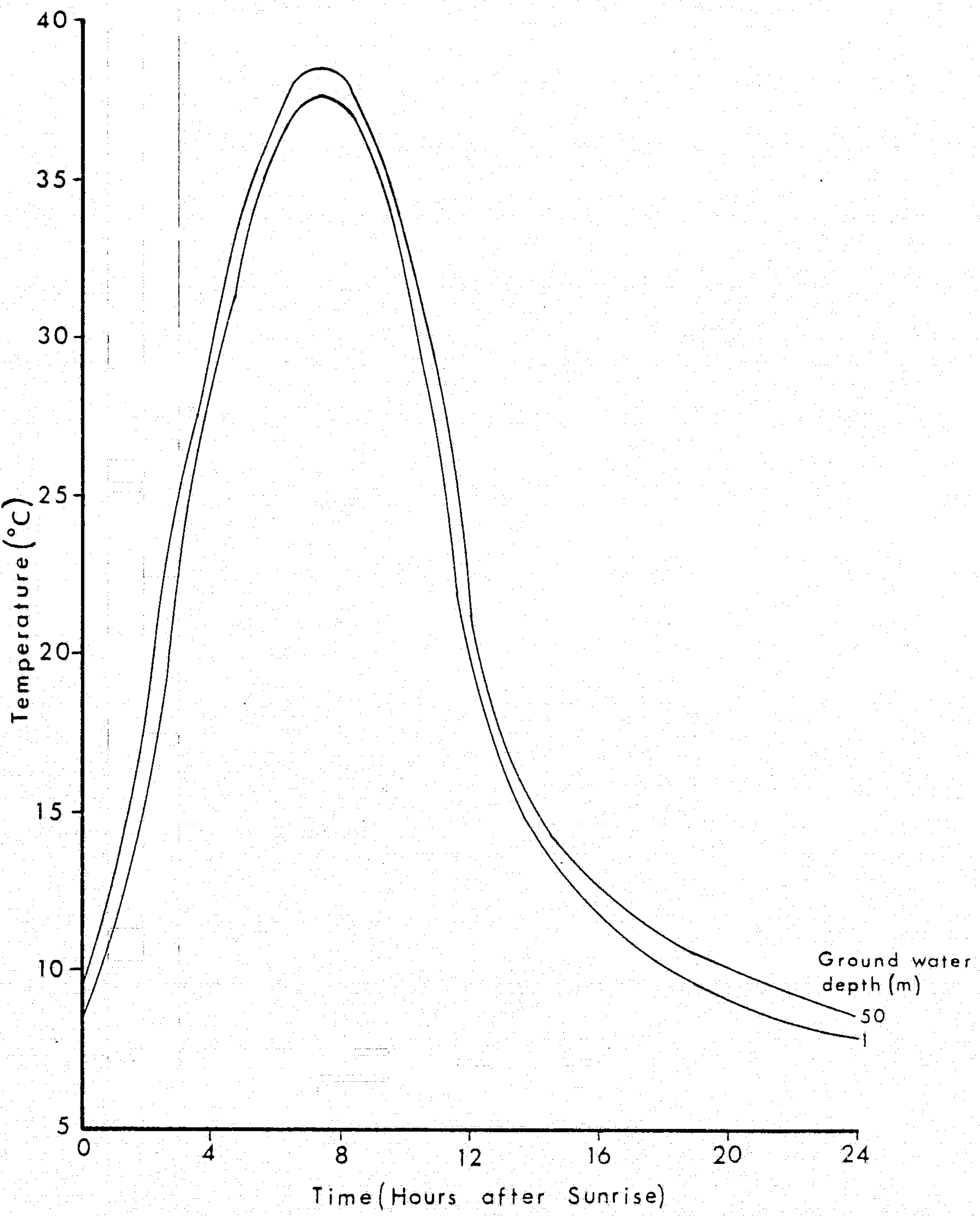


Figure 85: Theoretical effect of ground water depth on surface diurnal temperatures for August 10.

is not affected, but the absolute magnitude of diurnal temperatures through the cycle are affected. Variations in ground water depth can therefore theoretically be separated from variations in thermal inertia by the type of effect on the surface diurnal temperature curve. The absolute magnitude of the change in minimum and maximum temperatures is not great however. The relation between minimum and maximum temperature and ground water depth is a semi-logrithmic one (Fig. 86), with the strongest relations being;

$$T_{max} = 37.8 + 0.47 \log D$$

$$T_{min} = 8.0 + 0.47 \log D$$

where $T_{max,min}$ = Maximum and minimum surface temperatures (°C).
D = Ground water depth (meters).

Again, the minimum detectable surface temperature contrast is usually on the order of 0.5°C. The minimum detectable change of ground water depth under the best possible conditions is, therefore, on the order of one order of magnitude. The only way to use this data is by considering both the minimum and maximum temperatures. The temperature variations at a single point in time produced by varying thermal inertia across a scene are much greater than the variation that can be theoretically related to ground water depth. A more significant problem, though, is that of varying rates of evaporation. As mentioned previously, evaporation similarly should change the absolute magnitude of temperatures without strongly affecting

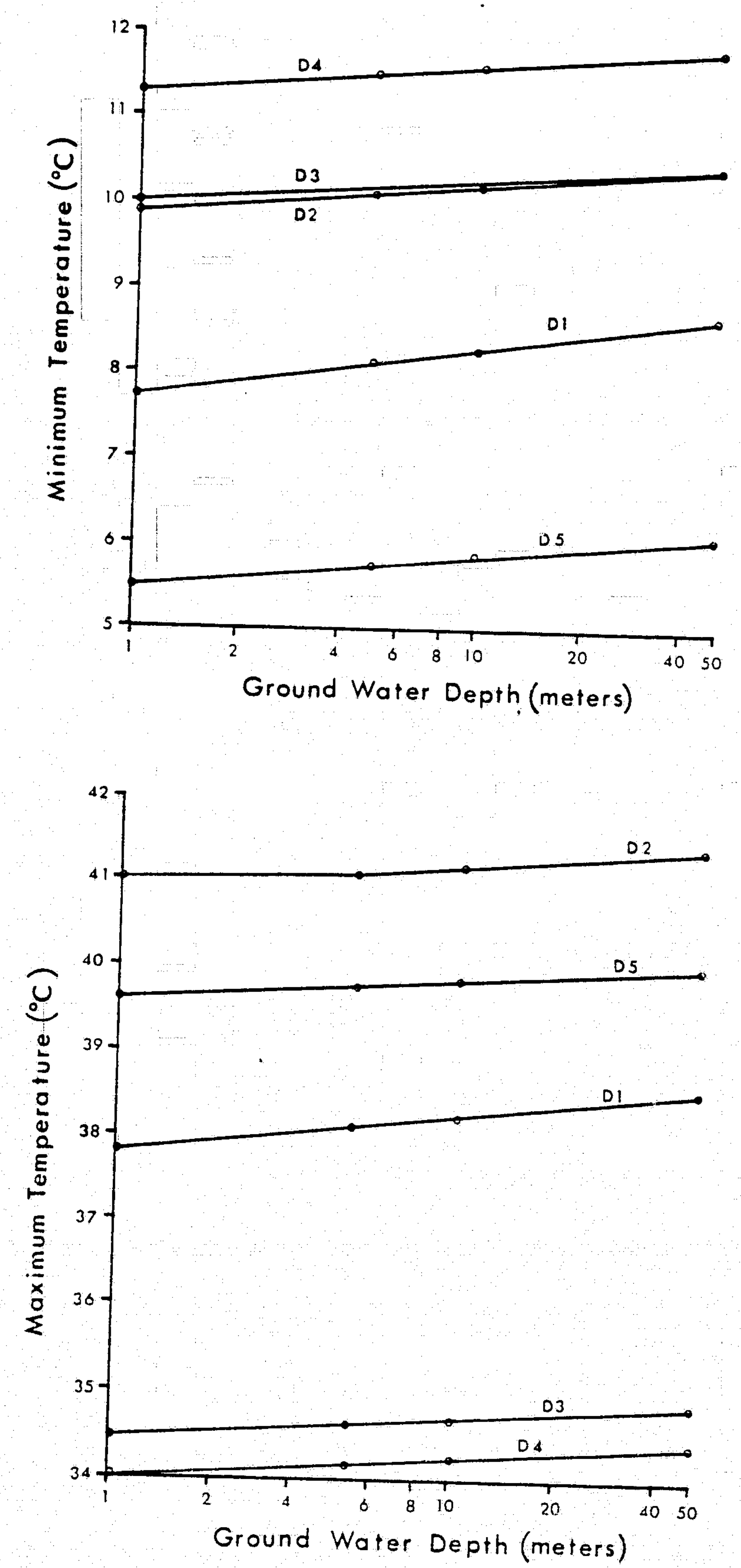


Figure 86: Theoretical relation between maximum and minimum surface temperatures and ground water depth.

the magnitude of diurnal variation. Temperature effects due to varying rates of evaporation may not be separable from those of varying ground water depth because they affect the diurnal temperature curve in similar ways. For moist soils to appear cool on thermal-infrared imagery, instead of warm as predicted by the thermal inertia/soil moisture relations, the effect of varying evaporation rates must be on the order of several degrees, much greater than effects of varying ground water depth. It is therefore considered likely that any previously observed relation between aquifer depth and radiometric temperature is, in fact, a relation between varying rates of evaporation and radiometric temperature. The spurious correlation between temperature and ground water depth occurs only because there is a relation between evaporation rates and ground water depth.

## SUMMARY

Aerial photography and thermal-infrared imagery are effective tools in regional ground water investigations, with a considerable savings in time and increase in accuracy resulting from their use. The degree of success in discrimination of hydrogeologic units in San Luis Basin depends primarily on the ground resolution, both because contrasts in geomorphic expression are greater than corresponding tonal or color contrasts and because soils and vegetation tend to mask color contrasts more than geomorphic contrasts. This is particularly

true in the San Luis Valley, where alluvial units are only expressed geomorphically, but is also valid for the San Juan Mountains, where tonal differences between units are much greater. Reflectance measurements of volcanic rocks did not determine any significant difference in the shape of the spectral reflectance curves of widely differing volcanic rock types.

Similar reflectance measurements of soils with varying moisture content contradict the conclusions of Piech and Walker (1974), showing no significant departure from the shape of the general spectral reflectance curve for soils and rocks. Measurements of saline soils, however, did show a reduced slope of increasing reflectance toward the photo-infrared region.

Both vegetation and saline soils can be used as keys to ground water depth. The distribution of phreatophytes depends both on depth to saturated sediment and on water quality, while saline soils distribution depends upon ground water depth, position within the flow system, and water quality. Saline soils are more dependable as a predictor than is vegetation distribution. Vegetation is a reliable predictor where it is present, but the absence of a particular vegetation type does not, for example, indicate deep ground water. Saline soils are absent only in areas of San Luis Valley that either have deep ground water, low salinity ground water, or where irrigation practices have obscured the soil salinity conditions.

As a single film type, color-infrared photography acquired in stereo offers the maximum usable information for regional ground water studies. This is because of the relative unimportance of rock color as an aid in hydrogeologic mapping and because of the relative importance of vegetation information in mapping geologic structures, in locating springs, and in estimating ground water depth.

The appearance of hydrogeologic units on thermal-infrared imagery is primarily a function of surface temperature. Diurnal surface temperatures are affected by the thermal inertia and spectral reflectance of the surface, by meteorologic variables, by evaporation rates, and by subsurface temperature effects. Variations in surface material result in variations in thermal inertia and spectral reflectance, causing a change in both the magnitude of temperatures throughout the diurnal cycle and the amplitude of temperature variation. Changes in soil moisture result in changes in thermal inertia, reflectance, and evaporative cooling rates. Increases in soil moisture therefore cause a decrease in the amplitude of diurnal temperature variation due to the increase in thermal inertia and a decrease in temperature through the cycle due to evaporative cooling.

Variation in ground water depth produces a variation in subsurface temperature distribution that is, in part, transmitted to the surface as an upward or downward shift in the surface diurnal temperature curve, without affecting the

amplitude of temperature variation. The effect is so small (on the order of 0.5°C for an order of magnitude change in ground water depth), however, that direct determination of ground water depth with present technology is impractical. More significant, the effect of ground water depth is not separable from the effect of evaporative cooling under varying moisture conditions.

The most successful application of thermal-infrared imagery in San Luis Valley is in the discrimination of bedrock from surficial units, discrimination between surficial units, and identification of areas of high soil moisture.

# CONCLUSIONS

1) Ground water recharge to the aquifers of San Luis Valley west of San Luis Creek is primarily from ground water flow in the volcanic aquifers of the San Juan Mountains. The high permeability and anisotropic nature of the volcanic rocks result in very little contrast in flow conditions between the San Juan Mountains and San Luis Valley.

2) Ground water recharge to the aquifers of eastern San Luis Valley is primarily from stream seepage into the upper reaches of the alluvial fans at the base of the Sangre de Cristo Mountains. Much of the recharge to the confined aquifer along the eastern edge of San Luis Valley is through the clays dividing the unconfined aquifer from the lower, confined aquifers.

3) The aquifers of San Luis Valley show a great deal of hydraulic interconnection. Development plans for one aquifer must therefore take into account the effect that development will have on the other aquifers and on surface water. In addition, the two mountain and one valley hydrologic provinces exhibit a great deal of interdependence. Consideration of San Luis Valley as a hydraulically separate entity is invalid.

4) The use of photography and thermal-infrared imagery results in a savings of time and increase in accuracy in regional hydrogeologic studies. The most information is produced by standard photo-interpretation of stereo color-infrared photography. Vegetation and geomorphic information are most useful in mapping hydrogeologic units and structure.

5) Volcanic rocks exhibit the same spectral reflectance curve as sedimentary rocks, with only the absolute magnitude of reflectance varying between units.

6) An increase in soil moisture does not result in a change in the shape of the spectral reflectance curve, only in a decrease in the absolute magnitude of reflectance.

7) Both saline soils and vegetation can be used to estimate general ground water depths, but both must be used with care. Saline soils are a more dependable indicator in San Luis Valley.

8) With present technology, it is not practical to directly estimate ground water depth using thermal-infrared imagery. Correlations between ground water depth and radiometric temperature noted in the literature are likely caused by increased evaporative cooling rates related to increased soil moisture. Estimation of evaporation from thermal-infrared imagery acquired during both the day and night may be feasible.

9) Thermal-infrared imagery does contain significant information usable in the discrimination of hydrogeologically-significant units and in estimation of moisture conditions.

## REFERENCES CITED

Anonymous, 1974, Age dates in Colorado: Isochron/west, no. 11, p. 22-32.

__________, 1976, Water for the desert: Denver Post, May 30, 1976, p. 68-71.

Back, W., 1966, Hydrochemical facies and ground water flow patterns in northern part of Atlantic Coastal Plain: U.S. Geol. Survey Prof. Paper 498-A, 42 p.

Bear, Jacob, 1972, Dynamics of fluids in porous media: American Elsevier Pub. Co., 764 p.

Behrendt, J.C., and Bajwa, L.Y., 1972, Bouger gravity map of Colorado: U.S. Geol. Survey Open-file Report.

Berry, F.A.F., 1959, Hydrodynamics and geochemistry of the Jurassic and Cretaceous systems in the San Juan basin, northwestern New Mexico and southwestern Colorado: Unpublished Ph.D. dissertation, Stanford Univ., 213 p.

Betters, D.R., 1975, A timber-water simulation model for lodgepole pine watersheds in the Colorado Rockies: Water Resources Research, v. 11, no. 6, p. 903-908.

Birman, J.H., 1969, Geothermal exploration for ground water: Geol. Soc. America Bull., v. 80, p. 617-630.

Blaney, H.F., and Criddle, W.D., 1962, Determining consumptive use and irrigation water requirements: U.S. Dept. Agr. Tech. Bull. 1275, 59 p.

Bolyard, D.W., 1956, Pennsylvanian and Permian stratigraphy in the Sangre de Cristo Mountains between La Veta Pass and Westcliff, Colorado: Unpublished M.Sc. thesis, Univ. of Colorado.

Bruns, D.L., 1971, Geology of the Lake Mountain Northeast Quadrangle, Saguache County, Colorado: Unpublished M.Sc. thesis, Colorado School of Mines, 79 p.

Bruns, D.L., Epis, R.C., Weimer, R.J., and Steven, T.A., 1971, Stratigraphic relations between Bonanza center and adjacent parts of the San Juan volcanic field, in H.L. James (ed.), Guidebook of the San Luis Basin, Colorado: 22nd Field Conference, New Mexico Geological Society, p. 183-190

Carpenter, L.G., 1891, Artesian wells of Colorado and their relation to irrigation: Colorado Agr. Coll. Exp. Station Bull. 16, p. 17-27.

Carslaw, H.S., and Jaeger, J.C., 1959, Conduction of heat in solids, 2nd edition: Oxford University Press, London, 510 p.

Cartwright, Keros, 1968a, Temperature prospecting for shallow glacial and alluvial aquifers in Illinois: Illinois State Geol. Survey Circ. 433, 41 p.

__________, 1968b, Thermal prospecting for ground water: Water Resources Research, v. 4, no. 2, p. 395-401.

__________, 1970, Groundwater discharge in the Illinois Basin as suggested by temperature anomalies: Water Resources Research, v. 6, no. 8, p. 912-918.

__________, 1971, Redistribution of geothermal heat by a shallow aquifer: Geol. Soc. America Bull., v. 82, no. 11, p. 3197-3200.

__________, 1974, Tracing shallow groundwater systems by soil temperatures: Water Resources Research, v. 10, no. 4, p. 847-855.

Chapin, C.E., 1971, The Rio Grande rift Part 1, Modifications and additions, in New Mexico Geol. Soc. Guidebook 22nd Field Conf., San Luis Basin, Colorado, 1971: p. 191-201.

Charron, J.E., 1969, Hydrochemical interpretation of ground-water movement in the Red River Valley, Manitoba: Inland Waters Branch, Dept. of Energy, Mines and Resources, Scientific Series no. 2, 31 p.

Chase, M.E., 1969, Airborne remote sensing for ground water studies in prairie environment: Canadian Jour. of Earth Sciences, v. 6, p. 737-741.

Chebotarev, I.I., 1955, Metamorphism of natural waters in the crust of weathering: Geochimica Cosmochimica Acta, v. 8, p. 22-48; p. 137-170.

Clark, S.P., 1966, Handbook of physical constants: Geol. Soc. of America Memoir 97, 587 p.

Colorado Water Conservation Board, 1959, Federal-State water resource planning development in Colorado: Closed basin drain, p. 100:32(1)-100:32(4).

Croft, A.R., 1944, Evaporation from snow: Bull. Am. Meteorology Soc., v. 25, p. 334-337.

Cruff, R.W., and Thompson, T.H., 1966, A comparison of estimating potential evapotranspiration from climatological data in arid and subhumid environments: U.S. Geol. Survey Open-file Report, 60 p.

Davis, S.N., 1969, Porosity, permeability of natural materials, in R.J.M. DeWiest (ed.), Flow Through Porous Media, Academic Press Inc., New York, p. 53-89.

Davis, S.N., and DeWiest, R.J.M., 1966, Hydrogeology: New York, John Wiley & Sons Inc., 463 p.

DeSitter, L.U., 1947, Diagenesis of oil-field brines: Am. Assoc. Petroleum Geologists Bull., v. 31, p. 2030-2040.

Domenico, P.A., 1972, Concepts and models in groundwater hydrology: McGraw-Hill Book Co., 405 p.

Emery, P.A., Boettcher, A.J., Snipes, F.J., and McIntyre, H.J., Jr., 1971, Hydrology of the San Luis Valley, south-central Colorado: U.S. Geol. Survey Hydrol. Inv. Atlas HA-381.

Emery, P.A., Dumeyer, J.M., and McIntyre, A.J., Jr., 1969, Irrigation and municipal wells in the San Luis Valley, Colorado: U.S. Geol. Survey Open-file Report, 7 p.

Emery, P.A., Patten, E.P., Jr., and Moore, J.E., 1975, Analog model study of the hydrology of the San Luis Valley, south-central Colorado: Colorado Water Conserv. Board Circ. 29, 21 p.

Emery, P.A., Snipes, R.J., and Dumeyer, J.M., 1972, Hydrologic data for the San Luis Valley, Colorado: Colorado Water Conserv. Board Basic-Data Release 22, 146 p.

Emery, P.A., Snipes, F.J., Dumeyer, J.M., and Klein, J.M., 1973, Water in San Luis Valley, south-central Colorado: Colorado Water Cons. Board Circ. 18, 26 p.

Epis, R.C., and Chapin, C.E., 1975, Geomorphic and tectonic implications of the Post-Laramide, Late Eocene erosion surface in the Southern Rocky Mountains, in Curtis, Bruce, ed., Cenozoic history of the Southern Rocky Mountains: Geol. Soc. America Memoir 144, p. 45-74.

Folk, R.L., 1968, Petrology of sedimentary rocks: Univ. of Texas, Austin, Texas, 170 p.

Freeze, R.A., 1969, Theoretical analysis of regional groundwater flow: Inland Waters Branch Scientific Series no. 3, Canadian Dept. of Energy, Mines, and Resources, 147 p.

Freeze, R.A., and Witherspoon, P.A., 1966, Theoretical analysis of regional groundwater flow:1: Water Resources Research, v. 2, no. 4, p. 641-656.

__________, 1967, Theoretical analysis of regional groundwater flow:2: Water Resources Research, v. 3, no. 2, p. 623-634.

__________, 1968, Theoretical analysis of regional groundwater flow:3: Water Resources Research, v. 4, no. 3, p. 581-590.

Gaca, J.R., and Karig, D.E., 1966, Gravity survey in the San Luis Valley area Colorado: U.S. Geol. Survey Open-file Report, 21 p.

Glanzman, R.K., 1972, Flouride in the confined ground water of the San Luis Valley, Colorado: Unpublished M.Sc. thesis, Colorado School of Mines.

Gray, D.M., 1970, Handbook on the principles of hydrology: National Research Council of Canada.

Hadsell, F.A., 1968, History of earthquake activity in Colorado: Quart. Colorado School of Mines, v. 63, p. 57-72.

Halverson, H.G., 1972, Seasonal snow surface energy balance in a forest opening: Pacific Southwest Forest and Range Experiment Station Report, 49 p.

Haxby, W.F., and Turcotte, D.L., 1976, Stresses induced by the addition or removal of overburden and associated thermal effects: Geology, v. 4, no. 3, p. 181-184.

Howe, R.H.L., 1958, Procedures of applying air photo interpretation in the location of ground water: Photogrammetric Eng., v. 24, p. 35.

Idso, S.B., Schmugge, T.J., Jackson, R.D., and Reginato, R.J., 1975, The utility of surface temperature measurements for the remote sensing of surface soil water status: Jour. of Geophys. Research, v. 80, no. 21, p. 3044-3049.

Jaeger, J.C., and Johnson, C.H., 1953, Note on diurnal temperature variation: Geofisica Pura e Applicata, v. 24, p. 104-106.

Johnson Division, 1966, Ground water and wells: Johnson Division, 440 p.

Johnson, R.B., 1969, Geologic map of the Trinidad quadrangle, south-central Colorado: U.S. Geol. Survey Misc. Geol. Inv. Map I-558.

______________, 1971, The Great Sand Dunes of Colorado, in H.L. James, Guidebook of the San Luis Basin, Colorado: New Mexico Geol. Soc. 22nd Field Conf., p. 123-128.

Kahle, A.B., Gillespie, A.R., Goetz, A.F.H., and Addington, J.D., 1975, Thermal inertia mapping: Proc. 10th Internat. Symp. on Remote Sensing of Environment, Univ. Michigan, Ann Arbor, v. 2, p. 985-994.

Kalensky, Zdenek, 1968, Psychological aspects of color photography and its effect on quantitative soil moisture interpretation: Presented at 11th Cong. Internat. Soc. Photogrammetry, Lausanne, Switzerland, 15 p.

Karig, D.E., 1964, Structural analysis of the Sangre de Cristo Range, Venable Peak to Crestone Peak, Custer and Saguache Co., Colorado: Unpublished M.Sc. thesis, Colorado School of Mines.

Keller, G.R., and Adams, H.E., 1976, A reconnaissance microearthquake survey of the San Luis Valley, southern Colorado: Bull. Seism. Soc. America, v. 66, no. 1, p. 345-347.

Kharaka, Y.K., 1975, Transport of water and solutes through geological membranes (abs): Trans. Am. Geophys. Union, v. 56, no. 12, p. 981.

Kharaka, Y.K., and Berry, F.A.F., 1974, The influence of geological membranes on the geochemistry of subsurface waters from Miocene sediments at Kettleman North Dome in California: Water Resources Research, v. 10, no. 2, p. 313-327.

Knepper, D.H., Jr., 1974, Tectonic analysis of the Rio Grande Rift Zone, central Colorado: Unpublished Ph.D. dissertation, Colorado School of Mines.

Kohler, M.A., Nordenson, T.J., and Baker, D.R., 1937, Evaporation maps for the United States: U.S. Weather Bureau Tech. Paper #37.

Krumbein, W.C., and Monk, G.D., 1942, Permeability as a function of the size parameters of unconsolidated sand: Petroleum Tech., p. 153-163.

Krynine, D.P., and Judd, W.R., 1957, Principles of engineering geology: McGraw-Hill Book Co., p. 61.

Larsen, E.S., and Cross, W., 1956, Geology and petrology of the San Juan region, southwestern Colorado: U.S. Geol. Survey Prof. Paper 258.

Liakopoulos, A.C., 1965, Variation of the permeability tensor ellipsoid in homogeneous, anisotropic soils: Water Resources Research, v. 1, no. 1.

Limbach, F.W., 1975, The geology of the Buena Vista area, Chaffee County, Colorado: Unpublished M.Sc. thesis, Colorado School of Mines, 98 p.

Lipman, P.W., 1968, Geology of Summer Coon volcanic center, eastern San Juan Mountains, Colorado: Quart. Colorado School of Mines, v. 63, no. 3, p. 211-237.

Lipman, P.W., Steven, T.A., and Mehnert, H.H., 1970, Volcanic history of the San Juan Mountains, Colorado, as indicated by potassium-argon dating: Geol. Soc. of America Bull., v. 81, p. 2329-2352.

Louis, C., and Pernot, M., 1972, Three-dimensional investigation of flow conditions of the Grand Maison damsite: Proc. Symp. on Percolation Through Fissured Rock, Stuttgart, p. T4-F1 to T4-F16.

Mifflin, M.D., 1968, Delineation of groundwater flow systems in Nevada: Desert Research Inst., Univ. of Nevada, Tech. Report #4, 110 p.

Myers, V.I., and Moore, D.G., 1972, Remote sensing for defining aquifers in glacial drift: Proc. 8th Internat. Symp. Remote Sensing of Environment, Univ. of Michigan, Ann Arbor, v. 1, p. 715-728.

Nettleton, L.L., 1942, Gravity and magnetic calculations: Geophysics, v. 7, no. 3, p. 293-310.

Nolting, R.M., 1970, Pennsylvanian-Permian stratigraphy and structural geology of the Orient-Cotton Creek area, Sangre de Cristo Mountains, Colorado: Unpublished M.Sc. thesis, Colorado School of Mines.

Parsons, M.L., 1970, Ground water thermal regime in a glacial complex: Water Resources Research, v. 6, p. 1701-1720.

Patton, H.E., 1909, Heat transference in soils: U.S. Dept. Agr., Bureau of Soils Bull. 59, 54 p.

Pearl, R.H., and Barrett, J.K., 1976, Geothermal resources of the upper San Luis and Arkansas valleys, Colorado, in, Epis, R.C., and Weimer, R.J.(ed.), Studies in Colorado field geology: Professional Contributions of Colorado School of Mines, N. 8, p. 439-445.

Peel, F.A., 1971, New interpretation of Pennsylvanian and Permian stratigraphy and structural history, northern Sangre de Cristo Range, Colorado: Unpublished M.Sc. thesis, Colorado School of Mines.

Peterson, R.C., 1971, Glaciation in the Sangre de Cristo Range, Colorado, in H.L. James, Guidebook of the San Luis Basin, Colorado: New Mexico Geol. Soc. 22nd Field Conf., p. 165-168.

Piech, K.R., and Walker, J.E., 1974, Interpretation of soils: Photogrammetric Eng., v. 40, no. 1, p. 87-94

Powell, W.J., 1958, Ground-water resources of the San Luis Valley, Colorado: U.S. Geol. Survey Water Supply Paper 1379, 284 p.

Quiel, Friedrich, 1975, Thermal/IR in geology: Photogrammetric Eng., v. 41, no. 3, p. 341-346.

Raines, G.L., and Lee, Keenan, 1974, Spectral reflectance measurements: Photogrammetric Eng., v. 40, no. 5, p. 547-550.

__________, 1975, In situ rock reflectance: Photogrammetric Eng., v. 41, no. 2, p. 189-198.

Robinson, T.W., 1958, Phreatophytes: U.S. Geol. Survey Water-Supply Paper 1423, 84 p.

Robinson, T.W., and Waite, H.A., 1938, Ground water in the San Luis Valley, Colorado, Regional planning, p. 6, upper Rio Grande: Natl. Resource Comm., Washington, D.C., p. 226-267.

Rowan, L.C., Offield, T.W., Watson, K., Cannon, P.J., and Watson, R.D., 1970, Thermal infrared investigations, Arbuckle Mountains, Oklahoma: Geol. Soc. America Bull., v. 81, p. 3549-3562.

Scott, G.R., 1953, Quaternary geology and geomorphic history of the Kassler quadrangle, Colorado: U.S. Geol. Survey Prof. Paper 421-A, 70 p.

__________, 1970, Quaternary faulting and potential earthquakes in east-central Colorado: U.S. Geol. Survey Prof. Paper 700-C, p. C11-C18.

Sellers, W.D., 1965, Physical climatology: Univ. of Chicago Press, Chicago, 272 p.

Siebenthal, C.E., 1910, Geology and water resources of the San Luis Valley, Colorado: U.S. Geol. Survey Water Supply Paper 240, 128 p.

Snow, D.T., 1968a, Rock fracture spacings, openings and porosities: Jour. Soil Mech. Found. Div. Am. Soc. Civil Engineers 94, (SMI), p. 73-91.

__________, 1968b, Hydraulic character of fractured metamorphic rocks of the Front Range and implications to the Rocky Mountain Arsenal well, in J.C. Hollister and R.J. Weimer (ed.), Geophysical and geological studies of the relationships between the Denver earthquakes and the Rocky Mountain Arsenal well: Quart. Colorado School of Mines, v. 63, no. 1, p. 167-199.

__________, 1972, Geodynamics of seismic reservoirs: Proc. Symp. on Flow Through Fractured Rock, German Soc. of Soil and Rock Mech., Stuttgart.

Steven, T.A., Lipman, P.W., Hail, W.J., Jr., Barker, Fred, and Luedke, R.G., 1974, Geologic map of the Durango quadrangle, Southwestern Colorado: U.S. Geol. Survey Misc. Inv. Series Map I-764.

Tóth, J., 1963, A theoretical analysis of groundwater flow in small drainage basins: Jour. of Geophys. Research v. 68, no. 16, p. 4795-4813.

Upson, J.E., 1941, The Vallejo Formation: new early Tertiary red-beds in southern Colorado: American Jour. of Science, v. 239, no. 8, p. 577-589.

U.S. Department of Commerce, Normal annual, May-September, October-April isohyetal maps.

U.S. Salinity Laboratory Staff, 1954, Diagnosis and improvement of saline and alkali soils: U.S. Dept. Agr. Handbook 60, 160 p.

Van Alstine, R.E., 1969, Geology and mineral deposits of the Poncha Springs NE Quadrangle, Chaffee County, Colorado: U.S. Geol. Survey Prof. Paper 626, 52 p.

Watson, Kenneth, 1975, Geologic applications of thermal infrared images: Proc. Inst. of Electrical and Electronics Engineers, v. 63, no. 1, p. 128-137.

Watson, Kenneth, Rowan, L.C., and Offield, T.W., 1971, Application of thermal modeling in the geologic interpretation of IR images: Proc. 7th Internat. Symp. Remote Sensing of Environment, Univ. of Michigan, Ann Arbor, v. 3, p. 2017-2053.

White, W.N., 1916, The San Luis Valley, Colorado, irrigation from artesian wells and general irrigation and drainage problems involved in land classification: Ground Water Branch, U.S. Geol. Survey Open-file Report.

Williams, D.E., 1970, Use of alluvial faults in the storage and retention of ground water: Ground Water, v. 8, no. 5, p. 25-29.

Wilm, H.G., and Dunford, E.G., 1948, Effect of timber cutting on water available for stream flow from a lodgepole pine forest: U.S. Dept. Agr. Tech. Bull. 968.

Wilson, W.W., 1965, Pumping tests in Colorado: Colorado Water Conservation Board Circ. 11, 361 p.

Winograd, I.J., 1971, Hydrogeology of ash-flow tuff: A preliminary statement: Water Resources Research, v. 7, no. 4, p. 994-1006.

Winograd, I.J., and Thordarson, William, 1975, Hydrogeologic and hydrochemical framework, south-central Great Basin, Nevada-California, with special reference to the Nevada Test Site: U.S. Geol. Survey Prof. Paper 712-C, 126 p.

Wolfe, E.W., 1971, Thermal IR for geology: Photogrammetric Eng., v. 37, p. 43-52.

Woodside, W., and Messmer, J.H., 1961, Thermal conductivity of porous media, 1, unconsolidated sands,2, consolidated rocks: Jour. Applied Physics, v. 32, p. 1688-1706.

Wychgram, D.C., 1972, Geology of the Hayden Pass-Orient Mine area, northern Sangre de Cristo Mountains, Colorado: A geologic remote sensing evaluation: Unpublished M.Sc. thesis, Colorado School of Mines.

# APPENDIX A: PERMEABILITY DETERMINATIONS

## Sieve/Permeameter Analysis

| Hydrogeologic Unit | Mean Diameter (mm) | Inclusive Graphic Standard Deviation | Hydraulic Conductivity ($10^{-3}$ cm/sec) Sieve | Permeameter |
|---|---|---|---|---|
| $Qf_1$ | 0.85 | 2.51 | 20.5 | 95.0 |
| | 1.05 | 2.14 | 50.8 | 105.0 |
| $Qf_2$ | 0.78 | 2.39 | 20.2 | 287.0 |
| | 1.13 | 1.36 | 163.0 | 123.0 |
| | 1.70 | 2.01 | 158.0 | 300.0 |
| | 2.60 | 0.97 | 1440. | 1333. |
| | 1.26 | 2.79 | 31.2 | 65.0 |
| | 0.76 | 1.36 | 73.9 | 238.0 |
| $Qf_3$ | 0.98 | 2.78 | 19.0 | 117.0 |
| | 0.16 | 1.35 | 3.3 | 33.0 |
| | 0.66 | 2.18 | 19.0 | 37.0 |
| | 0.29 | 1.73 | 6.6 | |
| | 0.47 | 1.10 | 39.7 | 66.0 |
| | 0.70 | 2.43 | 15.4 | 82.0 |
| | 1.03 | 1.70 | 86.9 | 236.0 |
| | 1.45 | 2.42 | 67.1 | 469.0 |
| | 1.8 | 2.56 | 86.1 | 138.0 |
| $Qf_4$ | 1.40 | 1.86 | 130.0 | 106.0 |
| Morainal Deposits | 0.76 | 2.39 | 19.2 | 172.0 |
| | 0.98 | 2.98 | 14.7 | 169.0 |
| Eolian Sands | 0.26 | 0.66 | 21.6 | 38.0 |
| | 0.17 | 0.91 | 6.4 | 32.0 |
| | 0.14 | 0.93 | 4.4 | |
| | 0.27 | 1.31 | 10.0 | 72.0 |
| | 0.17 | 0.82 | 7.2 | 20.0 |
| | 0.19 | 0.90 | 8.4 | 38.0 |
| | 0.26 | 0.85 | 16.9 | 39.0 |

Stream Discharge Measurements

| Station # | Creek | Date | River Mile | Wetted Perimeter (ft) | Discharge (cfs) | Gain (+) or Loss (-) (cfs) |
|---|---|---|---|---|---|---|
| 1 | San Isabel | 5/26/74 | 0 | 5.0 | 8.4 | |
| 2 | San Isabel | 5/26/74 | 1.2 | 5.0 | 4.95 | -3.45 |
| 3 | San Isabel | 5/26/74 | 2.5 | 5.0 | 5.4 | +0.45 |
| 4 | Wild Cherry | 5/26/74 | 0 | 6.0 | 3.9 | |
| 5 | Wild Cherry | 5/26/74 | 0.95 | 6.0 | 2.8 | -1.1 |
| 6 | Wild Cherry | 5/26/74 | 1.78 | 4.0 | 2.7 | -0.1 |
| 7 | Cotton | 5/26/74 | 0 | 8.6 | 15.7 | |
| 8 | Cotton | 5/26/74 | 0.75 | 8.6 | 12.0 | -3.7 |
| 9 | Cotton | 5/26/74 | 1.73 | 7.3 | 9.5 | -2.5 |
| 10 | Cotton | 5/26/74 | 3.43 | 6.7 | 7.95 | -1.55 |
| 11 | Cotton | 5/26/74 | 4.30 | 6.0 | 6.65 | -1.30 |
| 12 | Garner | 5/26/74 | 0 | 4.1 | 2.20 | |
| 13 | Garner | 5/26/74 | 0.4 | 4.1 | 1.45 | -0.75 |
| 14 | Valley View Hot | 5/26/74 | 0 | 3.0 | 1.2 | |
| 15 | Springs | 5/26/74 | 1.63 | 3.0 | 0.8 | -0.4 |
| 16 | N. Piney | 5/27/74 | 0 | 2.0 | 0.12 | |
| 17 | N. Piney | 5/27/74 | 0.41 | 0.0 | 0.0 | -0.12 |
| 18 | Hayden | 5/27/74 | 0 | 3.0 | 0.36 | |
| 19 | Hayden | 5/27/74 | 0.6 | 0.0 | 0.0 | -0.36 |
| 20 | Raspberry | 5/27/74 | 0 | 2.5 | 1.08 | |
| 21 | Raspberry | 5/27/74 | 0.84 | 2.5 | 0.89 | -0.19 |
| 22 | S. Zapata | 5/28/74 | 0 | 10.0 | 4.9 | |
| 23 | S. Zapata | 5/28/74 | 0.73 | 0 | 0.0 | -4.9 |

| Station # | Creek | Date | River Mile | Wetted Perimeter (ft) | Discharge (cfs) | Gain (+) or Loss (-) (cfs) |
|---|---|---|---|---|---|---|
| 24 | Middle Zapata | 5/28/74 | 0 | 3.6 | 0.79 | |
| 25 | Middle Zapata | 5/28/74 | 0.23 | 3.6 | 1.62 | +0.83 |
| 26 | Contribution from S. Zapata | 5/28/74 | 0.75 | | 1.7 | |
| 27 | Middle Zapata | 5/28/74 | 0.98 | 5.5 | 4.4 | +1.08 |
| 28 | Middle Zapata | 5/28/74 | 2.0 | 5.0 | 1.15 | -3.25 |
| 29 | Middle Zapata | 5/28/74 | 2.3 | 2.9 | 0.77 | -0.38 |
| 30 | Middle Zapata | 5/28/74 | 2.6 | 2.9 | 0.69 | -0.08 |
| 31 | Mosca | 5/28/74 | 0 | 2.3 | 0.96 | |
| 32 | Mosca | 5/28/74 | 0.3 | 2.3 | 0.55 | -0.41 |
| 33 | Mosca | 5/28/74 | 1.1 | 2.1 | 0.10 | -0.45 |
| 34 | Medano | 5/28/74 | 0 | 6.6 | 11.5 | |
| 35 | Medano | 5/28/74 | 2.8 | 9.0 | 4.5 | -7.0 |
| 36 | Medano | 5/28/74 | 5.4 | 0.0 | 0.0 | -4.5 |
| 37 | S. Crestone | 7/4/73 | 0 | 7.0 | 7.8 | |
| 38 | S. Crestone | 7/4/73 | 1.7 | 7.2 | 6.18 | -1.62 |
| 39 | S. Crestone | 7/4/73 | 5.8 | 6.1 | 4.2 | -1.98 |
| 37 | S. Crestone | 9/23/73 | 0 | 7.0 | 1.73 | |
| 38 | S. Crestone | 9/23/73 | 1.7 | 6.8 | 0.60 | -1.13 |
| 39 | S. Crestone | 9/23/73 | 5.8 | 0.0 | 0.0 | -0.60 |
| 40 | N. Crestone | 7/4/73 | 0 | 17.0 | 84.0 | |
| 41 | N. Crestone | 7/4/73 | 1.04 | 15.0 | 81.5 | -2.5 |
| 39 | Contribution from S. Crestone | 7/4/73 | 4.16 | | 4.2 | |
| 42 | N. Crestone | 7/4/73 | 4.16 | 15.0 | 73.0 | -12.7 |
| 43 | N. Crestone | 7/4/73 | 18.4 | 14.0 | 43.0 | -30.0 |
| 44 | N. Spanish | 7/3/73 | 0 | 11.2 | 30.7 | |
| 45 | N. Spanish | 7/3/73 | 1.05 | 10.5 | 13.8 | -16.9 |
| 46 | N. Spanish | 7/3/73 | 2.37 | 10.0 | 11.3 | -2.5 |
| 47 | N. Spanish | 7/3/73 | 5.8 | 9.9 | 9.2 | -2.1 |
| 48 | N. Spanish | 7/3/73 | 14.1 | 9.5 | 0.79 | -8.41 |

| Station # | Creek | Date | River Mile | Wetted Perimeter (ft) | Discharge (cfs) | Gain (+) or Loss (-) (cfs) |
|---|---|---|---|---|---|---|
| 49 | Deadman | 7/2/73 | 0 | 19.0 | 58.6 | |
| 50 | Deadman | 7/2/73 | 1.99 | 14.0 | 34.6 | -24.0 |
| 51 | Deadman | 7/2/73 | 4.25 | 13.6 | 20.6 | -14.0 |
| 52 | Deadman | 7/2/73 | 12.8 | 13.4 | 17.0 | -3.6 |
| 53 | Alpine | 6/25/73 | 0 | 4.6 | 2.37 | |
| 54 | Alpine | 6/25/73 | 0.47 | 4.2 | 2.41 | +0.04 |
| 55 | Alpine | 6/25/73 | 0.66 | 3.8 | 0.90 | -1.51 |
| 56 | Alpine | 6/25/73 | 0.76 | 0.0 | 0.0 | -0.90 |
| 57 | Cottonwood | 7/3/73 | 0 | 14.3 | 32.6 | |
| 58 | Cottonwood | 7/3/73 | 2.09 | 9.6 | 14.9 | -17.7 |
| 59 | Cottonwood | 7/3/73 | 4.17 | 10.0 | 12.3 | -2.6 |
| 60 | Cottonwood | 7/3/73 | 10.4 | 11.8 | 9.8 | -2.5 |
| 61 | Cottonwood | 7/3/73 | 18.8 | 6.0 | 3.0 | -6.8 |
| 62 | Willow | 7/4/73 | 0 | 16.0 | 38.5 | |
| 63 | Willow | 7/4/73 | 1.14 | 13.5 | 34.0 | -4.5 |
| 64 | Willow | 7/4/73 | 1.71 | 12.4 | 27.5 | -6.5 |
| 65 | Willow | 7/4/73 | 7.0 | 10.6 | 13.0 | -14.5 |
| 66 | Willow | 7/4/73 | 18.0 | 9.4 | 1.56 | -11.44 |
| 67 | Cedar | 7/2/73 | 0 | 2.4 | 0.65 | |
| 68 | Cedar | 7/2/73 | 1.14 | 1.3 | 0.03 | -0.62 |
| 69 | Carnero | 7/14/75 | 0 | 17.0 | 16.2 | |
| 70 | Carnero | 7/14/75 | 2.27 | 16.5 | 17.1 | +0.9 |
| 71 | Diversion | 7/14/75 | 3.59 | | 1.3 | |
| 71 | Carnero | 7/14/75 | 3.59 | 16.0 | 13.8 | -2.0 |
| 72 | Diversion | 7/14/75 | 7.38 | | 0.69 | |
| 72 | Diversion | 7/14/75 | 7.38 | | 10.3 | |
| 72 | Carnero | 7/14/75 | 7.38 | 8.0 | 2.42 | -0.39 |
| 73 | Diversion | 7/14/75 | 7.76 | | 0.50 | |
| 73 | Carnero | 7/14/75 | 7.76 | 8.0 | 2.14 | +0.22 |
| 74 | Carnero | 7/14/75 | 8.14 | 5.0 | 1.50 | -0.64 |

| Station # | Creek | Date | River Mile | Wetted Perimeter (ft) | Discharge (cfs) | Gain (+) or Loss (-) (cfs) |
|---|---|---|---|---|---|---|
| 75 | La Garita | 7/14/75 | 0 | 18.0 | 25.6 | |
| 76 | La Garita | 7/14/75 | 2.41 | 14.0 | 28.0 | +2.4 |
| 77 | Diversion | 7/14/75 | 5.72 | | 1.63 | |
| 77 | La Garita | 7/14/75 | 5.72 | 14.0 | 23.2 | -3.17 |
| 78 | Diversion | 7/14/75 | 6.48 | | 1.05 | |
| 79 | Diversion | 7/14/75 | 7.62 | | 0.62 | |
| 80 | La Garita | 7/14/75 | 10.18 | 19.0 | 23.8 | +2.27 |
| 81 | Saguache | 8/26/75 | | | 52.3 | |
| 81 | Tributary | 8/26/75 | | | 0.78 | |
| 82 | Diversion | 8/26/75 | | | 0.23 | |
| 83 | Diversion | 8/26/75 | | | 6.4 | |
| 83 | Saguache | 8/26/75 | | | 43.2 | -3.25 |
| 84 | Saguache | 8/26/75 | | | 48.35 | +5.15 |
| 84 | Tributary | 8/26/75 | | | 4.01 | |
| 85 | Diversion | 8/26/75 | | | 5.43 | |
| 85 | Diversion | 8/26/75 | | | 4.68 | |
| 85 | Saguache | 8/26/75 | | | 38.05 | -4.2 |
| 86 | Diversion | 8/26/75 | | | 3.33 | |
| 86 | Saguache | 8/26/75 | | | 34.78 | +0.06 |
| 87 | Diversion | 8/26/75 | | | 3.29 | |
| 87 | Saguache | 8/26/75 | | | 27.32 | -4.17 |
| 88 | Diversion | 8/26/75 | | | 1.45 | |
| 89 | Saguache | 8/26/75 | | | 27.16 | +1.29 |
| 90 | Diversion | 8/26/75 | | | 6.29 | |
| 91 | Saguache | 8/26/75 | | | 20.54 | -0.33 |
| 91 | Diversion | 8/26/75 | | | 9.04 | |
| 92 | Diversion | 8/26/75 | | | 1.61 | |
| 92 | Diversion | 8/26/75 | | | 2.83 | |
| 93 | Saguache | 8/26/75 | | | 5.37 | -1.69 |
| 94 | Diversion | 8/26/75 | | | 0.55 | |
| 95 | Saguache | 8/26/75 | | | 3.65 | -1.17 |
| 96 | Diversion | 8/26/75 | | | 0.63 | |
| 97 | Saguache | 8/26/75 | | | 0.76 | -2.26 |

Hydraulic Conductivity as Computed from Stream Seepage

| Hydrogeologic Unit | Creek | Hydraulic Conductivity ($10^{-3}$ cm/sec) |
|---|---|---|
| $Qf_3$ | San Isabel | 3.86 |
| | Wild Cherry | 1.29 |
| | Cotton | 3.85 |
| | Garner | 3.07 |
| | Zapata | 4.26 |
| | N. Spanish | 6.7 |
| | Deadman | 4.56 |
| | Cottonwood | 4.85 |
| | Willow | 6.05 |
| $Qf_2$ | Valley View Springs | 0.55 |
| | Hayden | 2.7 |
| | N. Piney | 1.98 |
| | Raspberry | 0.62 |
| | S. Zapata | 9.0 |
| $Qf_4$ | Mosca | 3.99 |
| Eolian Sands | Medano | 2.54 |
| | Alpine | 13.6 |
| | Cedar | 1.97 |

## Pump Tests

Three pump tests were completed during the course of the study, all in the town of Crestone (T. 43 N., R. 12 E.), and all within the Pinedale(?) age alluvial fan. Of the three, the test shown in Figure 86a is the most dependable, with the pumped well and the observation well being separated by a distance of 11.4 m (37.3 ft). A high degree of heterogeneity of the sediment is associated with the test of Figure 86b, as evidenced by the changing slope of the drawdown curve, making this test less dependable. The least dependable estimate is that of the test of Figure 87, where instrument malfunctions decreased the number of usable data points, and where drawdown was measured in the pumped well itself.

To analyze the pump test data, drawdowns were first adjusted using the Jacob Adjustment for unconfined wells;

$$s' = s - \frac{s^2}{2m}$$

where $s'$ = Adjusted drawdown.

$s$ = Measured drawdown.

$m$ = Saturated thickness of aquifer.

The adjusted drawdowns were then plotted against time (Figs. 86,87) on a semilogorithmic scale, and the Jacob Method for the solution of the nonequilibrium formula (Davis and DeWiest, 1966) was used to solve for the transmissivity and storage coefficient of the aquifer, by the formula;

$$T = \frac{264Q}{\Delta h}$$

$$S = \frac{0.3Tt_0}{r^2}$$

where T = Transmissivity (gallons per day per foot).

Q = Well discharge (gpm).

$\Delta h$ = Drawdown during one logorithmic scale division (Feet).

S = Storage coefficient.

$t_0$ = Intercept of the straight portion of the curve with zero drawdown (days).

r = Distance between the pumped and observation wells (Feet).

a)

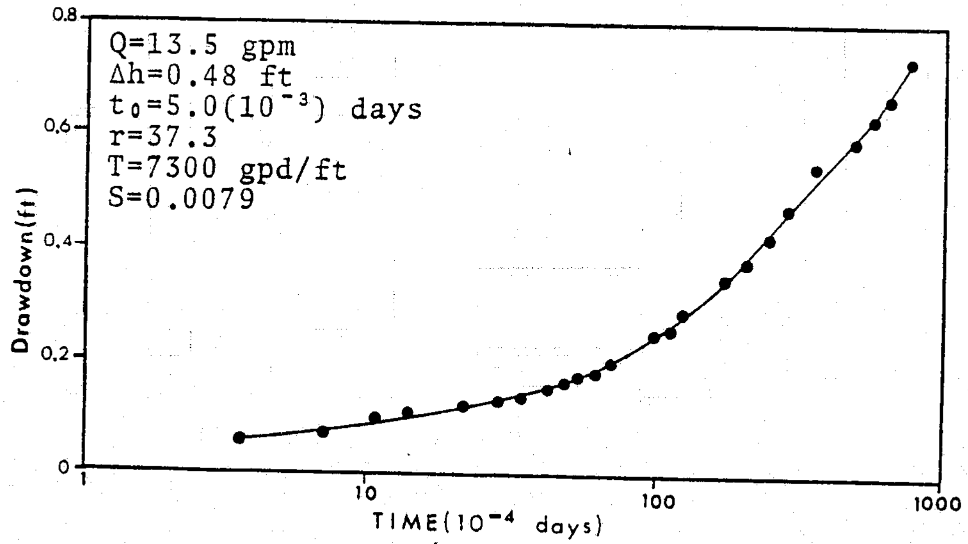


b)

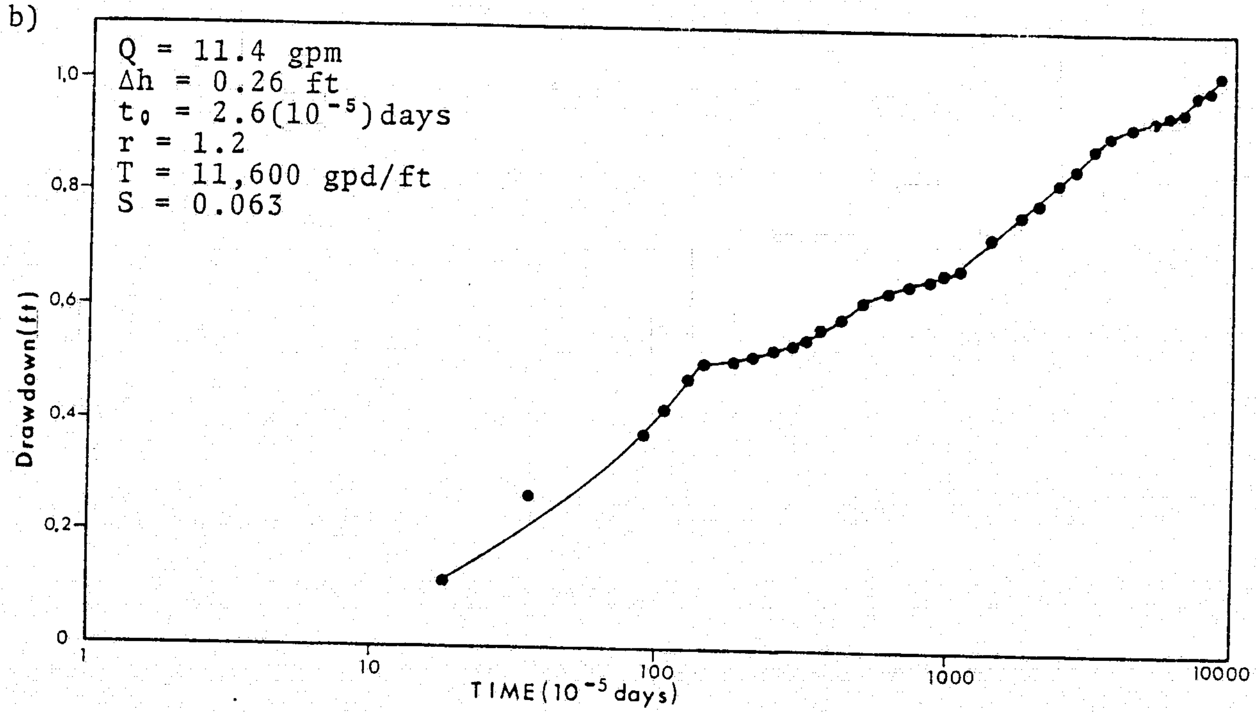


Figure 86. Pump test results.

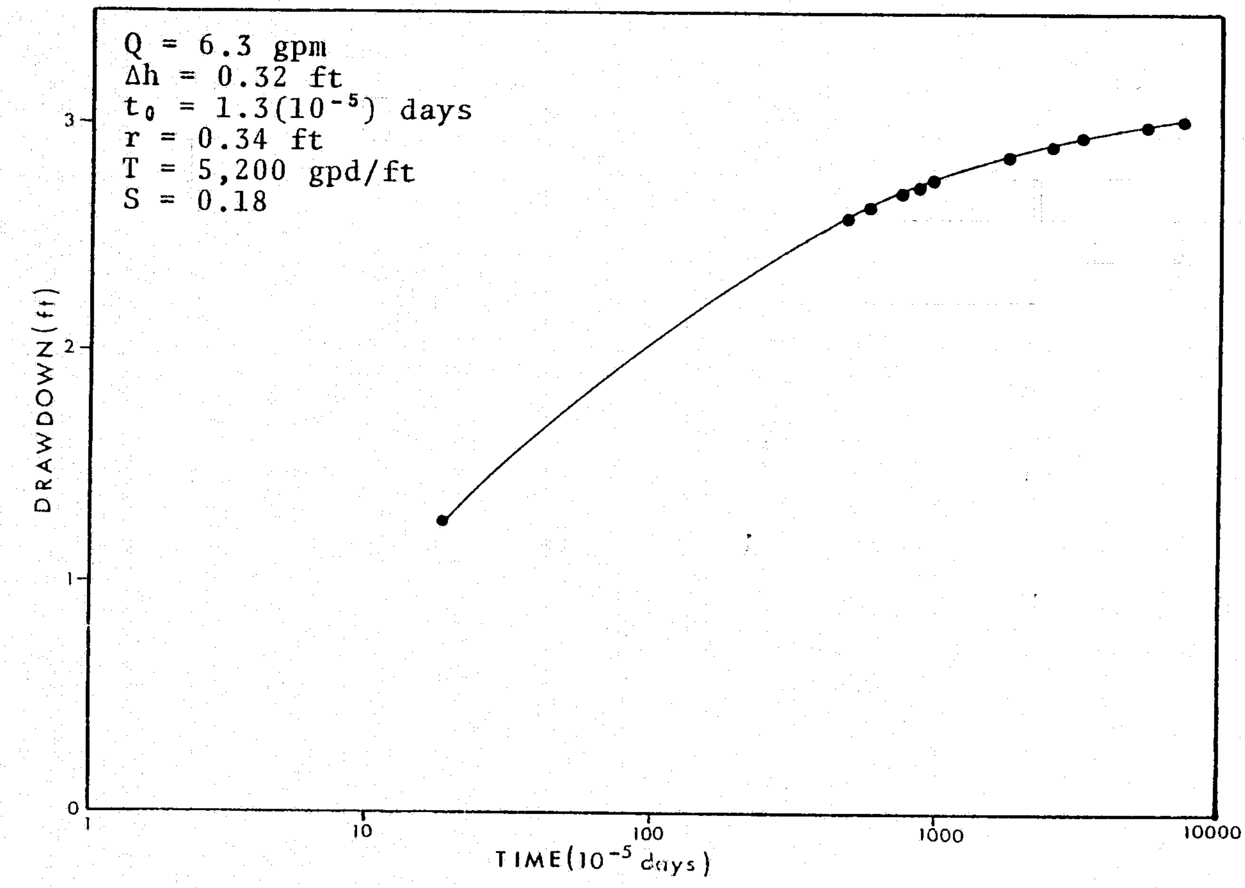


Figure 87. Pump test results.

## Computer Modelling

Estimates of the vertical permeability of the confining clay layers were made by matching measured piezometric values with theoretical piezometric values produced by a steady-state finite-difference model, as described previously.

On the west side of San Luis Valley, there is only one variable, the vertical permeability of the clays. The ranges of the theoretical and measured values are shown in Figure 88, for the best match obtained. Discrepancies between the two are believed to be due to extensive development of the aquifer along the west side of the valley, and the subsequent introduction of non-steady-state flow.

On the east side of San Luis Valley, there are two variables, the vertical permeability, and the extent of the confining clays. Lateral extent, however, has little influence once the clay is assumed to extend beyond the limit of flowing wells (Fig. 89), and solutions for clays extending to the Sangre de Cristo Fault, and pinching out 6 km east of the fault, are identical. Solutions shown are those of the best match for the eastern San Luis Valley.

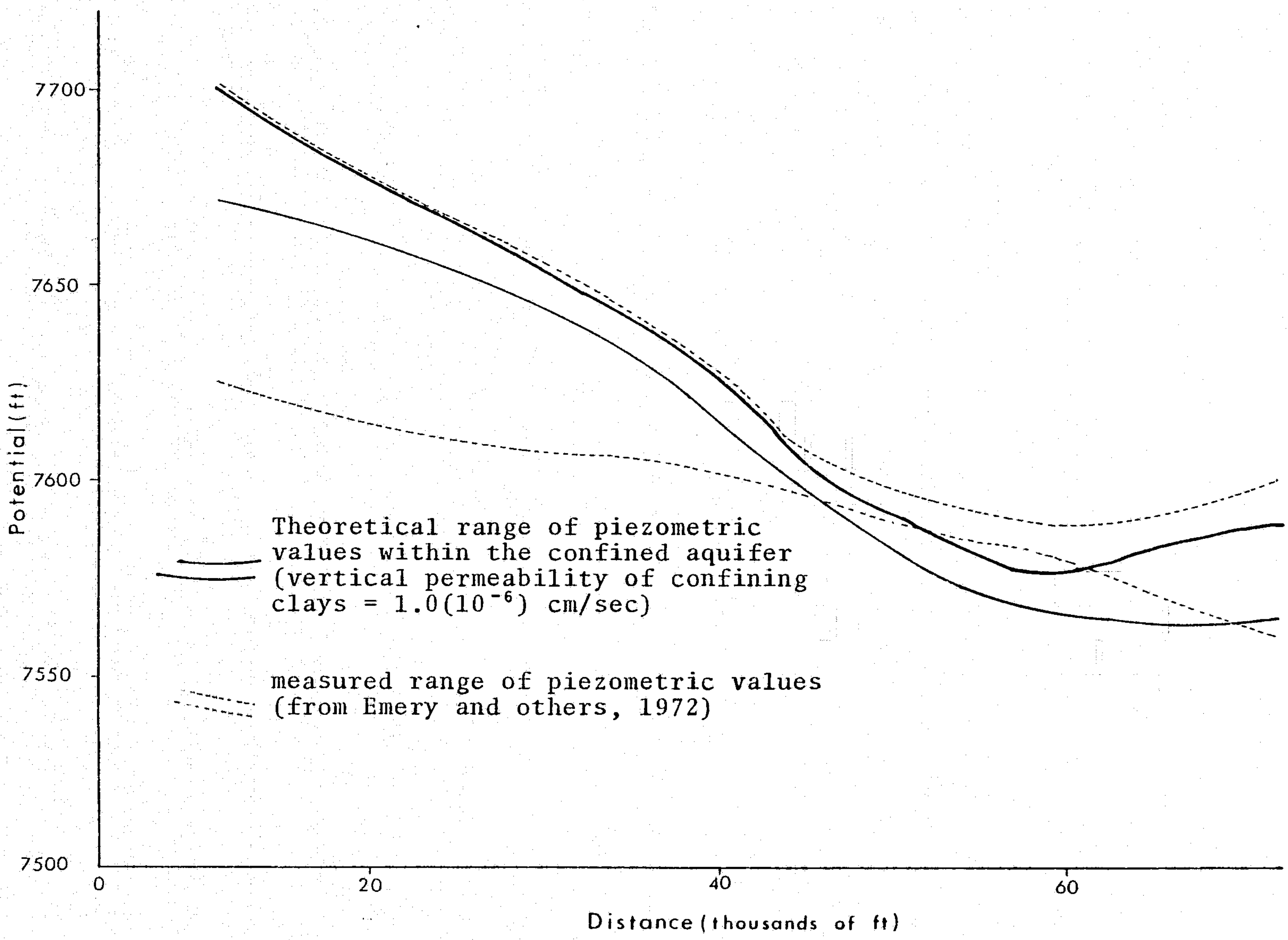


Figure 88: Theoretical and measured piezometric values, western San Luis Valley.

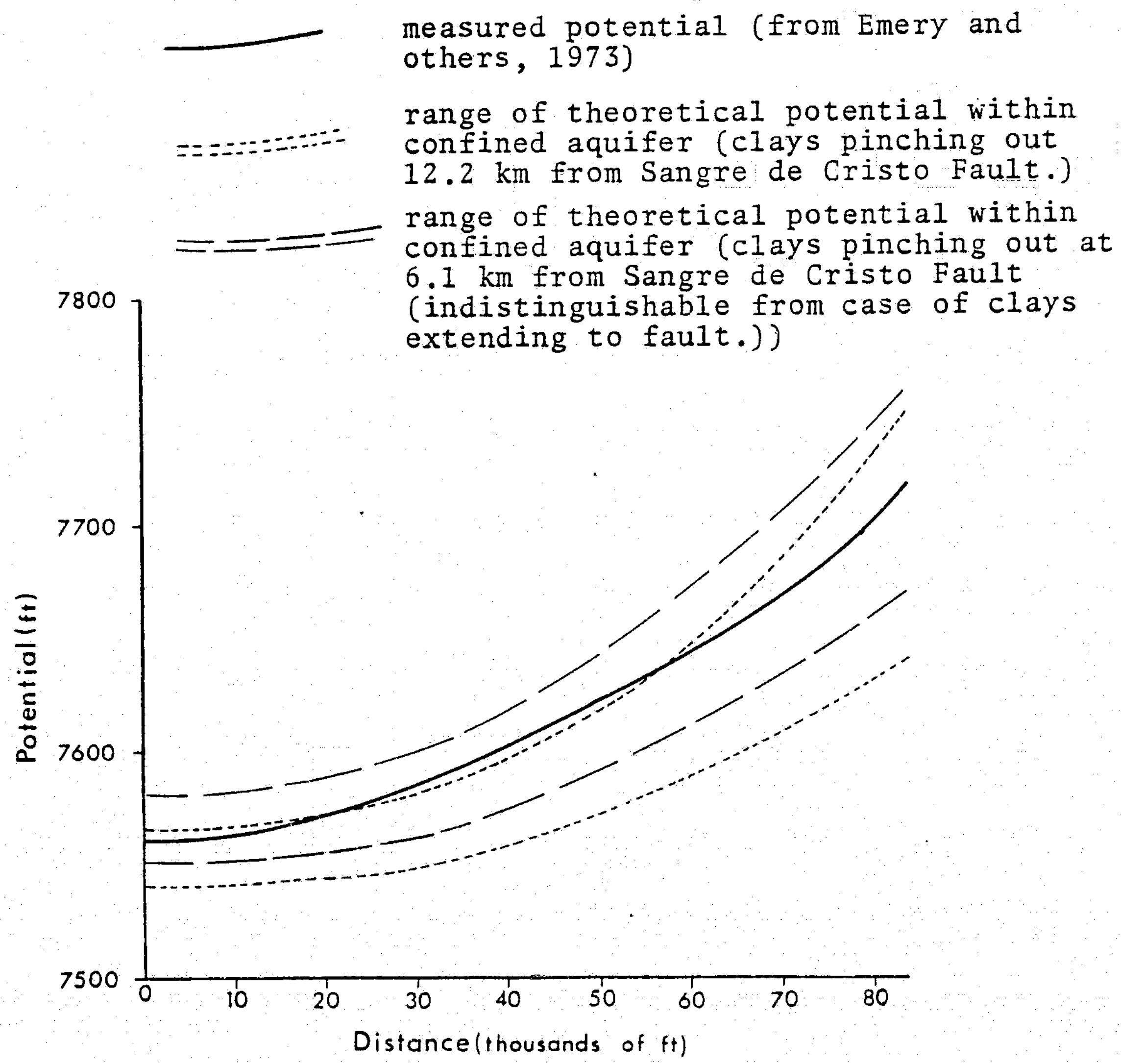


Figure 89: Theoretical and measured piezometric values, eastern San Luis Valley.

# APPENDIX B: WATER CHEMISTRY

## Introduction

Chemical analyses of water samples are divided into two separate sections. The first section (p. B2-B9) presents collection dates, pH, total dissolved solids, hardness, $SiO_2$, F, and Fe concentrations and sodium adsorption ratios and temperatures for all samples collected by this author for this study. The second section (p. B10-B19) presents the concentrations of the major ions (in epm) and the specific conductance of all samples used in this study, including both samples collected by this author and those of Emery and others (1972).

Water temperature data for samples obtained from the the unconfined aquifer are not given for wells that use either a pressure or storage tank.

The locations of all samples used in this report are shown on Plate 7.

See Plate 7 for location of all samples in this appendix.

Surface Water Samples Collected for this Report:

| Sample # | Source | Date of Collection | pH | Total Dissolved Solids (ppm) | Hardness (ppm $CaCO_3$) | Sodium Adsorption Ratio | $SiO_2$ (ppm) | F (ppm) |
|---|---|---|---|---|---|---|---|---|
| 1 | Stream | 7/2/73 | 7.4 | 109 | 50 | 0.22 | 14.0 | 0.33 |
| 2 | Stream | 7/2/73 | 7.4 | 48 | 20 | 0.09 | 6.8 | 0.40 |
| 3 | Stream | 7/3/73 | 7.4 | 33 | 16 | 0.05 | 5.5 | 0.13 |
| 4 | Stream | 7/3/73 | 7.5 | 38 | 17 | 0.07 | 4.3 | 0.34 |
| 5 | Stream | 7/4/73 | 7.8 | 40 | 20 | 0.06 | 5.5 | 0.25 |
| 6 | Stream | 7/4/73 | 7.7 | 96 | 22 | 0.06 | 4.3 | 0.18 |
| 7 | Stream | 7/4/73 | 8.2 | 49 | 25 | 0.05 | 4.1 | 0.21 |
| 8 | Spring | 5/20/74 | 7.6 | 262 | 140 | 0.40 | 18.5 | 1.02 |
| 9 | Spring | 5/22/74 | 8.9 | 154 | 40 | 0.68 | 40.0 | 0.44 |
| 10 | Stream | 5/26/74 | 8.0 | 67 | 30 | 0.11 | 7.5 | 0.01 |
| 11 | Stream | 5/26/74 | 8.0 | 91 | 50 | 0.11 | 8.5 | 0.20 |
| 12 | Stream | 5/26/74 | 8.1 | 143 | 100 | 0.08 | 3.5 | 0.20 |
| 13 | Stream | 5/26/74 | 8.1 | 255 | 160 | 0.13 | 8.0 | 0.65 |
| 14 | Stream | 5/27/74 | 8.0 | 71 | 30 | 0.11 | 12.5 | 0.31 |
| 15 | Spring | 5/27/74 | 8.2 | 194 | 105 | 0.35 | 16.5 | 0.69 |
| 16 | Stream | 5/27/74 | 8.1 | 80 | 35 | 0.19 | 14.0 | 0.53 |
| 17 | Stream | 5/27/74 | 7.9 | 84 | 55 | 0.20 | 6.0 | 0.42 |
| 18 | Stream | 5/28/74 | 8.0 | 45 | 20 | 0.13 | 10.5 | 0.44 |
| 19 | Stream | 5/28/74 | 7.7 | 45 | 30 | 0.08 | 4.5 | 0.31 |
| 20 | Spring | 5/28/74 | 7.3 | 156 | 80 | 0.41 | 16.5 | 0.65 |

| Sample # | Source | Date of Collection | pH | Total Dissolved Solids (ppm) | Hardness (ppm $CaCO_3$) | Sodium Adsorption Ratio | $SiO_2$ (ppm) | F (ppm) |
|---|---|---|---|---|---|---|---|---|
| 21 | Stream | 5/28/74 | 8.0 | 157 | 80 | 0.34 | 16.5 | 0.71 |
| 22 | Stream | 5/29/74 | 8.3 | 62 | 25 | 0.07 | 9.8 | 0.38 |
| 23 | Spring | 6/6/74 | 7.8 | 981 | 145 | 8.31 | 21.5 | 4.0 |
| 24 | Spring | 6/7/74 | 7.9 | 178 | 65 | 0.35 | 43.8 | 0.40 |
| 25 | Spring | 6/9/74 | 7.8 | 152 | 80 | 0.21 | 10.0 | 0.19 |
| 26 | Spring | 6/11/74 | 8.2 | 529 | 320 | 0.20 | 15.0 | 0.64 |
| 27 | Spring | 7/5/74 | 7.5 | 470 | 295 | 0.12 | 15.0 | 0.28 |
| 28 | Spring | 7/6/74 | 7.0 | 375 | 80 | 3.16 | 26.5 | 3.03 |
| 29 | Spring | 5/21/75 | 7.1 | 147 | 40 | 0.39 | 39.8 | 0.52 |
| 30 | Spring | 5/23/75 | 7.8 | 344 | 185 | 0.15 | 52.5 | 0.61 |
| 31 | Stream | 5/31/75 | 8.7 | 440 | 185 | 0.74 | 59.8 | 0.75 |
| 32 | Stream | 6/1/75 | 7.3 | 206 | 75 | 0.35 | 50.0 | 0.60 |
| 33 | Spring | 6/1/75 | 7.4 | 250 | 125 | 0.29 | 37.5 | 0.65 |
| 34 | Spring | 6/2/75 | 4.4 | 624 | 350 | 0.63 | 62.5 | 1.21 |
| 35 | Spring | 6/5/75 | 7.3 | 290 | 110 | 0.47 | 63.8 | 0.75 |
| 36 | Spring | 6/6/75 | 7.2 | 246 | 90 | 0.35 | 62.5 | 0.55 |
| 37 | Spring | 6/19/75 | 7.1 | 83 | 20 | 0.18 | 35.0 | 0.41 |
| 38 | Stream | 6/19/75 | 7.6 | 66 | 20 | 0.22 | 20.0 | 0.40 |
| 39 | Spring | 6/25/75 | 7.6 | 93 | 20 | 0.36 | 38.8 | 0.30 |
| 40 | Spring | 7/10/75 | 9.2 | 224 | 70 | 0.57 | 54.8 | 0.45 |
| 41 | Stream | 7/10/75 | 8.4 | 161 | 55 | 0.27 | 39.8 | 0.42 |
| 42 | Canal | 7/11/75 | 7.8 | 60 | 18 | 0.17 | 19.8 | 0.39 |
| 43 | Stream | 7/14/75 | 7.9 | 153 | 55 | 0.23 | 40.0 | 0.52 |
| 44 | Stream | 7/14/75 | 8.1 | 90 | 25 | 0.18 | 31.3 | 0.40 |

Surface water samples collected for this report:

| Sample # | Temp. (°C) | Fe (ppm) | Sample # | Temp. (°C) | Fe (ppm) |
|---|---|---|---|---|---|
| 1 | 7.4 | 0.05 | 23 | 10.0 | 0.05 |
| 2 | 8.5 | 0.02 | 24 | 14.0 | 0.05 |
| 3 | 6.5 | 0.01 | 25 | 10.0 | 0.08 |
| 4 | 6.2 | 0.05 | 26 | 12.0 | 0.09 |
| 5 | 8.4 | 0.03 | 27 | 6.5 | 0.12 |
| 6 | 9.3 | 0.05 | 28 | - | 0.07 |
| 7 | 9.1 | 0.02 | 29 | 7.0 | 0.10 |
| 8 | 8.0 | 0.00 | 30 | 4.0 | 0.01 |
| 9 | 15.0 | 0.03 | 31 | 9.0 | 0.00 |
| 10 | 6.0 | 0.05 | 32 | 10.0 | 0.04 |
| 11 | 7.0 | 0.01 | 33 | 9.0 | 0.02 |
| 12 | 9.0 | 0.04 | 34 | 13.0 | 0.40 |
| 13 | 12.0 | 0.04 | 35 | 8.0 | 0.47 |
| 14 | 7.5 | 0.02 | 36 | 8.0 | 0.00 |
| 15 | 17.0 | 0.02 | 37 | 4.0 | 0.04 |
| 16 | 8.5 | 0.03 | 38 | 12.0 | 0.05 |
| 17 | 15.0 | 0.04 | 39 | 6.0 | 0.06 |
| 18 | 7.0 | 0.05 | 40 | 28.0 | 0.00 |
| 19 | 7.0 | 0.05 | 41 | 20.0 | 0.10 |
| 20 | 9.0 | 0.05 | 42 | 12.0 | 0.05 |
| 21 | 9.0 | 0.05 | 43 | 12.0 | 0.13 |
| 22 | 12.0 | 0.05 | 44 | 11.0 | 0.10 |

Water Samples from Unconfined Aquifer Collected for this Report:

| Sample # | Date of Collection | pH | Total Dissolved Solids (ppm) | Hardness (ppm $CaCO_3$) | Sodium Adsorption Ratio | $SiO_2$ (ppm) | F (ppm) |
|---|---|---|---|---|---|---|---|
| 1 | 7/6/74 | 7.0 | 167 | 90 | 0.23 | 17.0 | 0.28 |
| 2 | 7/6/74 | 7.1 | 295 | 160 | 0.47 | 24.0 | 0.79 |
| 3 | 7/6/74 | 6.9 | 253 | 135 | 0.37 | 18.0 | 0.38 |
| 4 | 7/5/74 | 6.7 | 168 | 85 | 0.19 | 19.5 | 0.31 |
| 5 | 7/6/74 | 6.8 | 156 | 85 | 0.20 | 15.5 | 0.25 |
| 6 | 7/6/74 | 6.9 | 129 | 50 | 0.37 | 21.5 | 0.42 |
| 7 | 7/6/74 | 6.3 | 93 | 45 | 0.21 | 17.5 | 0.35 |
| 8 | 7/6/74 | 6.8 | 137 | 60 | 0.17 | 26.3 | 0.70 |
| 9 | 7/6/74 | 6.8 | 351 | 170 | 0.87 | 20.5 | 1.12 |
| 10 | 7/6/74 | 7.0 | 354 | 205 | 0.30 | 24.0 | 0.53 |
| 12 | 7/17/74 | 7.5 | 421 | 240 | 0.74 | 19.5 | 0.87 |
| 13 | 7/17/74 | 6.6 | 511 | 320 | 0.27 | 14.0 | 0.35 |
| 15 | 6/10/74 | 6.9 | 94 | 50 | 0.08 | 9.5 | 0.23 |
| 16 | 6/10/74 | 6.7 | 110 | 60 | 0.01 | 15.5 | 0.45 |
| 17 | 6/10/74 | 8.1 | 109 | 55 | 0.31 | 25.5 | 0.22 |
| 18 | 7/6/73 | 7.2 | 121 | 40 | 0.28 | 18.5 | 0.20 |
| 19 | 7/6/73 | 7.2 | 106 | 50 | 0.19 | 20.0 | 0.21 |
| 20 | 7/19/73 | 6.8 | 96 | 45 | 0.05 | 17.5 | 0.20 |
| 21 | 7/30/73 | 6.8 | 113 | 10 | 0.11 | 22.5 | 0.25 |
| 22 | 7/30/73 | 6.8 | 112 | 5 | 0.09 | 18.7 | 0.30 |
| 23 | 7/17/74 | 6.8 | 391 | 210 | 1.07 | 19.0 | 0.32 |
| 27 | 6/7/74 | 7.4 | 119 | 35 | 0.21 | 24.0 | 0.39 |
| 31 | 7/21/73 | 7.2 | 187 | 90 | 0.31 | 18.0 | 0.25 |
| 32 | 7/27/73 | 7.3 | 174 | 10 | 0.14 | 32.5 | 0.21 |
| 33 | 7/21/73 | 7.3 | 140 | 55 | 0.28 | 39.0 | 0.45 |
| 34 | 7/2/73 | 7.2 | 387 | 170 | 0.29 | 80.0 | 1.25 |
| 35 | 5/28/74 | 7.5 | 229 | 120 | 0.36 | 24.0 | 0.54 |
| 36 | 5/28/74 | 7.3 | 274 | 125 | 0.70 | 23.0 | 0.74 |
| 37 | 5/24/74 | 8.0 | 247 | 135 | 0.41 | 22.5 | 0.29 |

| Sample # | Date of Collection | pH | Total Dissolved Solids (ppm) | Hardness (ppm $CaCO_3$) | Sodium Adsorption Ratio | $SiO_2$ (ppm) | F (ppm) |
|---|---|---|---|---|---|---|---|
| 38 | 5/24/74 | 7.3 | 109 | 50 | 0.24 | 17.8 | 0.19 |
| 40 | 5/22/74 | 7.9 | 199 | 55 | 0.87 | 50.0 | 0.39 |
| 77 | 7/5/74 | 8.4 | 121 | 45 | 0.42 | 24.0 | 0.15 |
| 78 | 7/5/74 | 7.9 | 103 | 40 | 0.40 | 21.0 | 0.23 |
| 79 | 5/24/74 | 8.8 | 119 | 35 | 0.41 | 23.0 | 0.14 |
| 87 | 5/18/74 | 7.7 | 173 | 75 | 0.58 | 18.0 | 0.52 |
| 98 | 6/19/75 | 7.4 | 217 | 70 | 0.38 | 65.5 | 0.50 |
| 99 | 6/23/75 | 7.0 | 333 | 150 | 0.35 | 43.8 | 0.59 |
| 100 | 6/23/75 | 7.2 | 221 | 85 | 0.32 | 45.0 | 0.50 |
| 101 | 6/25/75 | 7.2 | 265 | 105 | 0.53 | 42.3 | 0.35 |
| 102 | 7/10/75 | 8.1 | 221 | 60 | 1.33 | 35.5 | 0.45 |
| 103 | 7/10/75 | 7.7 | 345 | 135 | 0.90 | 48.8 | 0.60 |
| 104 | 7/10/75 | 7.8 | 304 | 70 | 0.98 | 100.0 | 0.59 |
| 105 | 7/11/75 | 7.4 | 249 | 95 | 0.21 | 57.5 | 0.40 |
| 106 | 7/11/75 | 7.3 | 295 | 130 | 0.44 | 57.5 | 0.49 |
| 107 | 7/11/75 | 7.4 | 258 | 110 | 0.34 | 52.5 | 0.42 |
| 108 | 7/11/75 | 7.5 | 304 | 150 | 0.28 | 46.3 | 0.40 |
| 109 | 7/11/75 | 7.3 | 251 | 115 | 0.32 | 60.0 | 0.50 |
| 110 | 7/11/75 | 7.5 | 187 | 65 | 0.41 | 42.8 | 0.49 |
| 111 | 7/11/75 | 7.6 | 209 | 90 | 0.22 | 42.5 | 0.50 |
| 112 | 7/11/75 | 7.8 | 218 | 125 | 1.08 | 28.8 | 0.49 |
| 113 | 7/11/75 | 7.6 | 256 | 135 | 0.24 | 45.0 | 0.43 |
| 114 | 7/11/75 | 7.6 | 511 | 250 | 0.61 | 54.8 | 0.55 |
| 115 | 7/12/75 | 7.1 | 462 | 215 | 0.59 | 46.8 | 0.33 |

Water samples collected from the unconfined aquifer for this report:

| Sample # | Temp. (°C) | Fe (ppm) | Sample # | Temp. (°C) | Fe (ppm) |
|---|---|---|---|---|---|
| 1 | - | 0.05 | 36 | 12.0 | 0.05 |
| 2 | - | 0.06 | 37 | 14.0 | 0.05 |
| 3 | 9.0 | 2.50 | 38 | 16.2 | 0.10 |
| 4 | 9.0 | 0.04 | 40 | 13.0 | 0.01 |
| 5 | - | 0.03 | 77 | - | 0.05 |
| 6 | - | 0.03 | 78 | - | 0.03 |
| 7 | - | 0.05 | 79 | 17.0 | 0.15 |
| 8 | - | 0.05 | 87 | 15.0 | 0.05 |
| 9 | 10.5 | 0.05 | 98 | 9.0 | 0.01 |
| 10 | - | 0.06 | 99 | 8.0 | 0.05 |
| 12 | 10.5 | 0.05 | 100 | 6.0 | 0.00 |
| 13 | 10.0 | 0.05 | 101 | 8.0 | 0.00 |
| 15 | - | 0.05 | 102 | - | 0.04 |
| 16 | 10.6 | 0.05 | 103 | 13.0 | 0.03 |
| 17 | 12.8 | 0.04 | 104 | - | 0.01 |
| 18 | 16.0 | 1.50 | 105 | 13.0 | 0.04 |
| 19 | 14.3 | 0.02 | 106 | - | 0.05 |
| 20 | 19.2 | 0.00 | 107 | - | 0.02 |
| 21 | - | 0.05 | 108 | - | 0.01 |
| 22 | 15.5 | 0.05 | 109 | - | 0.00 |
| 23 | 8.5 | 0.04 | 110 | - | 0.00 |
| 27 | 9.0 | 0.05 | 111 | - | 0.07 |
| 31 | 11.0 | 0.85 | 112 | - | 0.01 |
| 32 | 14.0 | 0.85 | 113 | - | 0.01 |
| 33 | 16.6 | 0.45 | 114 | - | 0.05 |
| 34 | 27.0 | 1.35 | 115 | 9.0 | 0.03 |
| 35 | - | 0.07 | | | |

Water Samples from Confined Aquifer Collected for this Report:

| Sample # | Date of Collection | pH | Total Dissolved Solids (ppm) | Hardness (ppm $CaCO_3$) | Sodium Adsorption Ratio | $SiO_2$ (ppm) | F (ppm) |
|---|---|---|---|---|---|---|---|
| 5 | 6/10/74 | 8.5 | 192 | 25 | 2.54 | 48.8 | 0.77 |
| 6 | 6/10/74 | 8.3 | 180 | 50 | 0.65 | 25.0 | 0.43 |
| 7 | 6/10/74 | 8.2 | 145 | 55 | 0.70 | 23.8 | 0.38 |
| 8 | 7/17/74 | 7.3 | 206 | 85 | 0.85 | 18.5 | 0.38 |
| 19 | 7/6/73 | 7.8 | 173 | 22 | 2.29 | 52.5 | 0.65 |
| 20 | 7/3/73 | 7.7 | 169 | 40 | 1.09 | 60.0 | 0.60 |
| 25 | 7/21/73 | 7.4 | 342 | 15 | 1.86 | 80.0 | 2.40 |
| 29 | 7/2/73 | 7.9 | 890 | 35 | 14.0 | 82.5 | 1.20 |
| 63 | 5/22/74 | 8.2 | 192 | 30 | 1.79 | 55.0 | 0.65 |
| 78 | 5/24/74 | 8.2 | 130 | 50 | 0.55 | 24.0 | 0.12 |
| 79 | 5/24/74 | 8.2 | 135 | 50 | 0.55 | 26.0 | 0.22 |
| 93 | 5/24/74 | 8.6 | 123 | 40 | 0.59 | 33.8 | 0.35 |
| 94 | 5/24/74 | 9.7 | 126 | 40 | 0.68 | 30.0 | 0.25 |
| 95 | 5/24/74 | 8.5 | 103 | 30 | 0.55 | 28.5 | 0.12 |
| 96 | 5/24/74 | 9.0 | 109 | 35 | 0.61 | 20.0 | 0.20 |
| 98 | 7/9/75 | 8.1 | 295 | 65 | 2.32 | 30.8 | 2.50 |
| 99 | 7/10/75 | 8.1 | 229 | 75 | 1.15 | 26.0 | 0.69 |
| 100 | 7/10/75 | 7.9 | 248 | 100 | 0.77 | 27.5 | 0.35 |
| 101 | 7/10/75 | 7.9 | 283 | 93 | 0.86 | 53.0 | 0.46 |
| 102 | 7/10/75 | 8.2 | 233 | 50 | 2.10 | 33.8 | 1.10 |
| 103 | 7/10/75 | 7.9 | 248 | 70 | 0.86 | 57.5 | 0.85 |
| 104 | 7/10/75 | 7.4 | 264 | 105 | 0.42 | 52.5 | 0.50 |
| 105 | 7/10/75 | 7.3 | 381 | 110 | 0.48 | 52.5 | 0.42 |
| 106 | 7/10/75 | 8.2 | 210 | 45 | 0.43 | 100.0 | 0.46 |
| 107 | 7/12/75 | 7.7 | 153 | 35 | 0.32 | 70.0 | 0.40 |

Water samples collected from the confined aquifer for this report:

| Sample # | Temp. (°C) | Fe (ppm) | Sample # | Temp. (°C) | Fe (ppm) |
|---|---|---|---|---|---|
| 5 | 14.5 | 0.05 | 95 | 14.0 | 0.05 |
| 6 | 15.4 | 0.05 | 96 | 18.0 | 0.00 |
| 7 | 12.7 | 0.00 | 98 | 15.0 | 0.15 |
| 8 | 13.0 | 0.05 | 99 | 18.0 | 0.03 |
| 19 | 19.4 | 0.00 | 100 | 24.0 | 0.02 |
| 20 | 16.5 | 0.06 | 101 | 10.0 | 0.00 |
| 25 | 18.3 | 0.20 | 102 | 16.0 | 0.03 |
| 29 | 23.3 | 0.03 | 103 | 16.0 | 0.04 |
| 63 | 13.0 | 0.00 | 104 | 11.0 | 0.00 |
| 78 | 13.0 | 0.05 | 105 | 10.0 | 0.00 |
| 79 | 12.8 | 0.03 | 106 | 15.0 | 0.05 |
| 93 | 14.5 | 0.01 | 107 | 12.0 | 0.03 |
| 94 | 24.0 | 0.08 | | | |

## Major Ions - Surface Water

Source:

1 = Huntley, this report.
2 = Emery and others (1972).

Concentrations in equivalent parts per million. Conductance in micromhos per centimeter.

| Sample # | Source | Specific Conductance | Na | K | Ca | Mg | $HCO_3$ | $SO_4$ | Cl |
|---|---|---|---|---|---|---|---|---|---|
| 1 | 1 | 162 | 0.16 | 0.07 | 1.00 | 0.00 | 0.65 | 0.45 | 0.14 |
| 2 | 1 | 64 | 0.04 | 0.01 | 0.40 | 0.00 | 0.40 | 0.06 | 0.07 |
| 3 | 1 | 44 | 0.02 | 0.01 | 0.28 | 0.04 | 0.24 | 0.04 | 0.08 |
| 4 | 1 | 47 | 0.03 | 0.01 | 0.30 | 0.04 | 0.32 | 0.04 | 0.08 |
| 5 | 1 | 53 | 0.03 | 0.00 | 0.40 | 0.00 | 0.32 | 0.04 | 0.05 |
| 6 | 1 | 61 | 0.03 | 0.01 | 0.32 | 0.14 | 0.40 | 0.04 | 0.14 |
| 7 | 1 | 67 | 0.03 | 0.00 | 0.24 | 0.29 | 0.49 | 0.06 | 0.05 |
| 8 | 1 | 319 | 0.47 | 0.04 | 2.50 | 0.30 | 2.38 | 0.42 | 0.32 |
| 9 | 1 | 160 | 0.43 | 0.20 | 0.60 | 0.20 | 1.15 | 0.15 | 0.11 |
| 10 | 1 | 73 | 0.06 | 0.02 | 0.60 | 0.00 | 0.65 | 0.06 | 0.06 |
| 11 | 1 | 120 | 0.08 | 0.03 | 0.90 | 0.10 | 0.82 | 0.15 | 0.08 |
| 12 | 1 | 213 | 0.08 | 0.03 | 1.40 | 0.60 | 1.57 | 0.69 | 0.07 |
| 13 | 1 | 392 | 0.17 | 0.07 | 2.30 | 0.90 | 1.07 | 2.40 | 0.07 |
| 14 | 1 | 86 | 0.06 | 0.06 | 0.50 | 0.10 | 0.66 | 0.04 | 0.04 |
| 15 | 1 | 266 | 0.36 | 0.03 | 1.60 | 0.50 | 1.89 | 0.16 | 0.20 |
| 16 | 1 | 104 | 0.11 | 0.03 | 0.70 | 0.00 | 0.66 | 0.10 | 0.08 |
| 17 | 1 | 146 | 0.15 | 0.06 | 1.00 | 0.10 | 1.28 | 0.06 | 0.05 |
| 18 | 1 | 64 | 0.06 | 0.03 | 0.30 | 0.10 | 0.33 | 0.04 | 0.07 |
| 19 | 1 | 80 | 0.04 | 0.03 | 0.50 | 0.10 | 0.66 | 0.02 | 0.03 |
| 20 | 1 | 200 | 0.37 | 0.04 | 1.10 | 0.50 | 1.31 | 0.31 | 0.18 |
| 21 | 1 | 193 | 0.30 | 0.03 | 1.00 | 0.60 | 1.48 | 0.19 | 0.14 |
| 22 | 1 | 88 | 0.13 | 0.08 | 0.40 | 0.10 | 0.49 | 0.06 | 0.11 |
| 23 | 1 | 1302 | 10.00 | 0.25 | 2.60 | 0.30 | 5.74 | 5.21 | 1.69 |
| 24 | 1 | 200 | 0.43 | 0.08 | 1.20 | 0.10 | 1.39 | 0.06 | 0.21 |
| 25 | 1 | 213 | 0.19 | 0.04 | 1.40 | 0.20 | 1.31 | 0.42 | 0.14 |

| Sample # | Source | Specific Conductance | Na | K | Ca | Mg | $HCO_3$ | $SO_4$ | Cl |
|---|---|---|---|---|---|---|---|---|---|
| 26 | 1 | 698 | 0.36 | 0.08 | 4.60 | 1.80 | 2.54 | 4.79 | 0.07 |
| 27 | 1 | 589 | 0.21 | 0.04 | 3.70 | 2.20 | 2.79 | 3.64 | 0.07 |
| 28 | 1 | 459 | 2.83 | 0.04 | 1.40 | 0.20 | 1.72 | 2.60 | 0.51 |
| 29 | 1 | 206 | 0.25 | 0.29 | 0.60 | 0.20 | 0.70 | 0.35 | 0.42 |
| 30 | 1 | 472 | 0.20 | 0.13 | 2.80 | 0.88 | 2.90 | 0.49 | 0.38 |
| 31 | 1 | 659 | 1.00 | 0.08 | 2.80 | 0.88 | 4.20 | 0.42 | 0.28 |
| 32 | 1 | 259 | 0.30 | 0.13 | 1.10 | 0.39 | 1.60 | 0.25 | 0.19 |
| 33 | 1 | 359 | 0.32 | 0.13 | 1.90 | 0.59 | 2.20 | 0.25 | 0.21 |
| 34 | 1 | 1617 | 1.17 | 0.19 | 5.20 | 1.77 | 0.00 | 8.17 | 0.22 |
| 35 | 1 | 333 | 0.49 | 0.09 | 1.90 | 0.29 | 2.50 | 0.19 | 0.21 |
| 36 | 1 | 279 | 0.33 | 0.13 | 1.50 | 0.29 | 2.00 | 0.17 | 0.20 |
| 37 | 1 | 82 | 0.08 | 0.08 | 0.40 | 0.00 | 0.50 | 0.02 | 0.08 |
| 38 | 1 | 72 | 0.10 | 0.06 | 0.40 | 0.00 | 0.40 | 0.10 | 0.10 |
| 39 | 1 | 82 | 0.16 | 0.08 | 0.40 | 0.00 | 0.50 | 0.10 | 0.09 |
| 40 | 1 | 279 | 0.48 | 0.17 | 1.20 | 0.20 | 1.44 | 0.54 | 0.31 |
| 41 | 1 | 193 | 0.20 | 0.09 | 1.10 | 0.00 | 1.44 | 0.00 | 0.08 |
| 42 | 1 | 77 | 0.07 | 0.09 | 0.35 | 0.00 | 0.40 | 0.03 | 0.06 |
| 43 | 1 | 176 | 0.17 | 0.09 | 1.00 | 0.10 | 1.20 | 0.16 | 0.08 |
| 44 | 1 | 97 | 0.09 | 0.08 | 0.50 | 0.00 | 0.66 | 0.00 | 0.08 |

Major Ions - Unconfined Aquifer

Source:

1 = Huntley, this report.
2 = Emery and others (1972).

Concentrations in equivalent parts per million. Conductance in micromhos per centimeter.

| Sample # | Source | Specific Conductance | Na | K | Ca | Mg | $HCO_3$ | $SO_4$ | Cl |
|---|---|---|---|---|---|---|---|---|---|
| 1 | 1 | 240 | 0.22 | 0.03 | 1.70 | 0.10 | 1.39 | 0.42 | 0.11 |
| 2 | 1 | 385 | 0.59 | 0.03 | 2.50 | 0.70 | 2.54 | 0.73 | 0.21 |
| 3 | 1 | 300 | 0.43 | 0.04 | 2.00 | 0.70 | 1.80 | 1.21 | 0.11 |
| 4 | 1 | 240 | 0.21 | 0.03 | 1.60 | 0.10 | 0.90 | 1.04 | 0.11 |
| 5 | 1 | 226 | 0.18 | 0.04 | 1.50 | 0.20 | 0.82 | 1.04 | 0.07 |
| 6 | 1 | 146 | 0.26 | 0.02 | 0.90 | 0.10 | 1.15 | 0.15 | 0.11 |
| 7 | 1 | 113 | 0.14 | 0.02 | 0.60 | 0.30 | 0.74 | 0.15 | 0.11 |
| 8 | 1 | 160 | 0.22 | 0.03 | 1.00 | 0.20 | 1.15 | 0.16 | 0.11 |
| 9 | 1 | 492 | 1.13 | 0.05 | 2.60 | 0.80 | 0.98 | 3.54 | 0.28 |
| 10 | 1 | 472 | 0.43 | 0.06 | 3.20 | 0.90 | 0.66 | 4.17 | 0.07 |
| 11 | 2 | 1040 | 6.65 | 0.18 | 3.80 | 0.98 | 5.18 | 4.31 | 1.32 |
| 12 | 1 | 667 | 1.15 | 0.05 | 3.40 | 1.40 | 1.64 | 3.75 | 0.20 |
| 13 | 1 | 760 | 0.49 | 0.04 | 4.50 | 2.10 | 1.97 | 5.00 | 0.26 |
| 14 | 2 | 521 | 1.74 | 0.03 | 2.80 | 1.23 | 3.15 | 0.34 | 2.06 |
| 15 | 1 | 113 | 0.11 | 0.03 | 1.00 | 0.00 | 0.82 | 0.15 | 0.11 |
| 16 | 1 | 146 | 0.02 | 0.03 | 0.80 | 0.40 | 0.98 | 0.08 | 0.10 |
| 17 | 1 | 160 | 0.23 | 0.04 | 1.00 | 0.10 | 1.05 | 0.06 | 0.07 |
| 18 | 1 | 126 | 0.18 | 0.10 | 0.70 | 0.11 | 1.14 | 0.10 | 0.05 |
| 19 | 1 | 161 | 0.14 | 0.01 | 0.90 | 0.11 | 0.90 | 0.08 | 0.09 |
| 20 | 1 | 107 | 0.04 | 0.00 | 0.80 | 0.10 | 0.73 | 0.25 | 0.05 |
| 21 | 1 | 146 | 0.08 | 0.05 | 0.80 | 0.20 | 0.98 | 0.10 | 0.01 |
| 22 | 1 | 136 | 0.07 | 0.00 | 1.00 | 0.10 | 1.01 | 0.12 | 0.01 |
| 23 | 1 | 589 | 0.74 | 0.07 | 3.00 | 1.20 | 1.89 | 3.12 | 0.35 |
| 24 | 2 | 263 | 0.70 | 0.03 | 1.75 | 0.34 | 2.08 | 0.35 | 0.07 |
| 25 | 2 | 212 | 0.42 | 0.07 | 1.60 | 0.28 | 1.90 | 0.16 | 0.06 |

| Sample # | Source | Specific Conductance | Na | K | Ca | Mg | $HCO_3$ | $SO_4$ | Cl |
|---|---|---|---|---|---|---|---|---|---|
| 26 | 2 | 431 | 0.91 | 0.11 | 2.90 | 0.72 | 2.95 | 0.69 | 0.68 |
| 27 | 1 | 146 | 0.35 | 0.07 | 0.70 | 0.00 | 0.98 | 0.02 | 0.25 |
| 28 | 2 | 204 | 0.52 | 0.06 | 0.25 | 0.52 | 1.90 | 0.04 | 0.16 |
| 29 | 2 | 964 | 2.26 | 0.24 | 6.30 | 1.31 | 4.52 | 2.06 | 3.04 |
| 30 | 2 | 490 | 4.61 | 0.07 | 0.32 | 0.24 | 4.79 | 0.27 | 0.19 |
| 31 | 1 | 241 | 0.30 | 0.01 | 1.50 | 0.30 | 1.88 | 0.16 | 0.05 |
| 32 | 1 | 186 | 0.13 | 0.01 | 1.50 | 0.20 | 1.39 | 0.33 | 0.02 |
| 33 | 1 | 161 | 0.21 | 0.01 | 0.70 | 0.40 | 1.14 | 0.08 | 0.03 |
| 34 | 1 | 680 | 0.39 | 0.44 | 2.30 | 1.30 | 3.19 | 0.12 | 0.42 |
| 35 | 1 | 293 | 0.39 | 0.08 | 1.70 | 0.70 | 2.13 | 0.23 | 0.25 |
| 36 | 1 | 340 | 0.78 | 0.03 | 2.00 | 0.50 | 2.46 | 0.46 | 0.35 |
| 37 | 1 | 306 | 0.47 | 0.04 | 2.00 | 0.70 | 1.72 | 1.02 | 0.25 |
| 38 | 1 | 200 | 0.17 | 0.04 | 1.00 | 0.00 | 0.90 | 0.15 | 0.11 |
| 39 | 2 | 112 | 0.13 | 0.01 | 0.90 | 0.10 | 1.15 | 0.15 | 0.15 |
| 40 | 1 | 177 | 0.64 | 0.14 | 0.90 | 0.20 | 1.48 | 0.23 | 0.20 |
| 41 | 2 | 499 | 3.65 | 0.46 | 0.85 | 0.22 | 4.21 | 0.75 | 0.28 |
| 42 | 2 | 1920 | 16.50 | 3.41 | 0.60 | 0.16 | 17.00 | 2.54 | 1.55 |
| 43 | 2 | 678 | 3.87 | 0.21 | 2.30 | 0.90 | 5.25 | 1.27 | 0.79 |
| 44 | 2 | 401 | 2.39 | 0.23 | 0.55 | 0.34 | 2.07 | 0.75 | 0.45 |
| 45 | 2 | 532 | 1.87 | 0.22 | 2.55 | 0.90 | 3.11 | 1.77 | 0.56 |
| 46 | 2 | 542 | 0.30 | 0.20 | 3.20 | 0.90 | 3.84 | 1.04 | 0.04 |
| 47 | 2 | 503 | 0.91 | 0.17 | 3.15 | 1.15 | 3.41 | 0.85 | 0.28 |
| 48 | 2 | 488 | 1.17 | 0.15 | 2.95 | 1.07 | 3.70 | 3.75 | 0.15 |
| 49 | 2 | 365 | 0.83 | 0.10 | 2.40 | 0.68 | 3.38 | 0.35 | 0.07 |
| 50 | 2 | 173 | 0.32 | 0.06 | 1.15 | 0.34 | 1.57 | 0.17 | 0.02 |
| 51 | 2 | 113 | 0.20 | 0.05 | 0.80 | 0.15 | 0.99 | 0.09 | 0.01 |
| 52 | 2 | 460 | 1.35 | 0.10 | 2.90 | 0.56 | 3.61 | 0.73 | 0.15 |
| 53 | 2 | 276 | 0.61 | 0.09 | 1.75 | 0.48 | 2.39 | 0.29 | 0.08 |
| 54 | 2 | 295 | 0.43 | 0.12 | 1.80 | 0.79 | 2.23 | 0.38 | 0.08 |
| 55 | 2 | 495 | 1.00 | 0.18 | 4.00 | 0.38 | 3.97 | 0.96 | 0.17 |

| Sample # | Source | Specific Conductance | Na | K | Ca | Mg | $HCO_3$ | $SO_4$ | Cl |
|---|---|---|---|---|---|---|---|---|---|
| 56 | 2 | 394 | 0.61 | 0.12 | 2.90 | 0.52 | 3.23 | 0.35 | 0.07 |
| 57 | 2 | 270 | 0.61 | 0.19 | 1.75 | 0.32 | 2.10 | 0.38 | 0.04 |
| 58 | 2 | 531 | 1.39 | 0.23 | 3.15 | 0.98 | 3.61 | 1.27 | 0.42 |
| 59 | 2 | 392 | 0.83 | 0.15 | 2.55 | 0.80 | 3.25 | 0.48 | 0.11 |
| 60 | 2 | 309 | 0.43 | 0.15 | 2.40 | 0.26 | 2.07 | 0.58 | 0.15 |
| 61 | 2 | 225 | 0.52 | 0.09 | 1.40 | 0.35 | 1.77 | 0.44 | 0.10 |
| 62 | 2 | 467 | 0.96 | 0.16 | 3.40 | 0.48 | 3.41 | 0.50 | 0.18 |
| 63 | 2 | 447 | 0.91 | 0.17 | 2.95 | 0.82 | 3.34 | 0.79 | 0.21 |
| 64 | 2 | 1100 | 1.65 | 0.28 | 7.50 | 2.29 | 2.10 | 6.58 | 2.70 |
| 65 | 2 | 555 | 2.09 | 0.10 | 3.05 | 0.34 | 2.95 | 2.25 | 0.51 |
| 66 | 2 | 432 | 1.70 | 0.13 | 2.35 | 0.30 | 2.92 | 1.17 | 0.37 |
| 67 | 2 | 359 | 2.78 | 0.08 | 0.70 | 0.24 | 3.79 | 0.11 | 0.03 |
| 68 | 2 | 283 | 1.04 | 0.16 | 1.30 | 0.52 | 2.43 | 0.63 | 0.15 |
| 69 | 2 | 1130 | 2.43 | 0.38 | 6.65 | 2.46 | 3.54 | 5.75 | 2.45 |
| 70 | 2 | 1120 | 11.50 | 0.15 | 0.80 | 0.26 | 12.30 | 0.06 | 0.48 |
| 71 | 2 | 32100 | 452.00 | 2.46 | 8.90 | 32.00 | 117.00 | 245.00 | 147.00 |
| 72 | 2 | 3280 | 28.40 | 0.28 | 6.70 | 0.18 | 12.80 | 13.80 | 9.13 |
| 73 | 2 | 2280 | 24.60 | 0.14 | 0.14 | 0.06 | 25.10 | 0.01 | 1.77 |
| 74 | 2 | 7350 | 87.00 | 0.38 | 0.60 | 0.25 | 47.70 | 22.50 | 18.10 |
| 75 | 2 | 189 | 0.70 | 0.15 | 1.00 | 0.52 | 2.41 | 0.17 | 0.05 |
| 76 | 2 | 243 | 0.27 | 0.17 | 1.85 | 0.82 | 3.34 | 0.79 | 0.21 |
| 77 | 1 | 126 | 0.28 | 0.08 | 0.80 | 0.10 | 1.07 | 0.00 | 0.14 |
| 78 | 1 | 113 | 0.25 | 0.03 | 0.70 | 0.10 | 0.90 | 0.04 | 0.07 |
| 79 | 1 | 106 | 0.24 | 0.05 | 0.70 | 0.00 | 0.74 | 0.10 | 0.08 |
| 80 | 2 | 132 | 0.20 | 0.03 | 1.05 | 0.16 | 1.29 | 0.10 | 0.03 |
| 81 | 2 | 1730 | 17.40 | 0.38 | 0.26 | 0.25 | 10.40 | 4.46 | 2.85 |
| 82 | 2 | 13800 | 116.00 | 1.26 | 32.40 | 19.80 | 12.60 | 62.50 | 89.90 |
| 83 | 2 | 134 | 0.65 | 0.10 | 0.80 | 0.08 | 1.40 | 0.08 | 0.02 |
| 84 | 2 | 99 | 0.25 | 0.01 | 0.70 | 0.06 | 0.97 | 0.05 | 0.01 |
| 85 | 2 | 219 | 0.87 | 0.04 | 1.55 | 0.20 | 1.87 | 0.27 | 0.14 |

| Sample # | Source | Specific Conductance | Na | K | Ca | Mg | $HCO_3$ | $SO_4$ | Cl |
|---|---|---|---|---|---|---|---|---|---|
| 86 | 2 | 161 | 0.83 | 0.02 | 0.75 | 0.21 | 1.48 | 0.14 | 0.05 |
| 87 | 1 | 200 | 0.50 | 0.08 | 1.30 | 0.20 | 1.55 | 0.13 | 0.28 |
| 88 | 2 | 197 | 0.30 | 0.03 | 1.40 | 0.36 | 1.57 | 0.25 | 0.12 |
| 89 | 2 | 5910 | 47.80 | 0.59 | 12.20 | 13.50 | 8.66 | 54.40 | 12.70 |
| 90 | 2 | 3370 | 28.40 | 0.49 | 4.80 | 2.87 | 6.85 | 16.00 | 11.70 |
| 91 | 2 | 1170 | 4.48 | 0.14 | 6.85 | 1.80 | 6.20 | 2.90 | 1.61 |
| 92 | 2 | 1090 | 6.61 | 0.28 | 3.20 | 1.80 | 6.98 | 2.58 | 2.06 |
| 93 | 2 | 910 | 5.57 | 0.13 | 3.20 | 1.47 | 5.46 | 2.25 | 1.83 |
| 94 | 2 | 894 | 8.13 | 0.11 | 1.85 | 0.39 | 5.80 | 1.92 | 1.46 |
| 95 | 2 | 219 | 0.83 | 0.05 | 0.70 | 0.39 | 1.80 | 0.31 | 0.06 |
| 96 | 2 | 834 | 4.00 | 0.31 | 3.30 | 1.64 | 6.20 | 1.54 | 1.24 |
| 97 | 2 | 330 | 2.04 | 0.15 | 1.15 | 0.34 | 3.21 | 0.46 | 0.03 |
| 98 | 1 | 219 | 0.32 | 0.10 | 1.20 | 0.20 | 1.70 | 0.10 | 0.11 |
| 99 | 1 | 432 | 0.43 | 0.13 | 2.40 | 0.59 | 2.90 | 0.50 | 0.21 |
| 100 | 1 | 273 | 0.29 | 0.18 | 1.40 | 0.29 | 1.90 | 0.21 | 0.11 |
| 101 | 1 | 326 | 0.54 | 0.08 | 1.60 | 0.49 | 2.50 | 0.23 | 0.07 |
| 102 | 1 | 306 | 1.03 | 0.08 | 1.10 | 0.10 | 1.50 | 0.86 | 0.08 |
| 103 | 1 | 492 | 1.04 | 0.17 | 2.20 | 0.49 | 2.70 | 0.75 | 0.39 |
| 104 | 1 | 313 | 0.82 | 0.23 | 1.30 | 0.10 | 2.10 | 0.33 | 0.11 |
| 105 | 1 | 299 | 0.21 | 0.17 | 1.70 | 0.20 | 2.10 | 0.23 | 0.11 |
| 106 | 1 | 372 | 0.50 | 0.15 | 1.90 | 0.69 | 2.50 | 0.27 | 0.20 |
| 107 | 1 | 346 | 0.36 | 0.17 | 1.80 | 0.39 | 2.20 | 0.26 | 0.08 |
| 108 | 1 | 399 | 0.34 | 0.08 | 2.40 | 0.57 | 2.84 | 0.27 | 0.16 |
| 109 | 1 | 346 | 0.34 | 0.06 | 1.70 | 0.57 | 1.80 | 0.33 | 0.35 |
| 110 | 1 | 246 | 0.33 | 0.08 | 1.30 | 0.00 | 1.60 | 0.16 | 0.07 |
| 111 | 1 | 266 | 0.22 | 0.09 | 1.60 | 0.39 | 1.84 | 0.10 | 0.10 |
| 112 | 1 | 426 | 0.85 | 0.09 | 1.10 | 0.15 | 2.10 | 0.22 | 0.08 |
| 113 | 1 | 399 | 0.27 | 0.10 | 2.30 | 0.20 | 2.10 | 0.39 | 0.15 |
| 114 | 1 | 791 | 0.97 | 0.18 | 4.00 | 0.98 | 4.30 | 1.21 | 0.39 |
| 115 | 1 | 744 | 0.86 | 0.13 | 3.60 | 0.69 | 4.10 | 1.00 | 0.28 |

## Major Ions - Confined Aquifer

Source:

1 = Huntley, this report.
2 = Emery and others (1972).

Concentrations in equivalnet parts per million. Conductance in micromhos per centimeter.

| Sample # | Source | Specific Conductance | Na | K | Ca | Mg | $HCO_3$ | $SO_4$ | Cl |
|---|---|---|---|---|---|---|---|---|---|
| 1 | 2 | 982 | 6.65 | 0.31 | 3.50 | 0.56 | 5.74 | 3.52 | 1.10 |
| 2 | 2 | 376 | 0.37 | 0.03 | 2.60 | 1.14 | 2.40 | 1.43 | 0.04 |
| 3 | 2 | 293 | 0.21 | 0.02 | 2.35 | 0.63 | 2.10 | 0.83 | 0.01 |
| 4 | 2 | 220 | 1.74 | 0.02 | 0.60 | 0.00 | 1.85 | 0.35 | 0.05 |
| 5 | 1 | 200 | 1.27 | 0.05 | 0.40 | 0.10 | 1.56 | 0.06 | 0.11 |
| 6 | 1 | 178 | 0.92 | 0.04 | 1.00 | 0.00 | 1.48 | 0.15 | 0.21 |
| 7 | 1 | 173 | 0.52 | 0.03 | 1.00 | 0.10 | 1.23 | 0.15 | 0.13 |
| 8 | 1 | 285 | 0.78 | 0.04 | 1.60 | 0.10 | 1.39 | 0.87 | 0.21 |
| 9 | 2 | 295 | 0.70 | 0.03 | 1.95 | 0.46 | 2.07 | 0.05 | 0.90 |
| 10 | 2 | 258 | 0.87 | 0.04 | 1.50 | 0.32 | 2.07 | 0.54 | 0.14 |
| 11 | 2 | 163 | 0.32 | 0.10 | 1.05 | 0.28 | 1.44 | 0.17 | 0.07 |
| 12 | 2 | 542 | 5.04 | 0.10 | 0.85 | 0.28 | 6.03 | 0.08 | 0.05 |
| 13 | 2 | 944 | 9.09 | 0.33 | 0.80 | 0.45 | 10.63 | 0.01 | 0.08 |
| 14 | 2 | 911 | 9.26 | 0.28 | 0.36 | 0.04 | 9.38 | 0.00 | 0.54 |
| 15 | 2 | 225 | 1.78 | 0.02 | 0.50 | 0.00 | 1.67 | 0.56 | 0.03 |
| 16 | 2 | 228 | 1.96 | 0.07 | 0.18 | 0.06 | 2.36 | 0.03 | 0.06 |
| 17 | 2 | 555 | 5.39 | 0.28 | 0.42 | 0.14 | 6.00 | 0.03 | 0.09 |
| 18 | 2 | 236 | 1.78 | 0.17 | 0.48 | 0.00 | 2.26 | - | 0.07 |
| 19 | 1 | 170 | 1.08 | 0.01 | 0.35 | 0.10 | 1.31 | 0.06 | 0.07 |
| 20 | 1 | 185 | 0.69 | 0.01 | 0.80 | 0.00 | 1.14 | 0.06 | 0.07 |
| 21 | 2 | 219 | 1.74 | 0.11 | 0.46 | 0.08 | 2.22 | 0.02 | 0.06 |
| 22 | 2 | 726 | 7.26 | 0.23 | 0.32 | 0.16 | 7.90 | 0.01 | 0.14 |
| 23 | 2 | 1310 | 14.40 | 0.17 | 0.22 | 0.24 | [illegible].80 | 0.00 | 0.26 |
| 24 | 2 | 330 | 1.83 | 0.22 | 1.45 | 0.[illegible] | 3.28 | 0.00 | 0.26 |
| 25 | 1 | 347 | 1.60 | 0.17 | 1.20 | 0.[illegible] | 2.87 | 0.17 | 0.11 |

C-4

T-1864

| Sample # | Source | Specific Conductance | Na | K | Ca | Mg | $HCO_3$ | $SO_4$ | Cl |
|---|---|---|---|---|---|---|---|---|---|
| 26 | 2 | 1300 | 12.00 | 0.28 | 1.05 | 0.79 | 13.40 | 0.01 | 1.15 |
| 27 | 2 | 178 | 0.70 | 0.11 | - | - | 1.69 | 0.37 | 0.06 |
| 28 | 2 | 360 | 3.04 | 0.28 | 0.32 | 0.16 | 3.87 | 0.00 | 0.26 |
| 29 | 1 | 1375 | 8.26 | 0.42 | 0.60 | 0.11 | 9.34 | 0.08 | 0.35 |
| 30 | 2 | 1140 | 11.20 | 0.33 | 0.40 | 0.43 | 12.62 | 0.00 | 0.26 |
| 31 | 2 | 157 | 0.74 | 0.08 | 0.70 | 0.06 | 1.54 | 0.11 | 0.05 |
| 32 | 2 | 176 | 0.43 | 0.13 | 1.10 | 0.22 | 1.62 | 0.12 | 0.04 |
| 33 | 2 | 166 | 0.48 | 0.10 | 0.85 | 0.30 | 1.46 | 0.15 | 0.05 |
| 34 | 2 | 151 | 0.61 | 0.11 | 0.70 | 0.20 | 1.10 | 0.31 | 0.05 |
| 35 | 2 | 648 | 6.70 | 0.13 | 0.36 | 0.68 | 7.31 | 0.07 | 0.07 |
| 36 | 2 | 148 | 0.24 | 0.12 | 1.00 | 0.28 | 1.44 | 0.08 | 0.04 |
| 37 | 2 | 1830 | 19.90 | 0.41 | 0.40 | 0.73 | 21.30 | 0.01 | 0.14 |
| 38 | 2 | 214 | 1.43 | 0.13 | 0.60 | 0.08 | 1.84 | 0.29 | 0.04 |
| 39 | 2 | 159 | 1.13 | 0.13 | 0.18 | 0.00 | 1.44 | 0.09 | 0.04 |
| 40 | 2 | 547 | 5.39 | 0.12 | 0.24 | 0.08 | 5.77 | 0.00 | 0.05 |
| 41 | 2 | 3190 | 37.40 | 0.54 | 0.22 | 0.77 | 38.40 | - | 0.34 |
| 43 | 2 | 1880 | 19.70 | 0.36 | 0.44 | 0.79 | 21.10 | 0.00 | 0.79 |
| 44 | 2 | 214 | 0.36 | 0.08 | 1.30 | 0.55 | 1.70 | 0.22 | 0.10 |
| 45 | 2 | 132 | 0.43 | 0.04 | 0.85 | 0.00 | 1.26 | 0.10 | 0.02 |
| 46 | 2 | 136 | 0.21 | 0.14 | 0.85 | 0.40 | 1.30 | 0.09 | 0.03 |
| 47 | 2 | 159 | 0.36 | 0.23 | 0.85 | 0.28 | 1.51 | 0.10 | 0.05 |
| 48 | 2 | 156 | 0.28 | 0.19 | 0.90 | 0.28 | 1.51 | 0.08 | 0.04 |
| 49 | 2 | 144 | 0.65 | 0.19 | 0.55 | 0.08 | 1.25 | 0.17 | 0.05 |
| 50 | 2 | 630 | 6.52 | 0.10 | 0.20 | 0.00 | 6.58 | 0.18 | 0.06 |
| 51 | 2 | 644 | 6.65 | 0.12 | 0.16 | 0.11 | 7.03 | 0.01 | 0.07 |
| 52 | 2 | 391 | 3.78 | 0.16 | 0.24 | 0.04 | 3.05 | 0.50 | 0.22 |
| 53 | 2 | 1340 | 15.70 | 0.10 | 0.24 | 0.16 | 15.40 | 0.09 | 0.14 |
| 54 | 2 | 130 | 0.65 | 0.10 | 0.55 | 0.08 | 1.13 | 0.16 | 0.03 |
| 55 | 2 | 130 | 1.09 | 0.06 | 0.10 | 0.00 | 1.25 | 0.15 | 0.03 |
| 56 | 2 | 147 | 1.39 | 0.03 | 0.08 | 0.04 | 1.34 | 0.18 | 0.18 |

| Sample # | Source | Specific Conductance | Na | K | Ca | Mg | $HCO_3$ | $SO_4$ | Cl |
|---|---|---|---|---|---|---|---|---|---|
| 57 | 2 | 137 | 1.74 | 0.20 | 0.10 | 0.00 | 1.31 | 0.12 | 0.03 |
| 58 | 2 | 454 | 4.26 | 0.06 | 0.06 | 0.08 | 4.40 | 0.31 | 0.06 |
| 60 | 2 | 3610 | 43.50 | 0.31 | 0.60 | 0.22 | 41.50 | 0.01 | 3.01 |
| 61 | 2 | 1590 | 17.90 | 0.16 | 0.18 | 0.20 | 17.70 | 0.00 | 0.13 |
| 62 | 2 | 202 | 1.09 | 0.15 | 0.55 | 0.31 | 2.16 | - | 0.03 |
| 63 | 1 | 170 | 0.98 | 0.12 | 0.60 | 0.00 | 1.23 | 0.31 | 0.20 |
| 64 | 2 | 378 | 3.52 | 0.11 | 0.32 | 0.20 | 4.00 | - | 0.05 |
| 65 | 2 | 1520 | 17.00 | 0.23 | 0.32 | 0.35 | 17.20 | - | 0.15 |
| 66 | 2 | 1170 | 12.80 | 0.22 | 0.24 | 0.11 | 13.2 | - | 0.09 |
| 67 | 2 | 125 | 0.30 | 0.04 | 0.80 | 0.14 | 1.23 | 0.09 | 0.01 |
| 68 | 2 | 146 | 0.23 | 0.16 | 0.95 | 0.16 | 1.38 | 0.09 | 0.02 |
| 69 | 2 | 365 | 3.30 | 0.04 | 0.18 | 0.00 | 1.91 | 1.08 | 0.36 |
| 70 | 2 | 463 | 4.56 | 0.05 | 0.06 | 0.00 | 4.47 | 0.22 | 0.04 |
| 71 | 2 | 1540 | 17.04 | 0.18 | 0.26 | 0.01 | 17.48 | 0.10 | 0.12 |
| 72 | 2 | 1930 | 21.43 | 0.21 | 0.36 | 0.00 | 22.30 | 0.11 | 0.01 |
| 73 | 2 | 437 | 4.26 | 0.03 | 0.16 | 0.01 | 3.89 | 0.43 | 0.15 |
| 74 | 2 | 3320 | 38.34 | 0.41 | 0.80 | 0.04 | 40.97 | 0.06 | 0.53 |
| 75 | 2 | 2530 | 28.17 | 0.25 | 0.40 | 0.15 | 28.52 | 0.01 | 1.32 |
| 76 | 2 | 2090 | 23.13 | 0.30 | 0.26 | 0.57 | 23.60 | 0.00 | 0.78 |
| 77 | 2 | 575 | 5.86 | 0.08 | 0.20 | 0.19 | 6.09 | 0.03 | 0.03 |
| 78 | 1 | 146 | 0.39 | 0.04 | 0.80 | 0.20 | 0.98 | 0.27 | 0.10 |
| 79 | 1 | 153 | 0.39 | 0.08 | 1.00 | 0.00 | 0.98 | 0.26 | 0.11 |
| 80 | 2 | 159 | 0.30 | 0.67 | 0.95 | 0.38 | 1.64 | 0.27 | 0.07 |
| 81 | 2 | 266 | 2.30 | 0.10 | 0.32 | 0.08 | 2.74 | 0.12 | 0.01 |
| 82 | 2 | 316 | 2.56 | 0.08 | 0.24 | 0.05 | 2.78 | 0.31 | 0.03 |
| 83 | 2 | 351 | 3.39 | 0.03 | 0.18 | 0.04 | 3.27 | 0.01 | 0.18 |
| 84 | 2 | 257 | 2.21 | 0.04 | 0.34 | 0.04 | 2.51 | 0.18 | 0.02 |
| 85 | 2 | 469 | 4.34 | 0.12 | 0.08 | 0.00 | 3.79 | 0.54 | 0.33 |
| 86 | 2 | 213 | 1.73 | 0.11 | 0.44 | 0.08 | 2.03 | 0.19 | 0.04 |
| 87 | 2 | 463 | 4.08 | 0.01 | - | - | 2.92 | 0.00 | 0.13 |

| Sample # | Source | Specific Conductance | Na | K | Ca | Mg | $HCO_3$ | $SO_4$ | Cl |
|---|---|---|---|---|---|---|---|---|---|
| 88 | 2 | 323 | 3.08 | 0.02 | 0.20 | 0.01 | 3.28 | 0.10 | 0.02 |
| 89 | 2 | 218 | 2.13 | 0.01 | 0.10 | 0.04 | 1.80 | 0.16 | 0.23 |
| 90 | 2 | 324 | 3.39 | 0.02 | 0.18 | 0.00 | 3.02 | 0.22 | 0.03 |
| 91 | 2 | 174 | 0.82 | 0.03 | 0.90 | 0.09 | 1.59 | 0.14 | 0.04 |
| 92 | 2 | 94 | 0.56 | 0.01 | 0.35 | 0.00 | 0.85 | 0.11 | 0.01 |
| 93 | 1 | 120 | 0.37 | 0.05 | 0.80 | 0.00 | 0.82 | 0.15 | 0.14 |
| 94 | 1 | 144 | 0.43 | 0.05 | 0.80 | 0.00 | 0.98 | 0.10 | 0.08 |
| 95 | 1 | 100 | 0.30 | 0.04 | 0.60 | 0.00 | 0.82 | 0.04 | 0.06 |
| 96 | 1 | 97 | 0.36 | 0.03 | 0.70 | 0.00 | 0.90 | 0.10 | 0.15 |
| 97 | 2 | 83 | 0.33 | 0.01 | 0.48 | 0.08 | 0.78 | 0.07 | 0.04 |
| 98 | 1 | 412 | 1.87 | 0.08 | 1.20 | 0.10 | 2.30 | 0.94 | 0.14 |
| 99 | 1 | 319 | 1.00 | 0.09 | 1.30 | 0.20 | 1.80 | 0.67 | 0.17 |
| 100 | 1 | 366 | 0.77 | 0.09 | 1.60 | 0.39 | 1.80 | 1.02 | 0.10 |
| 101 | 1 | 359 | 0.83 | 0.10 | 1.60 | 0.25 | 1.80 | 1.21 | 0.11 |
| 102 | 1 | 332 | 1.48 | 0.09 | 0.90 | 0.10 | 1.50 | 0.94 | 0.14 |
| 103 | 1 | 279 | 0.72 | 0.13 | 1.20 | 0.20 | 2.10 | 0.17 | 0.14 |
| 104 | 1 | 326 | 0.43 | 0.13 | 1.70 | 0.39 | 2.30 | 0.23 | 0.17 |
| 105 | 1 | 333 | 0.50 | 0.10 | 1.80 | 0.39 | 2.50 | 0.27 | 0.17 |
| 106 | 1 | 313 | 0.29 | 0.15 | 0.90 | 0.00 | 1.10 | 0.15 | 0.14 |
| 107 | 1 | 160 | 0.19 | 0.13 | 0.60 | 0.10 | 0.90 | 0.06 | 0.05 |

## APPENDIX C: REFLECTANCE MEASUREMENTS

Fish Canyon Tuff

| Filter \ Sample # | 3 | 4 | 5 | 6 | 7 | 8 | 9 | 10 | 11 | 12 |
|---|---|---|---|---|---|---|---|---|---|---|
| NF | 10.9 | 13.7 | 31.4 | 11.6 | 13.5 | 28.3 | 12.6 | 11.3 | 17.4 | 12.4 |
| 2C | 9.5 | 10.9 | 22.6 | 9.6 | 12.6 | 22.0 | 12.3 | 10.3 | 13.0 | 10.6 |
| 8 | 10.0 | 11.4 | 28.9 | 10.2 | 12.0 | 19.1 | 11.6 | 10.5 | 13.8 | 11.3 |
| 15 | 9.9 | 11.6 | 34.7 | 7.1 | 13.7 | 34.9 | 12.7 | 10.7 | 14.2 | 11.5 |
| 22 | 11.4 | 12.9 | 20.2 | 11.6 | 13.7 | 19.1 | 12.8 | 11.0 | 17.0 | 12.4 |
| 57 | 10.3 | 10.7 | 25.7 | 9.3 | 11.9 | 30.6 | 13.1 | 10.0 | 13.4 | 10.8 |
| 89B | 22.2 | 22.2 | 38.3 | 22.2 | 23.2 | 40.4 | 22.2 | 20.0 | 30.8 | 19.2 |
| 25 | 11.6 | 14.5 | 36.0 | 11.7 | 14.5 | 45.1 | 13.5 | 11.2 | 18.5 | 12.4 |
| 92 | 12.1 | 15.4 | 37.9 | 12.9 | 15.3 | 29.8 | 13.3 | 12.1 | 27.6 | 13.0 |
| 87 | 25.2 | 27.7 | 37.4 | 23.9 | 24.6 | 30.3 | 23.1 | 20.5 | 33.7 | 23.1 |
| 47B | 9.1 | 8.1 | 15.2 | 7.3 | 10.3 | 13.2 | 9.4 | 9.1 | 9.1 | 8.8 |
| 70 | 13.7 | 16.6 | 40.4 | 13.5 | 14.9 | 39.5 | 14.1 | 12.2 | 24.8 | 12.7 |
| 87C | 27.0 | 30.7 | 40.2 | 26.6 | 26.2 | 27.5 | 26.2 | 23.6 | 32.9 | 23.6 |

Carpenter Ridge and Sapinero Mesa Tuffs

| Filter \ Sample # | 15 | 20 | 21 | 22 | 23 | 24 | 25 | 26 | 27 | 28 | 29 | 30 |
|---|---|---|---|---|---|---|---|---|---|---|---|---|
| NF | 13.5 | 17.4 | 17.4 | 17.4 | 14.1 | 10.4 | 10.4 | 17.4 | 15.1 | 15.7 | 7.8 | 8.0 |
| 2C | 13.5 | 14.9 | 15.5 | 15.3 | 12.6 | 9.7 | 9.3 | 12.3 | 13.3 | 13.2 | 7.2 | 7.6 |
| 8 | 12.7 | 16.0 | 15.8 | 16.0 | 13.1 | 9.6 | 9.6 | 13.5 | 14.9 | 13.0 | 8.4 | 7.6 |
| 15 | 13.1 | 15.7 | 16.0 | 16.3 | 14.0 | 9.6 | 9.4 | 12.4 | 14.0 | 14.0 | 7.9 | 7.9 |
| 22 | 14.3 | 21.8 | 23.6 | 20.0 | 15.5 | 9.9 | 10.1 | 16.5 | 15.4 | 15.1 | 8.3 | 7.9 |
| 57 | 11.0 | 14.4 | 15.3 | 14.4 | 12.0 | 9.5 | 9.3 | 15.7 | 12.9 | 12.6 | 7.6 | 7.7 |
| 89B | 25.2 | 33.8 | 34.4 | 31.3 | 28.0 | 14.8 | 15.7 | 33.3 | 27.4 | 25.1 | 12.1 | 13.6 |
| 25 | 14.7 | 30.5 | 24.3 | 21.3 | 16.6 | 9.9 | 9.6 | 21.3 | 16.6 | 16.6 | 8.2 | 9.0 |
| 92 | 15.7 | 27.6 | 27.2 | 27.2 | 21.3 | 10.5 | 10.5 | 22.6 | 20.3 | 19.3 | 6.6 | 8.9 |
| 87 | 27.0 | 38.5 | 38.5 | 37.1 | 21.9 | 15.9 | 16.4 | 33.8 | 31.8 | 31.5 | 13.2 | 11.9 |
| 47B | 9.8 | 11.6 | 11.6 | 11.9 | 10.3 | 9.1 | 9.1 | 11.8 | 11.7 | 11.1 | 6.9 | 6.5 |
| 70 | 16.1 | 32.9 | 24.5 | 32.9 | 21.6 | 10.8 | 11.2 | 29.7 | 27.5 | 29.7 | 8.6 | 7.9 |
| 87C | 26.2 | 36.1 | 35.4 | 38.3 | 29.9 | 17.6 | 16.5 | 33.0 | 27.4 | 29.7 | 12.9 | 14.5 |

Flows and Flow Breccias of Conejos Formation

| Filter \ Sample # | 1 | 2 | 31 | 32 | 33 | 34 | 35 | 36 | 37 | 38 | 39 | 40 |
|---|---|---|---|---|---|---|---|---|---|---|---|---|
| NF | 14.9 | 7.0 | 10.4 | 8.7 | 8.7 | 9.5 | 8.4 | 10.4 | 11.9 | 10.4 | 12.4 | 13.6 |
| 2C | 10.1 | 6.1 | 9.2 | 8.1 | 7.8 | 9.4 | 8.2 | 9.8 | 9.5 | 7.9 | 11.1 | 13.0 |
| 8 | 14.4 | 6.8 | 9.4 | 7.9 | 8.1 | 8.9 | 7.9 | 9.8 | 9.3 | 7.7 | 11.9 | 13.8 |
| 15 | 14.8 | 6.5 | 9.5 | 8.4 | 8.6 | 10.6 | 8.3 | 10.2 | 9.9 | 8.4 | 11.0 | 13.7 |
| 22 | 16.5 | 7.2 | 11.3 | 9.1 | 11.7 | 11.2 | 8.8 | 10.0 | 10.6 | 7.9 | 12.5 | 14.4 |
| 57 | 13.6 | 5.8 | 9.2 | 7.5 | 9.2 | 8.9 | 7.9 | 9.4 | 9.4 | 7.4 | 11.1 | 12.6 |
| 89B | 26.6 | 14.3 | 18.0 | 17.8 | 21.1 | 19.3 | 18.3 | 17.4 | 17.8 | 14.9 | 21.3 | 21.8 |
| 25 | 16.6 | 7.7 | 9.2 | 10.4 | 11.6 | 11.4 | 9.8 | 10.5 | 10.9 | 8.2 | 13.7 | 15.1 |
| 92 | 18.0 | 8.0 | 10.0 | 10.1 | 12.3 | 12.1 | 9.9 | 10.1 | 11.5 | 8.0 | 14.4 | 14.6 |
| 87 | 27.0 | 17.7 | 23.1 | 19.4 | 19.2 | 20.5 | 20.1 | 17.8 | 17.6 | 15.0 | 23.1 | 23.1 |
| 47B | 10.6 | 6.1 | 7.4 | 6.6 | 7.3 | 8.0 | 6.5 | 8.4 | 8.2 | 6.8 | 10.0 | 10.1 |
| 70 | 19.9 | 7.9 | 10.8 | 10.7 | 13.1 | 12.5 | 10.9 | 9.7 | 11.6 | 9.1 | 14.4 | 14.4 |
| 87C | 28.3 | 15.4 | 21.3 | 20.8 | 21.9 | 21.5 | 21.3 | 17.5 | 21.0 | 18.0 | 24.3 | 23.6 |

Air-Fall/Water-Laid Tuffs and Laharic Breccias

| Filter \ Sample # | 13 | 14 | 16 | 17 | 18 | 19 |
|---|---|---|---|---|---|---|
| NF | 35.5 | 39.1 | 56.5 | 28.3 | 39.1 | 28.3 |
| 2C | 23.9 | 34.8 | 56.2 | 33.8 | 36.5 | 15.2 |
| 8 | 27.4 | 45.0 | 60.4 | 36.6 | 43.4 | 16.0 |
| 15 | 26.7 | 40.9 | 64.7 | 37.9 | 39.6 | 22.5 |
| 22 | 22.6 | 50.1 | 62.7 | 38.9 | 40.0 | 23.2 |
| 57 | 31.6 | 50.6 | 58.3 | 33.1 | 36.1 | 23.4 |
| 89B | 35.3 | 57.6 | 59.6 | 45.4 | 50.0 | 45.4 |
| 25 | 43.8 | 49.8 | 64.2 | 45.1 | 40.9 | 29.0 |
| 92 | 29.8 | 49.6 | 61.1 | 44.1 | 49.6 | 33.1 |
| 87 | 48.4 | 57.9 | 76.9 | 48.1 | 50.0 | 45.7 |
| 47B | 26.3 | 34.2 | 50.9 | 19.2 | 30.2 | 15.2 |
| 70 | 42.3 | 63.3 | 68.9 | 40.4 | 46.3 | 38.4 |
| 87C | 45.2 | 50.0 | 62.0 | 40.4 | 50.0 | 46.2 |

Saline Soils

| Filter \ Sample # | 41 | 42 | 43 | 44 | 45 |
|---|---|---|---|---|---|
| NF | 39.1 | 28.3 | 50.0 | 50.0 | 25.4 |
| 2C | 25.2 | 15.7 | 38.4 | 41.7 | 15.7 |
| 8 | 43.1 | 22.9 | 50.3 | 45.1 | 14.6 |
| 15 | 35.8 | 21.9 | 42.1 | 37.8 | 27.6 |
| 22 | 36.7 | 18.1 | 37.0 | 44.5 | 31.6 |
| 57 | 27.7 | 22.9 | 39.0 | 39.4 | 15.7 |
| 89B | 31.5 | 35.5 | 41.9 | 50.0 | 35.8 |
| 25 | 43.7 | 30.4 | 49.8 | 49.8 | 24.1 |
| 92 | 41.3 | 31.2 | 51.8 | 51.8 | 34.2 |
| 87 | 50.5 | 39.8 | 49.7 | 46.7 | 39.2 |
| 47B | 15.2 | 12.1 | 33.1 | 23.9 | 12.9 |
| 70 | 48.0 | 35.7 | 54.0 | 49.3 | 42.4 |
| 87C | 50.0 | 37.4 | 49.0 | 58.1 | 42.1 |

Soil Sample 1: Sandy Silt

| Filter | Soil Moisture (% Dry Weight) | | |
|---|---|---|---|
| | 0.0 | 8.8 | 17.9 |
| NF | 11.4 | 7.9 | 5.8 |
| 2C | 9.1 | 6.7 | 5.5 |
| 8 | 9.1 | 6.5 | 7.3 |
| 15 | 10.1 | 7.2 | 7.7 |
| 22 | 10.6 | 7.5 | 7.6 |
| 57 | 8.3 | 5.3 | 6.5 |
| 89B | 22.2 | 20.1 | 15.7 |
| 25 | 13.6 | 8.0 | 8.0 |
| 92 | 14.1 | 8.1 | 6.7 |
| 87 | 21.5 | 15.9 | 16.4 |
| 47B | 5.6 | 3.5 | 4.3 |
| 70 | 14.3 | 9.0 | 9.6 |
| 87C | 19.1 | 18.0 | 16.9 |

Soil Sample 2: Silty-Sandy Gravel

| Filter | Soil Moisture (% Dry Weight) | | | |
|---|---|---|---|---|
| | 1.3 | 6.5 | 10.9 | 15.3 |
| NF | 15.6 | 8.9 | 7.1 | 7.0 |
| 2C | 12.5 | 7.5 | 6.1 | 5.9 |
| 8 | 14.1 | 7.8 | 6.1 | 5.8 |
| 15 | 14.8 | 8.4 | 6.2 | 6.9 |
| 22 | 15.3 | 9.3 | 7.5 | 7.5 |
| 57 | 11.2 | 7.1 | 5.4 | 5.3 |
| 89B | 24.8 | 19.0 | 14.2 | 13.8 |
| 25 | 16.3 | 10.1 | 7.8 | 7.9 |
| 92 | 19.2 | 12.1 | 9.0 | 8.1 |
| 87 | 25.9 | 20.9 | 17.1 | 17.8 |
| 47B | 8.1 | 5.2 | 3.8 | 4.1 |
| 70 | 18.3 | 13.2 | 10.5 | 9.9 |
| 87C | 25.4 | 19.7 | 15.5 | 15.7 |

Soil Sample 3: Clay

| Filter | Soil Moisture (% Dry Weight) | | |
|---|---|---|---|
| | 0.0 | 12.3 | 21.9 |
| NF | 18.5 | 17.4 | 14.6 |
| 2C | 16.4 | 15.1 | 12.5 |
| 8 | 17.4 | 16.0 | 12.6 |
| 15 | 17.9 | 16.6 | 13.0 |
| 22 | 25.7 | 19.4 | 14.9 |
| 57 | 15.7 | 14.0 | 9.4 |
| 89B | 28.1 | 26.4 | 22.8 |
| 25 | 24.3 | 18.9 | 15.8 |
| 92 | 24.8 | 22.1 | 17.6 |
| 87 | 30.0 | 27.7 | 24.1 |
| 47B | 13.0 | 9.4 | 7.1 |
| 70 | 27.9 | 22.6 | 17.3 |
| 87C | 27.2 | 25.2 | 20.6 |

Soil Sample 4: Dark Organic Silt

| Filter | Soil Moisture (% Dry Weight) 1.4 | 12.3 |
|---|---|---|
| NF | 8.9 | 8.7 |
| 2C | 8.6 | 7.1 |
| 8 | 9.7 | 7.6 |
| 15 | 9.7 | 7.5 |
| 22 | 10.8 | 7.5 |
| 57 | 9.6 | 6.4 |
| 89B | 17.8 | 14.0 |
| 25 | 11.2 | 7.7 |
| 92 | 13.3 | 9.2 |
| 87 | 17.0 | 14.8 |
| 47B | 8.8 | 5.7 |
| 70 | 11.8 | 8.8 |
| 87C | 16.2 | 15.7 |

Soil Sample 5: Gray Clay

| Filter | Soil Moisture (% Dry Weight) 0.0 | 17.0 | 23.2 |
|---|---|---|---|
| NF | 17.4 | 15.0 | 13.4 |
| 2C | 13.0 | 12.2 | 11.3 |
| 8 | 12.6 | 12.2 | 11.6 |
| 15 | 13.2 | 12.9 | 12.7 |
| 22 | 14.4 | 15.1 | 13.8 |
| 57 | 14.1 | 12.0 | 11.5 |
| 89B | 22.2 | 23.5 | 22.6 |
| 25 | 21.1 | 15.8 | 15.3 |
| 92 | 26.6 | 18.9 | 17.3 |
| 87 | 25.8 | 25.9 | 24.6 |
| 47B | 15.6 | 8.8 | 9.5 |
| 70 | 27.5 | 17.7 | 15.7 |
| 87C | 29.5 | 27.5 | 25.2 |

Soil Sample 6: Gravelly Sand

| Filter | Soil Moisture (% Dry Weight) | | |
|---|---|---|---|
| | 1.3 | 10.2 | 17.9 |
| NF | 17.1 | 7.3 | 6.9 |
| 2C | 13.8 | 6.3 | 5.7 |
| 8 | 15.7 | 6.5 | 6.1 |
| 15 | 16.0 | 6.7 | 6.5 |
| 22 | 17.5 | 7.6 | 6.9 |
| 57 | 13.6 | 6.1 | 5.6 |
| 89B | 25.0 | 14.6 | 22.2 |
| 25 | 17.4 | 8.3 | 8.1 |
| 92 | 18.3 | 8.9 | 8.8 |
| 87 | 25.2 | 15.2 | 16.3 |
| 47B | 9.8 | 4.8 | 4.7 |
| 70 | 18.6 | 9.8 | 9.4 |
| 87C | 25.5 | 14.6 | 15.3 |

Soil Sample 7: Sandy Gravel ($Qf_3$)

| Filter | Soil Moisture (% Dry Weight) | | |
|---|---|---|---|
| | 0.0 | 4.0 | 7.3 |
| NF | 12.6 | 8.3 | 8.3 |
| 2C | 10.4 | 7.0 | 7.1 |
| 8 | 10.6 | 7.3 | 7.6 |
| 15 | 11.0 | 7.7 | 7.9 |
| 22 | 13.8 | 9.2 | 8.6 |
| 57 | 9.6 | 6.4 | 6.7 |
| 89B | 22.5 | 18.1 | 16.6 |
| 25 | 14.3 | 10.4 | 9.7 |
| 92 | 15.6 | 11.3 | 10.9 |
| 87 | 22.9 | 18.5 | 18.1 |
| 47B | 7.1 | 4.7 | 5.5 |
| 70 | 15.9 | 12.3 | 11.8 |
| 87C | 21.9 | 18.3 | 16.5 |

Soil Sample 8: Eolian Sand

| Filter | Soil Moisture (% Dry Weight) | | |
|---|---|---|---|
| | 0.0 | 11.3 | 11.8 |
| NF | 11.6 | 10.9 | 8.2 |
| 2C | 14.4 | 9.5 | 7.3 |
| 8 | 14.5 | 9.4 | 7.7 |
| 15 | 15.1 | 9.8 | 8.0 |
| 22 | 15.5 | 10.4 | 8.3 |
| 57 | 11.7 | 8.7 | 9.5 |
| 89B | 16.8 | 16.8 | 13.9 |
| 25 | 16.6 | 12.1 | 11.6 |
| 92 | 19.1 | 11.9 | 9.7 |
| 87 | 24.5 | 16.4 | 9.6 |
| 47B | 11.6 | 6.4 | 7.3 |
| 70 | 22.1 | 13.0 | 10.4 |
| 87C | 26.1 | 15.7 | 20.2 |

## APPENDIX D: GRAVITY MEASUREMENTS

For location of stations, see Plate 8

| Station | Latitude | Elevation (Ft) | Observed Gravity (gals) | Bouger Gravity (mgals) (2.67 gm/cc) |
|---|---|---|---|---|
| B1 | 38°15'06" | 7957 | 979.2719 | -276.9 |
| B2 | 38°11'18" | 7808 | 979.2850 | -267.1 |
| 1 | 38°11'18" | 7791 | 979.2813 | -271.8 |
| 2 | 38°11'18" | 7770 | 979.2777 | -276.7 |
| 3 | 38°11'16" | 7753 | 979.2772 | -278.1 |
| 4 | 38°11'15" | 7754 | 979.2775 | -277.8 |
| 5 | 38°11'15" | 7779 | 979.2753 | -278.5 |
| 6 | 38°11'41" | 7800 | 979.2756 | -277.5 |
| 7 | 38°12'07" | 7825 | 979.2759 | -276.4 |
| 8 | 38°12'34" | 7869 | 979.2759 | -274.4 |
| 9 | 38°12'34" | 7893 | 979.2750 | -273.8 |
| 10 | 38°12'45" | 7941 | 979.2734 | -272.8 |
| 11 | 38°12'54" | 7980 | 979.2724 | -271.7 |
| 12 | 38°13'02" | 8056 | 979.2695 | -270.2 |
| 13 | 38°13'06" | 8076 | 979.2688 | -269.7 |
| 14 | 38°13'11" | 8099 | 979.2681 | -269.3 |
| 15 | 38°13'23" | 8152 | 979.2664 | -268.1 |
| 16 | 38°13'28" | 8172 | 979.2651 | -268.3 |
| 17 | 38°13'48" | 8304 | 979.2608 | -265.2 |
| 18 | 38°14'00" | 8475 | 979.2533 | -262.7 |
| 19 | 38°13'00" | 7906 | 979.2758 | -277.9 |
| 20 | 38°13'25" | 7959 | 979.2747 | -271.6 |
| 21 | 38°13'38" | 7973 | 979.2745 | -271.1 |
| 22 | 38°13'50" | 8005 | 979.2735 | -270.5 |
| 23 | 38°14'03" | 8021 | 979.2731 | -270.2 |
| 24 | 38°14'09" | 8061 | 979.2715 | -269.5 |
| 25 | 38°14'29" | 8076 | 979.2710 | -269.6 |
| 26 | 38°14'42" | 8084 | 979.2712 | -269.4 |
| 27 | 38°14'36" | 8131 | 979.2689 | -268.6 |
| 28 | 38°14'20" | 8219 | 979.2655 | -266.4 |
| 29 | 38°14'10" | 8330 | 979.2611 | -263.9 |
| 30 | 38°11'15" | 7832 | 979.2733 | -277.3 |
| 31 | 38°11'15" | 7833 | 979.2718 | -275.7 |
| 32 | 38°11'15" | 7956 | 979.2696 | -273.5 |
| 33 | 38°11'15" | 8052 | 979.2668 | -270.6 |
| 34 | 38°11'15" | 8143 | 979.2635 | -268.4 |
| 35 | 38°11'15" | 8209 | 979.2597 | -268.3 |
| 36 | 38°10'55" | 8332 | 979.2532 | -266.9 |
| 37 | 38°11'07" | 8413 | 979.2499 | -265.6 |
| 38 | 38°11'15" | 8462 | 979.2478 | -265.0 |

| Station | Latitude | Elevation (Ft) | Observed Gravity (gals) | Bouger Gravity (mgals) (2.67 gm/cc) |
|---|---|---|---|---|
| 39 | 38°11'25" | 8574 | 979.2427 | -263.6 |
| 40 | 38°24'20" | 8745 | 979.2413 | -273.6 |
| 41 | 38°24'37" | 8920 | 979.2316 | -273.2 |
| 42 | 38°24'52" | 8953 | 979.2290 | -274.2 |
| 43 | 38°25'05" | 8989 | 979.2296 | -271.8 |
| B3 | 37°39'55" | 7753 | 979.2547 | -254.9 |
| 44 | 37°36'28" | 7718 | 979.2519 | -254.8 |
| 45 | 37°36'27" | 7738 | 979.2518 | -253.7 |
| 46 | 37°36'26" | 7810 | 979.2506 | -250.6 |
| 47 | 37°36'25" | 7884 | 979.2484 | -248.4 |
| 48 | 37°36'25" | 7970 | 979.2452 | -246.4 |
| 49 | 37°36'27" | 8062 | 979.2409 | -245.2 |
| 50 | 37°36'26" | 8144 | 979.2369 | -244.3 |
| 51 | 37°36'27" | 8246 | 979.2320 | -243.0 |
| 52 | 37°36'28" | 8347 | 979.2270 | -242.0 |
| 53 | 37°36'22" | 8401 | 979.2244 | -241.2 |
| 54 | 37°44'48" | 8138 | 979.2590 | -234.6 |
| 55 | 37°44'49" | 8184 | 979.2572 | -233.8 |
| 56 | 37°44'49" | 8203 | 979.2570 | -232.8 |
| 57 | 37°44'47" | 8220 | 979.2562 | -232.5 |
| 58 | 37°44'45" | 8251 | 979.2548 | -232.0 |
| 59 | 37°44'46" | 8289 | 979.2535 | -231.1 |
| 60 | 37°44'44" | 8327 | 979.2514 | -230.8 |

## APPENDIX E: TEMPERATURE MEASUREMENTS

All temperatures were measured at 70 cm depth. See Plate 8 for location of measurement.

| Station # | Date | Temperature (°C) | Ground Water Depth (m) |
|---|---|---|---|
| 1 | 8/10/75 | 21.6 | 73 |
| 2 | | 20.4 | 46 |
| 3 | | 20.5 | 20 |
| 4 | | 16.2 | 6 |
| 5 | | 16.0 | 4.6 |
| 6 | | 17.4 | 1.8 |
| 7 | | 14.2 | 0.9 |
| 8 | | 12.7 | 3.4 |
| 9 | | 14.5 | 0.9 |
| 10 | | 14.9 | 0.9 |
| 11 | | 14.2 | 3.0 |
| 12 | | 19.8 | 7.3 |
| 13 | | 20.8 | 13 |
| 14 | | 20.8 | 18 |
| 15 | | 21.1 | 15 |
| 16 | | 19.6 | 93 |
| 17 | | 17.8 | ? |
| 18 | 8/12/75 | 20.6 | 24 |
| 19 | | 22.6 | 12 |
| 20 | | 14.4 | 0.9 |
| 21 | | 21.0 | 2.1 |
| 22 | | 19.4 | 3.4 |
| 23 | | 19.9 | 2.7 |
| 24 | | 21.2 | 2.7 |
| 25 | | 20.4 | 2.7 |
| 27 | | 20.2 | 2.7 |
| 28 | | 19.3 | 2.7 |
| 29 | | 21.0 | 3.7 |
| 30 | | 19.8 | 1.5 |
| 31 | 8/13/75 | 17.4 | 4.0 |
| 32 | | 20.2 | 4.6 |
| 33 | | 19.0 | 4.0 |
| 34 | | 19.1 | 2.1 |
| 35 | | 18.3 | 1.5 |
| 36 | | 21.0 | 6.1 |
| 37 | | 22.0 | 6.4 |
| 38 | | 21.7 | 4.3 |
| 39 | | 21.1 | 6.1 |
| 40 | | 23.0 | 21. |

| Station # | Date | Temperature (°C) | Ground Water Depth (m) |
|---|---|---|---|
| 41 | 8/13/75 | 21.7 | 15. |
| 42 | | 21.0 | 14. |
| 43 | | 21.7 | 12. |
| 44 | | 21.6 | 12. |
| 45 | | 17.0 | 1.8 |
| 46 | | 17.5 | 1.5 |
| 47 | | 20.5 | 2.1 |
| 48 | | 21.9 | 2.7 |
| 49 | | 20.8 | 2.7 |
| 50 | 8/14/75 | 20.3 | 3.0 |
| 51 | | 20.1 | 2.7 |
| 52 | | 19.6 | 1.5 |
| 53 | | 19.4 | 1.5 |
| 54 | | 20.2 | 7.6 |
| 55 | | 21.2 | 9.8 |
| 56 | | 20.4 | 12. |
| 57 | | 19.5 | 26. |
| 58 | | 20.0 | 30. |
| 59 | | 19.2 | 49. |
| 60 | | 17.0 | 6.1 |
| 61 | | 17.0 | 1.8 |
| 62 | | 19.0 | 0.9 |
| 63 | | 19.8 | 9.1 |

# APPENDIX F: FORTRAN IV PROGRAM FOR SIMULATION OF DIURNAL TEMPERATURE VARIATIONS

## Introduction

This program is designed to compute diurnal temperature variations at the surface and in the sub-surface to some user-defined depth where diurnal temperature variations are insignificant. Vertical node spacing (variable XH) is set at 1 cm, and the program allows the user to select the depth of the basal, constant-temperature boundary (maximum depth of 5 m).

Heat flow beneath the surface is assumed to be entirely one-dimensional and conductive. Heat loss from the surface is radiative only. Heat is added to the surface by both insolation and sky radiation. The sky radiation term includes both radiation from the sky and from clouds. Convective heat loss from the earth's surface may be taken into account by decreasing the "effective" sky temperature.

Because of a general lack of information on the meteorologic factors that determine sky radiation and cloud transmittance, the model does not have predictive capability. While cloud transmittance and sky temperature may vary significantly in the physical situation, these variables are assumed constant for the model. In this study, the simulation model was calibrated by adjusting cloud transmittance (CLD) and sky temperature (TSKY) until a match with field temperature variations was achieved. The model can then be

used to study the effects of varying the physical properties of the surface, the meteorologic variables, and the temperature at the base of the model.

Initial conditions are set by assuming a linear temperature gradient between the surface and the basal, constant-temperature boundary. The effect of this initial assumption disappears after the first 24 hours of simulation. Only temperature values obtained for the second 24 hours of simulation were used for this study.

Output from this program is a printout that lists the input variables and the temperature at 0, 10, 20, 30, 40, 50, 60, 70, 80, and 100 cm for each time step. All times listed are based on sunrise(time=0).

## Documentation

Input variables list:

| Input Variable | Description |
|---|---|
| MD | The number of days the simulation is allowed to run. |
| NS | The part of the solar declination cycle at the beginning of simulation (equals 1 if the initial date is between June 21 and December 22, equals 2 if the initial date is between December 23 and June 20) |
| MT | Maximum number of time steps to be taken. Used only when user wishes to limit the simulation to less than one day. Otherwise this variable is set to equal 1440/DELTM. |

| Input Variable | Description |
|---|---|
| IMAX | Maximum number of iterations allowed in the computation of the surface temperature (convergence is usually reached after 2-3 iterations). |
| JBASE | Nodal value at the basal, constant-temperature boundary. Node spacing = 1 cm, surface node = 1. Maximum value = 501 (1 m). |
| DELTM | The length of the time step, in minutes. |
| BDEC | The declination angle at the beginning of the cycle, in degrees. |
| AL | The latitude of the modeled site, in degrees. |
| TB | The temperature at the base of the model ($^{o}C$). |
| TOL | Error tolerance for the convergence of the surface temperature solution (0.01 $^{o}C$ was used in this study). |
| TA | Mean monthly surface temperature(used only for initial condition. Approximately equal to the mean monthly air temperature ($^{o}C$) + 5$^{o}C$). |
| ALPHA | Thermal diffusivity of the surface ($cm^2/sec$). |
| TCOND | Thermal conductivity (mcal/cm-sec-$^{o}C$) |
| ALBEDO | Solar reflectance (%). |
| EMISS | Emissivity of the surface. |
| CLD | Cloud transmittance (Usually varies between 0.1 and 0.3). |
| TSKY | Sky temperature ($^{o}K$). |
| TS | Surface temperature at the beginning of simulation ($^{o}C$ at sunrise). |

Input Variable Format:

| Card | Variables | Format |
|---|---|---|
| 1 | MD,NS,MT,IMAX,JBASE | 5I |
| 2 | DELTM,BDEC,AL,TB,TOL,TA | 6F |
| 3 | ALPHA,TCOND,ALBEDO,EMISS,CLD,TSKY,TS | 7F |

Notes:

1) The sequence of data cards given above may be repeated any number of times. The final data card in the data deck should have a Ø (zero) followed by a comma in the first two columns.

2) The I format specifies that each integer value is followed by a comma. The F format specifies that each real value is written explicitly, with a decimal point in all cases, and followed by a comma.

REPRODUCIBILITY OF THE
ORIGINAL PAGE IS POOR

```
      COMMON XH,X(5Ø1),R,BETA,RM1,GAMMA,ALFA,W(5Ø1),
     1DENOMG(5Ø1),U(2,5Ø1),DELTA(5Ø1),G(5Ø1),NDAY,T,IMAX,
     2TOL,JBASE,JBASE1,C1,C4
C
C     READ IN DATA
C
    5 READ(5,1Ø) MD,NS,MT,IMAX,JBASE
   1Ø FORMAT(5I)
      IF(MD .EQ. Ø) GO TO 11ØØ
      READ(5,2Ø) DELTM,BDEC,AL,TB,TOL,TA
   2Ø FORMAT(6F)
      READ(5,3Ø) ALPHA,TCOND,ALBEDO,EMISS,CLD,TSKY,TS
   3Ø FORMAT(7F)
C
C     SET GRID SPACINGS AND COMPUTE CONSTANTS
C
      XH=1.Ø
      X(1)=Ø.Ø
      DO 7Ø J=2,5Ø1
             X(J)=(X(J-1)*XH)
   7Ø CONTINUE
      DO 75 J=1,5Ø1
             X(J)=X(J)/1ØØ.Ø
   75 CONTINUE
      DELTS=DELTM*6Ø.Ø
      R=DELTS*ALPHA/(XH*XH)
      BETA=1.Ø+R
      RM1=1.Ø-R
      GAMMA=R/2.Ø
      ALFA=R/2.Ø
      W(2)=GAMMA/BETA
      DENOMG(2)=GAMMA/W(2)
      DO 14Ø J=3,5ØØ
             W(J)=GAMMA/(BETA-(ALFA*W(J-1)))
             DENOMG(J)=GAMMA/W(J)
  14Ø CONTINUE
      S=(1.Ø-(ALBEDO/1ØØ.Ø))*Ø.Ø333*CLD
      THCOND=TCOND/1ØØØ.Ø
      SB=1.355E-12
      C1=EMISS*SB*XH/THCOND
      C2=XH/THCOND
      C3=SB*XH*(TSKY**4.Ø)/THCOND
      PI=3.14159
      DEC=BDEC*PI/18Ø.Ø
      RLAT=AL*PI/18Ø.Ø
      COSL=COS(RLAT)
      SINL=SIN(RLAT)
      NSTEP=144Ø.Ø/DELTM
      NHCYC=NSTEP/2
```

```
      JBASE1=JBASE-1
      GRAD=(TB-TA)/X(JBASE)
      DO 18Ø J=2,JBASE1
         U(1,J)=TA + X(J)*GRAD
  18Ø CONTINUE
      DO 19Ø J=1,5Ø1
         IF(J .GE. JBASE) U(2,J)=TB
  19Ø CONTINUE
      U(1,1)=TS
      U(2,1)=TS
      U(1,JBASE)=TB
      U(2,JBASE)=TB
C
C     PRINTING DIRECTIONS AND OUTPUT OF CONSTANTS
C
      WRITE(6,2Ø5) ALPHA,TCOND,ALBEDO,EMISS
  2Ø5 FORMAT(1H1,2ØHTHERMAL DIFFUSIVITY=,F7.5,
     11ØH SQ CM/SEC,/1H ,21HTHERMAL CONDUCTIVITY=,F8.5,
     219H MCAL/CM-SEC-DEG. C,/1H ,7HALBEDO=,F4.1,
     38HPERCENT,/1H ,11HEMISSIVITY=,F4.2)
      WRITE(6,21Ø) AL,BDEC,TB,X(JBASE)
  21Ø FORMAT(1H ,19HTEST SITE LATITUDE=,F5.2,8H DEGREES,/
     11H ,4ØHDECLINATION ANGLE AT BEGINNING OF CYCLE=,
     2F5.2,8H DEGREES,/1H ,23HCONSTANT TEMPERATURE OF,
     3F6.2,22H DEGREES AT A DEPTH OF,F7.2,7H METERS,///)
      WRITE(6,215)
  215 FORMAT(1X,35X,25HTEMPERATURE AT A DEPTH OF,///1H ,
     11ØHDAY   HOUR,15X,4HØ CM,4X,5H1Ø CM,4X,5H2Ø CM,4X,
     25H3Ø CM,4X,5H4Ø CM,4X,5H5Ø CM,4X,5H6Ø CM,4X,
     35H7Ø CM,5X,5H8Ø CM,5X,5H1.Ø M,)
C
C     START DAY COUNTER. CALCULATE ALL TERMS THAT ARE
C     ONLY DAY-DEPENDENT.
C
      DO 1ØØØ I=1,MD
         NDAY=I
         IF(NS .EQ. 1) DEC=DEC-Ø.ØØ439
         IF(NS .EQ. 2) DEC=DEC+Ø.ØØ439
         IF(DEC .GT. Ø.4) NS=1
         IF(DEC .LT. -Ø.4) NS=2
         T=Ø.Ø
         SINDEC=ABS(SIN(DEC))
         COSDEC=COS(DEC)
C
C     START DIURNAL CHANGES. CALCULATE TERMS THAT ARE
C     TIME DEPENDENT.
C
         DO 1ØØØ K=1,NSTEP
            THR=T/6Ø.Ø
            IF(K .GT. MT) GO TO 1ØØØ
```

REPRODUCIBILITY OF THE
ORIGINAL PAGE IS POOR



```
                  IF(K .GT. NHCYC) GO TO 4ØØ
                  TT=PI*T/72Ø.Ø
                  SINT=SIN(TT)
                  COSZ=COSL*COSDEC*SINT+SINL*SINDEC
                  Y=1.Ø/COSZ
                  XMZ=1.Ø-Ø.2*SQRT(Y)
                  SF=S*XMZ*COSZ
                  C4=C2*SF+C3
                  CALL TEMP
                  GO TO 6ØØ
  4ØØ             SF=Ø.Ø
                  C4=C3
                  CALL TEMP
C
C      OUTPUT OF DATA
C
  6ØØ WRITE(6,6Ø5) NDAY,THR,U(2,1),U(2,11),U(2,21),U(2,31),
     1U(2,41),U(2,51),U(2,61),U(2,71),U(2,81),U(2,1Ø1)
  6Ø5 FORMAT(1H ,I3,F7.2,1ØF9.2)
      T=T+DELTM
 1ØØØ CONTINUE
      GO TO 5
 11ØØ STOP
      END


      SUBROUTINE TEMP
      COMMON XH,X(5Ø1),R,BETA,RM1,GAMMA,ALFA,W(5Ø1),
     1DENOMG(5Ø1),U(2,5Ø1),DELTA(5Ø1),G(5Ø1),NDAY,T,IMAX,
     2TOL,JBASE,JBASE1,C1,C4
      IF(NDAY .EQ. 1 .AND. T .EQ. Ø.Ø) GO TO 2ØØ
C
C     COMPUTATION OF SURFACE TEMPERATURE BY NEWTON'S
C     METHOD.
C
      DO 1ØØ I=1,IMAX
         XNUM=U(1,1)+C1*((U(1,1)+273.Ø)**4.Ø)-U(1,2)-C4
         XDEN=1.Ø+4.Ø*C1*((U(1,1)+273.Ø)**3.Ø)
         U(2,1)=U(1,1)-XNUM/XDEN
         DIFF=ABS(U(2,1)-U(1,1))
         IF(DIFF .LE. TOL) GO TO 2ØØ
         U(1,1)=U(2,1)
  1ØØ CONTINUE
C
C     COMPUTATION OF TEMPERATURE WITH DEPTH USING THE
C     CRANK-NICHOLSON METHOD.
```

```
C
  2ØØ DO 3ØØ J=2,JBASE1
            DELTA(J)=Ø.5*R*(U(1,J+1)+U(1,J-1))+RM1*U(1,J)
  3ØØ CONTINUE
      G(2)=(DELTA(2)+ALFA*U(2,1))/BETA
      DO 4ØØ J=3,JBASE1
            G(J)=(DELTA(J)+ALFA*G(J-1))/DENOMG(J)
  4ØØ CONTINUE
      DO 5ØØ I=2,JBASE1
            J=JBASE+1-I
            U(2,J)=W(J)*U(2,J+1)+G(J)
  5ØØ CONTINUE
      DO 6ØØ J=1,JBASE
            U(1,J)=U(2,J)
  6ØØ CONTINUE
      RETURN
      END
```